THE ADSORPTIVE PROPERTIES OF OLIGOMERIC, NON-IONIC SURFACTANTS FROM AQUEOUS SOLUTION

A thesis submitted for the degree of Doctor of Philosophy

by

Kirsten Jane Holland.

Department of Chemistry, Brunel University

May 1998

Declaration

I hereby certify that this thesis has been composed entirely by myself, that the work presented is my own and that any collaborative work has been duly acknowledged.

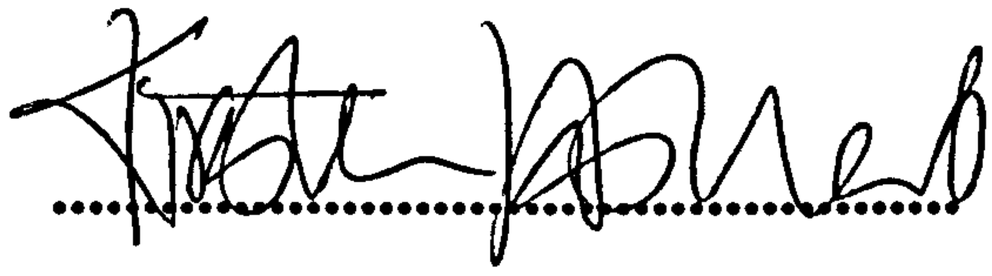

Kirsten Holland, May 1998.

Acknowledgements.

I wish to express my gratitude to my supervisor, Professor Paul A. Sermon, for the guidance and encouragement that he gave throughout my three years at Brunel.

My thanks also go to the EU for the financial assistance received.

There are many, many others who helped me during my time spent working for this degree. In particular, I would like to thank Dr Anne Young for her constant help and interest, in particular, in the light and neutron scattering work, and also Mr Brian Wheals for so generously allowing me to use the HPLC equipment in his laboratory and for providing much sound technical advice.

My appreciation also goes to the many colleagues and friends in the laboratory who made my time at Brunel so enjoyable; they know who they are.

Finally, this thesis would not have been completed without the unceasing support, both financial and emotional, given by my parents. My thanks go to them, and also to my sister Elizabeth and to Jonathan, for their constant encouragement and patience.

ABSTRACT

Surfactants from the `Triton' range, manufactured by Rohm and Haas, Germany, were used to study the adsorptive behaviour of non-ionic surfactants (of the alkyl polyoxyethylene type) from aqueous solution onto mineral oxide surfaces. The oligomeric distributions of the surfactants were characterised using the HPLC technique. Two gradients were used: a normal phase gradient was used to study the surfactants from non-aqueous solution; an unusual gradient, which could not be definitively categorised as either normal or reversed phase and which was developed at Brunel, was used to analyse surfactants directly from aqueous solution.

Quartz was used as a model mineral oxide surface. The quartz surface was characterised using a range of techniques: scanning electron microscopy (SEM), X-ray photoelectron spectroscopy, X-ray fluorescence analysis, Fourier transform-infra red spectroscopy and BET analysis. It was found that washing the quartz with concentrated HCl removed any calcium ions present on the surface and also removed O^{2-} ions. Calcining the sample removed carbonaceous materials from the surface and also caused a decrease in the surface area. The quartz was shown to be non-porous by SEM and BET analysis.

The adsorption experiments for this study were carried out using a simple tumbling method for which known ratios of surfactant in aqueous solution and quartz silica were mixed together for a known length of time. The amounts of surfactant present were measured using ultra-violet analysis and the HPLC techniques mentioned above. It was found that the smallest oligomers were adsorbed the most. An addition of salt to the system caused an overall increase in adsorption of the bulk surfactant, and increase in temperature caused an initial decrease in adsorbed amounts before the plateau of the isotherm and a final increase in bulk adsorption at the plateau of the isotherm. The oligomeric adsorption generally appeared to mirror the behaviour of the bulk surfactant.

Atomic force microscopy (AFM), dynamic light and neutron scattering studies were used to analyse the character of the adsorbed surfactant layer. It was shown that the layer reached a finite thickness that corresponded to a bilayer of adsorbed surfactant. According to AFM data, this value of thickness was not consistent over the whole of the quartz surface.

CONTENTS

CHAPTER 1: Introduction.

It is the purpose of this chapter to provide a general introduction to oil recovery and surfactant chemistry, and to introduce the point that surfactant behaviour in aqueous solution, important in the oil industry amongst others, determines whether it is environmentally feasible to use certain surfactants in bulk industrial processes and domestic/industrial cleaners.

1.1. Part One: Surfactant Chemistry.

Surfactants are materials which are capable of reducing the surface tension between two phases; they can therefore control surface and interfacial tensions, wettability, dispersion stability and rheology.

Surfactant molecules are amphiphilic, one section being oleophilic and the other being hydrophilic, and this permits their miscibility in both aqueous and non-aqueous systems. The hydrophilic section of the surfactant molecule is known as the *head group* whereas the oleophilic region is known as the *tail*. There are four main categories of surfactant: anionic where the head group is negatively charged; cationic where the head group is positively charged; ampholytic or neutral where the charge on the head group depends upon the pH; and non-ionic where the head group is uncharged. Table 1.1 shows examples of each type of surfactant.

Despite the structural differences mentioned above, all of the surfactant types have a similar property in that at a certain critical concentration there is a formation of aggregates of surfactant molecules, these aggregates are known as micelles. The critical concentration at which micelles form is known as the CMC and this can be determined with relative ease as micelle formation strongly affects the physical properties of surfactants. Surface tension, electrical conductivity and light scattering all show a sharp change when plotted as a function of concentration of surfactant in solution (see Figure 1.1). These breaks all occur at roughly the CMC when plotted versus concentration, ln concentration and $(\text{concentration})^{0.5}$ - different concentration functions are used as the break in the property is then easier to discern.

Table 1.1: Examples of Surfactants.

Type of Surfactant	Example	Head Group
ANIONIC: R_nOSO_3Na	Sodium dodecyl sulphate.	OSO_3^-
CATIONIC: R_nNR_3Br	Decyltrimethyl ammonium bromide	N^+Me_3
AMPHOLYTIC: $R_nN^+(H_2)COO^-$	Alkyl betaines	$NHCOO^-$
NONIONIC: $R_nO(CH_2CH_2O)_nOH$	Polyethene oxides	$(CH_2CH_2O)_nOH$

The behaviour of surfactants in solution can be explained by the two moieties of the molecule attempting to separate out into distinct phases hence minimising the area of contact between them.

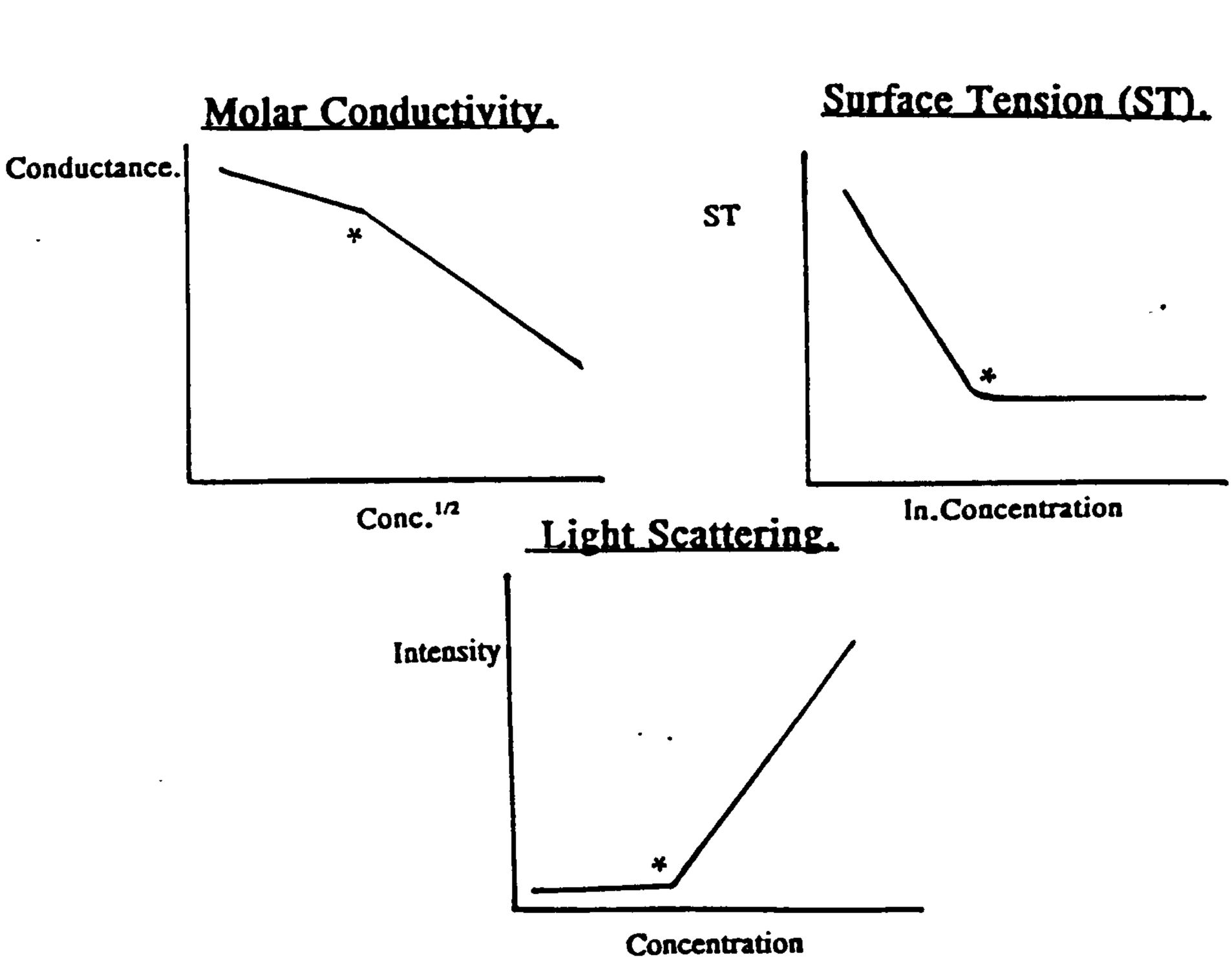

Figure 1.1: The Effects of the CMC (denoted by *) on the Physical Properties of Surfactants in Aqueous Solution.

Factors Affecting the CMC of Surfactants.

i) Hydrophobic Group. In aqueous solution, the larger the tail of a surfactant molecule the lower the CMC. This property of surfactants is predictable because the larger the hydrophobic moiety of a molecule the greater the need to separate from the aqueous phase. The decrease is greater for branched hydrophobic chains. As the chain length increases, the CMC also decreases until beyond C_{18}, the CMC remains unchangeable.

ii) Hydrophilic Group. In aqueous solution, ionic surfactants have higher values for their CMC than non-ionics with the same tail. The more ionic parts a surfactant has, the larger the CMC. For surfactants containing ethene oxide groups, the CMC decreases with the number of ethene oxide units present since this incurs hydrophobicity to the molecule.

iii) Electrolytes. In aqueous solution, the presence of an electrolyte decreases the CMC; this effect is stronger for anionics than non-ionics. In anionic surfactants this effect is due to the decrease in repulsion between the charged head groups in the micelle. For non-ionics, the reduction in CMC is due to the "salting out" of the head group.

iv) Organic Solvents. Small amounts of solvents, present as impurities or as by-products of the manufacturing process, may alter the CMC. Polar organic molecules cause a decrease in the CMC, particularly short chain molecules which are easily incorporated into the micelle. Larger molecules would be held in the outer region of the micelle and this effect helps lessen the repulsion between charged head groups in anionic micelles. The reduction in the CMC is strongest for straight chain solvent molecules and the effect increases with the chain length of the impurity.

v) Temperature. The CMC first reduces with increase in temperature and then increases. These strange effects are due to two opposing forces. A temperature increase causes the dehydration of the head group of the surfactant which in turn induces micellisation. Also, a temperature increase causes a disruption of the water molecules surrounding the tail which discourages micellisation. The resultant of these forces determines whether the CMC increases or decreases.

Micelle Shape.

Since 1913, when McBain first suggested that soaps formed electrically charged aggregates in solution (1), micelles have been well investigated. Initially most of these studies were carried out on anionic species and the micelles were considered to be spherical in shape (2). Later, pioneering studies by McBain using X-ray diffraction showed that micelles of both anionic and non-ionic species formed lamellar type structures which were capable of solubilising hydrocarbons (3-5). During the 1950's, much work was carried out on surface active agents using light scattering and viscometry to measure micellar molecular weights, micelle shape and surface charge (in the case of anionics) (6-12). Values of molecular weights of micelles were determined to be of the order of 30,000 Da and although there was some disagreement between workers, any differences were believed to be due to assumptions made concerning monomer concentrations and micelle size above the CMC during modelling of the surfactant systems (12).

Despite the work of McBain (3-5), the shape of anionic micelles was often assumed to be spherical; with a core of hydrocarbon surrounded by hydrated polar head groups which rose above the surface of the micelle core (7,9,10). The size of the micelles was found to be dependent on the length of the hydrocarbon chain and the state of charge on the head group. Stigter et al (9) proposed that, initially, small spherical micelles were formed which interacted to form larger aggregates in order to increase the number of surfactant molecules incorporated into each micelle.

The micellar structure of non-ionic species was also studied in-depth (13-15) and these molecules produced ellipsoidal shaped micelles the size of which was dictated by the length of the hydrocarbon tail and the size of the head group (13). Again, a growth in micellar molecular weight above the CMC was explained by the association of smaller micellar units producing larger aggregates (16). Attwood (16) predicted a rod-like structure for non-ionic micelles at high surfactant concentrations. Tanford (17) constructed a coherent set of equations which took into account the energetic favourability of transferring an alkyl chain section of a monomer into a micelle core and the opposing forces of head group repulsion. This was done for both anionic and non-ionic surfactants and it was concluded that there was an initial association of small micelles to form disk-like or oblate ellipsoidal shapes which changed structure to form rod-shaped or prolate ellipsoidal micelles (see Figure 1.2). Other studies, which use

the Scaling Laws derived for polymer solutions, also predict this change of micelle structure (18). It is now known that micelle shape plays a key role in controlling properties of the surfactants that are important in many technological applications (19); as a consequence, ways of controlling and modifying micellar shape are being developed (20).

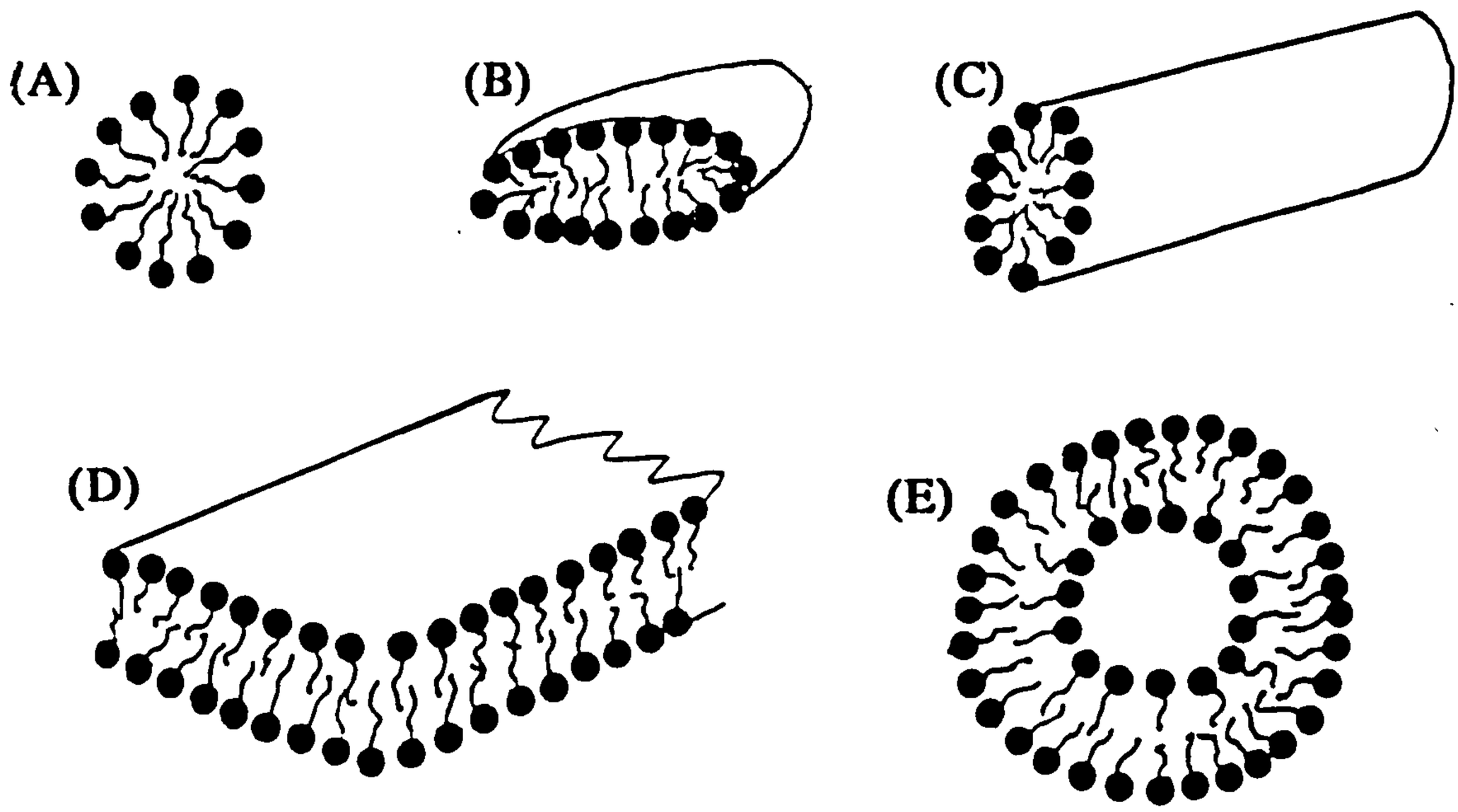

Figure 1.2: Examples of the Structures of Micelles.

[(A) most simple model - spherical, (B) oblate (disk-like) structure, (C) cylindrical (rod-like) structure, (D) lamellar structure, (E) spherical vesicle]

1.2 Uses of Surfactants.

Commercially, surfactants are extremely important materials and have many applications: use as detergents in washing powders and liquids, in the paint industry where they are used as stabilisers, as solubilisers in biological systems, as flocculants in the water industry, as emulsifiers for agricultural chemicals and during EOR. van Os et al (21) provide an extremely comprehensive guide to the applications of non-ionic surfactants. Almost all of these applications are controlled by surfactant adsorption at a surface, be it a rock surface, a liquid/solid interface or that of a colloidal particle.

It is extremely difficult to obtain a precise figure for amounts of surfactant produced

for industrial and household use from the literature. Although the general trend seems to be that surfactant production has risen steadily over the past decade. One survey carried out in 1990 estimated that the worldwide surfactant production was approximately 840,000 tonnes, whereas approximately 750,000 tonnes were produced in 1985 (22). It is thought that the amounts of non-ionic surfactants produced for industrial and domestic use is in the region of 300,000 tonnes in the UK (23) and between 300,000 and 360,000 tonnes in the USA (24,25).

1.3. Colloidal Stability and Surfactant Adsorption.

Forces between Particles.

Two types of forces govern when two similar particles approach each other in a liquid medium: attractive (van der Waals') and repulsive (electrostatic). A solid particle in a colloidal solution may become electrically charged through a number of causes:

i) ionisation of surface groups such as -COOH at a certain pH,

ii) isomorphous substitution, e.g., Al replaces Si in the surface layer of clay,

iii) specific adsorption of one type of ion from solution, or

iv) differential ionic solution, ie, in AgI, Ag dissolves preferentially leaving a negatively charged surface.

An 'atmosphere' of charged ions, carrying opposite charge to the colloidal particle, develops around the spherical particle as the system attempts to maintain electrical stability; this neutralising region is referred to as the *diffuse electrical double layer* (see Figure 1.3). The charge on the particle is distributed over its surface and is balanced by the charge in the double layer. The thickness of the double layer decreases with an increase in the electrolyte concentration. Figure 1.3 is a simple version of the double layer; thermal motion causes the ions to be spread out in space and thus they form a *diffuse* double layer.

The stability of such colloidal systems can be controlled by the addition of electrolyte, surfactants and or polymers. When two particles approach one another and their double layers overlap, there is an osmotic pressure build-up, due to the high concentration of ions between the particles, which causes the solvent to move into the overlap region. This results in particle repulsion and is known as 'electrostatic repulsion'. On compression of the double layer by further electrolyte addition the electrostatic repulsion may be reduced.

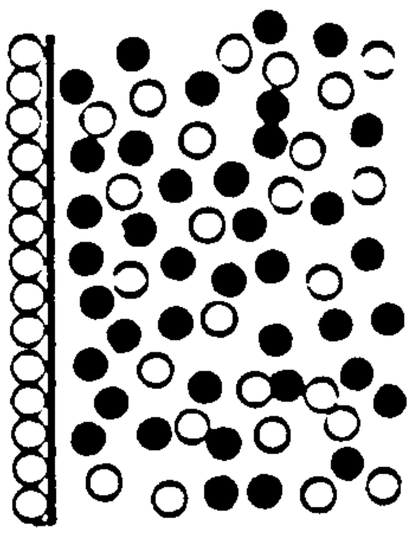

Figure 1.3: The Electrical Double Layer.

(The filled-in circles represent particles of opposite charge to the empty circles)

"Steric repulsion" is caused by the adsorption of surfactants or polymers onto the surface of a particle. There are two components of steric repulsion: (i) if close-packed adsorbed layers of surfactant/polymer on separate particles approach each other, the groups are unable to inter-penetrate resulting in steric repulsion, and (ii) if the layers and solvent are 'like' then the tails and loops will interpenetrate and cause an increase in the osmotic pressure, which results in the solvent diffusing to the region between the particles and repulsion occurs. Figure 1.4 below shows the combined energy of *electrostatic and dispersive forces* in a colloidal system:

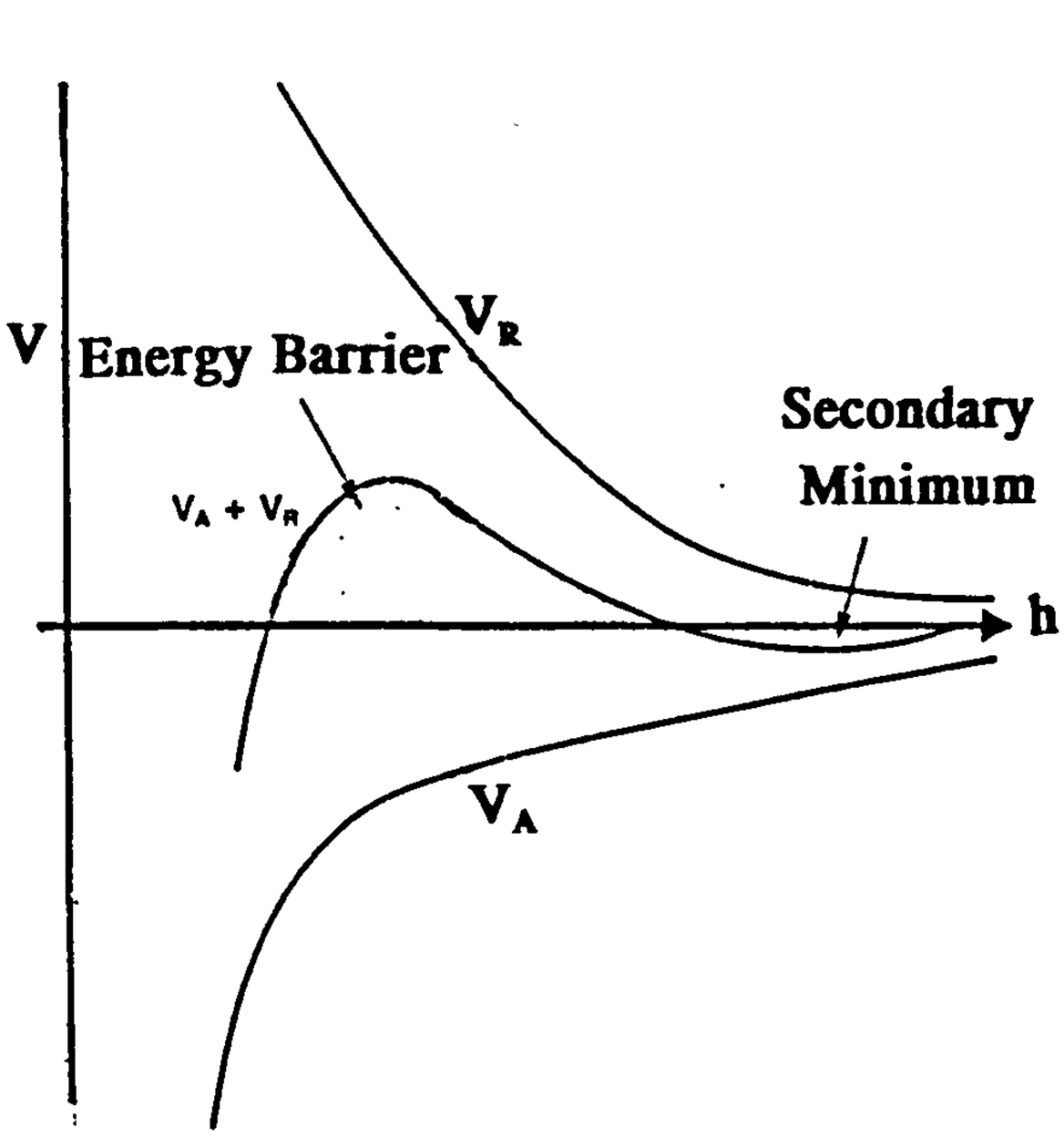

Figure 1.4: Energy Paths of Colloidal Particles due to Electrostatic Forces as the Interparticle Separation (h) is Varied.

(V_R denotes repulsive potential and V_A denotes attractive potential).

For smaller particles, an increase in ionic surfactant addition would increase the repulsive energy barrier and so promote colloidal stability. Larger particles are more

problematic in that they have a tendency to settle at the bottom or top of the container under gravity. In these cases, the energy minimum is exploited by increasing electrolyte concentration which enables the large particles to be held together in a 'loose floc'. Figure 1.5 shows the combined energy profile of *steric and dispersive forces*:

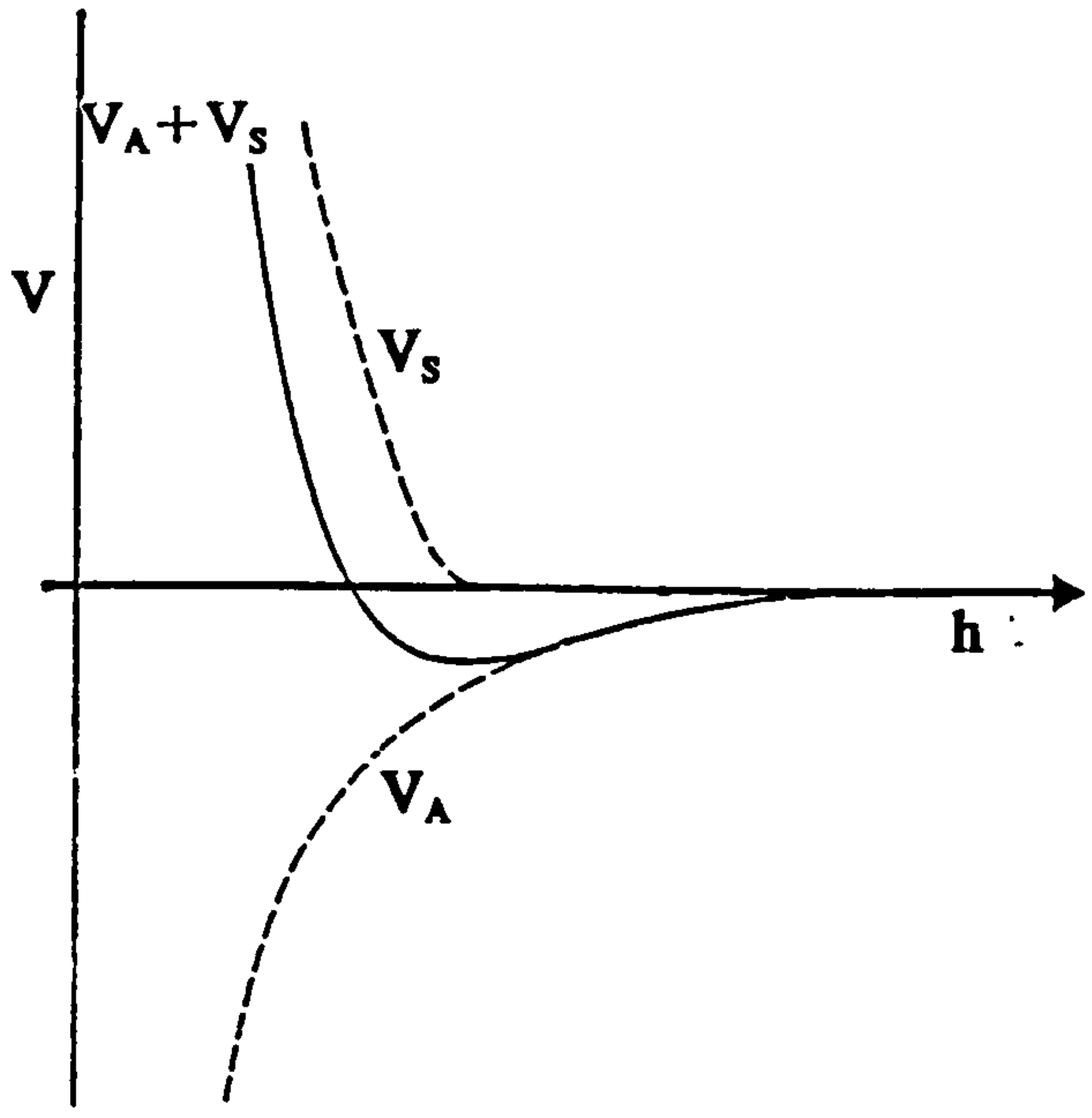

Figure 1.5: Energy Path of Colloidal Particles due to Steric Forces as a Function of h.

(V_A denotes attractive potential; V_S denotes the steric repulsive potential).

Non-ionic surfactants are capable of providing steric repulsions to colloidal particles, especially effective surfactants are block copolymer surfactants such as: poly(oxyethylene)-poly(oxypropylene)-poly(oxyethylene) or EO-PO-EO. These surfactants provide steric repulsion on hydrophobic surfaces via adsorption of the PO group and the EO groups forming a steric barrier. The depth of the minimum on the energy profile is related to the length of the EO section of the molecule. These effects are of great importance in products such as paints.

Examples of Other Applications:

Froth Flotation. Minerals and ores such as those of copper, nickel, zinc and lead are obtained from natural resources in the form of mixtures. To release the mineral desired the mixtures are often ground and separated by sieving. This is a difficult process which can be made easier by froth flotation. The ground ore is added to water

with 'frothers' and air is then blown into the suspension. Particles then float to the top of the vessel and are separated. The addition of 'collectors' ensure the selectivity of a particular mineral.

Detergency. There are two mechanisms of cleaning. (1) Oily soils are removed from clothing or other surfaces by 'roll-up'. Surfactant adsorption causes a decrease in the contact angle of the soil with the solid, the oil is therefore easily removed by a gentle agitation. (2) The adsorption of an anionic surfactant onto particulate dirt pulls the particles into solution and stabilises them. Re-deposition of the particles back onto the solid is hindered by anionic surfactants and co-polymers.

Corrosion Inhibition. Iron and steel constructions are prone to rust and corrosion particularly from water and brine. The adsorption of surfactants onto the metal surface provides an hydrophobic barrier to the water and brine solutions.

Bridging Flocculation. In colloidal solutions, the addition of low concentrations of high molecular weight polymers can cause flocculation of the system. Segments at remote areas on the same molecule may become connected to differing particles and so draw these particles together. This phenomenon is exploited in water treatment where addition of a few ppm of polyacrylamide cause flocculation of any particulate matter in solution.

Solubilisation. Non-ionic surfactants are used to solubilise oils present in pesticide formulations and also in products such as air fresheners. Anionic surfactants are used to keep these formulations stable and prevent phase separation.

1.4 Non-ionic Surfactants.

Octyl phenyl polyethoxylates have long held a prominent position in the field of non-ionic surfactants (26). Their structure is shown below:

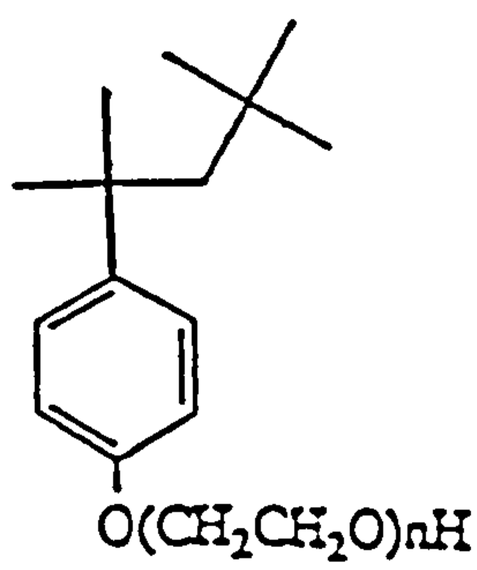

The molecules are taken to be homogeneous in terms of the R group section of the molecule. The polyethoxylate head group appears to have a Poisson distribution number of ethoxylate groups in the molecule, the average number for Triton X-100 being 9-10 (according to the manufacturer, Rohm and Haas), as shown. Other members of the Triton *family* include

TX-114 where n=7

TX-165 where n=16

TX-305 where n=30 (the values of n are averages).

TX-100 is produced by the reaction of octylphenol with ethylene oxide.

$$C_8H_{17}\text{-}(C_6H_4)\text{-}OH + n\text{-}CH_2CH_2\overset{\diagdown O \diagup}{} \rightarrow C_8H_{17}\text{-}(C_6H_4)\text{-}O(CH_2CH_2O)_nH$$

The reaction occurs via a stepwise polymerization of the -OH group of the octylphenol; of course, only an average length of chain can be achieved from this process as shorter and longer ethene oxide chains will be produced also (the assumption that the distribution of length of ethene oxide chains is a Poisson distribution must be proved mathematically from results gained by HPLC [see page 40]). The octylphenol used in the process is itself a technical product manufactured by the petroleum industry from dimerized isobutylene and phenol (27).

The Poisson distribution is an approximation of the well documented binomial distribution (28). The binomial distribution is the most important example of a *discrete* distribution, that is, a distribution used to fit a set of data which are classified in two groups (e.g., where each sample member is to be judged by some yes or no basis such as 'hit' or 'miss'). The binomial distribution is defined as

$$P_n(x) = C^n_x p^x q^{n-x} \ (x=0,1,2,3,.....,n),$$

where $P_n(x)$ = probability of getting exactly x hits in n trials,

C^n_x = number of combinations of n things taken x at a time

= $n!/x!(n-x)!$ [where $0!=1$],

p = the probability of a random item being a 'hit',

q = the probability of a random item being a 'miss' [i.e., $p+q=1$].

The mean of x in n trials is μ (=np).

The Poisson distribution is used as an approximation to the binomial distribution when n is large and p is small, and is defined as

$P(X) = m^x e^{-m} / x!$ (x=0,1,2,.....)

where m = np of the approximated binomial distribution = μ = the mean of the Poisson distribution.

The Poisson distribution can be used in its own right; it was used as an important piece of statistical investigation during the Second World War in 1944 to test the randomness of bombings carried out on London by the then newly invented V1 rocket, or doodlebugs (29). The conditions necessary for application of the Poisson distribution are as follows:-

- the mean of the distribution must be known,
- p is small and n is large,
- the mean remains constant as n is large,
- the occurrence of the event must be purely at random.

<u>Application of the Poisson Distribution to the Homologues of TX-100.</u>

The mean of the distribution was calculated to be 9.099; the statistical probabilities and Poisson probabilities were calculated (m for the Poisson calculation was taken to be 9.099). Table 1.2 shows the results; comparison of the statistical probabilities with the Poisson probabilities shows that the two values correspond well thus confirming that the ethene oxide chain length distribution in the bulk surfactant does indeed have a Poisson distribution.

The first studies on Triton X-100 were carried out during the late 1940's (5) using X-ray diffraction and these concluded that the molecules did not produce a lamellar type micelle structure as had been discovered for anionic species and other non-ionic species. In the 1950's the micelles were considered to be spherical in shape and highly hydrated with approximately 150 monomers per micelle (29). During the 1970's, Robson and Dennis (30) described the size, shape and hydration of micelles by following theoretical considerations based on viscometry measurements. They

proposed an oblate ellipsoidal micellar shape, as was agreed for other surfactants (17), although they proposed that, in fact, the micelle had an almost spherical appearance due to the non-uniform distribution of ethoxylate chain lengths around the micelle core.

This work was inspirational to many groups and knowledge of the Triton X-100 molecule has certainly increased a great deal since the beginning of the 1980's. Paradies (31) and Brown et al (32) have produced comprehensive descriptions of the Triton X-100 micelle as having an oblate ellipsoidal structure with a radius of gyration of approximately 5nm when completely hydrated, and an aggregation number of 150. The external surface of the micelle is described as being *highly* convoluted, complex and hydrated. These micelles are thought to aggregate at high concentrations, although few studies of this surfactant have been made at concentrations high above the CMC. Some groups still use the spherical model when carrying out studies on TX-100 (33).

1.5. Environmental Concerns Relating to Surfactants.

Virtually all used surfactants are discharged into sewage systems and from there into river systems, and as surfactants are used in such large quantities both industrially and domestically there is a need to increase awareness about their behaviour in the natural environment (34,35). It has been estimated (see page 6) that of the 300,000 tonnes of non-ionic surfactants produced in the UK, 60% are discharged in waste-water (23). In the past, the levels of surfactant-induced foam in rivers led to the abolition of branched alkylbenzenesulphonates (ABS), which were replaced by linear alkylbenzenesulphonates (LAS) surfactants, which are readily biodegraded in comparison to (ABS) (36). More recently, the less visible effects of surfactants upon the environment are recognised as being increasingly problematic.

The primary treatment of sewage involves sedimentation, and this can be interrupted by the presence of surfactants in the waste. The surfactants emulsify any oils and greases present thus reducing their removal as scum from the sedimentation tanks. The secondary stage of sewage treatment involves air being bubbled through the dilute sewage to allow aerobic degradation of the organic content. Again if surfactants are present foaming can occur which reduces oxygen transfer within the system.

Table 1.2: Analysis of the Distribution of Ethene Oxide Chain Lengths within Bulk TX-100.

Ethene oxide chain length	Occurrences of chain length in bulk surfactant (taken as intensity of HPLC peak)	Probability of particular chain length being present in the bulk surfactant	Poisson probability of chain length occurring in the bulk surfactant
1	1	0.0014	0.0010
2	3	0.0042	0.0046
3	9.5	0.0130	0.0140
4	24	0.0330	0.0320
5	40	0.0640	0.0580
6	66	0.0920	0.0880
7	83	0.1150	0.1150
8	93	0.1290	0.1300
9	90	0.1250	0.1320
10	79.5	0.1100	0.1200
11	67	0.0930	0.0990
12	53	0.0740	0.0750
13	40	0.0560	0.0530
14	29	0.0400	0.0340
15	18	0.0250	0.0210
16	11	0.0150	0.0120
17	7	0.0097	0.0063

In the natural environment, surfactants continue to retard oxygen uptake by gathering at the air-water interface. Aquatic life is therefore dependent on the surfactant content of the water in which they live.

The structure of TX-100 and a closely related surfactant based on a precursor of nonyl phenol have low biodegradability in aqueous systems due to the branched oleophilic regions of the molecules. The nonylphenol is used to produce the commercial surfactant shown below:

$$C_9H_{19}\text{-}(C_6H_4)O\text{-}(CH_2CH_2O)_nH$$

Aerobic attack of these molecules results in a stepwise cleavage of the hydrophilic ethylene oxide chain, leading to shorter ethylene oxide chain lengths and increased hydrophobicity. These reactions reduce the solubility of the surfactants in water and the effects are increased for molecules with branched alkyl groups (36), but remain unaffected by the length of the alkyl chain. The molecules containing the shorter ethoxylate chains have been shown to have low to moderate biodegradability in river water and tend to adsorb onto hydrophobic matter. Large amounts have been found in river sediments and these findings together with comments by and similar to those stated by Giger et al (24) that nonylphenol (NP) and short chain nonylphenolethoxylates (NPEs) are highly toxic to aquatic organisms, have led to NPE's being removed from cleaning products in some countries in Europe (37) and have induced much research to be undertaken in America (38).

Alkyl phenol polyethoxylates, in particular NPEs, have attracted much attention in the light of new research that suggests surfactant intake by humans, via the re-use of water, may be affecting the male reproductive system. Studies (39) of the oestrogenic properties of NPEs along with other river pollutants, following the discovery of "feminised" male fish (i.e. those that produce the female yolk protein found in eggs) in some of Britain's rivers, have been undertaken. Up until very recently, it had not been known exactly what causes this problem although research in the US suggests NPEs are the likely cause (23,40,41). A group at Edinburgh, however, has recently proposed three types of chemical (octylphenols, bisphenol A and butyl benzene phthalate) as definite oestrogen mimicks (42). It is clearly important therefore that research into alkyl phenol polyethoxylates, their adsorptive properties and the manner in which they

behave in solution needs to be fully understood if we are to succeed in minimising the afore-mentioned environmental problem.

1.6. Part Two: The Oil Industry.

Crude Oil.

Petroleum, or crude oil, is principally a complex mixture of hydrocarbons which exist both in a gaseous and liquid state in the natural reservoir, indeed, the Latin origins of the word "petroleum" are "petra" meaning rock and "oleum" meaning oil. The hydrocarbons present within petroleum are of mixed structural forms: alkanes, cycloalkanes, alkenes and heterocyclics. Elemental analysis of petroleum reveals it to be composed of hydrogen and carbon predominantly together with minor elements (such as S,N, and O) and trace quantities of phosphorus and heavy metals (e.g.V and Ni).

Since 1945, products from the petroleum industry have dominated not only the energy market but also the chemical industry. Thus a vast number of end-use chemicals (i.e. cosmetics, detergents, synthetic rubbers, fibres, lubricants, paints and adhesives) can be produced from crude oil (see Table 1.3).

1.7 Distribution of Oil Reservoirs.

Most of the world's oil reserves are situated in areas remote from the main centres of consumption and are in inhospitable environments such as deserts, jungles and beneath the oceans. Many countries produce oil either in large or small amounts (see Table 1.4). There are six main areas where oil is found in large quantities:

North America (US,Canada,Mexico)
Middle East (Saudi Arabia,Iran,Kuwait,Iraq)
Russia
Caribbean (Venezuela,Columbia,Trinidad)
Africa (Libya,Algeria,Nigeria)
Far East (mainly Indonesia)

Table 1.4 shows that the Middle East has a dominant position with regard to the world's oil reserves and production. The greater part of oil produced in the Middle East is exported since these countries need relatively little oil themselves when compared to Europe and America. In the 1960's and 1970's most of the oil used by

Britain and Western Europe came from this region; this left Europe particularly vulnerable to oil prices set by Middle Eastern countries, as shown by the OPEC crises of 1973/1974 and 1979/1980 and more recently during the Gulf War. The vulnerable position of the West has lead to the exploration of oil being extended to rather obscure locations such as in the Atlantic Ocean surrounding the Falkland Islands and even under the grounds which surround Windsor Castle (43). Europe now has considerable oil production in the North Sea. Figure 1.6 shows the price of crude oil since 1861.

Table 1.3: Products from the Oil Industry.

MAIN PRODUCT	GROUP PRODUCTS
GASOLINES	refinery gases industrial gases domestic gases motor spirits chemical feedstocks white spirit
MIDDLE DISTILLATES	kerosine gas oil diesel oil aviation fuels
FUEL OIL	light fuel oil medium fuel oil heavy fuel oil
OTHER PRODUCTS	bitumen lubricants and greases waxes detergents

Apart from a period in the 1950's and 1960's oil prices have fluctuated sharply throughout the years although at present the oil market is calm relative to the tumult of previous years (see Figure 1.6). Such fluctuations have an effect on the economic potential for EOR.

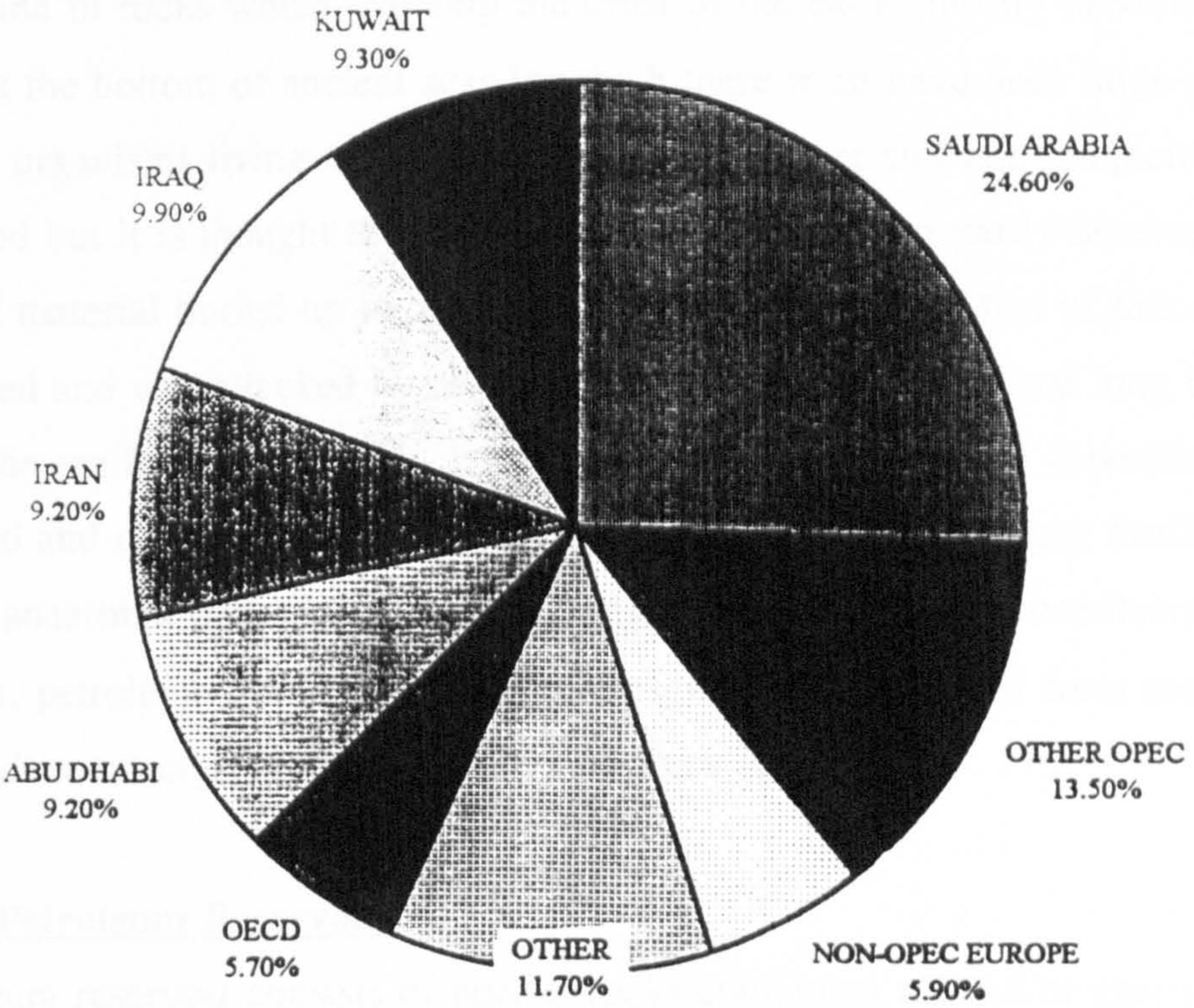

Table 1.4: The Distribution of Oil Reservoirs.

(The estimates contained in this table are those published in [44]).

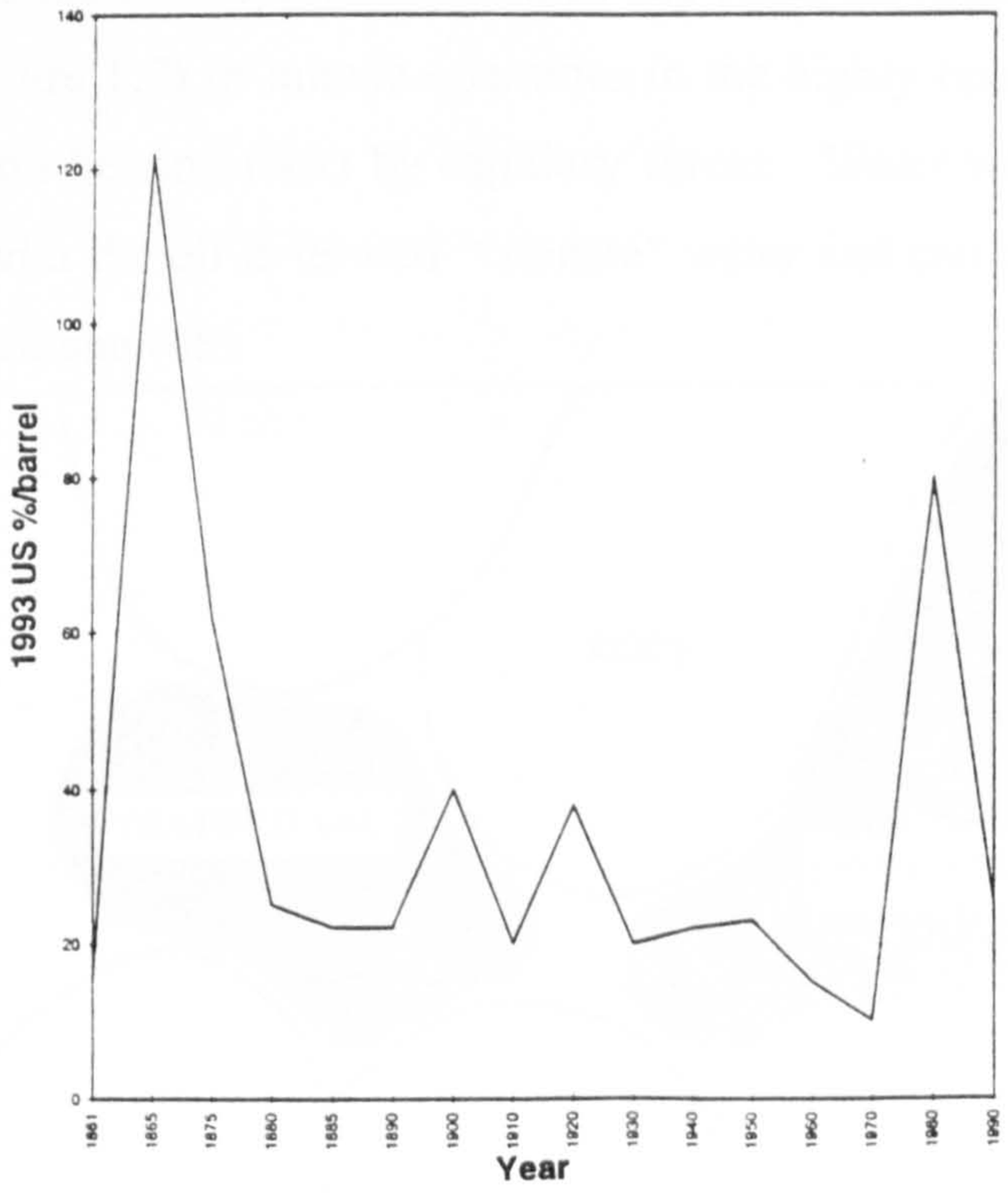

Figure 1.6: The Price of Crude Oil since 1861.

(taken from [44]).

1.8 Oil Formation.

Oil is found in rocks which make up the crust of the earth; mostly in sedimentary rock formed at the bottom of ancient seas in which there must have been large quantities of primitive organisms living. The natural origins of oil are still not completely understood but it is thought that petroleum was formed from partly decomposed animal and plant material buried up to 500 million years ago (45). Most of this organic matter died and was attacked by aerobic bacteria and hence oxidised long before it reached the sea bed. Some of it, however, was buried by rapidly depositing layers of mud, sand and dead sea plants (which reduced the amount of oxygen available), allowing anaerobic transformation from fatty acids to petroleum constituents. In very few cases, petroleum has also been found in igneous rock formed from molten lava which underwent crystallisation millions of years ago.

1.9 The Petroleum Reservoir.

A petroleum reservoir consists of porous rocks containing oil and/or gas; it may occur in sand, shales, limestones, dolomites or quartz. The reservoir oil varies from light gasolines to heavy viscous accumulations. The oil pool is said to be undersaturated if gases are completely dissolved in the oil, but is saturated if gases have separated into a free phase above the oil. Below impervious cap-rock, oil is often trapped as oil-droplets (see Figure 1.7) in minute quantities in the highly complex pore channels (present within oil bearing rock) by capillary forces. Water which is trapped in the pores together with the oil is termed "connate" water and can occupy up to 50% of the reservoir pore volume (46).

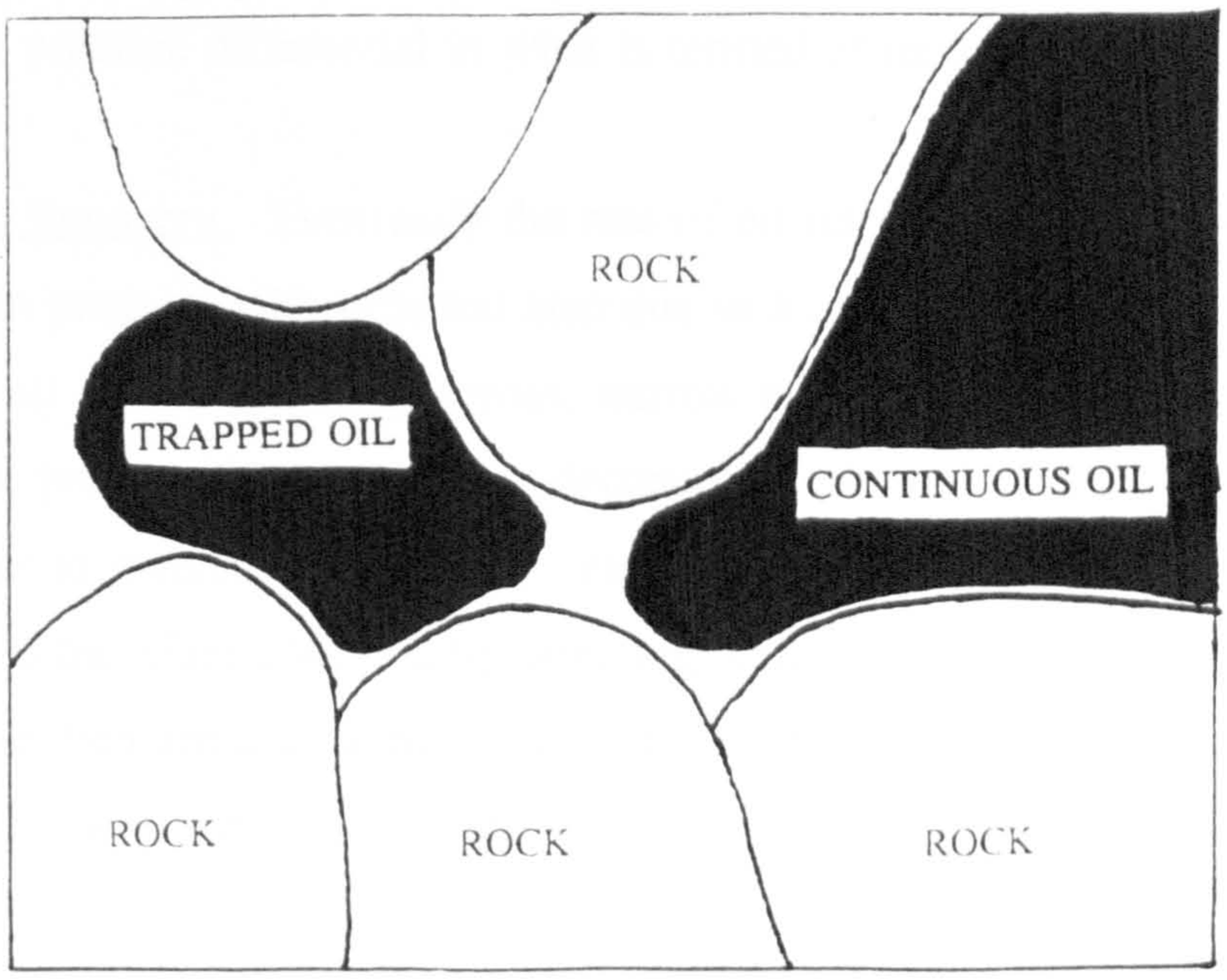

Figure 1.7: The Trapping of Oil in the Reservoir.

1.10 Recovery Mechanisms.

The three main stages to the modern day oil recovery process are shown below:-

PRIMARY (1^0) RECOVERY
natural flow

SECONDARY (2^0) RECOVERY
waterflood
gas injection

TERTIARY (3^0) RECOVERY
miscible gas injection
chemical processes
thermal processes
miscellaneous

The primary (1^0) and secondary (2^0) stages of recovery discussed later utilise conventional methods of oil recovery; these have been used for decades. At the end of secondary recovery almost 65%-70% of the original "oil-in-place" remains in the reservoir (46,47); the remaining oil is therefore the target of the tertiary stage of oil mobilisation.

Primary (1°) Recovery. When the drilling of an oil well initially begins, the pressure at the well head is less than the pressure under which the oil at the bottom of the well exists due to the presence of pressurised gases, and so the oil is forced to the well head by this natural pressure differential in what is termed 1° recovery.

Secondary (2°) Recovery. Eventually the rate of oil release diminishes mainly due to the reduction in pressure with time but also due to a decrease in rock permeability as the remaining oil is held in highly porous, narrow capillaries, and the increase in oil viscosity as the pressure in the reservoir decreases. Additional pressure must be applied in order to maintain productivity; these processes are known as 2° recovery. Additional oil is therefore collected by pumping water into the well. Carbon dioxide and thermal injection are also sometimes used. Thermal methods are used mostly for the recovery of heavy, viscous oils since increasing an oils' temperature decreases its viscosity.

Tertiary (3°) or Enhanced Oil Recovery. The remaining oil is trapped in highly porous areas of rock and is the target of the third stage of oil recovery: **tertiary or enhanced oil recovery (EOR).** This recognises that the oil is trapped due to two main effects:

1)Macroscopic Effects. The oil residue is left in reservoir areas which have not been swept by displacing fluid. During the 1° and 2° processes the injected water or gases travel along high permeability layers in the rock in preference to the alternative path of complex pore networks thereby *missing* large amounts of the trapped oil.

2)Microscopic Effects. The oil is trapped in the rock pores in the form of discontinuous ganglia which are completely surrounded by water; these are difficult to mobilise in a simple pressure drive flow since very large pressure gradients are needed to overcome the restraining capillary pressure.

Relevant EOR methods include thermally- and chemically-based processes along with more unique and adventurous methods (48-50).

EOR may be classified by four major categories.

(a) thermal processes include:
steam injection
steam flooding
hot waterflood
in-situ combustion or fire flooding.

(b) Miscible displacement include:
miscible hydrocarbon process
enriched gas process
carbon dioxide injection
nitrogen injection.

(c) Miscellaneous processes include:
genetic / microbial engineering
mining techniques
foam flooding.

(d) Chemical processes include:
polymer flooding
caustic flooding
surfactant flooding

Each process usually fits either a specific set of reservoir conditions or a specific oil type. Despite these limitations most reservoirs have processes which are already mastered and which therefore enable oil to be recovered more efficiently.

Thermal Processes.

Steam flooding is one of the processes most frequently applied to EOR. It requires steam to be injected into an oil reservoir. This condenses, supplying heat to the rock and fluid in the reservoir and so induces thermal expansion of the oil and a decrease in the oil's viscosity (51). There are certain limitations to steam flooding regarding reservoir depth and type of oil in the reservoir (46,52); although fuel for steam generation and the removal of pollutants from the flue gases is expensive, steam flooding is still one of the most economical EOR methods. Hot water methods seem to be less efficient at transferring energy to the oil within the reservoir. **In-situ combustion** is used for heavy oil mobilisation and involves the burning of oil. The hot gases formed push the "thinned oil" (where the oil thinning is caused by the heat from combustion) towards the well-head. The combustion needs oxygen provided at high pressure and this requires stringent safety regulations, which in turn involve high costs, to avoid explosive conditions being produced. The combustion products in the form of CO_2, NO_x and unused oxygen are difficult to handle and require expensive instrumentation. **Forward** and **backward** combustion are variations of this approach. **Forward combustion** means that the combustion zone is initiated at one well, by oxygen injection, and oil production occurs at nearby producing wells. **Backward (or reverse) combustion** means that the combustion zone is set up as forward combustion but the oxygen is injected at adjacent wells; very few fields have been tested for this EOR process.

Miscible flood processes.

These are based on an understanding of the interfacial tension forces between the injected species and the oil. During this process a slug of solvent (e.g. condensed hydrocarbon gases, CO_2, inert gases and certain alcohols) that is miscible with oil in the reservoir is injected into the well. **The miscible slug process** requires a hydrocarbon liquid, usually propane, to be injected into the reservoir followed by gas injection to drive the slug through the reservoir to the well head. The pressure must be high to maintain miscibility of the slug, and so this process is applicable to reservoirs at depths of 610m-760m (52). **The enriched gas process** uses the principle that the natural gas floods mentioned above can be especially effective when enriched with light hydrocarbons. The injection is sometimes driven through the reservoir by a dry gas or a mixture of gas and water.

An injection of nitrogen and some flue gases is often used as a replacement for hydrocarbon slugs as they become miscible with light crude oils at high reservoir pressures. Nitrogen is relatively accessible anywhere in the world (but is expensive to separate from O_2 in air) and therefore can be used in hostile environments where other injection fluids would not be available. Its' disadvantage is that the inert gases lower the calorific value of gases produced. Combustion products also contain moisture, CO_2 and NO which render them corrosive at high pressures (52). **Carbon dioxide injection** (53,54) involves oil being saturated with carbon dioxide. When the injected carbon dioxide is above the critical pressure of carbon dioxide, there is an increase in the volume of the oil, a lowering of its viscosity and, under correct conditions, a single phase mixture of oil and carbon dioxide is formed (52,55). Carbon dioxide flooding may also be carried out either as a miscible or immiscible process by simultaneous injection of carbon dioxide and water or alternating slugs of carbon dioxide and water (56). Carbon dioxide is advantageous due to its low cost and its availability in large amounts from the natural deposits which tend to occur near to oil and gas producing areas. Problems with this approach include the corrosive properties of carbon dioxide/water mixtures due to formation of HCOOH and the very low viscosity of the carbon dioxide/oil mixtures which leads to "fingering", or areas of carbon dioxide-rich oil being produced (57). In-depth tests on CO_2 injection have been carried out (52,53).

<u>Miscellaneous.</u>

Microbial processes involve the injection of bacteria, which are capable of making surfactants or carbon dioxide, into the reservoir in order for them to react with the oil under the anaerobic conditions of the reservoir. It is hoped to develop suitable bacterial species that could survive the high temperatures of deep wells, although none have yet been identified (46). **Mining techniques** involve boring tunnels above or below the reservoir. Tunnels above the oil provide a useful means by which to apply thermal energy or detergent solutions to the reservoir; those below the reservoir may be used as cavities for holding oil driven down by gravity (58,59). **Foam processes.** Gases have extremely low viscosities and hence high mobilities. If surfactants are injected along with these gases a foam is produced. The foam permits improved efficiency of both horizontal and vertical sweeps due to the relatively low mobility of the foam when compared to gas alone (45,60). The main disadvantage of this method is the short life time that the foam has in the presence of oil and also, as previously mentioned, surfactants can be extensively adsorbed onto rock surfaces thus diminishing

their efficiency. **Water-alternating-gas (WAG) processes.** These processes mimic the mobility effects of foam injection, the difference being that water and gases are injected in slugs alternatively. These systems are extremely complex and are yet to be understood fully (46).

Chemical Processes.

Polymer flooding is used to increase the viscosity of the displacing water, thereby rendering the injected water less mobile than the oil. The process leads to the polymer slug acting as a 'piston' and increasing sweep efficiencies throughout the reservoir. Problems occur with polymer adsorption or entrapment and polymer degradation at the high reservoir temperatures (but pH and/or salinity may also be important) these phenomena all add to polymer flooding being relatively ineffective during EOR (46,52). **Caustic flooding.** Oil recovery from waterflooding is increased when alkali is added to the water. This phenomenon was not understood in the early 1980's (51), but it is now appreciated that the alkali is in fact reacting with any organic acids present in the reservoir oil to form a surfactant which reduces the interfacial tension between the oil and water via an extremely complex set of reactions. The effects of adding an alkali solution are diminished if divalent cations are present. In sea water these are unavoidable (46). Caustic flooding also has no effect if there are no organic acids present in the oil originally. There is some recent research which has studied the effects of adding small amounts of surfactant in the form of alcohol ethoxy sulphates to the alkali solutions (61); these mixtures were capable of reducing the interfacial tension of oil for a larger length of time than if alkali alone was used. **Surfactant flooding** aims to lower the oil-water interfacial tension using surfactants. Decreasing interfacial tension at the oil-water interface reduces the resistance of ganglia to deform and therefore increases the likelihood of their travelling through the pore necks within the rock. The approximate interfacial tension (IFT) between the crude oil and brine is 20-30 mN/m; using surfactant/polymer blends this value can be lowered to 0.1-1.0 μN/m (47,62). After initial injection of the surfactant (which may well be oil-derived [see page 10]), a mixture of a suitable alcohol and a polymer-water slug, which forms a microemulsion, is added to push the detergent and oil towards the well-head (see Figure 1.8).

An emulsion consists, most commonly, of either a dispersion of fine oil droplets in an aqueous medium (an oil-in-water emulsion), or of a dispersion of aqueous droplets in

Initial injection of a surfactant slug causes the oil ganglia to deform.

SURFACTANT SLUG

OIL GANGLIA

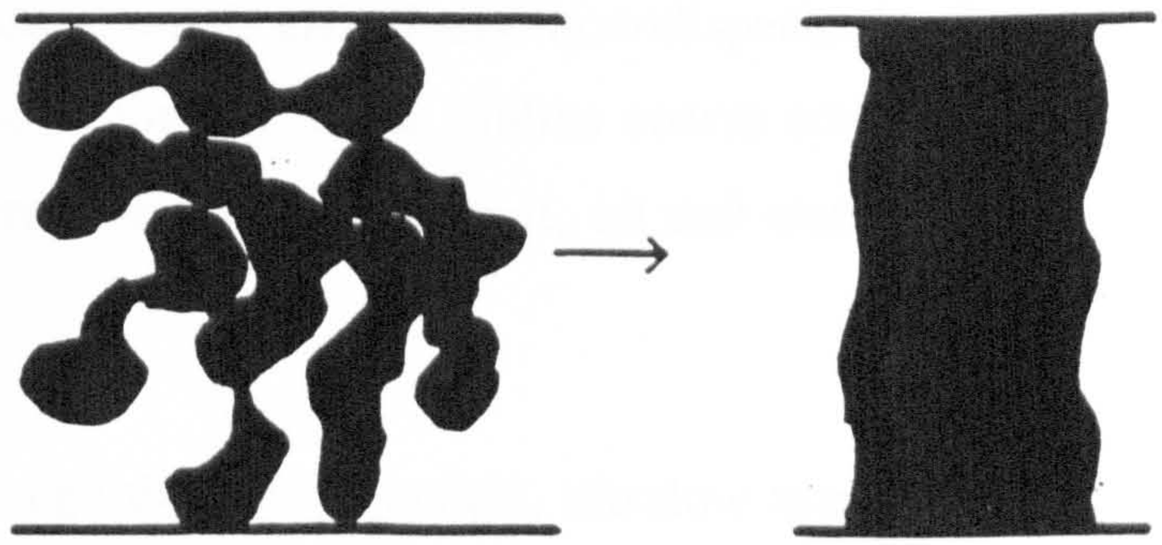

The ganglia form a `bank' of oil.

SURFACTANT SLUG

OIL BANK

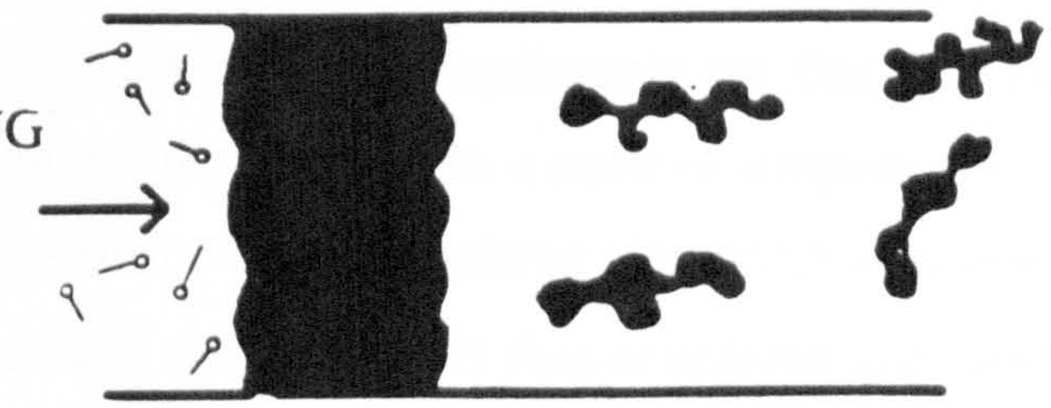

A mixture of alcohol and a polymer-water slug is then added in order that a microemulsion is formed, and thus ultra-low interfacial tensions are reached between the oil and brine.
The mixture is then pushed towards the well-head.

ALCOHOL/POLYMER/BRINE BLEND

OIL

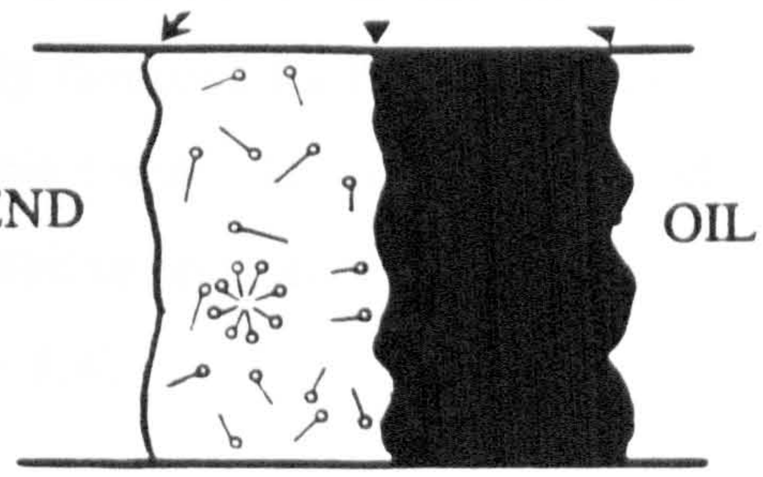

Figure 1.8. Oil Recovery by Surfactant Flooding.

oil (water-in-oil emulsion). The type of emulsion formed depends on the ratio of the amounts of the two phases (63). The droplets formed are considered to be "swollen" micelles having a lamellar structure. Those emulsions in which the interfacial tension between the two phases falls to < 1 μN/m form spontaneously. These clear emulsions are known as microemulsions and produce small, effectively monodisperse droplets which can scatter light and are thermodynamically stable, unlike coarse emulsions. In order to form microemulsions a mixture of alcohol, surfactant, oil and water in the correct ratio is needed.

For a microemulsion mix to travel through the pore channels, ultralow interfacial tensions must be achieved at the tail end of the oil bank. If this does not occur oil would be lost due to entrapment. Many groups have worked on this problem (62,64) and many surfactant systems have been designed using derivatised surfactants and surfactant blends, and have been found to be extremely effective in reaching the required interfacial tensions (65-67). Field tests, however, are often fraught with difficulties and disappointments. The disadvantages of surfactants are that they are highly temperature-dependent, forming microemulsions in a narrow temperature window only outside of which they de-form. Other problems also occur as a result of surfactant adsorption onto the rock surface with the effect that enormous quantities of chemicals are needed during surfactant flooding. It is recognised that new surfactants or surfactant mixes must be developed to ensure surfactant flooding has a place in future EOR (46).

If surfactant flooding is to remain a viable method for EOR then suitable replacements will be needed for the alkylphenols currently favoured by the oil industry as the basic surfactant for microemulsion flooding. These chemicals are currently under investigation due to their lack of biodegradability and hence their derogatory effects on marine and fresh-water wildlife (see section 1.4).

1.11 The Concerns of EOR.

Health and Safety.

Most oil companies provide protection for their workers through (often self-imposed) regulations for health and safety beyond the highly stringent legal requirements of the United States and Europe (68,69).

The dominant environmental elements that present the greatest risk to humans working in the oil industry are drilling-mud materials, additives, noise and the products of the catalytic cracking process during refining of the crude stock. Refinery workers are exposed mostly to lighter molecular weight substances which are considered less carcinogenic than the heavier refinery products; also, as the refinery process is carried out in a *closed* environment, inhalation of these products is kept to a minimum. Protective clothing worn by workers decreases the contact of substances, which cause dermatitis.

Zinc dialkyl dithio phosphates (ZDDPs) and calcium alkyl phenates (CAP's) are two important and widely used groups of oil additives. Due to their widespread usage they have been extensively tested on animals in the laboratory and have been found to cause eye damage, skin irritation and to effect the reproductive organs of male rabbits (69).

Despite the latter rather macabre findings researchers do not consider ZDDP's or CAP'S to be a risk to workers or the general public due to the large exposure time and amounts of chemical needed to cause any effect; however, workers are protected against dermatitis and eye-damage by protective clothing.

Put briefly, protective clothing, protective ventilation and well-informed workers are all utilized to reduce the risk of harm coming to employees.

Widespread debate concerning the effect of industrial processes on the environment has often dominated government agendas over the last decade or so. Whether short term (e.g. oil or product spills) or long term (e.g. the "greenhouse effect" or the depletion of the ozone layer).

The oil industry is a large, visible target for the governments of the world and the general public alike, and in the late 1980's it came under the scrutiny of governments and environmental pressure groups.

In 1985 the United States Environmental Protection Agency (EPA) introduced the Clean Air and Clean Water Acts both of which require strict performance standards for the reduction of volatile organic compounds and sulphur dioxide emissions from natural gas processing plants and the elimination of any discharge into the oceans (70).

Also, the Hazards and Solid Waste Amendments of 1984 introduced a mandatory ban on landfill disposal of certain chemical wastes which include some petroleum solvents and solvent sludges (71). These alterations in the way oil plants are run and their technology together with the phase-out of leaded petrol have added to cost increases for oil refineries and have forced smaller refineries out of business (71).

In many countries, oil companies are now legally required to publish their emissions so ensuring that they are kept at reasonably low levels. BP gave themselves a target of a 50% reduction in hydrocarbon emissions to air and a 66% reduction in emissions to water by 1997 (72). R&D groups in most major oil companies are developing novel ways to monitor the environment for toxic emissions since stringent emission legislation has been introduced. Shell Research has developed a system which uses optical techniques to measure the concentrations of a wide range of atmospheric pollutants over distances of 0.5km (73). In addition, oyster larvae which are sensitive to pollutants are currently being used to check conditions of water samples taken from sites close to oil production plants (73).

New technology is also being developed that utilizes emissions previously treated as waste. These products usually have further use in either the petroleum industry or the chemical or pharmaceutical industries. For example, the rejuvenation of acetonitrile from acrylonitrile manufacturing means that the acetonitrile produced can be used by the pharmaceutical industry to make synthetic insulin for diabetes sufferers (72). In addition, an ethene cracker situated in Scotland creates greatly reduced quantities of effluent (72).

In 1981, an oil company in Venezuela started research into methods that could be used to make the thick, viscous oil that is characteristic of those regions more useful to industry (i.e. to develop a formulation that would be less viscous in consistency and therefore easier to transport and handle). It was found that a mixture of the bitumen oil, water and non-ionic surfactant in the ratio 68:30:2, respectively, produced an emulsion that had the consistency of black ink, and that was stable in the region 278K - 343K (73). This mixture was tried as a fuel (known as "orimulsion"), which, when it was burned, was found to have several advantages. The soot particles and hydrocarbons burn out completely, thus the ash content on burning is low in comparison to, say, coal; there was also found to be a reduction in the amounts of NO_x

formed because of the low temperature of the flame produced. Work has been done in the past few years to attempt to understand the mechanism of combustion of bitumen/water slurries, and to compare this with other fuels (74).

Environmental protection is an international issue which the oil industry, if the literature is to be believed, is attempting to deal with as efficiently and effectively as time and costs will allow. There are some who feel that, while environmental concern over some parts of the oil industry is justified, at other times it is unreasonable and places unnecessary heavy financial burden on an industry that is already showing symptoms of hard times (71,75).

1.12 Aims of Programme and Purpose of Work.

Surfactant adsorption is highly significant in many sections of industry, from domestic cleaners to oil recovery. One sees that oil-derived surfactants can, if optimised, be used in blends to ease further oil recovery from wells. This optimisation needs to be efficient and "environmentally friendly". It was the purpose of this work to consider polydispersed, non-ionic surfactants, and to elucidate the mechanism of their adsorption onto silica and the nature of the adsorbed layer with variation of surfactant molecular design, salinity, pH and temperature. The work was to include a study of individual oligomeric adsorption and the thickness and density of the adsorbed layer as a whole.

References.

(1) J.W.McBain; Trans.Far.Soc.,9,99-100 (1913) .

(2) R.W.Mattoon;R.S.Steams;W.D.Harkins; J.Chem.Phys,15,209-210 (1947).

(3) J.W.McBain;S.S.Marsden;J.Chem.Phys., 15,211-212 (1947).

(4) E.Gonick;J.W.McBain;J.Am.Chem.Soc.,69,334-336 (1947).

(5) S.S.Marsden;J.W.McBain;J.Phys.Chem.,52,110-130 (1948).

(6) P.Debye;J.Phys.Colloid Chem.,53,1 (1949).

(7) K.J.Mysels; J.Phys.Chem.,58,303-307 (1954).

(8) D.Stigter;K.J.Mysels; J.Phys.Chem.,59,45-54 (1955).

(9) D.Stigter;R.J.Williams;K.J.Mysels;J.Phys.Chem.,59,330-335 (1955).

(10) H.V.Tartar;A.L.Lelong;J.Phys.Chem.,59,115-1190 (1956).

(11) E.W.Anacker;J.Phys.Chem.,62,41-47 (1958).

(12) K.J.Mysels;L.H.Princen;J.Phys.Chem.,63,1699-1700 (1959).

(13) M.J.Schick;S.M.Atlas;F.R.Eirich;J.Phys.Chem.,66,1326-1333 (1962).

(14) J.M.Corkill;J.F.Goodman;T.Walker;Trans.Far.Soc.,63,759-772 (1967).

(15) R.H.Ottewill;C.C.Storer;T.Walker;Trans.Far.Soc.,63,2796-2802 (1967).

(16) D.Attwood;J.Phys.Chem.,72(1),339-345 (1968).

(17) C.Tanford;J.Phys.Chem.,78(24),2469-2479 (1974).

(18) T.Kato;S.Aizai;T.Seimiya;J.Phys.Chem.,94(18),7255-7259 (1990).

(19) P.D.I.Fletcher;Curr.Opin.Colloid Interface Sci.,1(1),101-106 (1996).

(20) R.Zana;T.A.Hatton;Nature,362,228-230 (1993).

(21) N.M.van Os (Ed.); Nonionic Surfactants Organic Chemistry. Marcel Dekker Inc., New York (1998).

(22) D.R.Karsa (Editor); Industrial Applications of Surfactants (special publication No 59), Royal Society of Chemistry, Cambridge (1990).

(23) G.Vines; New Scientist, 147, 22 (1995).

(24) M.Ahel;J.McEvoy;W.Giger; Environmental Pollution, 79,243 (1993).

(25) M.J.Schick; Nonionic Surfactants; Surfactant Science Series, Vol.1, Marcel Dekker Inc., New York (1967).

(26) R.M.Weinheimer;P.T.Varineau; Polyoxyethylene Alkylphenols. In Nonionic Surfactants Organic Chemistry. Marcel Dekker Inc., New York; 30-39 (1998).

(27) L.M.Kushner;W.D.Hubbard;J.Phys.Chem.,58,1163-1167 (1955).

(28) E.L.Bauer; A Statistical Manual for Chemists. Academic Press, New York and London (1971).

(29) E.L.Crow;F.A.Davis;M.W.Maxfield; Statistics Manual. Dover Publications Inc.,

New York (1979).

(30) R.J.Robson;E.A.Dennis;J.Phys.Chem.,81(11),1075-1078 (1977).

(31) H.Hasko Paradies;J.Phys.Chem.,84,599-607 (1980).

(32) W.Brown;R.Rymden;J.van Stam;M.Almgren;G.Svensk;J.Phys.Chem.,93, 2512-2519 (1989).

(33) K.S.Rao;P.S.Goyal;B.A.Dasannacharya;V.K.Kelkar;C.Manohar;S.V.G.Memon, Pramana-J.Physics,37(4),311-319 (1991).

(34) R.Mosler;T.A.Hatton;Curr.Opin.Colloid Interface Sci.,1(4),540-547 (1996).

(35) P.Van der Meeren;W.Verstraete;Curr.Opin,Colloid Interface Sci.,1(5), 624-634 (1996).

(36) L.Kravetz; J.P.Salanitro; P.B.Dorn; K.F.Guin; J.Am.Oil.Chem.Soc., 68,610 (1991).

(37) A.Marcomini;W.Giger;Anal.Chem.,59,1709 (1987).

(38) C.G.Naylor;J.P.Mieuve;W.J.Adams;J.A.Wecks;F.J.Castaldin;L.D.Ogle; R.R.Romano;J.Am.Oil Chem.Soc.,69(7)695-703 (1992).

(39) Chemistry & Industry, page 76 (2/2/1998).

(40) S.Connor;Independent on Sunday (4/9/1994).

(41) S.Connor;Independent on Sunday (4/6/1995).

(42) L.Rogers; The Sunday Times (29/10/1995).

(43) M.Smith; The Independent (4/12/1994).

(44) BP Statistical Review of World Energy, June 1993.

(45) A.F.Fox; "Our Petroleum Industry", B.P. Company Ltd. (1970).

(46) R.A.Dawe; J.Chem.Tech.Biotechnol.,51,361-393 (1991).

(47) D.O.Shah; Annual Symp.EOR and Improved Drilling Tech.(Edit.Linville). 5th Symp.1-11 (1979).

(48) V.A.Kuuskran;G.Stosur; EOR:A Look at Its Technical and Economic Viability,9th Energy Technology Conference,777-792 (1984).

(49) M.Baviere; Basic Concepts in EOR Processes, volume 33; Elsevier (1991).

(50) J.S.Huang;R.Varadaj;Curr.Opin.Colloid Interface Sci.,1(4),535-539 (1996).

(51) E.F.Herbeck;R.C.Heintz;J.R.Hastings; Petroleum Engineer,24-34 (Aug.1976).

(52) R.V.Shankland; Chemtec.,684-688 (Nov.1982).

(53) R.H.Jacoby; In Situ,11(2+3) 145-167 (1987).

(54) E.F.Herbeck;R.C.Heintz;J.R.Hastings; Petroleum Engineer (May 1976).

(55) F.J.Fayers;R.I.Hawes;J.D.Mathews; J.Petroleum Tech.,1617-1627 (Sept.1981)

(56) N.Mungan; J.Canadian Petroleum Tech.,31(9),13-15 (1992).

(57) D.H.Smith; A.C.S. Symposium Series,No.373."Promise and Problems".

(58) B.Williams; Oil Gas Journal; 79(35),17 (1981).

(59) T.H.Maugh; Science, 207(4437)1334 (1980).

(60) J.Ali;R.W.Burley;C.W.Nutt; Ind.Chem.Eng.Res.Des.,63,101-110 (1985).

(61) A.Bhardwaj;S.Hartland; J.Dis.Sci.and Tech.,14(1),87-116 (1993).

(62) K.C.Taylor;L.L.Schramm; Colloids and Surfaces,47,245-253 (1990).

(63) M.Akhtar; PhD Thesis, Brunel University (1997).

(64) K.C.Taylor;B.F.Hawkins; Advances in Chemistry Series,231,263-293 (1992).

(65) D.J.Miller;S.P.Van Halasz;M.Schmidt;A.Holst;G.Pusch;J.Pet.Sci.& Eng.,6, 63-72 (1991).

(66) Y.C.Chiu;H.J.Hwang; Colloids and Surfaces, 28,53-65 (1987).

(67) S.Thomas;S.P.Supon;S.M.F.Ali; J.Can.Pet.Tech.,29(1),22-28 (1990).

(68) "The World of BP," Information published by Employee Communications and Services,BP plc,November 1992.

(69) M.Moody-Stuart; Environmental Action - a shared responsibility; Shell Intern.Pet.Comp.Publication, 1994.

(70) R.K.Hewstone; Regulatory Toxicology & Pharmacology, 5(3),284-293 (1985).

(71) L.E.Modesitt Jr.; J.Pet.Tech., 1113-1118 (1987).

(72) BP Chemicals Ltd.Publication; Health,Safety and the Environment, May 1992.

(73) M.Wade;F.Biffra; Research Communications of Shell Intern.Pet.Comp.Ltd., Shell Research Cloister Press, August 1993.

(74) E.Hampartsoumian;B.Hannud;A.Williams; J.Inst.Energy, 66,13 (1993)

(75) A.D.Koen; Oil and Gas Journal, 90(28),14-17 (1992).

CHAPTER 2: Materials and their Characterisation.

2.1 Surfactant Materials.

The surfactants used were members of the 'Triton' series of surfactants and were purchased from Rohm and Haas. Their basic structure is shown below:

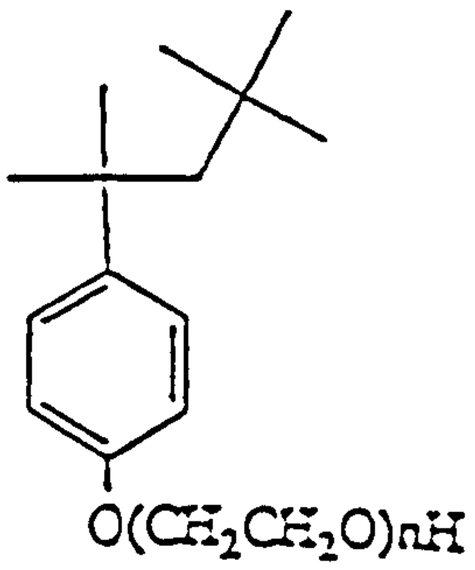

Triton X-114 n=7-8
Triton X-100 n=9-10
Triton X-165 n=16
Triton X-305 n=30

A monodisperse oligomer was synthesised via a three stage reaction sequence using chloroethoxy ethane and hexaethylene glycol (1). The sequence is shown below:

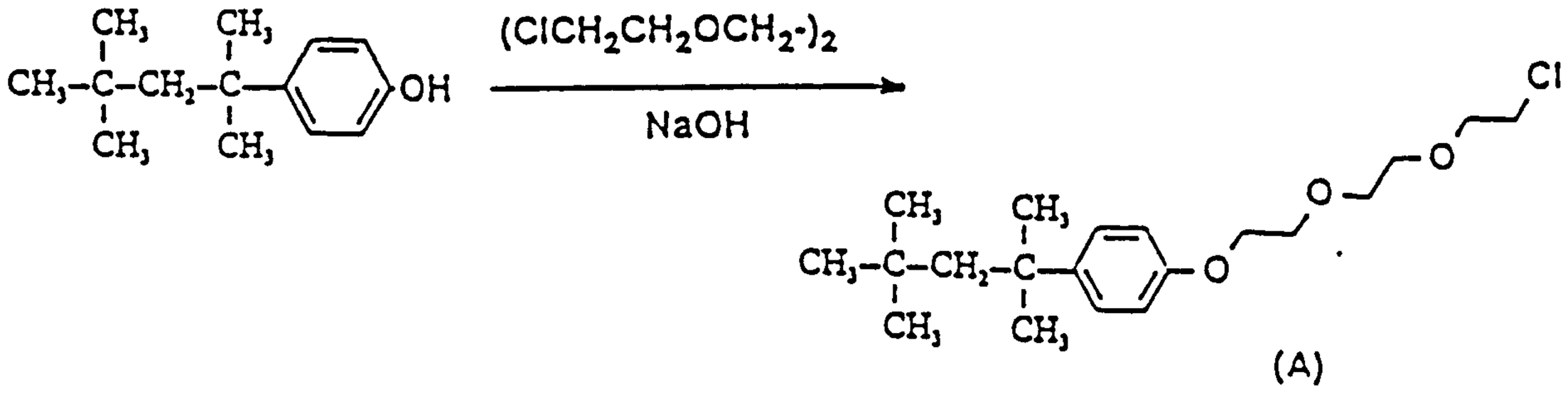

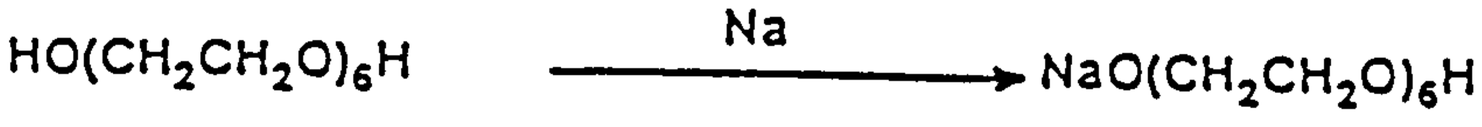

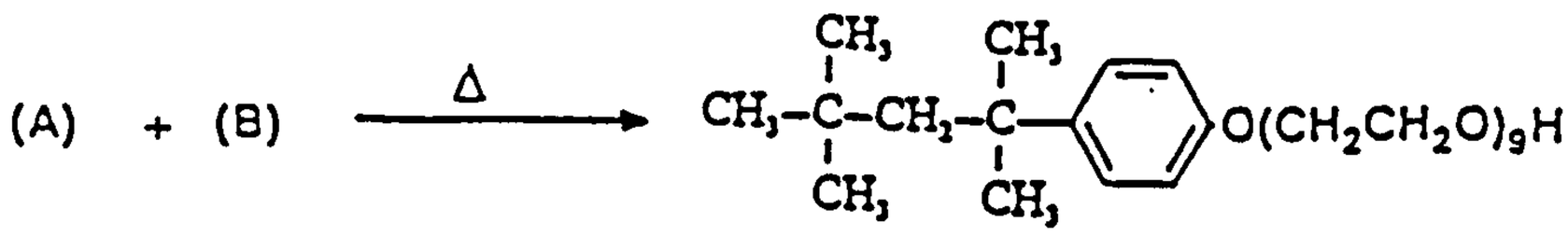

2.2 Adsorbent Materials.

The silica used in this work was in the form of natural quartz (as this would be the most comparable form of quartz to rock surfaces) and was obtained from Silfraco (C-600 grade). The quartz was analyzed using X-ray fluorescence, X-ray photoelectron spectroscopy, scanning electron microscopy, Fourier transform infra-red spectroscopy and N_2 and Kr adsorption at 77K before and after the following pretreatments:

(i) **Acid washing.** This involved washing the quartz with concentrated HCl to remove any inorganic chloride ions present. A 0.1wt%-0.2wt% aqueous suspension of the quartz was made up and conc.HCl was added dropwise until a pH of 1.5 was achieved. At this point, the suspension was filtered using a sintered funnel and the pH of the silica suspension was then increased to a value of approximately 5 by subsequent washings with distilled water. This acid washed silica is referred to as QB throughout the thesis.

(ii) **Calcination.** Quartz samples were calcined in a clean, dry oven at 1273K for varying times in order to observe the effects on surfactant adsorption of removing silanol surface groups. This quartz is referred to as QC throughout this thesis.

2.3 Surfactant Characterisation.

The commercial importance of surfactants, both industrially and domestically, means that there is a need for fast and accurate methods of analysis. The information most necessary for a non-ionic surfactant includes:

i) the distribution of the ethene oxide oligomers,

ii) the percentage of each oligomer present,

iii) the concentration and nature of substituents on any aromatic ring or hydrophilic group, and

iv) the total amount of impurities present.

Users of such surfactants may need to know the oligomeric composition of their samples in differing phases, generally oil and aqueous and also emulsion phases.

2.4 Chromatographic Analysis of Surfactants.

There are many forms of chromatographic procedure, most of which have been used to attempt the separation of commercial ethoxylated alkyl phenols according to their differing oligomers. Unfortunately most of these procedures have proved problematic for the elucidation of the oligomeric spread. Chromatography allows the separation of compounds, according to their size and polarity, by their retention on an adsorbent. Thin layer and paper chromatography have fallen short of requirements due to problems of

reproducibility and quantification (2,3). Gas chromatography has had some success in separating oligomers (4), but is unsatisfactory for the accurate quantisation of oligomers with more than fifteen ethene oxide groups present because of their lack of volatility, even after derivatisation. One group (5) have successfully used size exclusion chromatography to analyse ethoxylated surfactants by using new column technology, a non-aqueous carrier solvent and some operational optimisation. The authors claim to have separated oligomers over a wider and higher size range than the most up-to-date HPLC techniques, and the method appears to be able to deal with a wide range of surfactant type.

Liquid chromatography overcomes the aforementioned problems of long analysis times, lack of specificity and poor accuracy. First developed in 1941 by Martin and Synge, it involves the use of a stationary/solid phase and liquid/mobile phase into which the sample is dispersed. Liquid chromatography is very versatile due to the large variety of stationary and mobile phases available. High performance liquid chromatography (HPLC) is similar to liquid chromatography; the main difference being that the liquid phase is forced through the system under pressure. During analysis, the sample is partitioned between the mobile and stationary phases according to its partition coefficient. This leads to a differential rate of migration and hence separation. Adsorption of the sample onto the stationary phase is a competitive process between the solvent and solute molecules.

There are two modes of liquid chromatography: normal phase where the stationary phase is polar and the mobile phase is relatively non-polar; and reversed phase liquid chromatography which incorporates a non-polar stationary phase and a relatively polar mobile phase. During HPLC, there is the possibility of widely varying the mobile phase during one run to cater for the varying polarities of the compounds in the mixture. This is known as gradient elution and allows HPLC a much larger range of selectivity than the average liquid chromatography range (4).

UV and fluorescence detectors are most commonly used during HPLC analysis. UV/vis detection has the limitation that only species with a chromophore can be detected and the detector response is dependent on the molecular structure. Other detection methods, such as evaporative light scattering (6), mass spectroscopy (7,8) and diode array detection (9), have therefore been developed.

2.5 Analysis of Non-Ionic Surfactants using HPLC.

Many workers have studied the analysis of non-ionic surfactants over the past two decades with the result of great improvements being made in their elucidation. By the late 80's groups found that normal phase HPLC could be used to characterise surfactants containing up to twenty ethene oxide units using isocratic methods (10) and gradient elution (11,12). Good separations were also obtained by Desbene et al (13) using a reversed phase isocratic elution.

Sophisticated normal phase gradients are now being developed that will allow the elucidation of a mixture of surfactants with a wide range of ethene oxide units. Anghel et al (14) have succeeded in separating oligomers containing up to 40 ethene oxide groups and other groups have determined the oligomeric distribution of surfactants within differing emulsion phases (15). Gradients are also being developed which will allow one to look more closely at the structure of the alkyl chain section of alkyl phenols (14), as the para, meta and ortho isomers of alkyl phenols were being shown to have a separation which was superimposed onto the ethoxylate separation (16).

Jandera (17) has been able to describe the retention and selectivity of an oligomeric series using the same mathematical approach that he used for an homologous series. Elegant mathematics has been used which allow the possibility of prediction of the retention and selectivity of oligomers in reversed phase chromatography.

Other classes of surfactants have also been studied using HPLC; sulphated polyethoxylates and other anionic surfactants are extensively used in the oil and detergent industries. Both reversed (18-20) and normal phase gradients (16) have been used for anionic surfactant elucidation. Ogura et al (21) designed a piece of commercial equipment which quantitates linear alkyl benzene sulphonates in detergents. The new method uses ion-spray mass spectrometry, thus cutting out the more usual multi-technique approach used by HPLC (i.e. wet chemistry chromatographic and spectroscopic methods).

There have been few publications concerning cationic species which also have commercial importance in the detergent industry as fabric softeners. Most cationic surfactants cause problems due to their non-UV absorbing nature and therefore other detection techniques such as conductometry have been used (22).

There is now a need for the development of a method which will give a quantitative analysis of alkyl phenyl ethoxylates in waste waters, because there have been major environmental concerns regarding the lack of biodegradability of branched chain alkyl groups within non-ionic surfactants and the build-up of foam in sewage works, streams and rivers. The methods for waste water analysis must be capable of dealing with the compositional complexity of surfactant mixtures. Ahel and Giger (23) first described how HPLC could be used to analyze environmental samples in 1985, and the process is still used (24,25). The method requires a lengthy extraction process, during which fractions of the surfactant to be analysed may be lost (26), followed by normal phase HPLC (27). Until recently, few gradients have been available which would allow surfactant analysis direct from an aqueous eluent. One of these gradients was developed by Mengerink et al (28) using a water/acetonitrile gradient and a C_{18} column. Although this gradient provided good separations of oligomers of up to 25 ethoxylate units, the retention times were up to 45 min (29).

2.6 Experimental Method for Analysis of Surfactants from a Non-Aqueous Solution.

Initially Triton X-114, X-100, X165 and X-305 were studied using normal phase HPLC. The analysis was performed using a Gilson system (Anachem Ltd.) with automated injection via a 20μl loop. UV detection has long been used for the analysis of surfactants in bulk in aqueous solution owing to their sharp absorption of UV light at 275nm (see Figure 2.1); UV was also used during the HPLC analysis of oligomers. It was assumed that all of the oligomers had the same absorptivity at the set wavelength (275nm). The pumps were controlled using an Apple IIe computer and the chromatograms were traced using a Gilson chart recorder. A DuPont technical report (29) suggested the use of a cyano column with the following operating conditions:

Mobile Phase: solvent A: hexane
solvent B: 2-methoxyethanol / isopropanol (65:35)

Gradient: **solvent B, 2% - 50% in 20 min. Linear hold at 50% for 5 min.**

Column: **CN, 4.6mmx25cm**

Flow rate: **2cm^3/min**

Temperature: **298K**

The samples were prepared as 0.1% (wt/vol) solutions in solvent B.

2.7 Results for analysis of Surfactants from Non-Aqueous Solution.

Figures 2.2-2.5 show the chromatograms obtained for samples of the Triton family of non-ionic surfactants. In the initial experiments, time was measured along the abscissa of the chromatogram and absorbance measured along the ordinate. The apparatus used was not capable of providing an in-depth analysis of the UV absorbance of each oligomer, thus only retention times are shown here. At this stage it was necessary only to observe whether the oligomers could be separated using this technique. As can be seen, a Poisson distribution is obtained (see section 1.4) which reflects the distribution of oligomers within the surfactants. The least polar oligomers are eluted first since they have less affinity for the polar column and therefore a lower extent of retention. The larger oligomers are adsorbed onto the cyano column via a series of electrostatic interactions between the column and the ethoxylate chain. As the gradient continues, the polarity of the flushing solvent increases and so the more polar oligomers (i.e. those with a larger number of ethoxylate units present) are eluted until eventually all of the surfactant is driven off the column.

Figures 2.2 and 2.3 show chromatograms of the smaller molecular weight surfactants, their retention times are comparable and the oligomeric separation is good, although a higher injection concentration of TX-114 was needed to obtain a clear separation. The negative peaks at the beginning of both of the traces are most probably due to the sample-solvent effect. Samples should ideally be dissolved in the solvent mix that initiates the gradient, however, due to the larger surfactants having a low solubility in apolar solvents this was not carried out during experimentation. Injection of a sample dissolved in a solvent other than the gradient initiator may result in a temporary disturbance of the phase system which can lead to inferior chromatographic traces.

Figures 2.4 and 2.5 show the chromatograms obtained for the larger surfactants. The retention times are longer for these surfactants due to the relative hydrophilicity of the longer ethoxylate chains when compared to TX-114 and TX-100. Figure 2.5 shows the trace obtained for the largest surfactant molecule. The chromatogram shows a "bunching" of peaks which is due to the size exclusion effect. This is an effect commonly seen for surfactants having twenty or more oligomers. The poor resolution is caused by the decreasing relative differences between the molecular weights of successive oligomers and the lack of accessibility of the larger oligomers to the column pores (i.e. size exclusion). This leads to weaker retention.

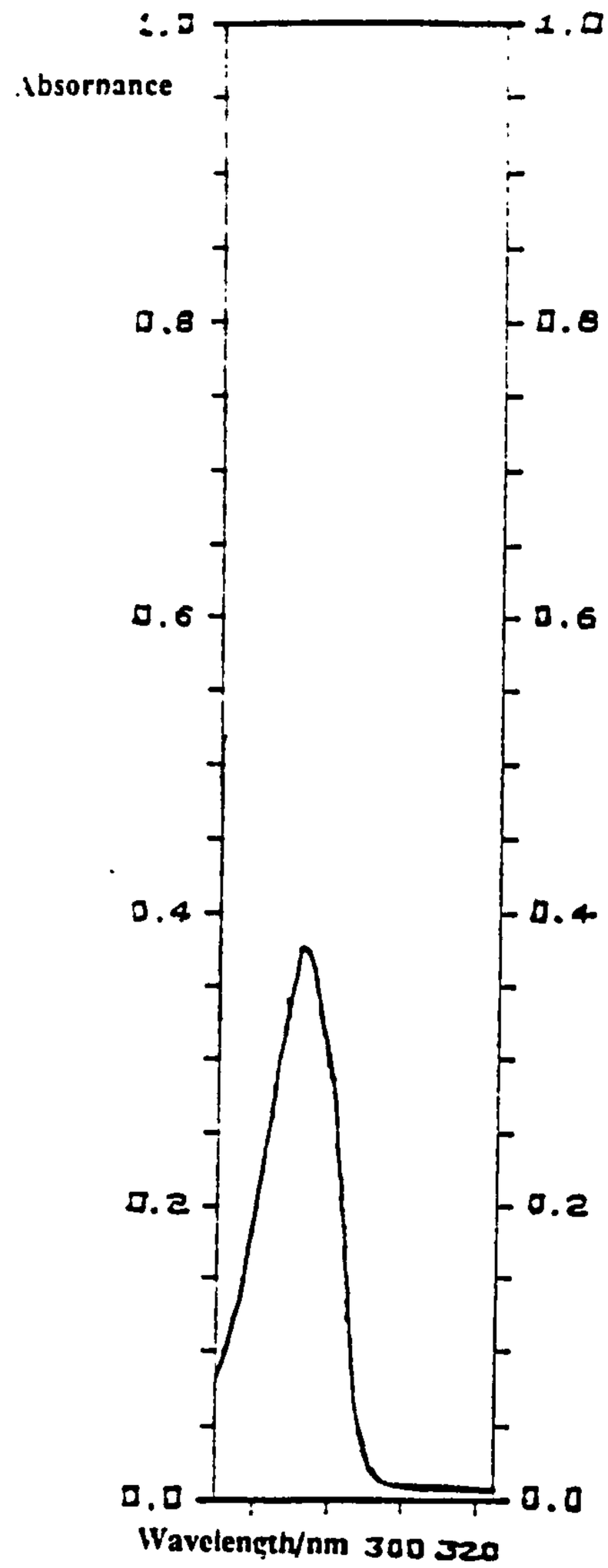

Figure 2.1: UV Absorption Typical of that seen for Surfactants in the Triton Series.

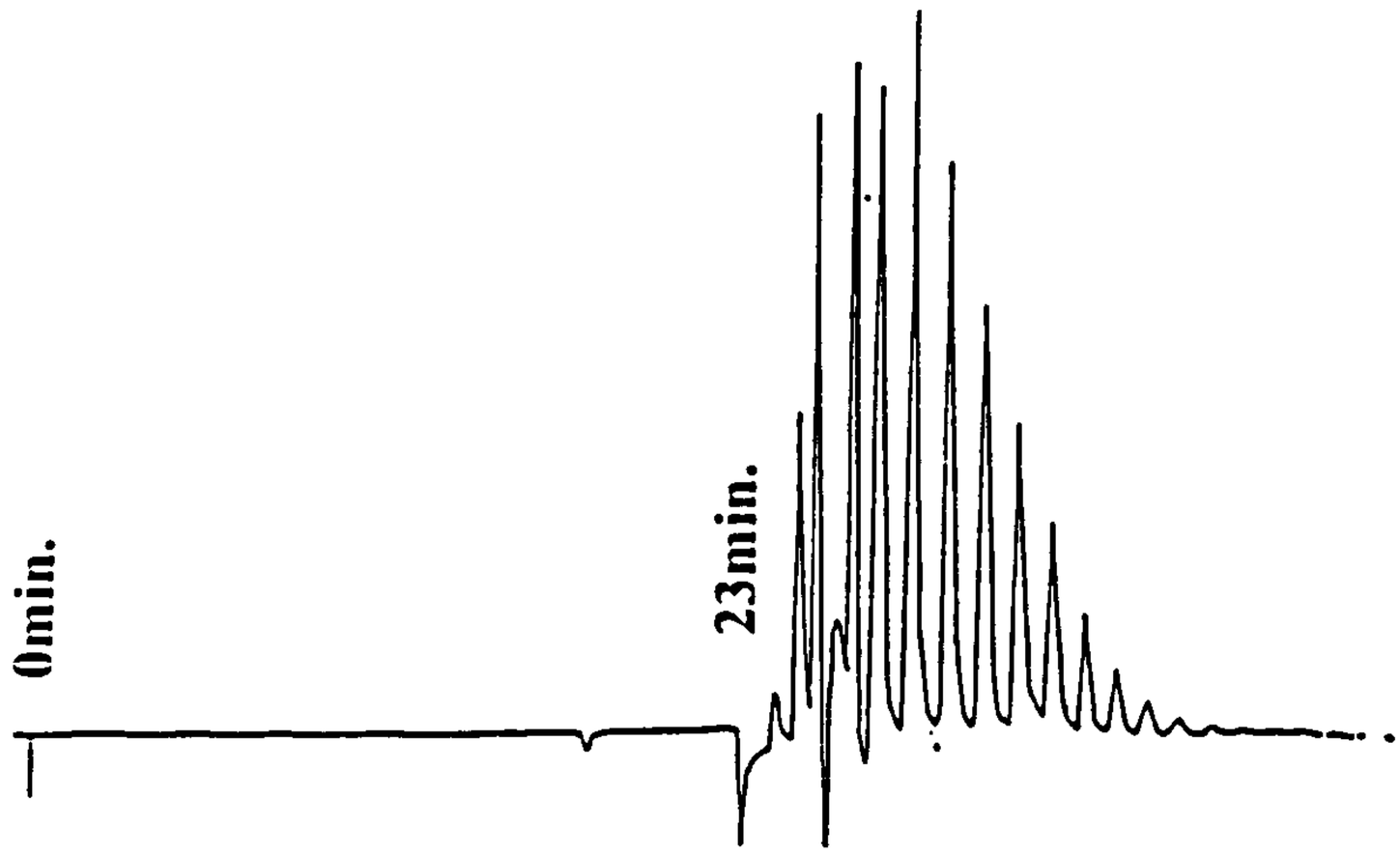

Figure 2.2: HPLC Trace for 3.73mmol/l TX-114.

(Retention time = 23min)

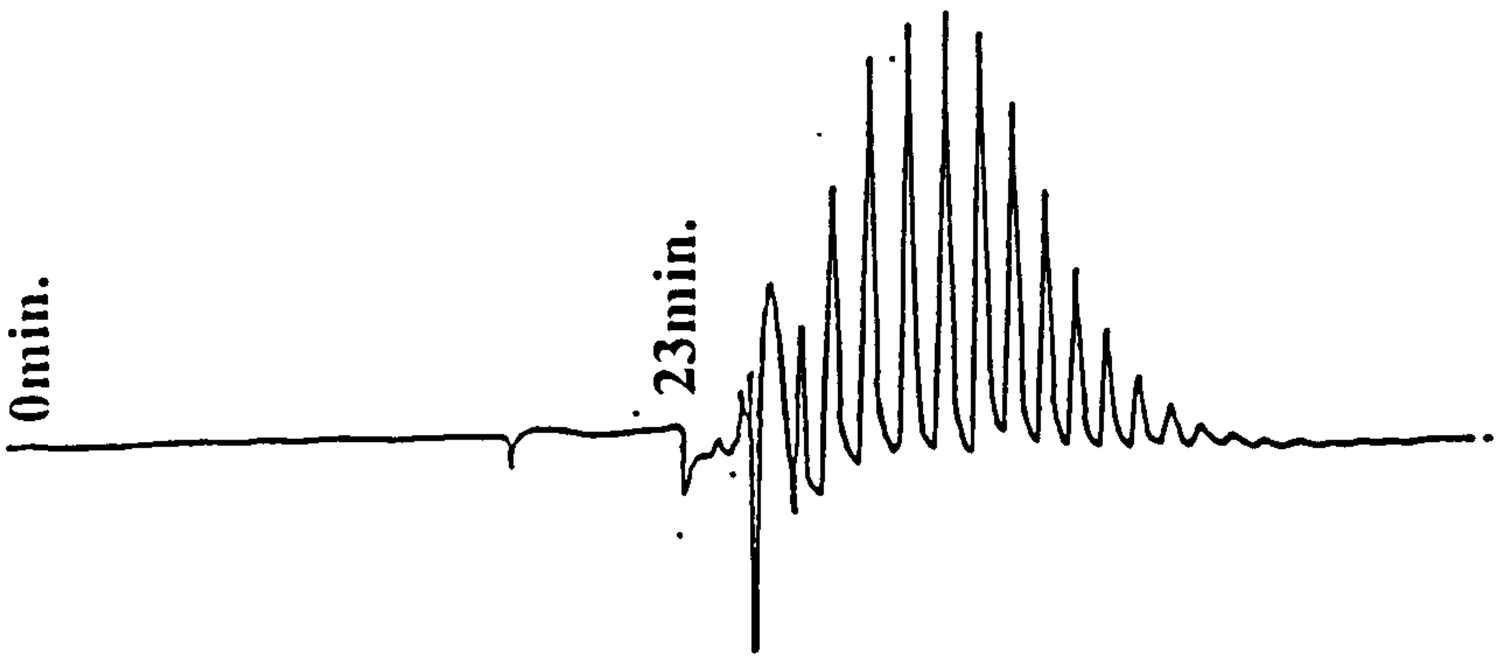

Figure 2.3: HPLC Trace for 1.6mmol/l TX-100.

(Retention time = 23min)

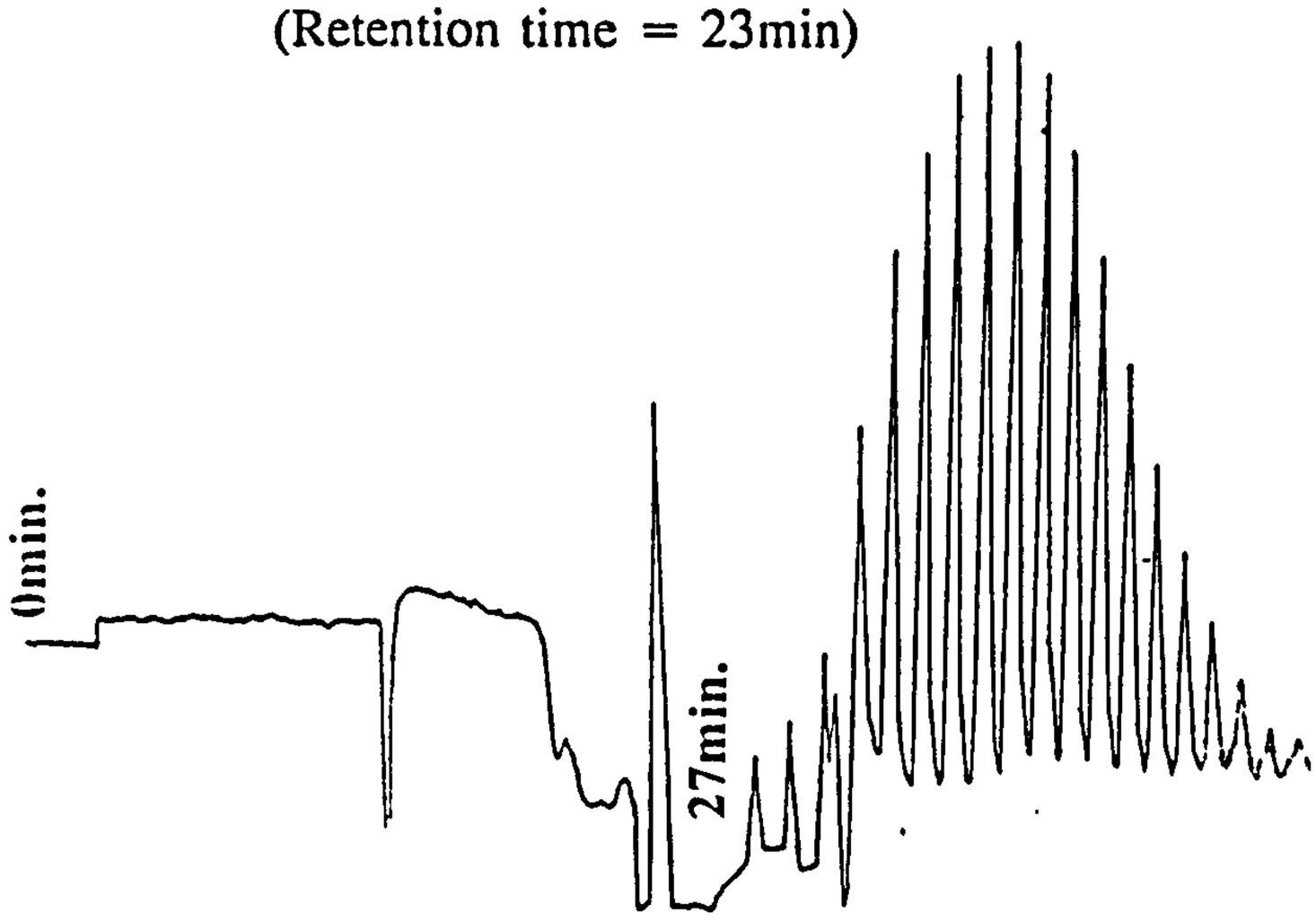

Figure 2.4: HPLC Trace for 1.07mmol/l TX-165.

(Retention time = 27min)

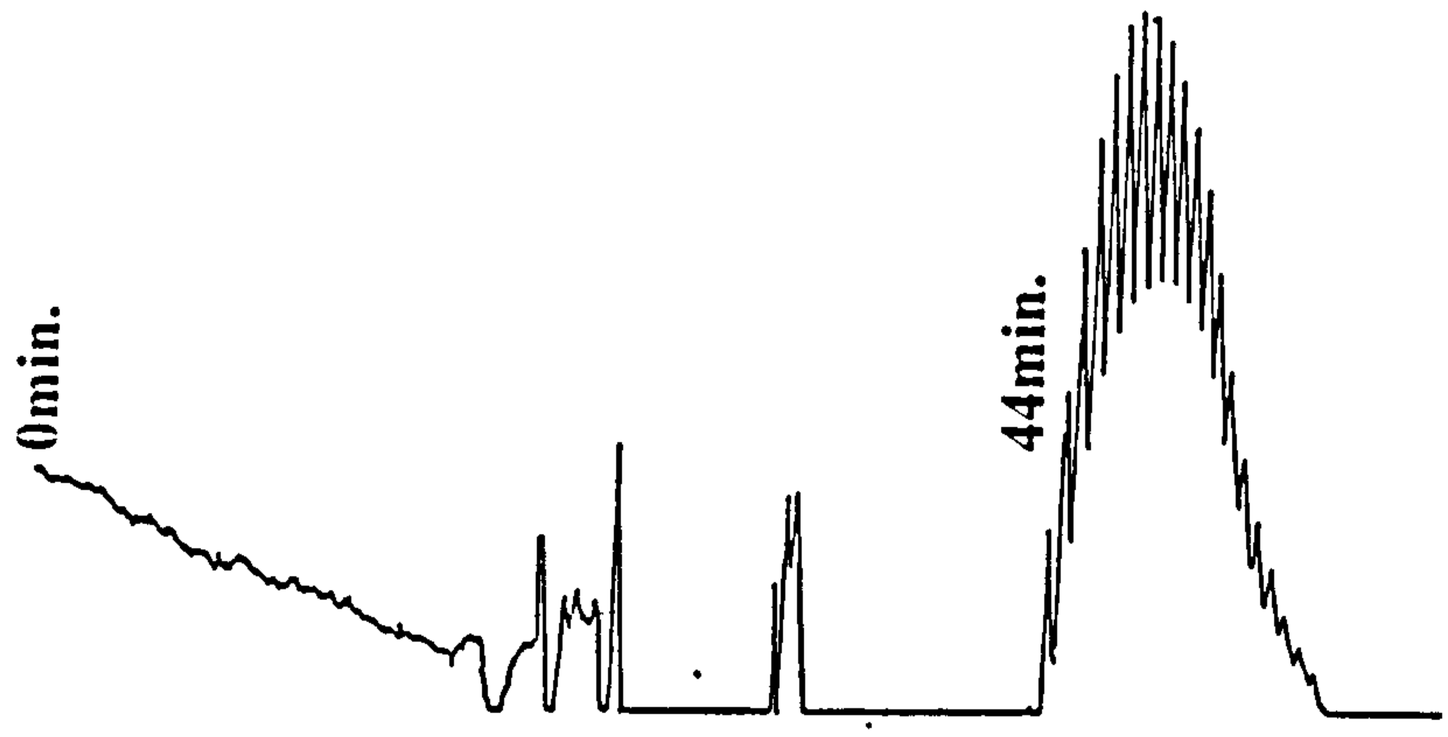

Figure 2.5: HPLC Trace for 0.65mmol/l TX-305.

(Retention time = 44min)

2.8. Experimental Method for Analysis of Surfactants from Aqueous Solution.

The majority of the work carried out for this thesis involved considering TX-100 in aqueous solution. A gradient developed here at Brunel (1,30) enabled the author to inject aqueous surfactant samples directly onto the HPLC system.

A Varian 9100 system with automated injection and fluorescence detection was used to conduct this analysis. The column was packed with a commercial silica (Spherisorb, 5μm) which was supplied by Phase Sep. and the following operating conditions were used:

Mobile Phase: solvent A: pH3 buffer (based on a disodium hydrogen phosphate, water and phosphoric acid mixture).
solvent B: acetonitrile

Gradient: solvent B, 25% - 50% in 12 min, reinjection after 20 min.

2.9. Results for Analysis of Surfactants from Aqueous Solution.

Figures 2.6-2.9 show examples of surfactant elution using this gradient. Again, the traces mirror the Poisson distribution of the ethoxylate chains in the surfactants. The system did not require a lengthy extraction of the surfactant from the aqueous solution, even to high degrees (5%) of salinity, and had a shorter analysis time. Smaller amounts of surfactant were needed for good oligomeric separation, making the gradient favourable for analysis of environmental samples. This gradient works due to the low pH of buffer which keeps the silanol groups of the silica packing protonated. As the concentration of acetonitrile increases, the silica surface is subtly altered together with the binding force between the surface and the surfactant molecules; the competition between the solvent molecules and the surfactant molecules for the protonated silanol groups of the stationary phase increases. As the pH increases with the gradient, so the larger surfactant oligomers are eluted. On examination of the chromatograms for TX-165 and TX-305 (see Figures 2.8 and 2.9), it would seem that this gradient is not as effective as the normal phase HPLC gradient at separating out the larger molecules; this is due to their hydrophilicity and thus their high solubility in the gradient initiator. It must also be mentioned that good separation of the surfactants was specific to Spherisorb silica only; other silicas with comparable surface areas and pore diameters are apparently not capable of separating the oligomers of alkylphenolpolyethoxylates (1).

It is not valid to assume that the largest peak on the chromatograph corresponds to the

oligomer having, say for TX-100, 10 ethene units because the possibility of drift cannot be ruled out. In order to label the peaks, a sample of polydisperse TX-100 was spiked with a monodisperse sample of known ethoxylate chain length and HPLC was carried out. The chromatogram is shown in Figure 2.10. As one can see, the n=9 oligomer is clearly visible.

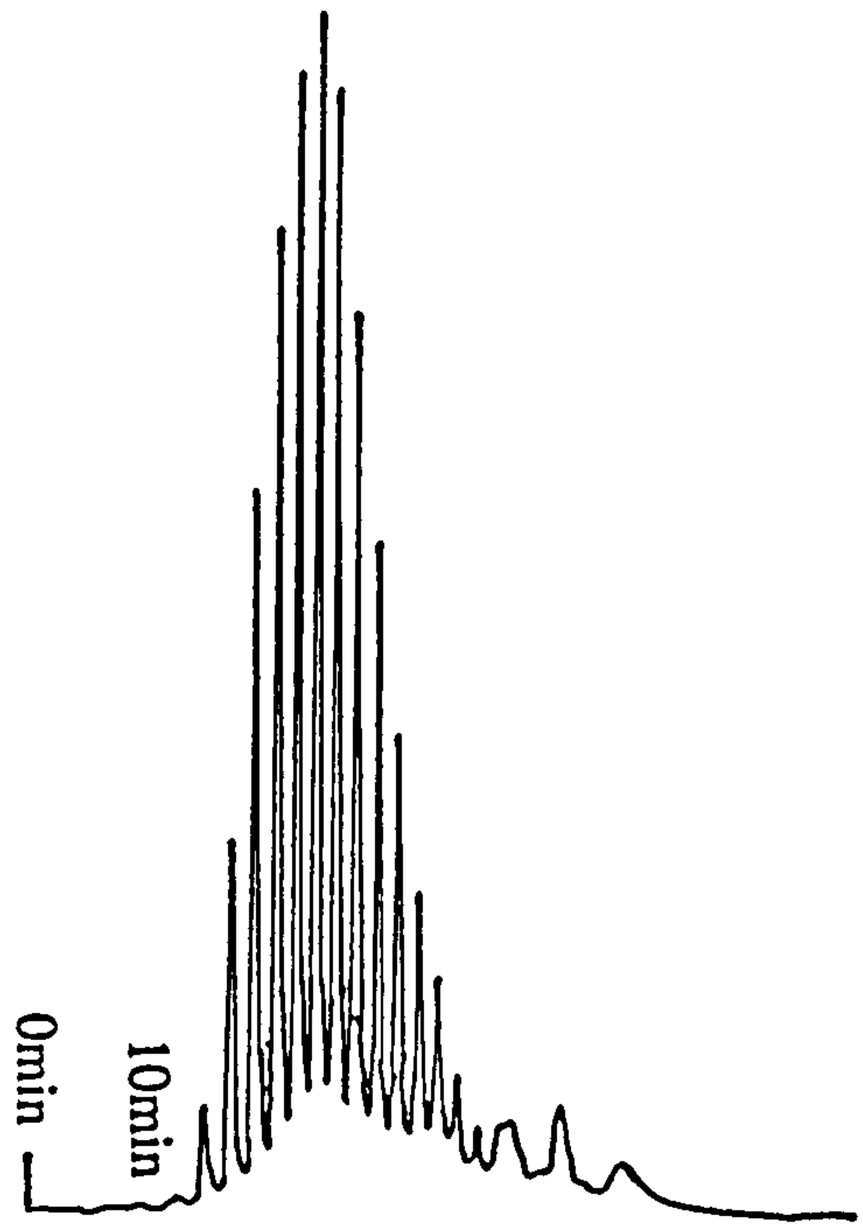

Figure 2.6: HPLC Trace of 0.41mmol/l TX-114.

(Retention time = 10min)

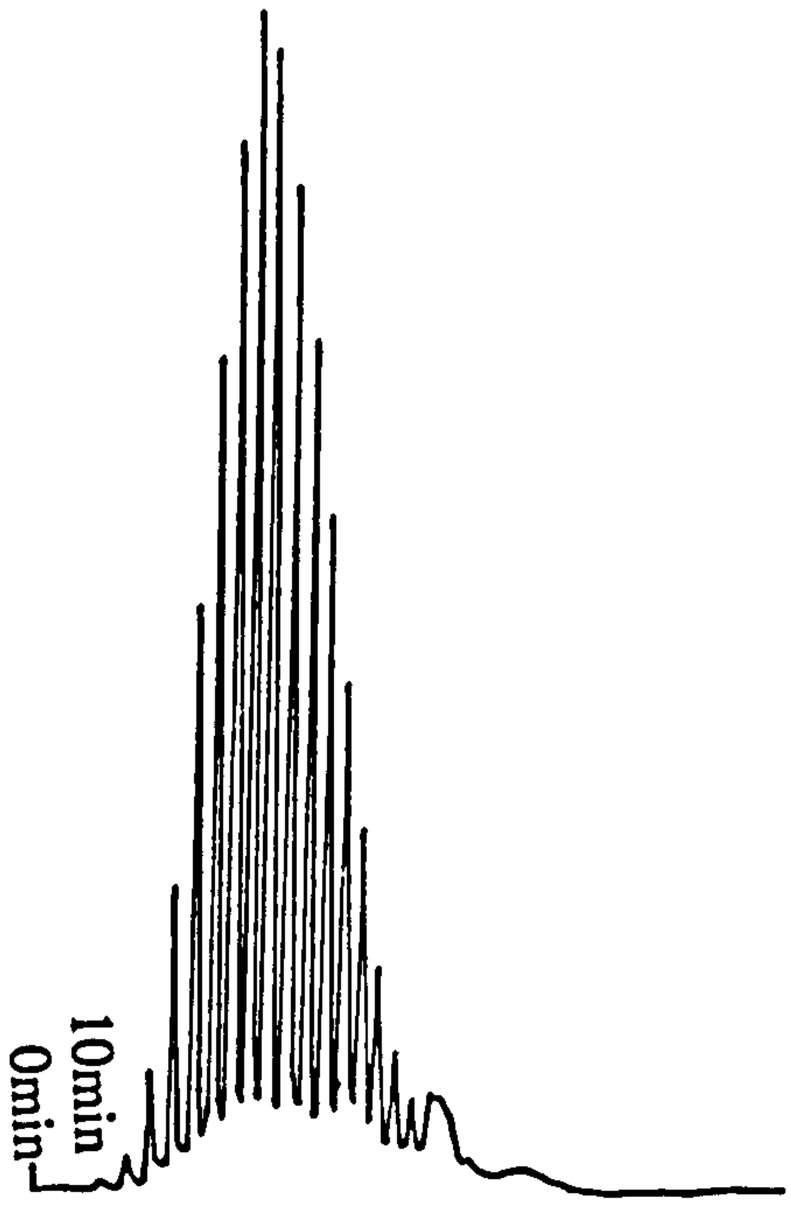

Figure 2.7: HPLC Trace of 0.35mmol/l TX-100.

(Retention time = 10min)

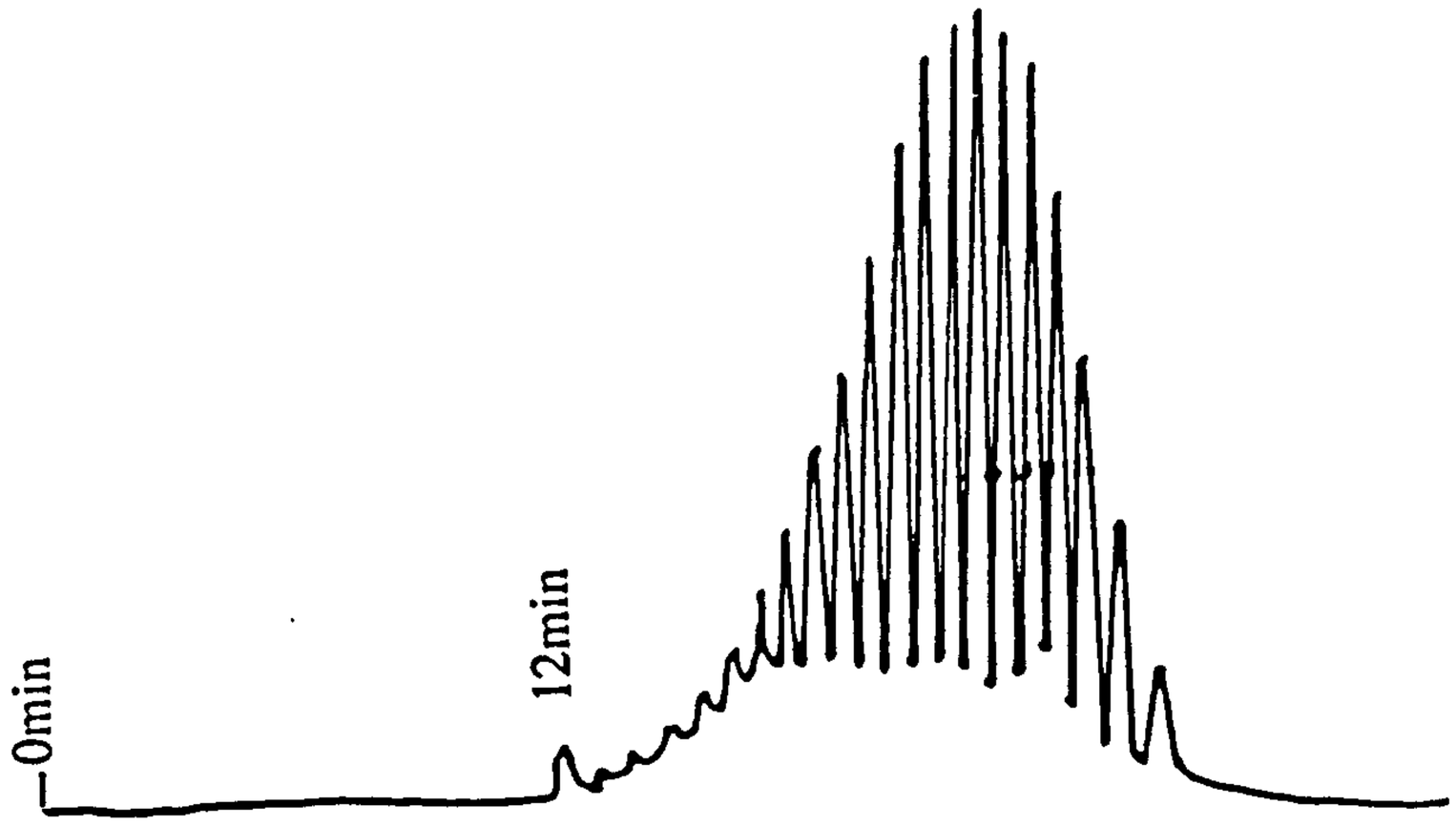

Figure 2.8: HPLC Trace of 0.30mmol/l TX-165.

(Retention time = 12min)

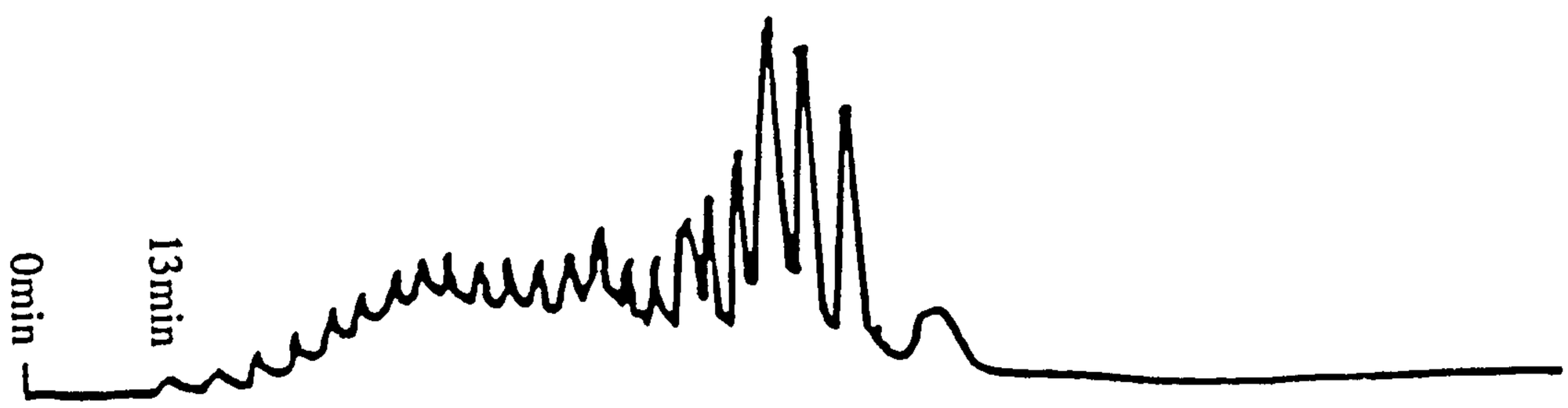

Figure 2.9: HPLC Trace of 0.97mmol/l TX-305.

(Retention time = 13min)

Figure 2.10: HPLC Trace of 0.32mmol/l TX-100 + 1.66mmol/l n=9 ethoxylate units.

2.10. Theory and Experimental Method of Surface Tension Analysis.

As previously mentioned, surfactants are active at the interface between two phases; they accumulate at the interface and as a result tend to modify the surface tension at that interface. A surfactant solution has a surface populated by a monolayer of adsorbed molecules. These molecules are in a state of lower free energy than the molecules in the bulk solution. As the surface tension of a liquid is related to the mechanical work required to create unit area of surface, then adsorption of surfactant at the interface should lower the surface tension of the pure liquid due to the low free energy of the surfactant molecules at the interface. Thermodynamics allows one to arrive at a precise relationship between the amounts of species at the surface and its effect on the surface tension of the liquid. Gibbs first derived the relationship between quantity of species per unit area of the surface and the change in surface tension in 1878.

Consider two phases, a and b, in contact; their volumes being V_a and V_b respectively. The total system is composed of several components J, each one being present in the amount n_J. The surface area of the interface is a well defined area σ. The total Gibbs function for the system is G. The components are not distributed uniformly throughout the phases and the sum of the Gibbs functions for the two phases differs from the total Gibbs function by an amount called the surface Gibbs function,

$$G^\sigma = G - (G^a + G^b). \qquad (2.1)$$

Similarly, if the bulk contains an amount n_J^a in phase a (and n_J^b in phase b), then the total amount J differs from their sum by the amount

$$n_J^\sigma = n_J - (n_J^a + n_J^b). \qquad (2.2)$$

The surface excess Γ_J of the substance is expressed in terms of the amount per unit area of the surface, and is defined as the excess material present in the surface phase due to adsorption over and above that which would be present if the bulk concentration were continued right up to the interface.

$$\Gamma_J = n_J^\sigma / \sigma. \qquad (2.3)$$

Both n_j^σ and Γ_j can be either positive or negative depending on whether there is an accumulation or deficiency of substance at the interface. A change in G is brought about by changes in temperature (T), pressure (p), surface area (σ) and the amount of component (n_j) present:

$$dG = -SdT + Vdp + \gamma d\sigma + \Sigma\mu_j dn_j. \qquad (2.4)$$

where γ = surface tension, μ = chemical potential of the components and S denotes entropy.

When this is applied to say G^σ,

$$dG^\sigma = -S^\sigma dT + \sigma d\gamma + \Sigma\mu_j dn_j^\sigma. \qquad (2.5)$$

It is important to note that at equilibrium, the chemical potentials of the components in phases a and b and at the interface are equal. This expression integrates at constant temperature to

$$G^\sigma = \sigma\gamma + \Sigma_j\mu_j n_j^\sigma. \quad (2.6)$$

As one is seeking a connection between the change in surface tension and the change in composition, then by comparing the equation $dG^\sigma = \sigma d\gamma + \gamma d\sigma + \Sigma n_j^\sigma d\mu_j + \Sigma\mu_j dn_j^\sigma$ with (2.5) at constant T (dT=0) one arrives at

$$\sigma d\gamma + \Sigma_j n_j^\sigma d\mu_j = 0, \quad \text{at constant T.} \qquad (2.7)$$

Dividing through by σ then gives the *Gibbs surface tension equation*:

$$d\gamma = -\Sigma_j\Gamma_j d\mu_j \qquad (2.8)$$

For a solution containing only two components, a solvent (1) and an uncharged surface active solute (2):

$$-d\gamma = \gamma_1 d\mu_1 + \Gamma_2 d\mu_2 \qquad (2.9)$$

The conventional way of writing the above equation is to position the interface so that surface excess of the solvent (1) is equal to zero:

$$-d\gamma = \Gamma_2 d\mu_2 \quad (2.10)$$

For changes in surfactant concentration

$$d\mu_2 = RT.d\ln a_2, \quad \text{where } a_2 \text{ is the activity of component 2} \quad (2.11)$$

Combining equations 2.10 and 2.11 gives:

$$\Gamma_2 = -(1/RT).(d\gamma/d\ln a_2) \quad (2.12)$$

When dilute surfactant solutions are being used then the activity of the solute can be approximated to the concentration so that:

$$\Gamma_2 = -(1/RT).(d\gamma/d\ln c_2). \quad (2.13)$$

This is the most commonly used form of the Gibbs equation. There are certain limitations to the equation due to the assumptions that the surfactant is a single component, that the activity of the dilute surfactant is equal to that of its concentration and that a dividing surface for which the surface excess of the solvent is zero can be defined.

The surface tension curves for the Triton surfactants in aqueous solution were measured manually using the Du Nouy ring method at 298K. Solutions of varying concentration were made up in distilled water and left for 24h to reach equilibrium before measurements were taken using a torsion balance (Whites Elect.Inst.Co.Ltd). The measurements were all reproducible to +/- 0.25mN/m.

2.11. Results of Surface Tension Analysis.

Figures 2.11-2.14 show the surface tensions obtained for TX-114, TX-100, TX-165 and TX-305 at 298K in aqueous solution with varying concentration. They all show the familiar pattern of decreasing surface tension with increasing concentration of surfactant until a final and constant value of surface tension is reached. When surfactant is added to an aqueous solution, surfactant monomers adsorb at the air/water interface, thus causing a decrease in surface tension of the water. Initially the surfactant molecules will position themselves so that their hydrocarbon regions are lying flat along the surface; as the concentration of surfactant added to the solution increases, the number of monomer

molecules adsorbing onto the surface increases also, thereby causing the gradual lowering of the surface tension; the tails of the molecules become entangled with each other but the mutual repulsion of the head-groups prevents a dense surface population being formed. At the CMC, the air/water interface will hold the maximum number of surfactant monomers allowable by the afore-mentioned forces and so the majority of monomer molecules added to the solution will be incorporated into micelles and not adsorbed onto the surface, thus the surface tension at this point remains constant. The adsorption of surfactant molecules at the surface of water is a dynamic process that reaches equilibrium when the numbers of molecules entering and leaving the interface in a given time are equal.

The CMCs of the surfactants were obtained as illustrated in Figure 2.11; the point at which the surface tension becomes a constant value is assumed to occur at the CMC of the surfactant.

On examining Figure 2.15, it is important to note that the larger molecules are not as surface active (i.e. inefficient at lowering the surface tension) as the smaller ones. One reason for this is that the larger molecules have a larger HLB (hydrophile/lipophile balance) value and so will remain in the bulk solution; the smaller molecules are less hydrophilic and so tend to spread themselves along the surface of the liquid. Another reason for the difference in surface tension decrease is that the larger molecules have larger head groups and the extra repulsion resulting from this hinders their adsorption onto the surface. Table 2.1 shows the value of CMC, number of ethoxylate units and surface tension at the CMC.

There is often a dip in the surface tension at points just below the CMC. This is most likely to be due to the presence of impurities in the system that are more surface active than the sample being studied. At points just below the CMC these impurities, if strong enough, can override the effects of the surfactant until either dilution reduces their levels to very small amounts or the addition of surfactant causes surfactant effects to be the strongest. The surface tension curves seen in Figures 2.11-2.14 do not show severe signs of impurity.

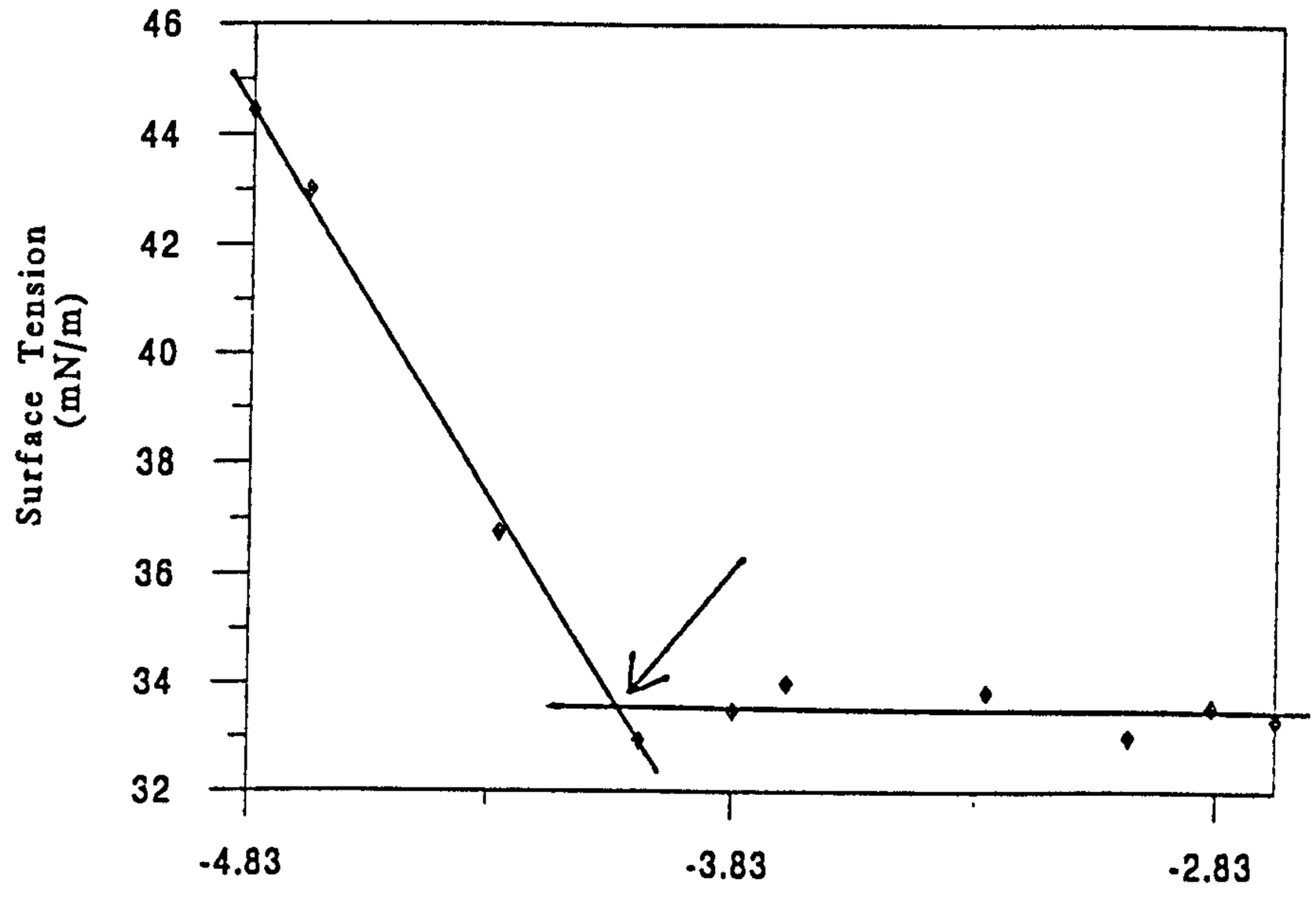

Figure 2.11: Surface Tension Curve measured at 298K for TX-114.

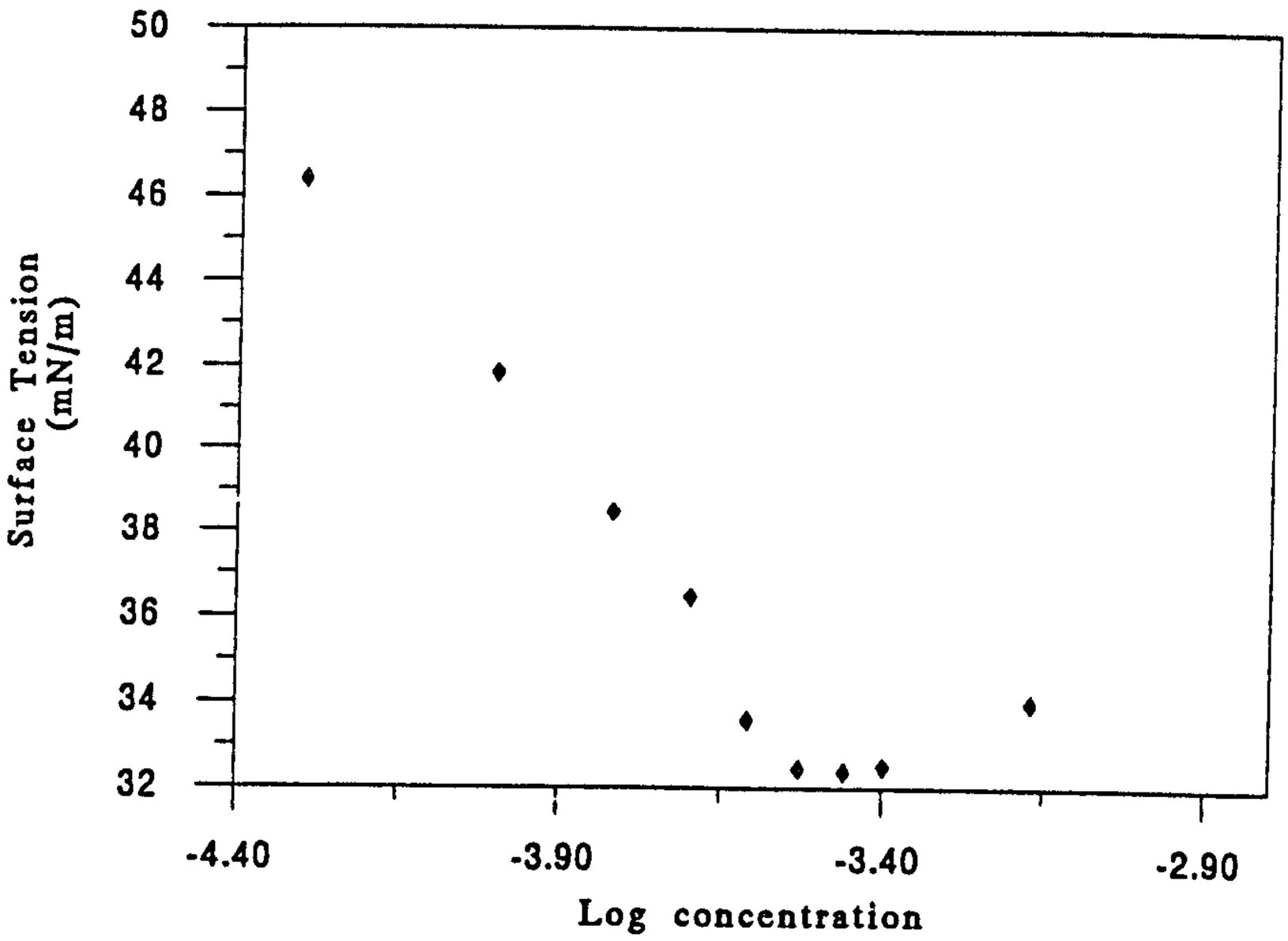

Figure 2.12: Surface Tension Curve measured at 298K for TX-100.

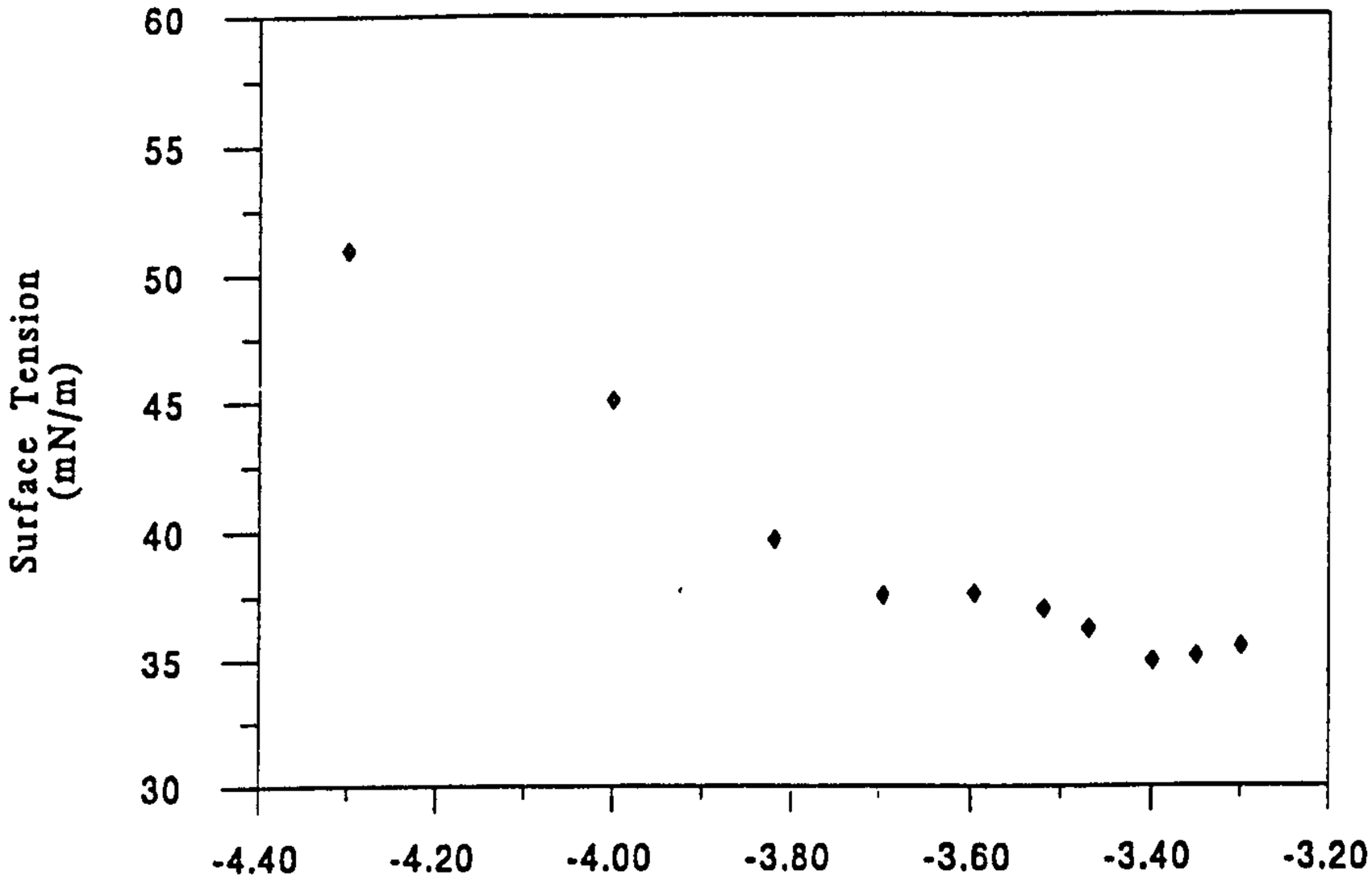

Figure 2.13: Surface Tension Curve measured at 298K for TX-165.

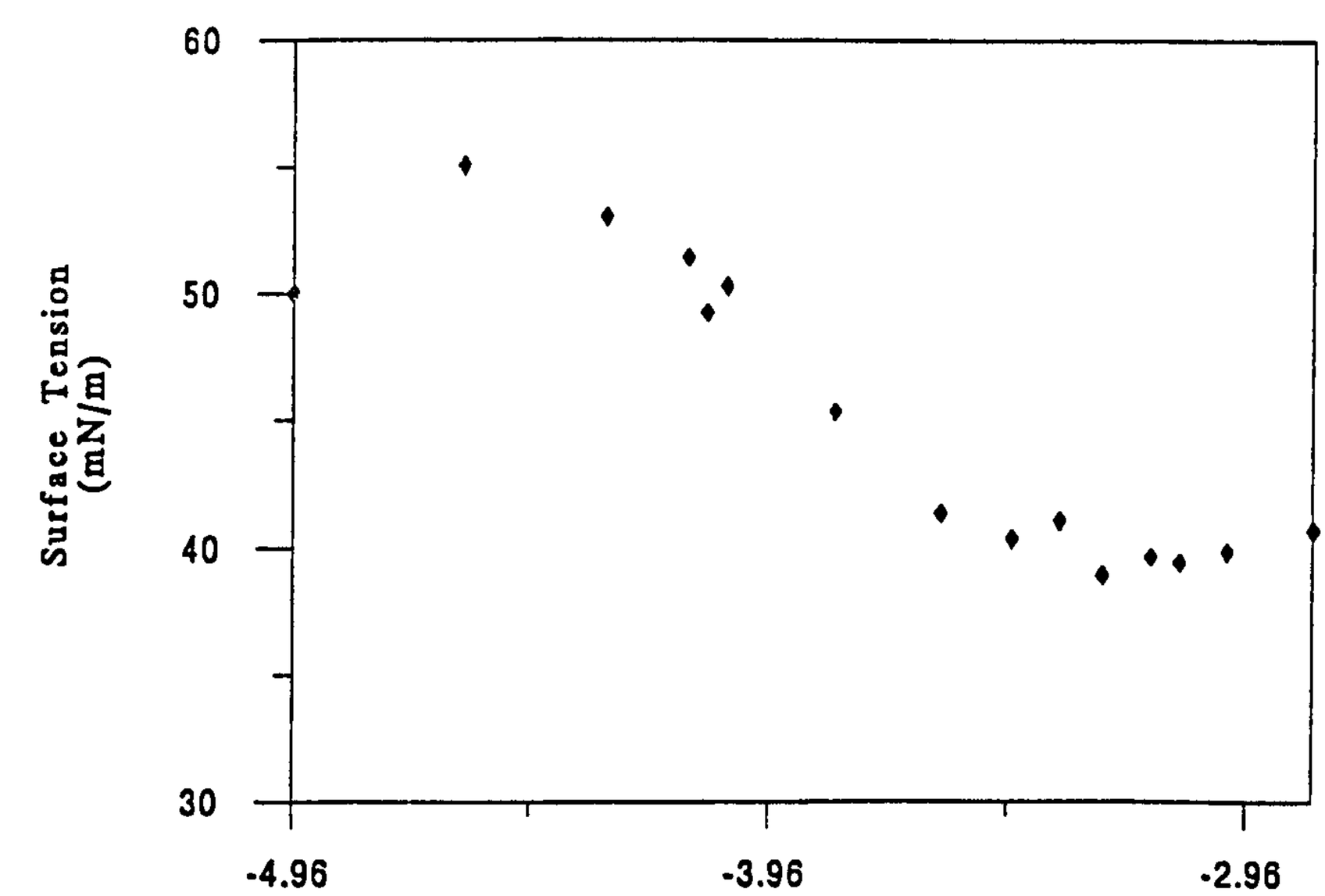

Figure 2.14: Surface Tension Curve measured at 298K for TX-305.

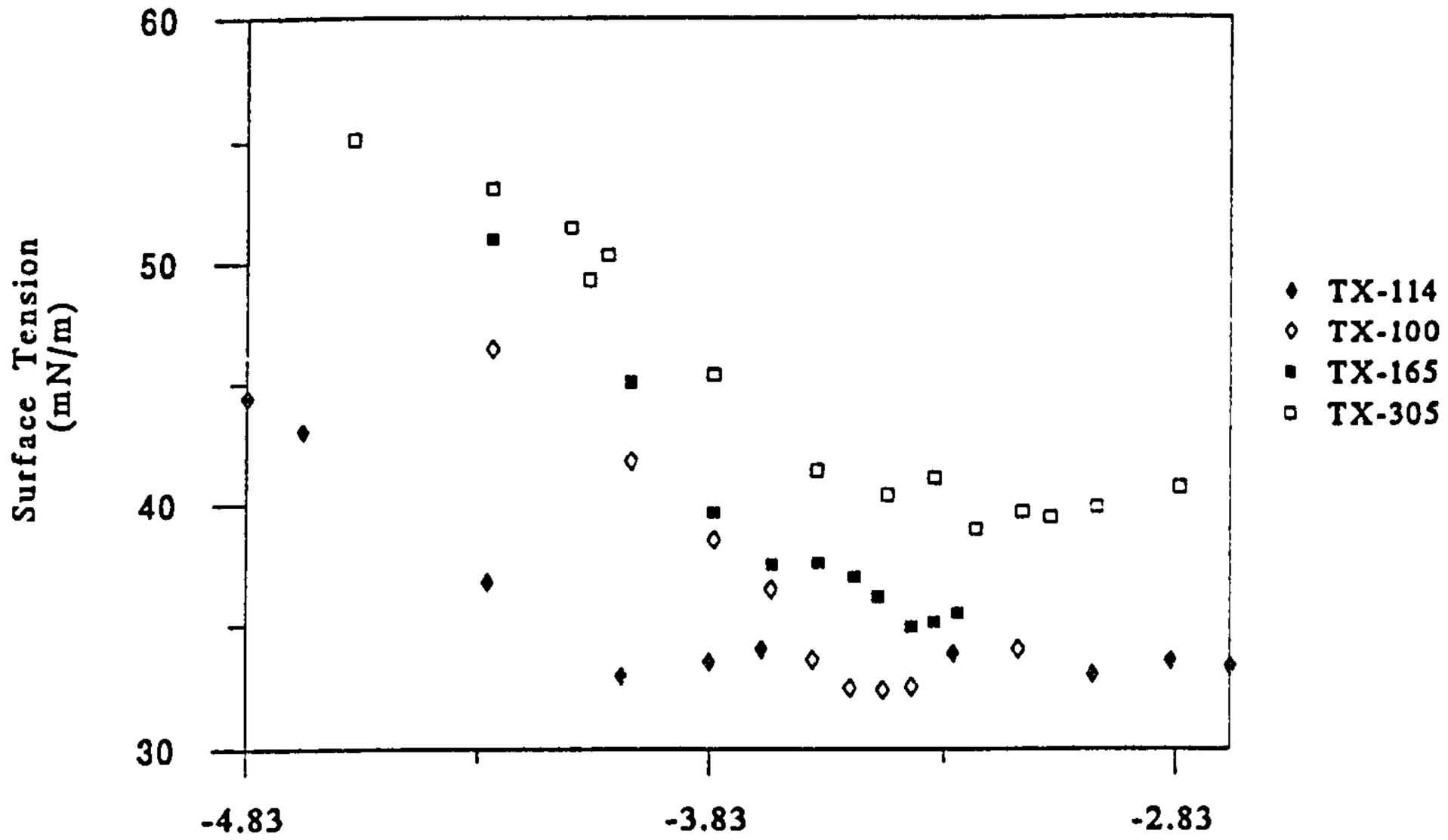

Figure 2.15: Superposition of Surface Tension Curves measured at 298K for TX-114, TX-100, TX-165 and TX-305.

Table 2.1 shows the variation of CMC with ethoxylate number. As previously stated, the longer the ethoxylate chain the less surface active the molecule. This effect is due to the increased hydrophilicity of the molecule and the extra repulsion due to the increased size of head group. The CMC also increases with ethoxylate chain length (n) since the larger molecules are more stable in the monomeric form in aqueous solution due to their relatively high hydrophilicity.

There will certainly be errors in the values obtained for γ at the CMC of the surfactant and thus the calculation of the CMC itself, due to the reading from the graph. A very loose estimation of the error of γ at the CMC would be approximately +/- 0.5mN/m, from the graph.

Table 2.1: Variation of CMC and γ at the CMC with Average Ethoxylate Chain Length (n) for Triton Surfactants.

Surfactants (n)	CMC (μmol/dm^3)	γ at CMC (mN/m)
TX-114 (7-8)	59	34
TX-100 (9-10)	193	33
TX-165 (16)	221	35
TX-305 (30)	390	40

2.12 Characterisation of the Quartz.

2.13 X-Ray Fluorescence (XRF) Theory and Experimental Method.

Analysis of minerals by XRF was first carried out in the early 1960's and by the early 1970's, XRF was accepted as a true competitor of analysis of sand and clays in terms of accuracy and precision (31). Since then, the scope of XRF has grown to include analysis of more complex materials such as glasses, glazes, ferrites and pottery amongst others. XRF has several advantages over other analytical techniques due to (i) the ease of interpretation of the spectra, (ii) the ease of X-ray excitation from the bulk samples by

higher energy X-rays. This being a non-destructive process, the method can be used to study antiques or archaeological artifacts. Figure 2.16 shows a schematic diagram of the XRF analytical system.

The X-ray tube (capable of producing X-rays of an energy at least 5keV greater than that of the studied X-rays) produces the primary beam of X-rays incident to the sample. These X-rays impinge on the atoms in the sample (see Figure 2.17) and cause electrons from the K,L and M shells to be ejected due to transfer of energy from the incident rays to the electrons. The remaining electrons in the higher energy shells then fall to fill the holes left by the excited electrons and in doing so ensure that an X-ray is emitted with energy which is characteristic of that atom.

As a sample emits many energies from all of the elements present within itself, the X-rays must be differentiated by either (a) diffraction from a single crystal (wavelength dispersion) or (b) using an energy sensitive X-ray detector (energy dispersion). The equipment used during analysis at Brunel consisted of an energy dispersive Si(Li) detector.

Energy dispersion works by using an intrinsic silicon semiconductor with a precisely defined band gap (3.65eV for silicon). Electrons in the semiconductor are promoted to the conduction band as an X-ray hits the detector. This electron movement is amplified to give a voltage pulse and all pulses detected are then sorted according to their voltage. In this way, the XRF technique provides an energy spectrum of all the elements within a sample.

2.14 XRF Results.

XRF was used to gain information on the level of impurities within the silica, and to detect any differences between the solids which had been pre-treated. An Oxford Instruments XR300 energy dispersive X-ray fluorescence spectrometer was used for the analysis. The instrument was calibrated using a copper oxide standard that was obtained from Microanalysis Consultants of Cambridge. All of the spectra obtained from the XRF analysis showed the main KLM peaks for the various atoms present. These were identified using the instrument software.

Figures 2.18-2.21 show the XRF spectra obtained for the quartz samples. Figure 2.18 shows the quartz as received and indicates the presence of trace quantities of potassium,

calcium, iron and also silicon. The large double peak to the right of the silicon peak is known as a tube line and is due to the detection of the characteristic X-rays from the rhodium tube. Figure 2.19 shows the spectra obtained for the QB, the levels of calcium seem to have reduced by approximately half, but the quantities of potassium and iron remain unchanged. Calcining the sample for 1h seems to have little effect on the ionic composition of the sample (see Figure 2.20) although at 16h of heat treatment all of the ions present are reduced by approximately half (Figure 2.21).

To reiterate, pre-treating the quartz with conc.HCl does little to remove the levels of potassium and iron present, whereas calcination for 16 h results in a reduction in levels of all the ions initially present in the sample.

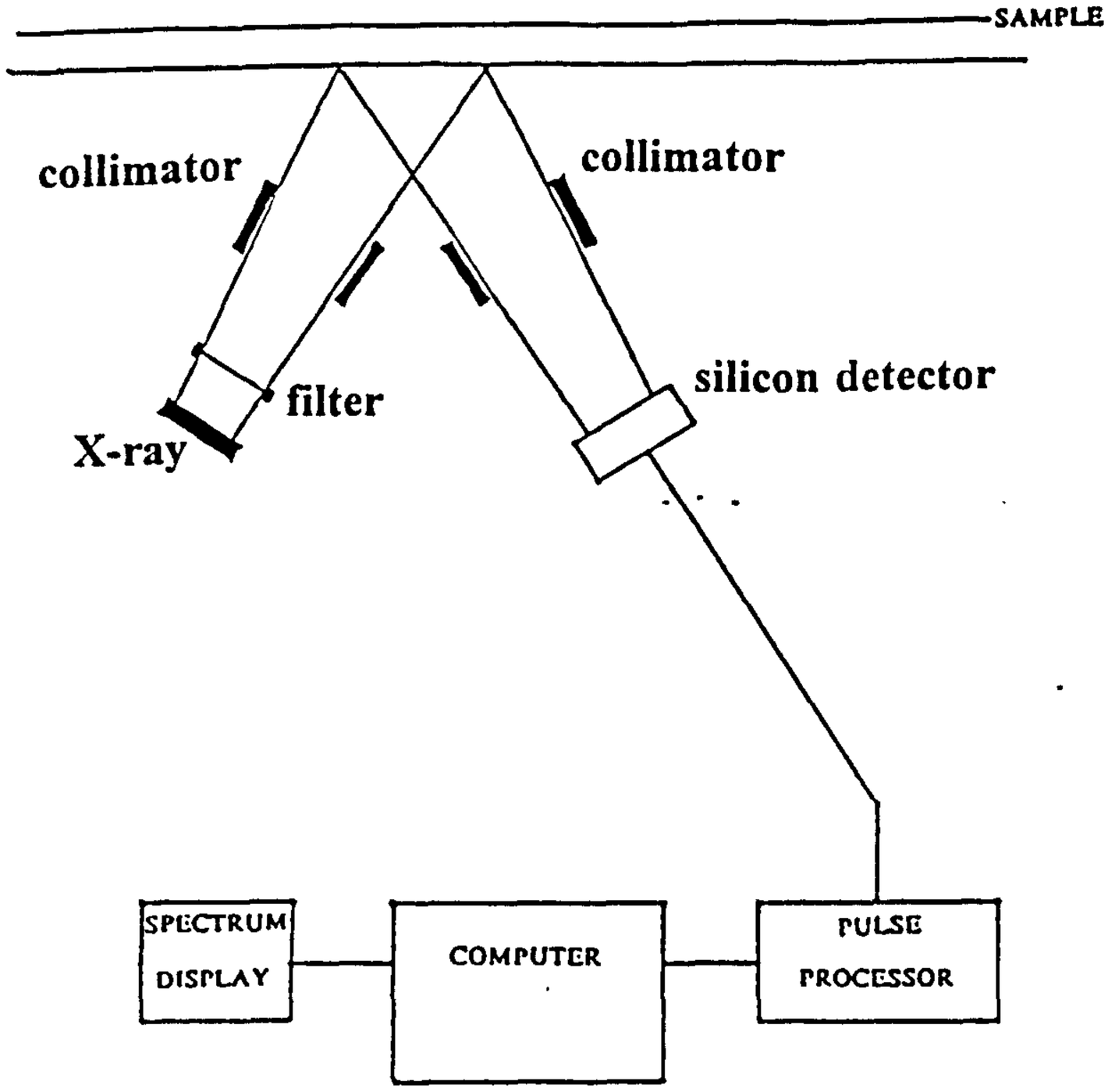

Figure 2.16: Schematic Diagram of the XRF System Used.

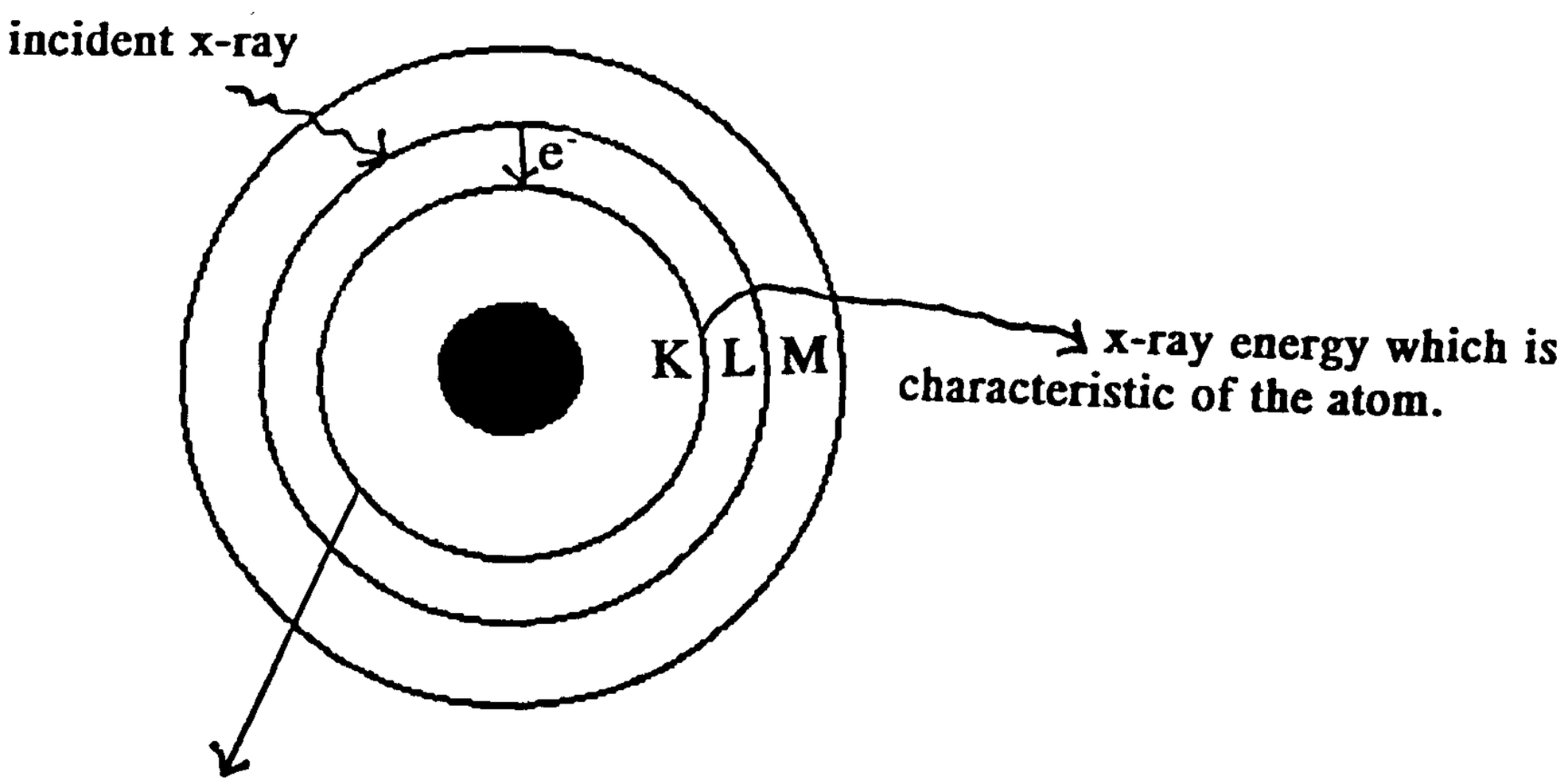

Figure 2.17: Electron Movement in Atoms undergoing XRF Analysis.

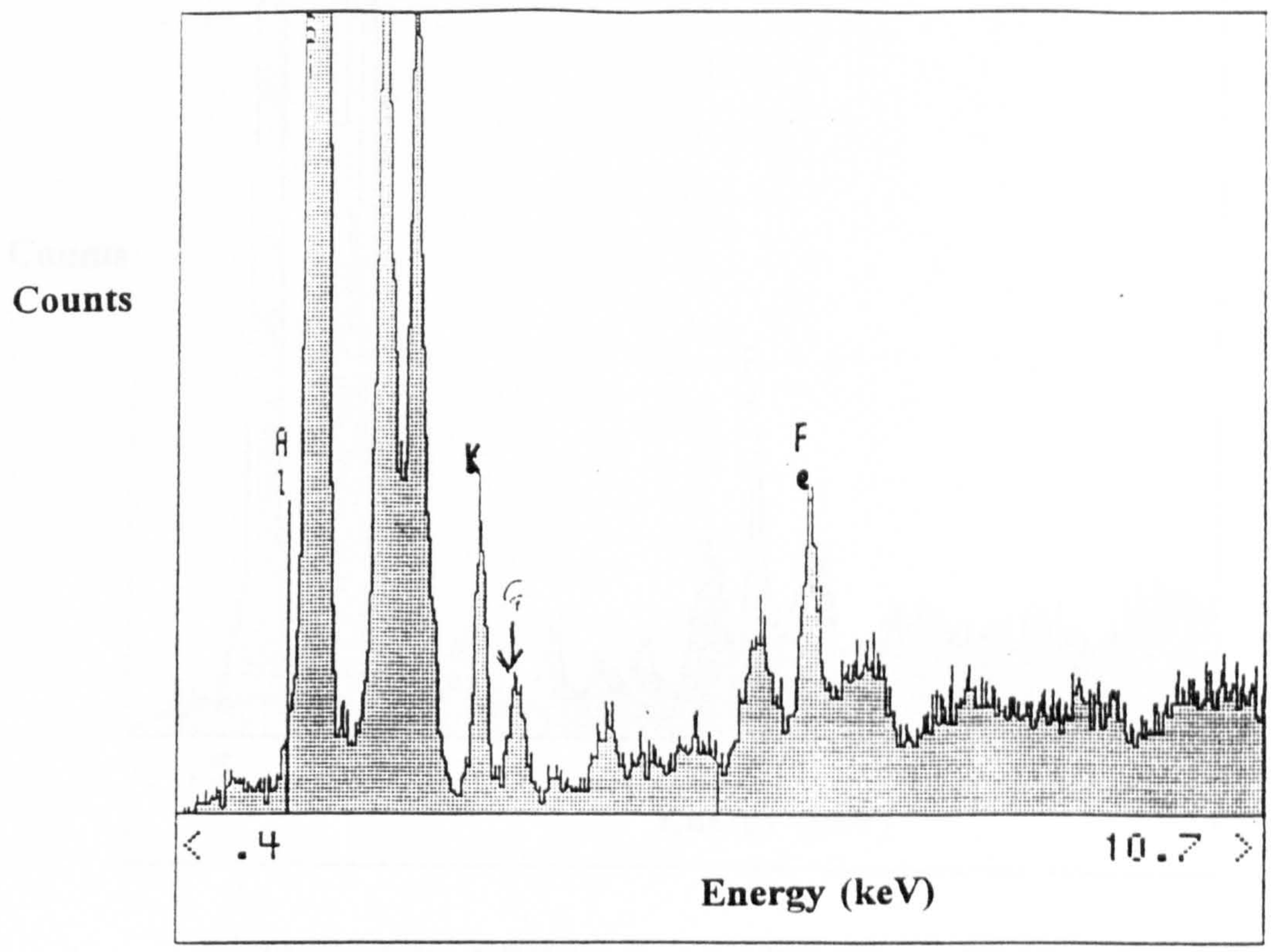

Figure 2.18: XRF Analysis of Quartz as Received

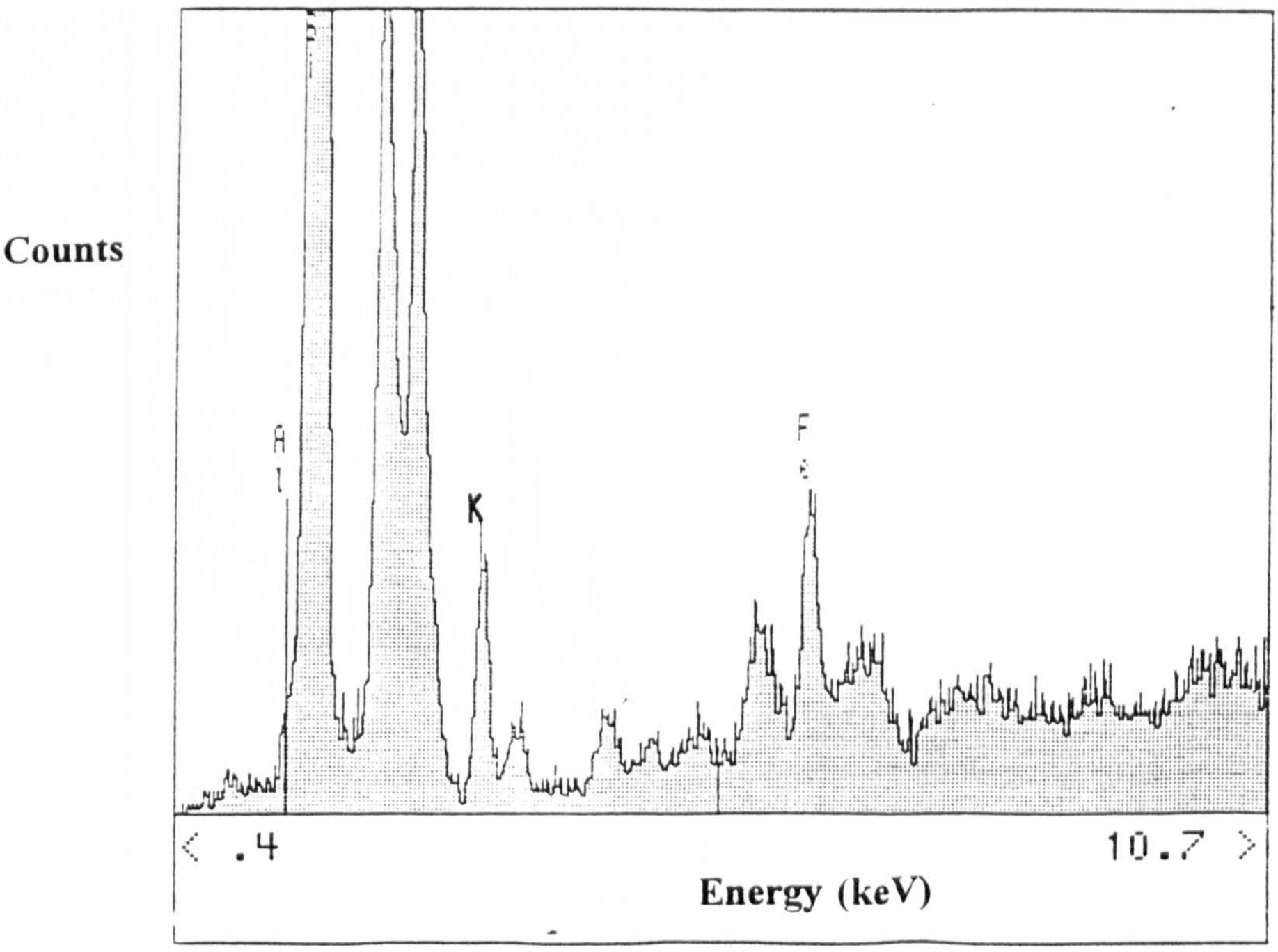

Figure 2.19: XRF Analysis of QB

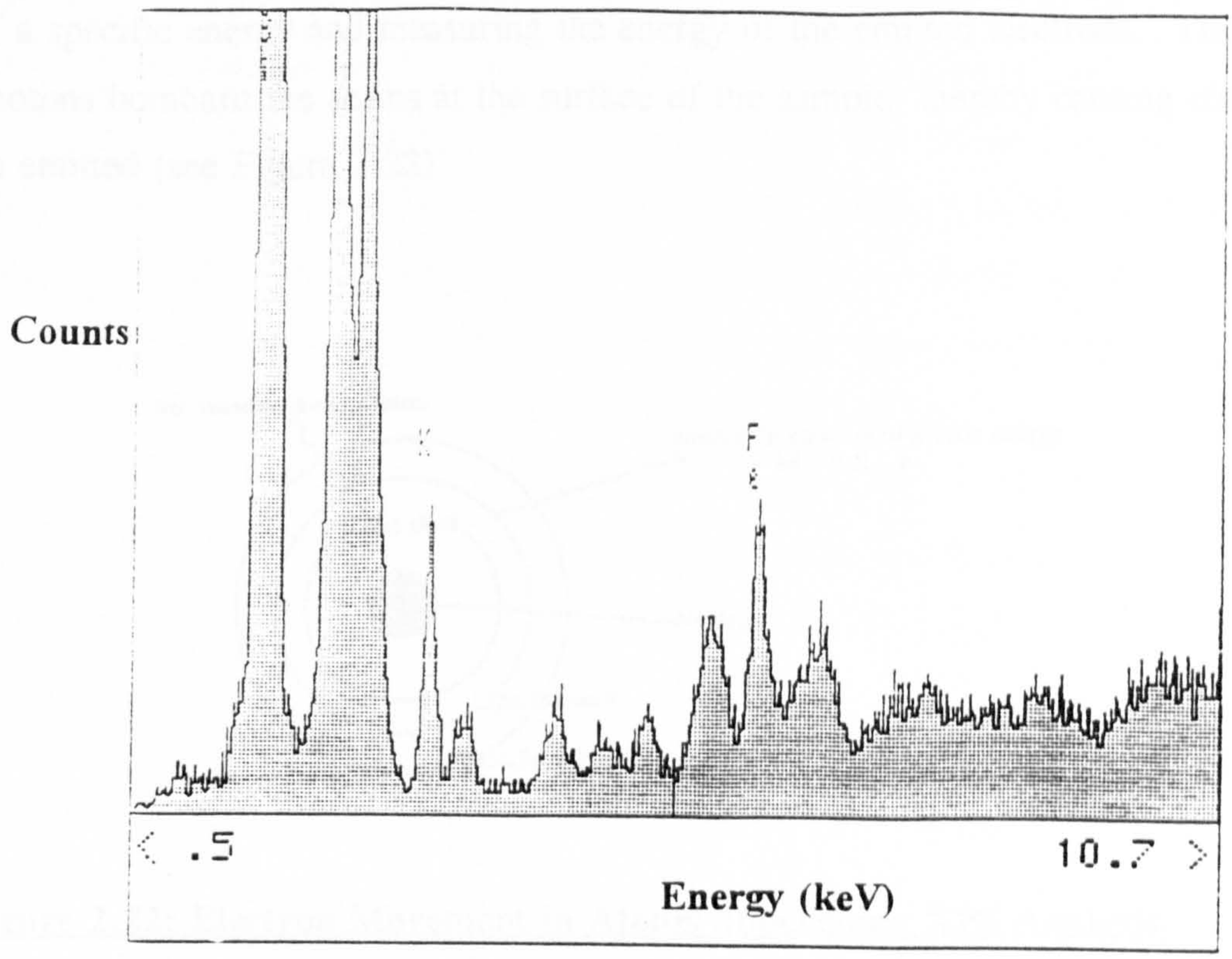

Figure 2.20: XRF Analysis of QC (1h at 1273K)

Figure 2.21: XRF Analysis of QC (16h at 1273K)

2.15 X-Ray Photoelectron Spectroscopy (XPS). Theory and Experimental Method.

Analysis of a surface by XPS involves irradiating a sample under vacuum with X-rays of a specific energy and measuring the energy of the emitted electrons. The X-ray photons bombard the atoms at the surface of the sample, thereby causing electrons to be emitted (see Figure 2.22)

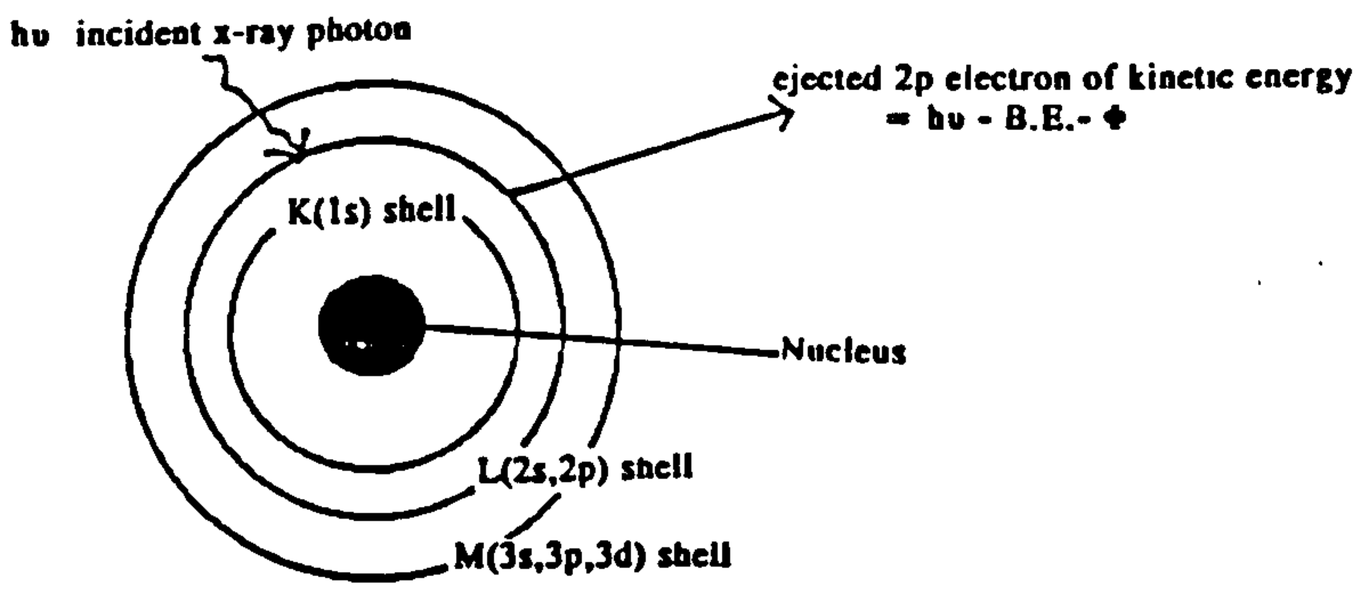

Figure 2.22: Electron Movement in Atoms undergoing XPS Analysis.

The probability of an electron being emitted from say the 2p orbital is different from the probability of electron emittence from the 3p orbital and so the spectrum obtained is a plot of the number of electrons from a spectral line (1s, 2s, 2p etc) vs. their kinetic energy. Each element has a characteristic spectrum from which quantitative data can be obtained. The emitted electrons are detected according to their kinetic energy via an electron spectrometer. The electrons incident to the detector are scanned for different energies by an applied electrostatic field prior to the analyzer. Electrons are detected by a photomultiplier and the electron count for a given time and energy is recorded.

XPS was used to detect any impurities in the surfaces of the samples of quartz with a Fisons Surface Science (formerly VG Scientific) ESCAlAB 210 XPS Spectrometer instrument. The quartz surfaces were analysed as received. The apparatus was calibrated every 2-3 months using either copper, silver or gold foil standards.

2.16 Experimental and Results.

Figures 2.23-2.26 show XPS spectra received for the quartz samples. The peaks marked are from elastically scattered electrons which have lost no energy in reaching

the analyzer. The steadily rising background is due to inelastically scattered electrons which have lost energy on emergence from the sample. The sharp peaks to the left of the spectra are photoelectron lines. To the right of each spectrum lie the broader "Auger" lines which are due to Auger emission. The small peak to the left of the main carbon and oxygen photoelectron lines are due to X-ray satellites, which are formed when the X-ray source is non-monochromatic and has some minor components at higher energies. The broader peaks to the right of the main carbon and oxygen peaks are called energy loss lines and are due to electron-electron interactions which set up bulk and surface electron oscillations known as 'surface plasmons'. Table 2.2 shows the atomic percentages for each atom present in the sample surface. These values are calculated by the software, which takes the raw intensity and, after treating with an instrumental transmission factor (=-1.04 at Brunel), divides this intensity value by a "sensitivity factor" (32).

As can be seen from the values set out below, the C/Si ratio appears to be reduced by heat treatment and to a lesser extent by acid washing. The carbonaceous material could originate from carbon residue on the sample (either atmospheric hydrocarbon material or an idiosyncrasy of the pumping system in the X-ray photon spectrometer) and/or the presence of carbonaceous material on the tape upon which the quartz was mounted. In any case this carbon layer is efficiently removed by heat treatment.

The XPS analysis also shows the O^{2-}:Si^{44} levels to fall with both acid washing and heat treatment.

Table 2.2: Atomic Ratios determined by XPS.

SAMPLE	Si_{2s}	C_{1s}	O_{1s}	C/Si	O/Si
QA: Quartz as received	9.9	58.3	31.6	5.89	3.19
QB	11.4	54.5	34.1	4.78	2.99
Quartz calcined at 1273K for 1h	15.9	41.3	42.5	2.60	2.67
QC: Quartz calcined at 1273K for 16h	23.17	15.2	61.61	0.66	2.66

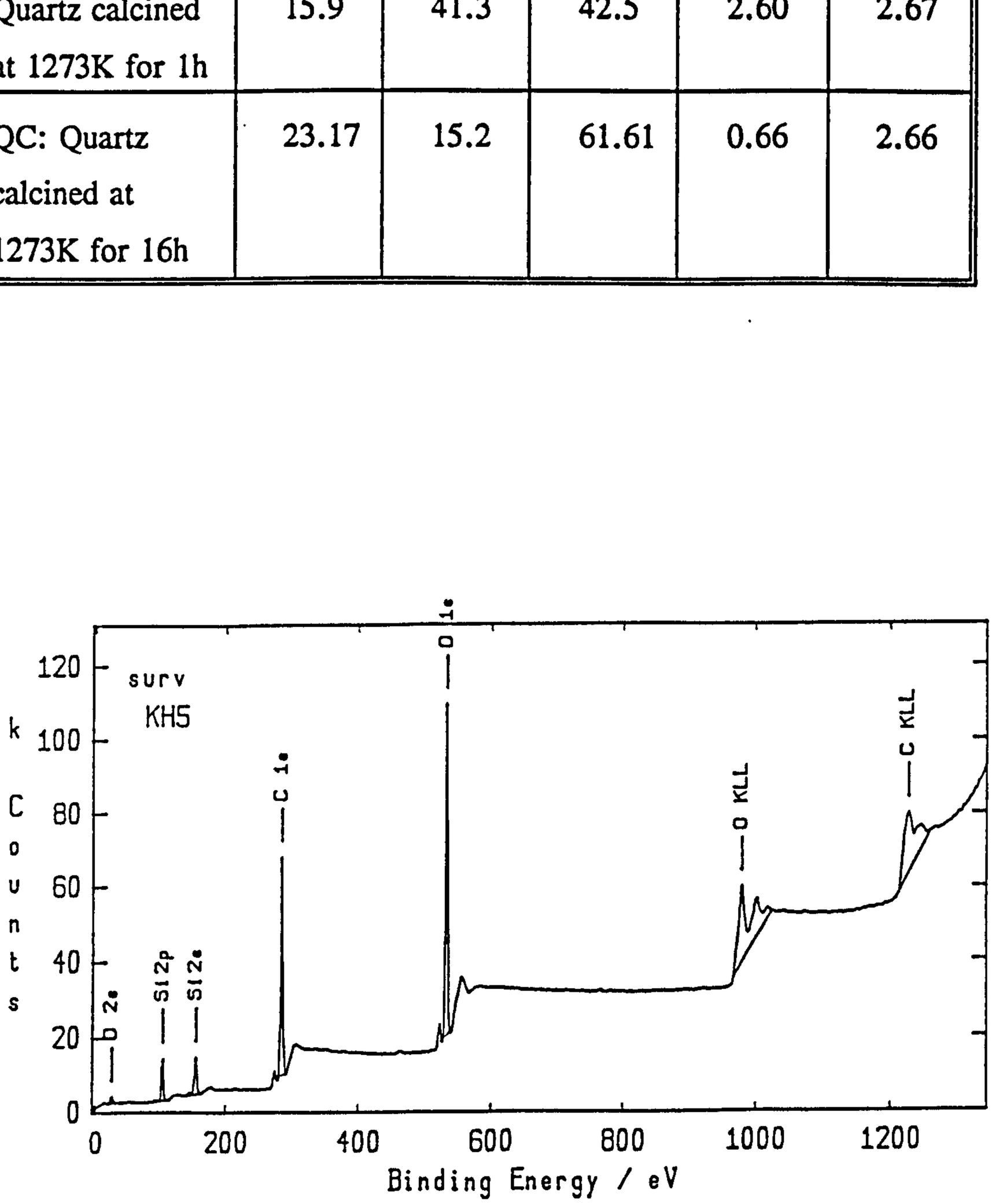

Figure 2.23: XPS Analysis of Quartz as Received.

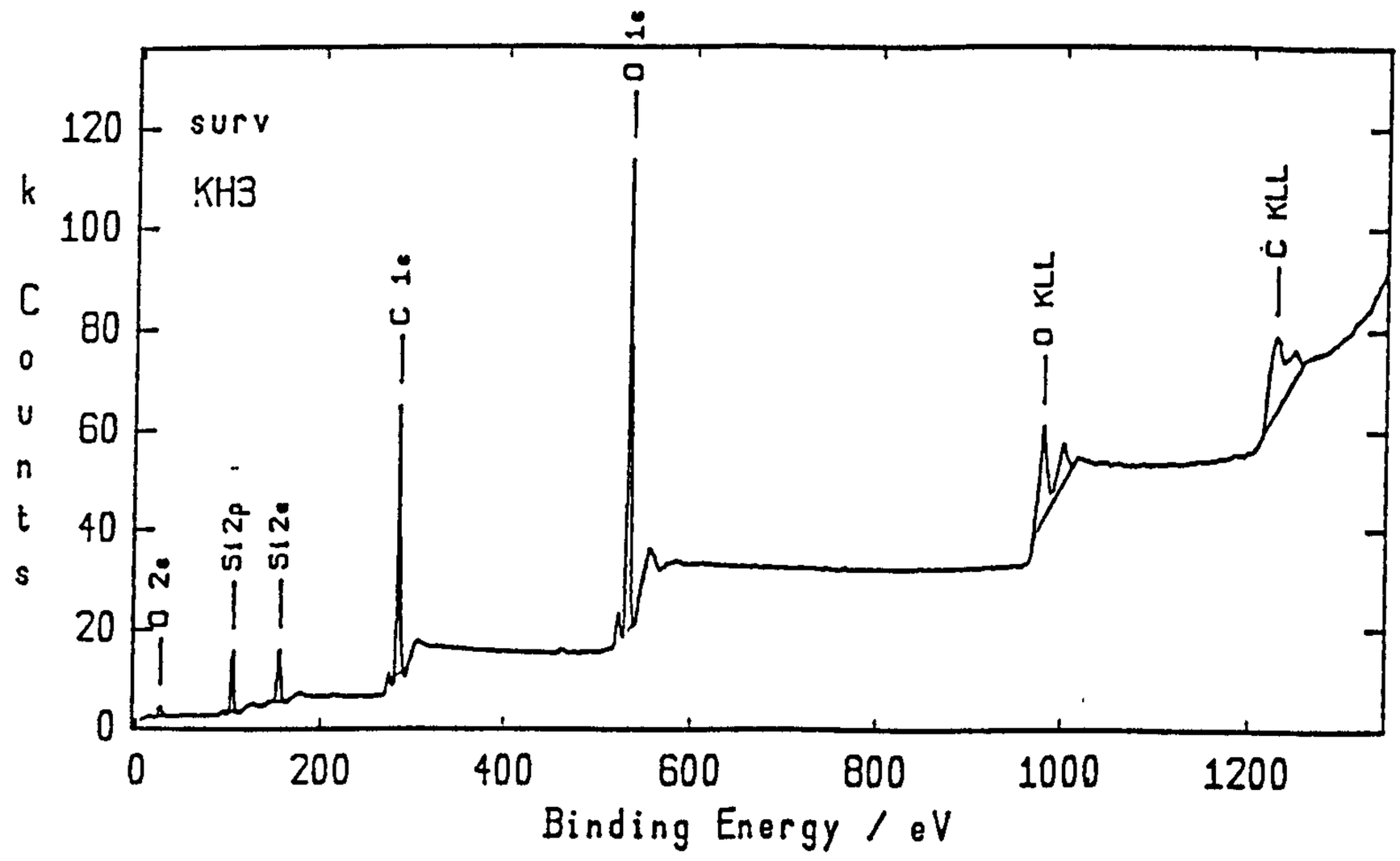

Figure 2.24: XPS Analysis of QB.

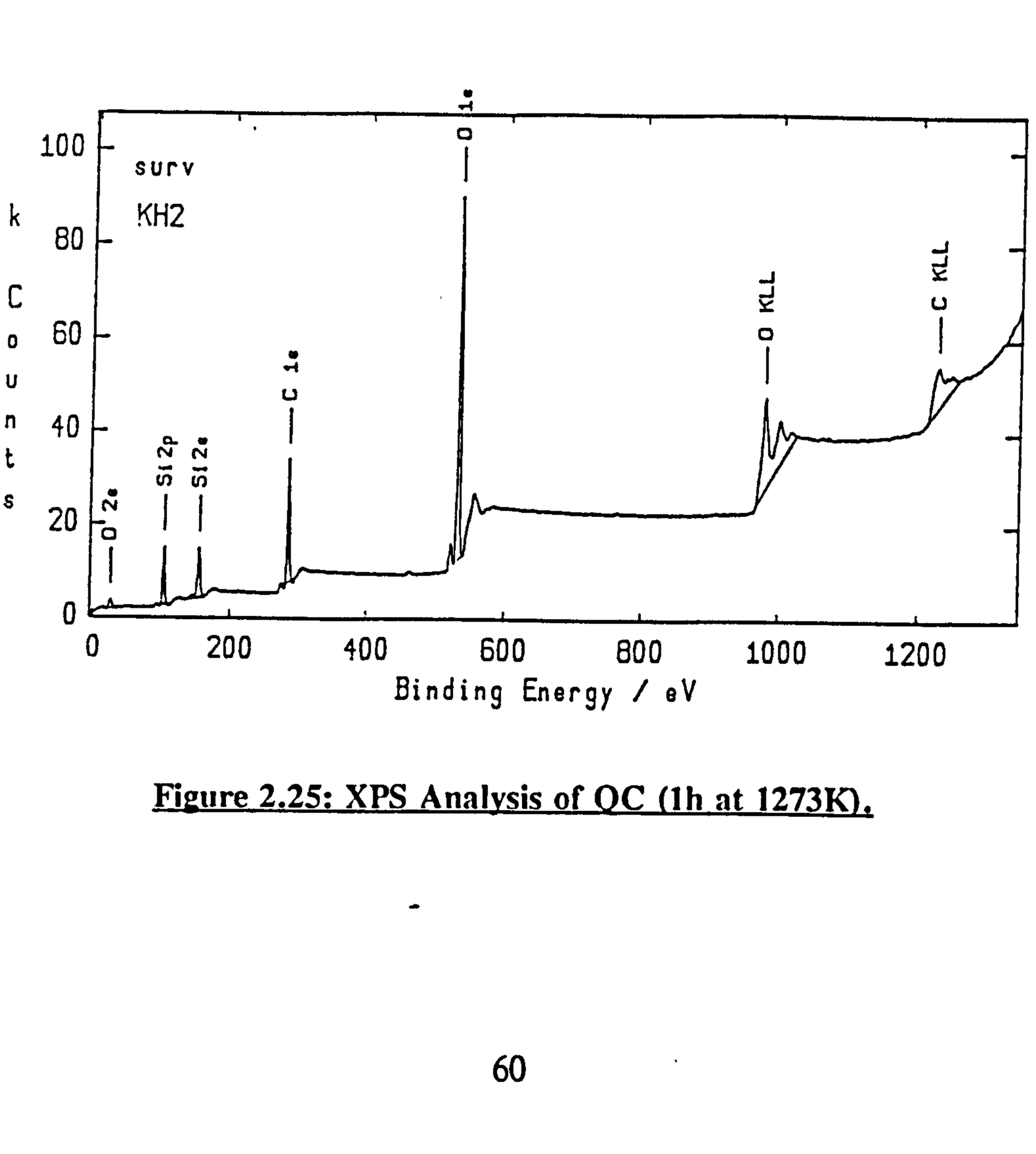

Figure 2.25: XPS Analysis of QC (1h at 1273K).

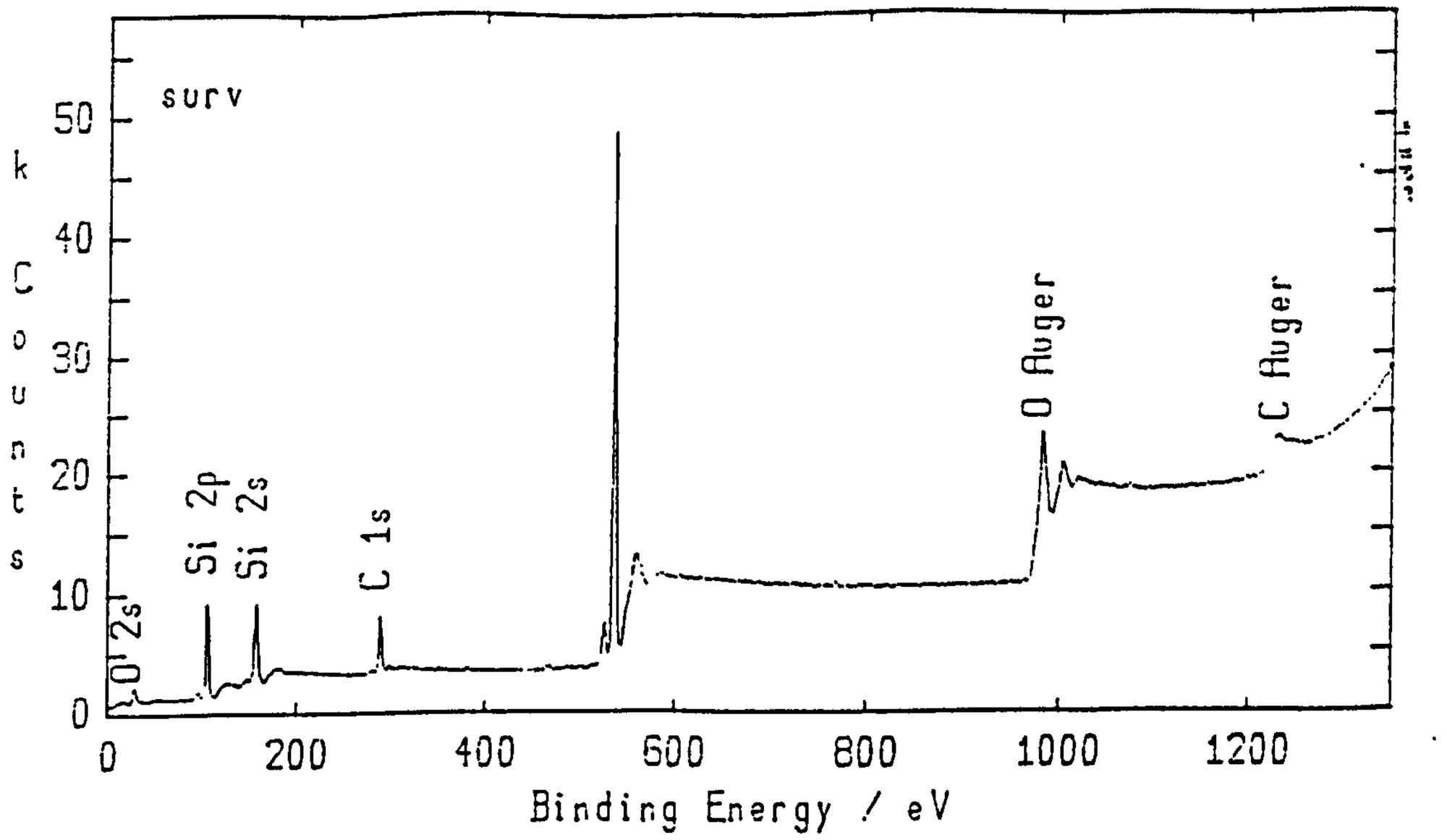

Figure 2.26: XPS Analysis of QC (16h at 1273K).

2.16 Scanning Electron Microscopy, Theory and Experimental Method.

The scanning electron microscope (SEM) permits the observation and characterisation of organic and inorganic materials and surfaces at the μm or sub-micron level. The sample is irradiated with a focused electron beam either statically or in a sweeping motion across the surface. Many signals are produced upon this irradiation, namely, secondary electrons, backscattered electrons, Auger electrons and X-rays characteristic of the specimen. The SEM uses signals obtained from the secondary and backscattered electrons as these vary with surface topography as the beam sweeps across the surface. The secondary electron emission allows high resolution images to be obtained since the emission originates from the impact area of the beam. Figure 2.27 shows a schematic drawing of a SEM.

The electron source or gun produces a beam of electrons whose diameter is too large to produce a sharp image at high magnification. The lenses are used therefore to reduce the diameter and thereby place a finely focused electron beam onto the specimen. The electron beam will usually generate a spot size of less than 10nm on the sample surface (33). The beam then interacts with the surface and generates signals which can be used to form an image. In order to produce an image on the display unit the beam-sample interaction is measured from point to point across the surface. This is achieved

by controlling the electron beam movement by using two pairs of electromagnetic deflection coils. One pair bends the beam back onto the axis. The magnification of the image is the ratio of the size of the image on the viewing screen to the size of the irradiated section of the surface. The signals generated from the electron beam interaction with the sample are made up of secondary electrons and backscattered electrons as previously described; an Everhart-Thornley (E-T) electron detector is used to collect the signals. Figure 2.28 shows a diagram of the E-T electron detector. The screen in front of the collector is held at a voltage of approximately +300V which draws the electrons towards it and on into the scintillator which is itself at a voltage of +12kV. The highly energetic electrons strike the scintillator material and light is produced which travels to a photomultiplier via a light pipe. The light is then converted to an amplified signal which varies according to the incoming electron signal as the beam crosses the specimen surface. A camera records the image via a second cathode ray tube.

SEM was used to examine the changes in surface or pore structure of the silica samples, if any, with heat treatment. The samples were made up into an aqueous suspension and a small droplet of this mounted onto a specimen stub. The samples were then dried in a clean, low temperature oven and once dry were sputter-coated with gold. This practice of coating the sample with a conductive layer is used to prevent build-up of electrons on the surface; electron accumulation occurs on non-conducting materials due to the lack of a conductance to ground.

2.17 SEM Results.

Figures 2.29 and 2.30 show the electron micrographs obtained for QB at increasing magnification. Figures 2.31 and 2.32 show the micrographs obtained for QC which had been calcined for 16h at 1273K. In all cases, the silica appeared non-porous and particle sizes varied from the sub-micron level up to 6μm. The surface structure and particle morphology of the silica appeared to be unaffected by heat treatment.

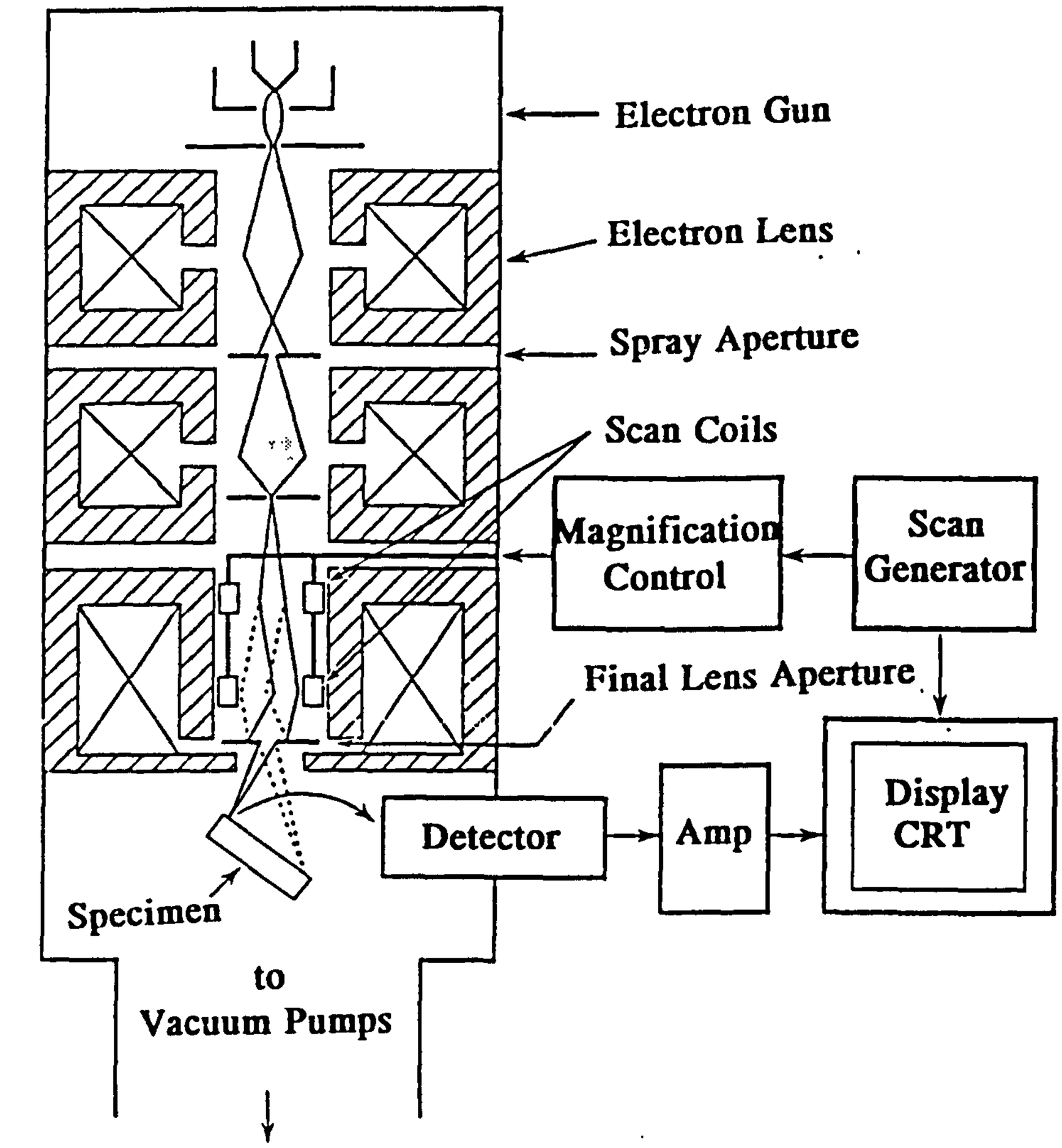

Figure 2.27: The Scanning Electron Microscope.

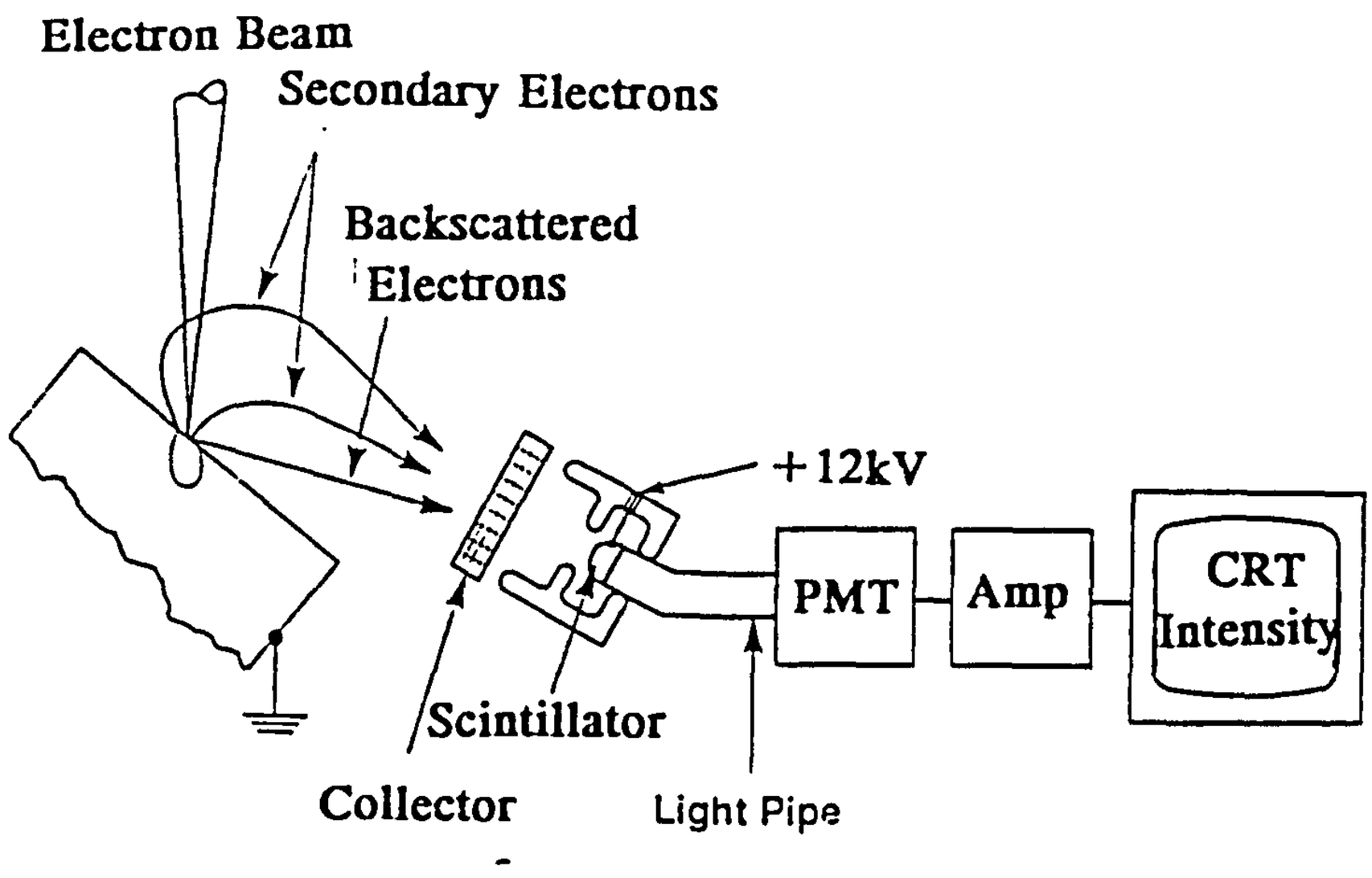

Figure 2.28: The Everhart-Thornley Electron Detector.

Figure 2.29: SEM Image of QB (x4000, 4mm=1μm).

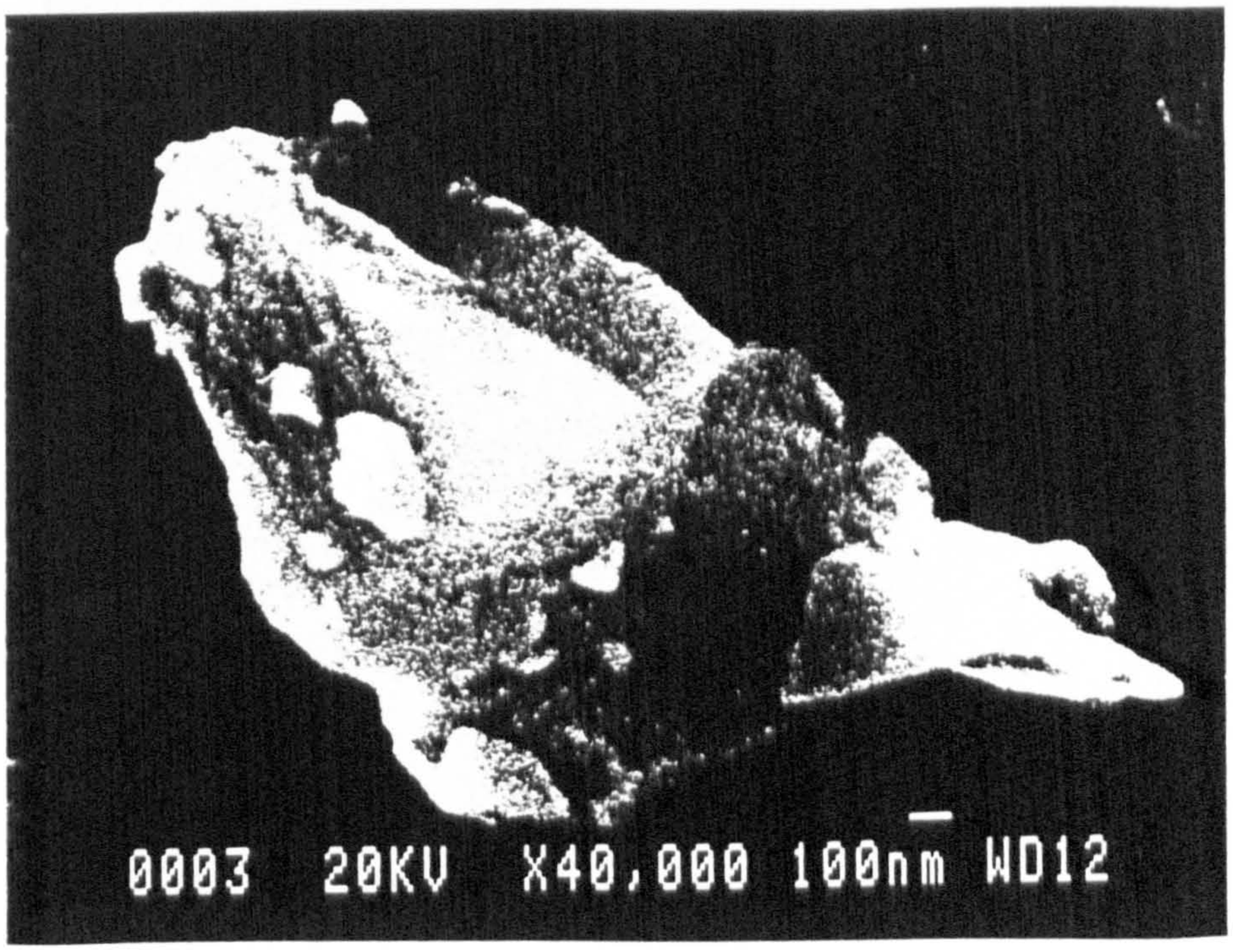

Figure 2.30: SEM Image of QB (x40000, 4mm=100nm).

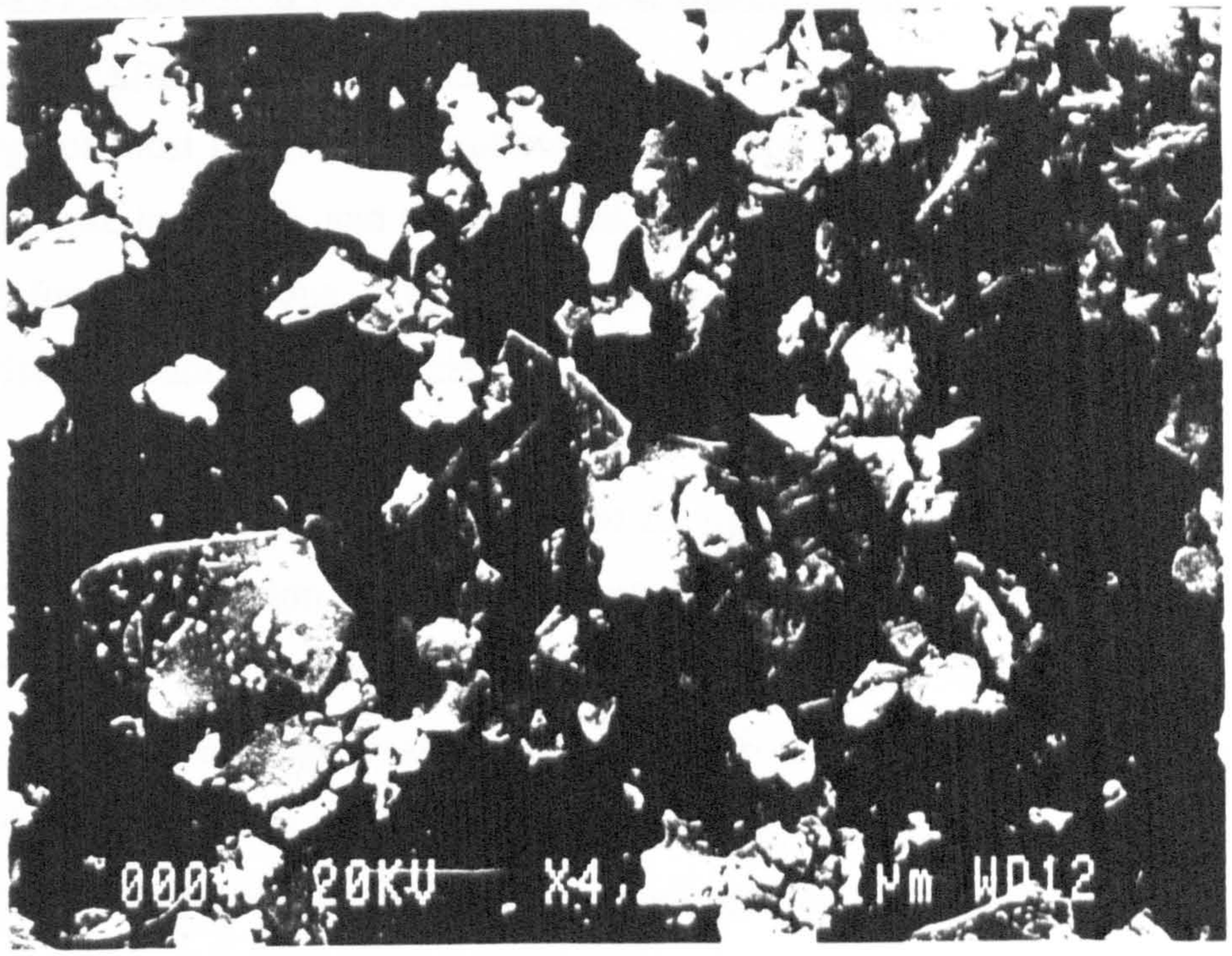

Figure 2.31: SEM Image of QC (16h at 1273K, x4000, 4mm=1μm).

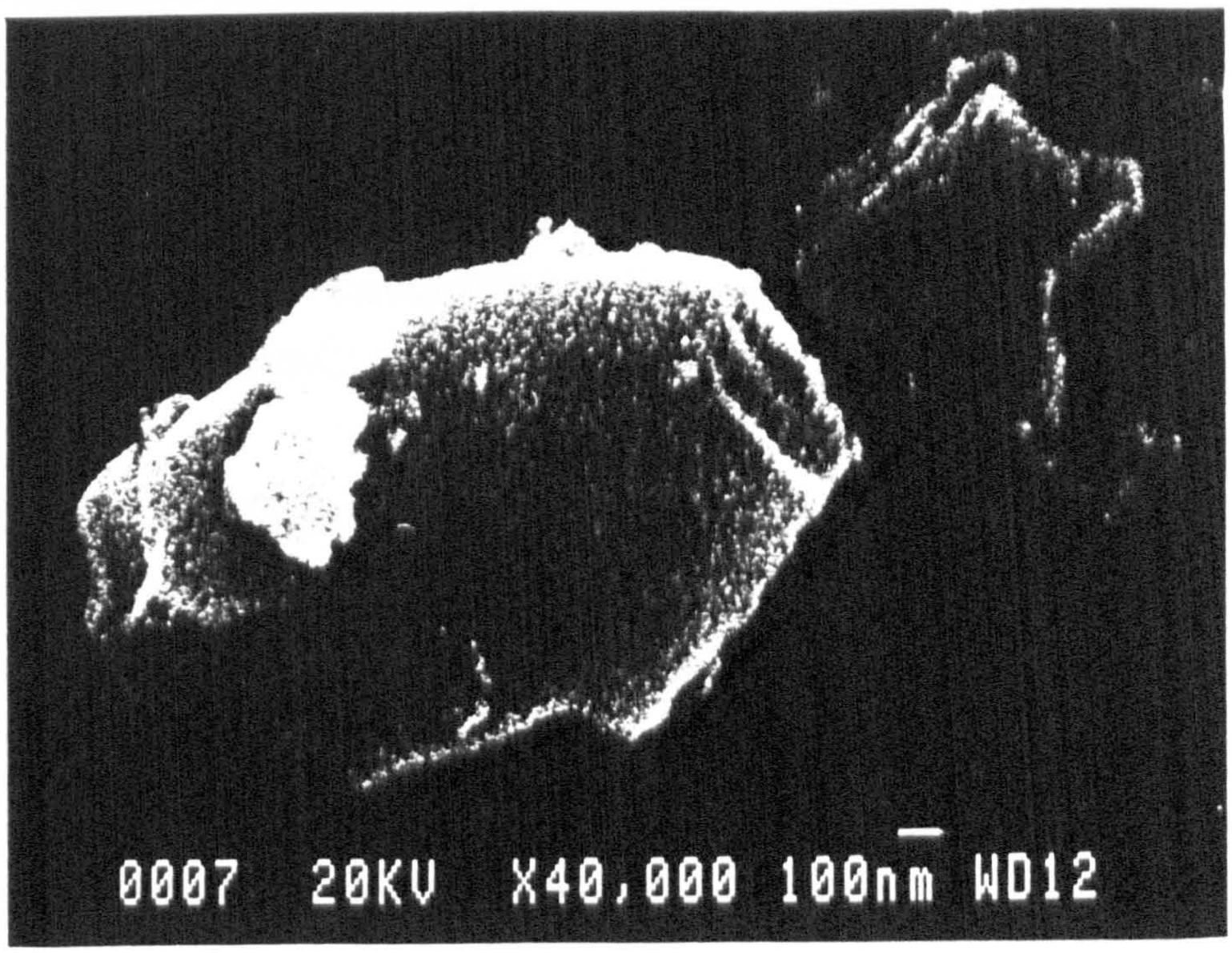

Figure 2.32: SEM Image of QC (16h at 1273K, x40000, 4mm=100nm).

2.18 Fourier Transform Infra-Red (FT-IR) Spectroscopy.

Theory and Experimental Method.

The energy of most molecular vibrations corresponds to that of the IR region of the electromagnetic spectrum, and these vibrations have frequencies that are characteristic of certain functional groups. Thus groups of molecules can be identified by their characteristic vibrational frequencies.

The IR spectrometer consists of a source of IR light which is split into two beams of equal intensity. One beam is passed through the sample under examination and if a sample molecule vibrates with a frequency within the region of the source range of frequencies, then the sample may absorb energy from the source beam. The spectrum is scanned by comparison of the two beam intensities and consists of a chart showing absorption of IR light versus the inverse wavelength or frequency.

The method of Fourier transform analysis uses a beam of IR radiation which is split into two. The beams are passed through the sample with one beam traversing a longer path than the other. On recombination of the beams, an interference pattern occurs that is the sum of all the interference patterns at each wavelength. The difference between the paths of the beams is systematically changed and a signal is produced that varies with the path length. As the total signal is the sum of all of the sine waves for each frequency, Fourier transformation is used to separate out the component frequencies. A final spectrum of % transmission against frequency is obtained. FT-IR is much faster than straight forward IR spectroscopy since it is not necessary to scan each frequency individually.

Selection Rules for IR Absorption. For a molecule to absorb IR radiation, the molecule and radiation must interact, for this to occur the molecule must contain a fluctuating dipole, and hence an electric field which will then interact with the fluctuating electric field of the IR radiation. At room temperature, molecules are constantly vibrating; some vibrations are considered as vibrations of the whole molecule, whilst others are more localized. These localized vibrations are either stretching or bending, and are useful in the identification of certain functional groups.

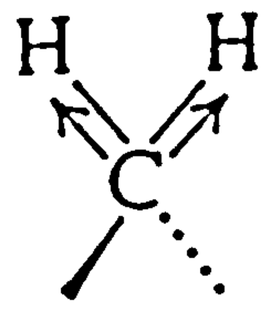

Symmetric

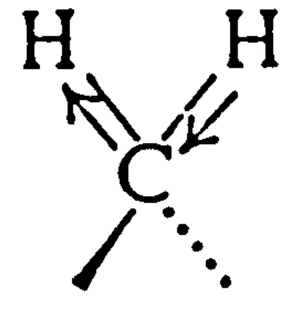

Asymmetric

Stretching.

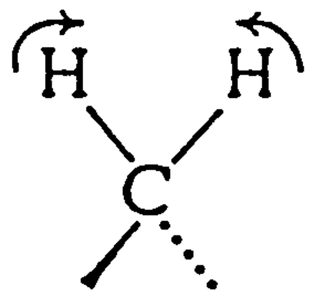

scissoring

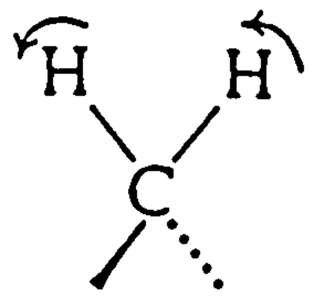

Rocking

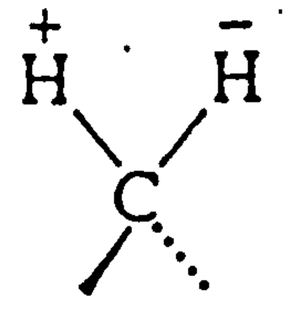

Twisting

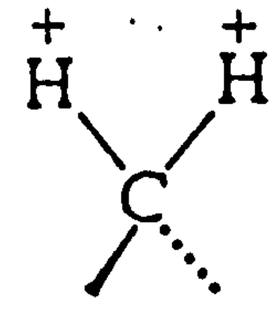

Wagging

Bending.

Stretching vibrations are larger than bending vibrations. Vibrations from the molecule as a whole give rise to bands at lower energies. Also, as the bond strength increases, so the frequency increases. Overtone bands occur at multiple frequencies of strong bands (e.g. a strong band at 800cm^{-1} may have an overtone at 2400cm^{-1}). Combination bands, as their name suggests, are the result of interaction between two or more bands.

The quartz samples were prepared by pressing into a KBr disk and the analysis of the quartz in this form was carried out using a Perkin Elmer 1710 FT-IR spectrometer in transmission mode. The KBr used was kept in a dry atmosphere and only removed for disk pressing. In order to discuss the results obtained from FT-IR, it is necessary to describe the structure of the quartz surface. There are several differing types of hydroxyl group on the surface of quartz:

(A)

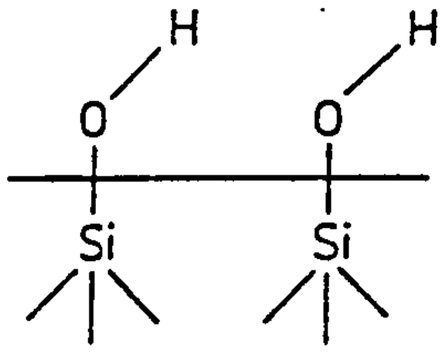

(B)

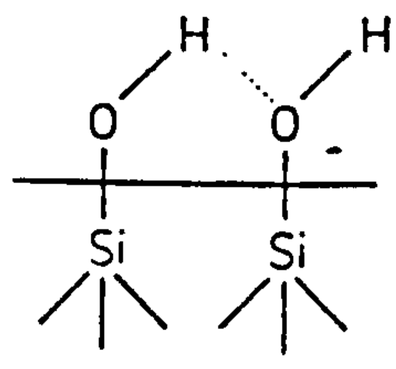

(C)

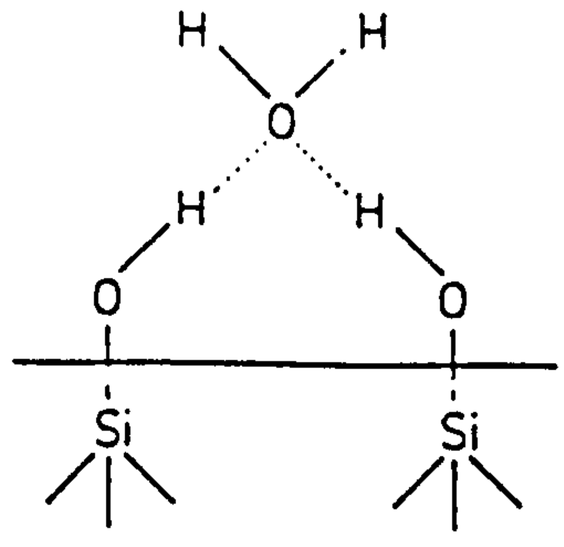

(A) shows free hydroxyl groups that are isolated on the quartz surface and are separated by a distance of 0.31nm (34). (B) shows bound or vicinal hydroxyl groups that have O-O distances of <0.31nm; these groups are hydrogen-bonded together. (C) shows the state of a "wet" sample, water becomes hydrogen-bonded to the hydroxyl groups on the quartz surface. Table 2.3 shows the bands for certain significant functional groups.

Table 2.3: Wavenumbers of Significant Bands for Silica Samples.

GROUP	BAND /cm^{-1}	REMARKS
Si-O	1110-1000 900-600	
Si-H	2550-2090 1010-700	
water in solution	3710	
free -OH	3690 and 3620	sharp peak
H-bonded -OH	3600-3200	broad
water of crystallisation	3600-3100 1640-1615	weak bands

2.19 FT-IR Results.

Figures 2.33 and 2.34 show IR spectra of the quartz as received and QB. The large broad peak to the left hand side of each spectra is due to the presence of water in the sample and to the bound hydroxyl groups on the quartz surface. On the left of these broad bands sharper peaks can be seen, these are due to free hydroxyl groups on the surface of the quartz. The peaks to the right of each spectra are due to Si-O-Si stretching, Si-H stretching and the presence of water in the sample. Figure 3.35 shows the spectrum obtained for the QC. As can be seen, there did not appear to be any water or hydroxyl groups present in the sample, although there are some weak peaks present due to siloxane stretching.

Zhuravlev (35) studied the effects of heat treatment on the hydroxyl populations of various silicas. It was proposed that the hydroxyl population of all silicas lies in the

range of 4.2-5.7 OH groups nm^{-2} and is independent of the structural characteristics of the silica type; Nevskaia et al (36) also found a similar value (approximately 4.2 OH groups per nm^2) for untreated quartz. It is generally agreed that dehydroxylation of silica begins at 473K forming less polar siloxane groups:

$$2(Si\text{-}OH) \text{ converts to } Si\text{-}O\text{-}Si + H_2O$$

After being heated to temperatures of approximately 673K the hydroxyl population is reduced to 0.5 and the sample is free of physically adsorbed water. When the sample is heated to 1373K, there is almost complete removal of hydroxyl groups from the surface of the sample. A sample displays maximum surface activity if it is fully hydroxylated and is free of physically adsorbed water. As the sample shown in figure 2.35 was calcined at 1273K, it can be assumed from the IR spectrum obtained that the hydroxyl population on the surface was negligible.

Figures 2.36 and 2.37 show spectra obtained for QC samples that were tumbled in distilled water for 6 and 24 h respectively. It can be seen that there is a slight return of a peak at approximately $3400cm^{-1}$ that indicates the presence of water and bound surface hydroxyl groups. It was not possible from these spectra to observe the presence of free hydroxyl groups on the quartz surface.

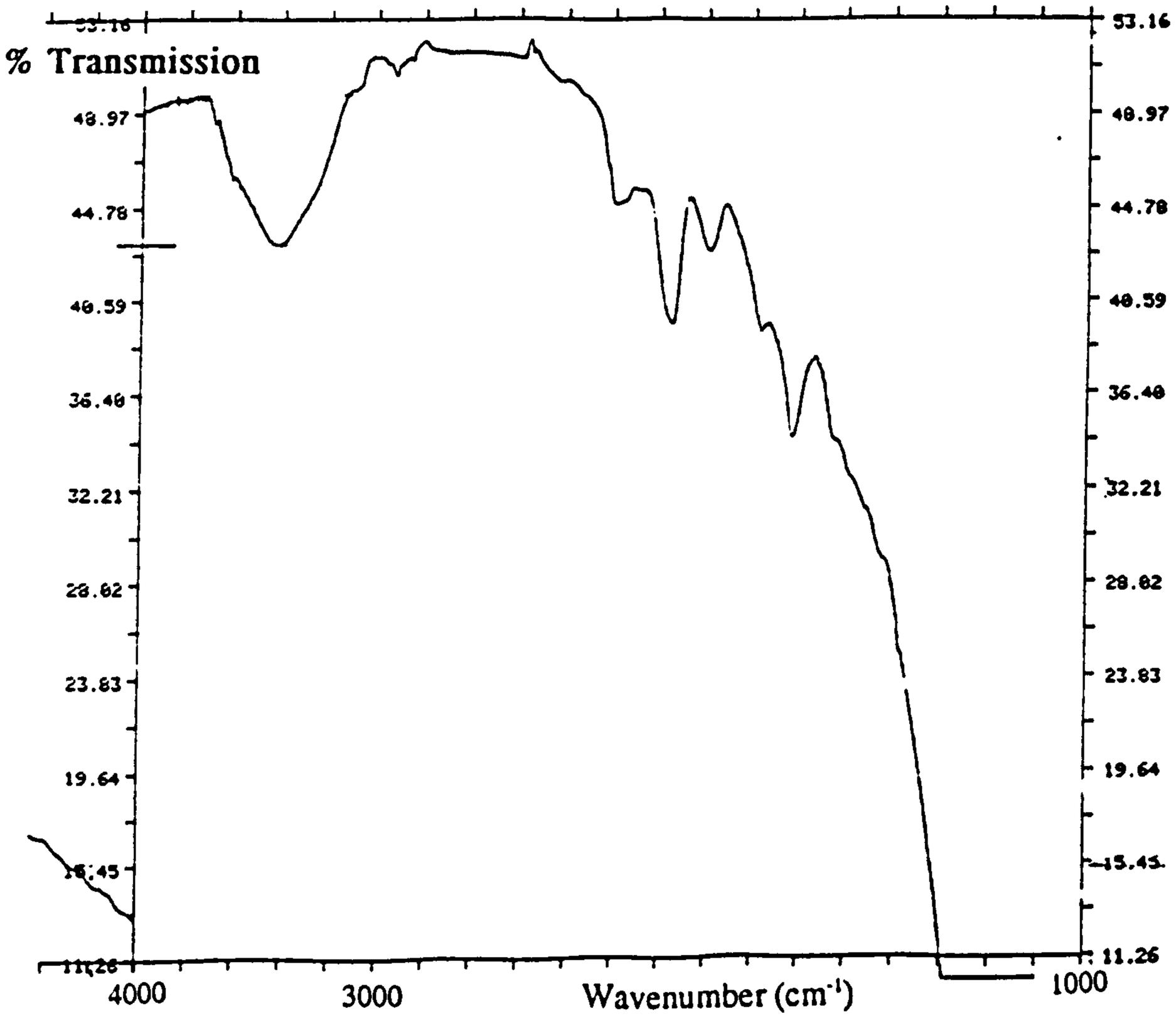

Figure 2.33: FTIR of Quartz as Received.

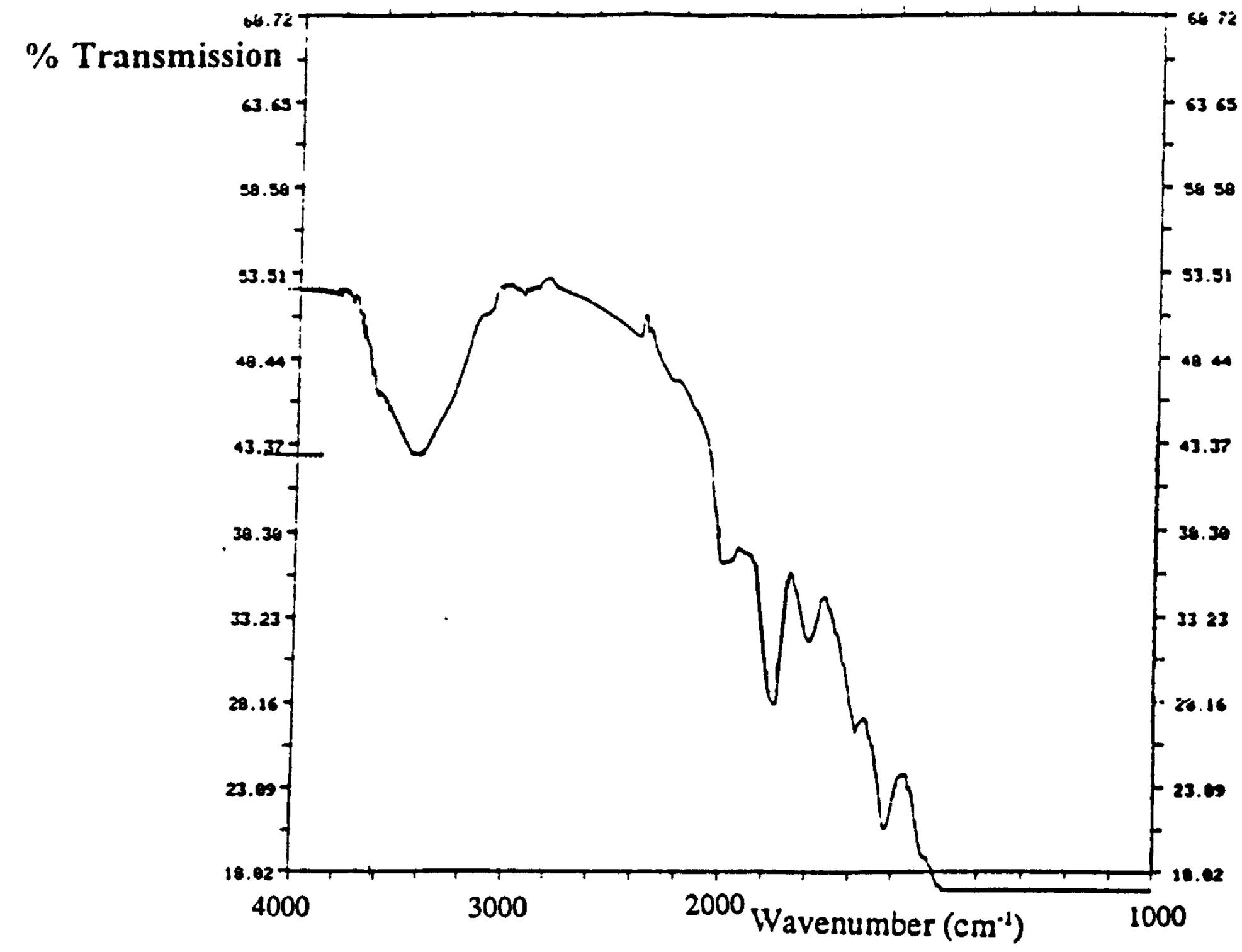

Figure 2.34: FTIR of QB.

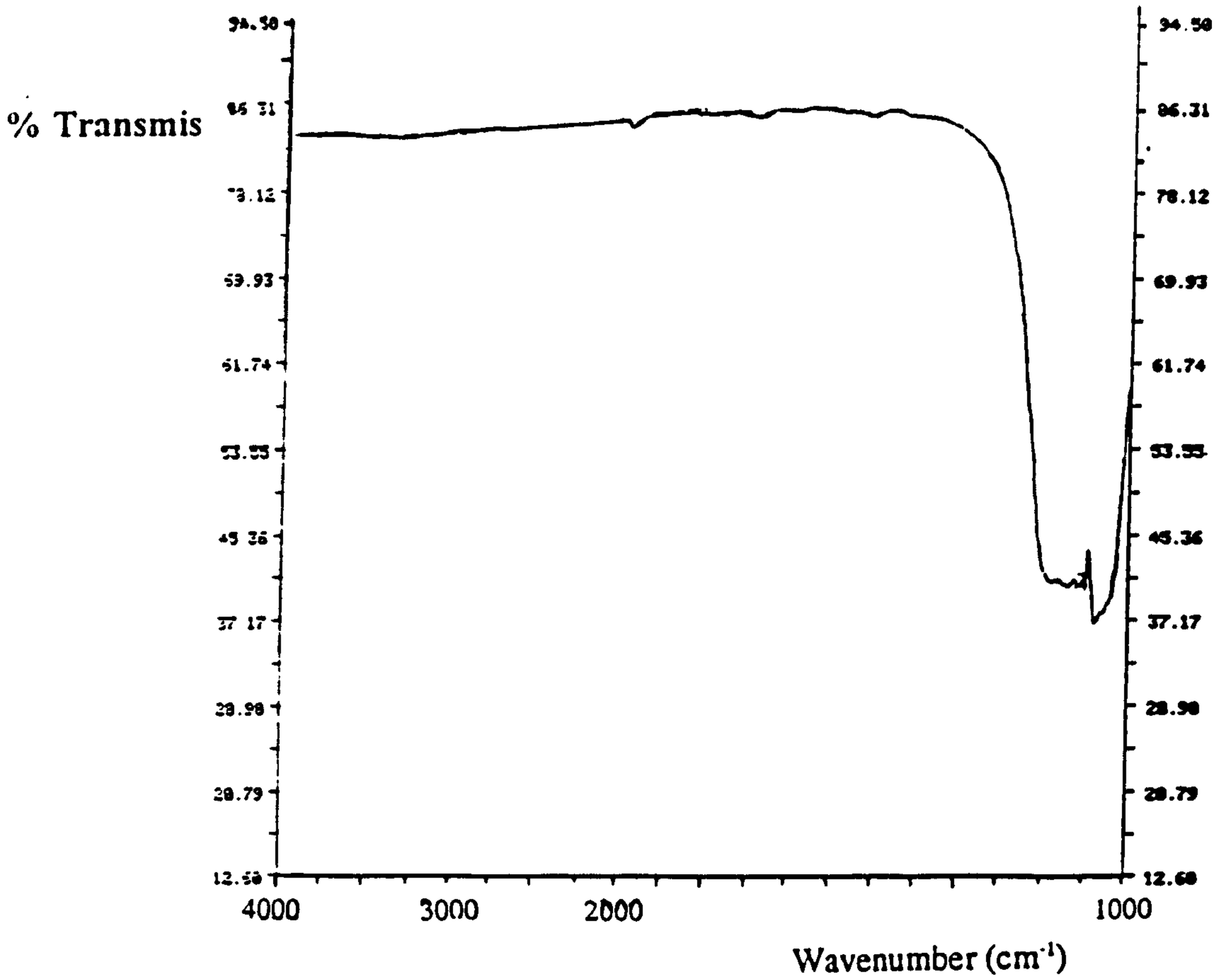

Figure 2.35: FTIR of QC (16h at 1273K).

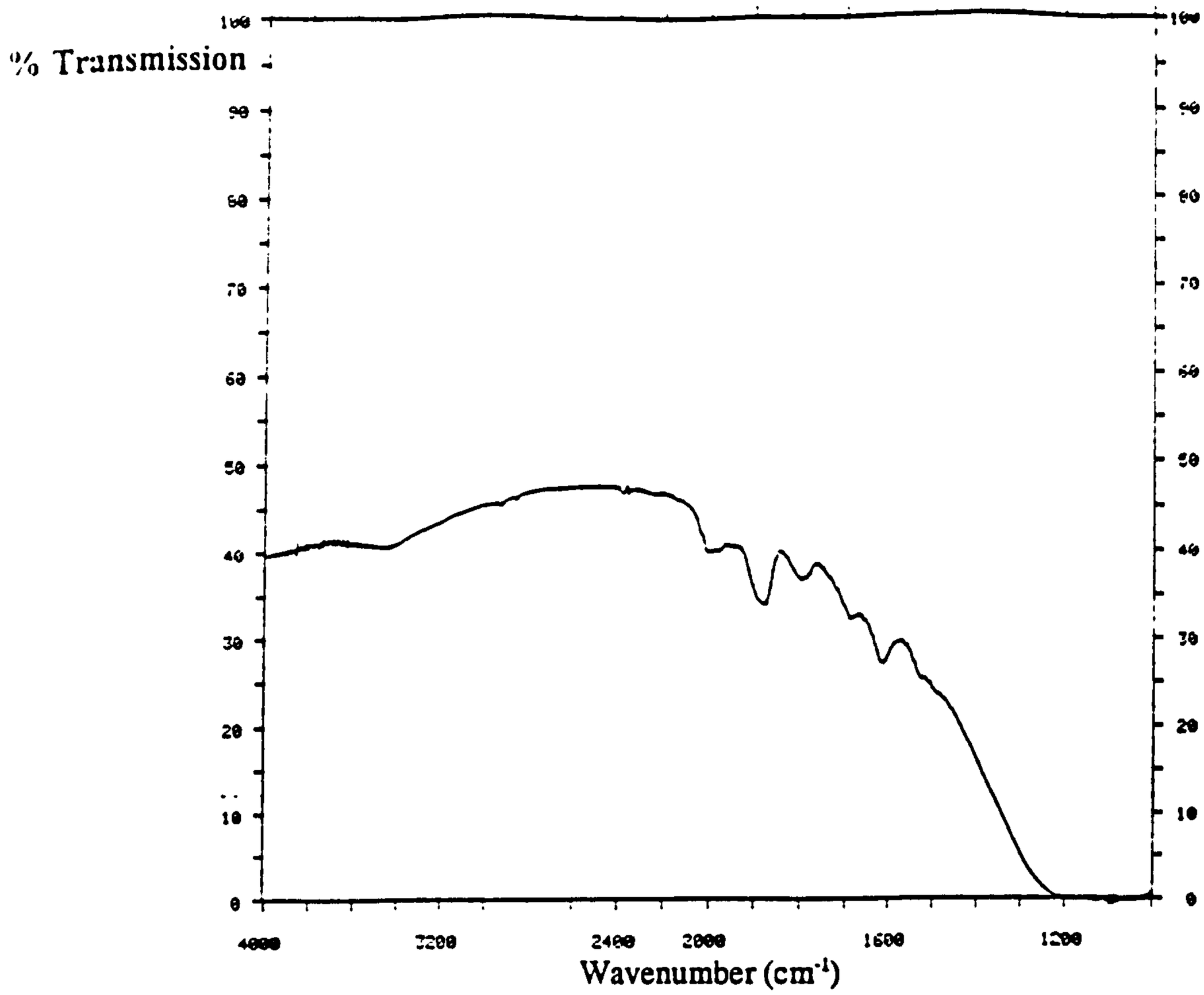

Figure 2.36: FT-IR Analysis of QC (16h at 1273K), tumbled in distilled water for 6h.

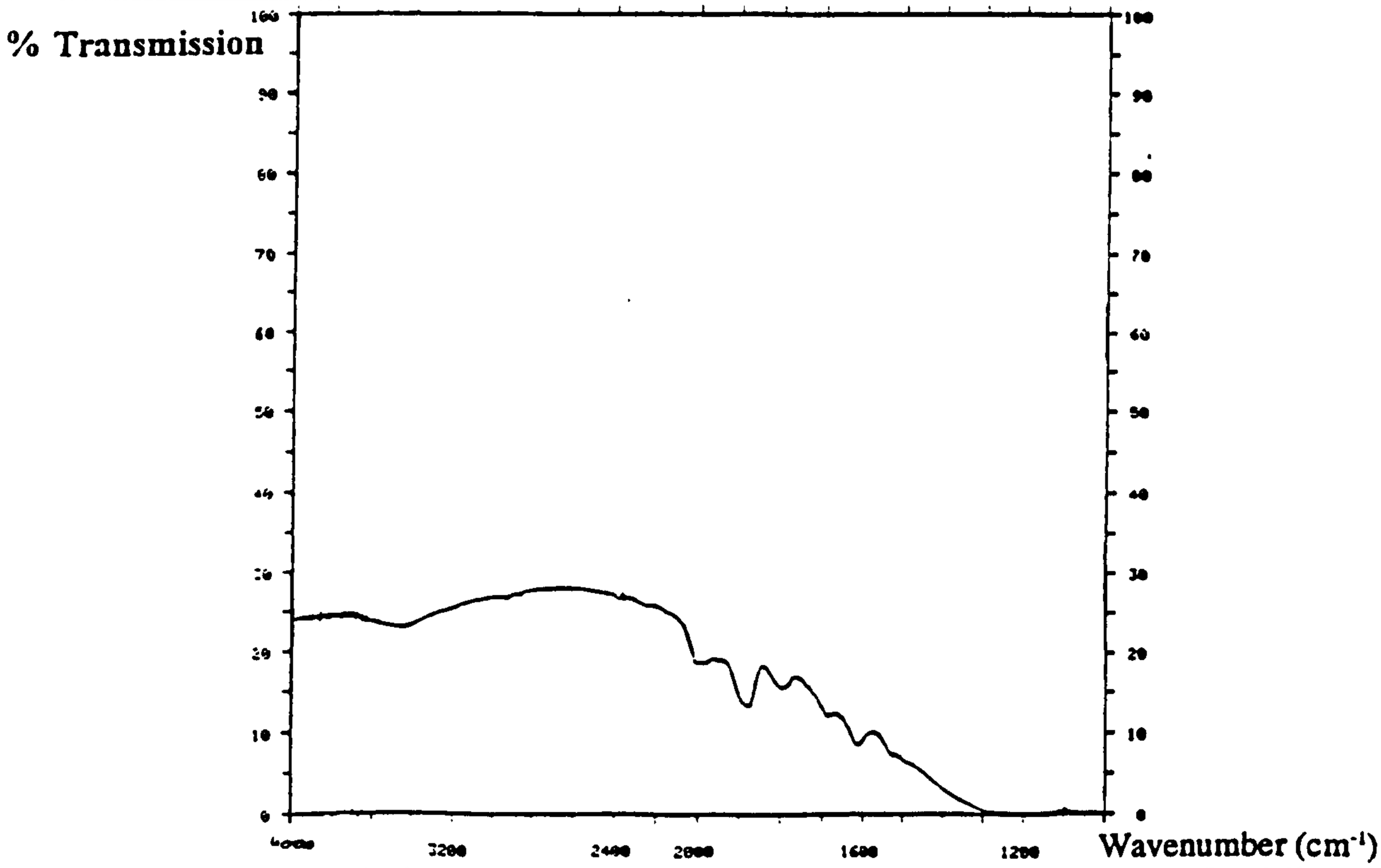

Figure 2.37: FT-IR Analysis of QC (16h at 1273K), tumbled in distilled water for 24h.

FT-IR analysis on the quartz samples using a microscope that was connected to the FT-IR spectrometer was performed; this technique allows the quartz to be analyzed without the presence of KBr or other impurities. Figures 2.38 and 2.39 show the spectra obtained for quartz as received and QB respectively. The spectra display absorption bands in similar positions to the spectra measured in transmission. Again, the large peak at approximately 3600 cm^{-1} is due to the presence of water and hydrogen-bonded hydroxyl group and is present in both spectra. The peaks due to free hydroxyl groups and bound hydroxyl groups seem to be more clearly visible on these spectra as long, sharp peaks that shoulder the rather broad band at 3600cm^{-1}. Figures 2.38 and 2.39 show sharp peaks at 3750cm^{-1} that correspond to free, isolated hydroxyl groups; also present are peaks at 3690cm^{-1} which are indicative of isolated silanols that are interacting with impurities, these peaks are stronger than the ones corresponding to free hydroxyl groups for these samples. Figure 2.40 shows the spectrum obtained for QC, the presence of water is clearly visible in this spectrum when compared to the transmission spectrum but it is smaller than the band in the same position for the washed silica. There also seems to be some IR absorption corresponding to free hydroxyl groups and isolated, bound hydroxyl groups at 3750cm^{-1} and 3660cm^{-1} respectively. Figure 2.41 shows the spectrum measured for calcined quartz that was tumbled for 24 h in distilled water. The main broad peak at 3600cm^{-1} has not changed in size when compared to Figure 2.35.

Although the spectra obtained by IR measured using a microscope are not conclusive in a quantitative sense as to whether the hydroxyl groups, either free or bound, return on contact with water, they do seem to indicate the presence of isolated OH groups. The difference in the spectra, however, are not clear enough for one to use them to carry out quantitative analysis. The only obvious point that one can conclude from these spectra is that the bound hydroxyl groups disappear upon calcination of the silica sample and seem to reappear slightly when the sample is re-emersed in water.

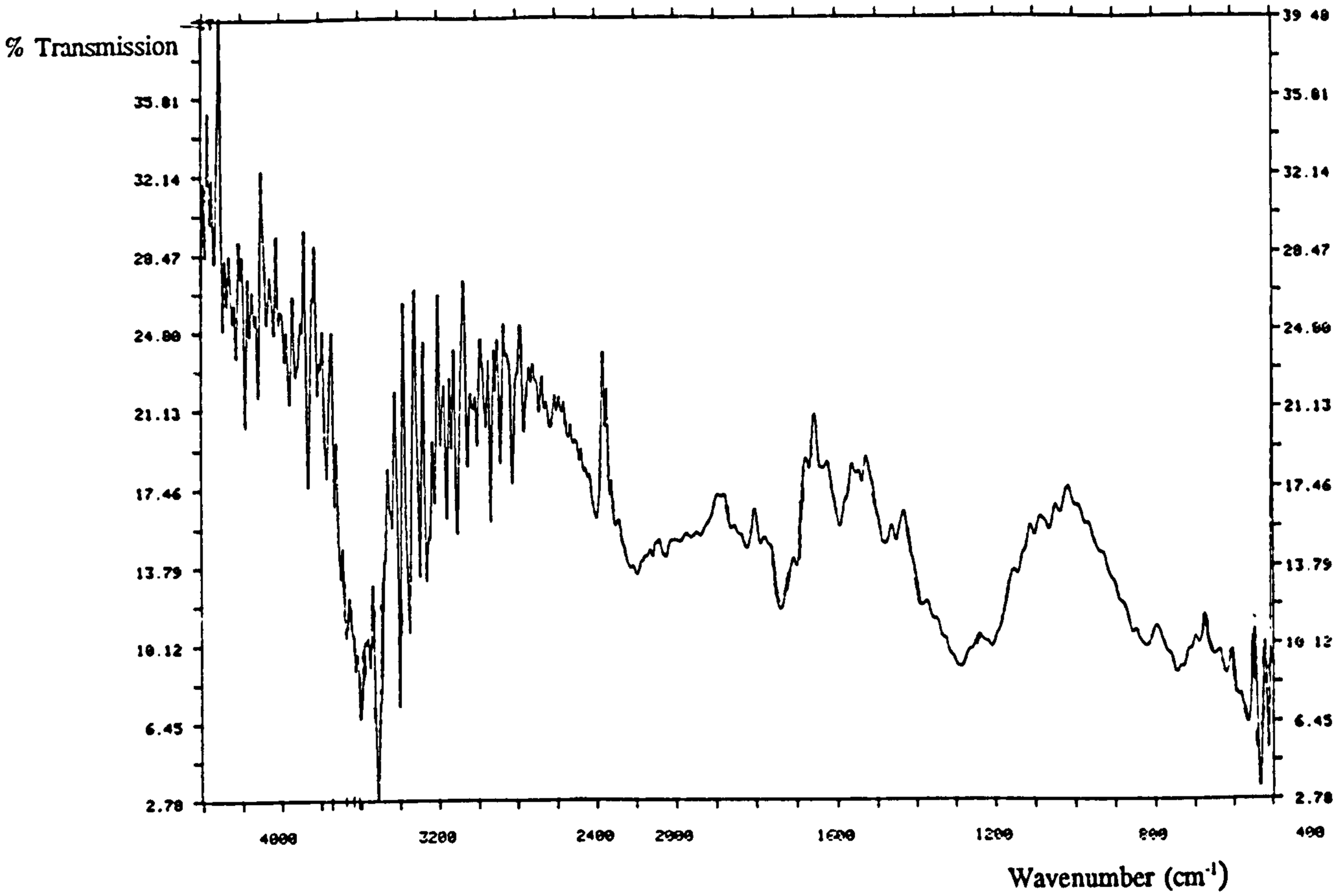

Figure 2.38: Micro-FTIR of Quartz as Received.

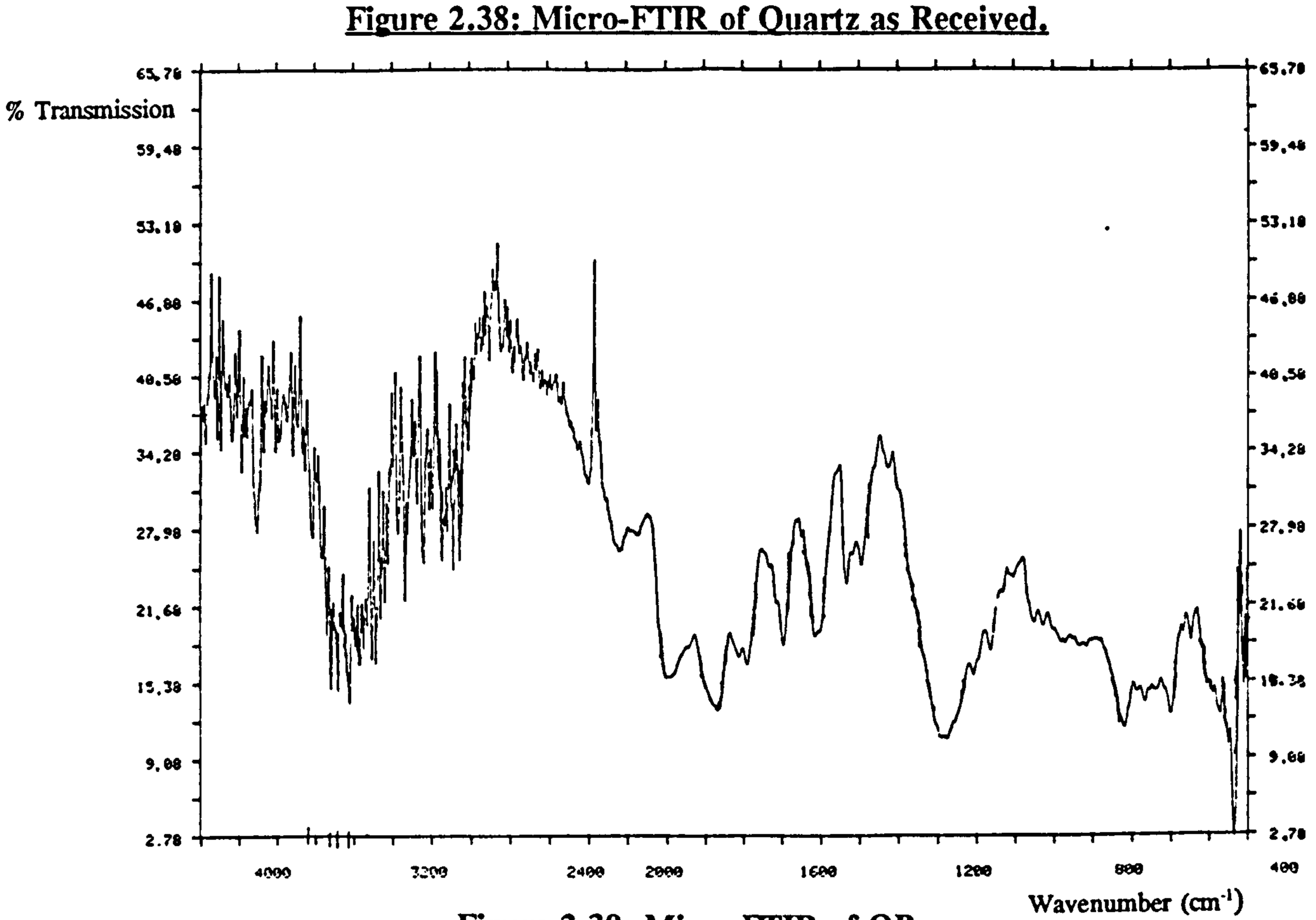

Figure 2.39: Micro-FTIR of QB.

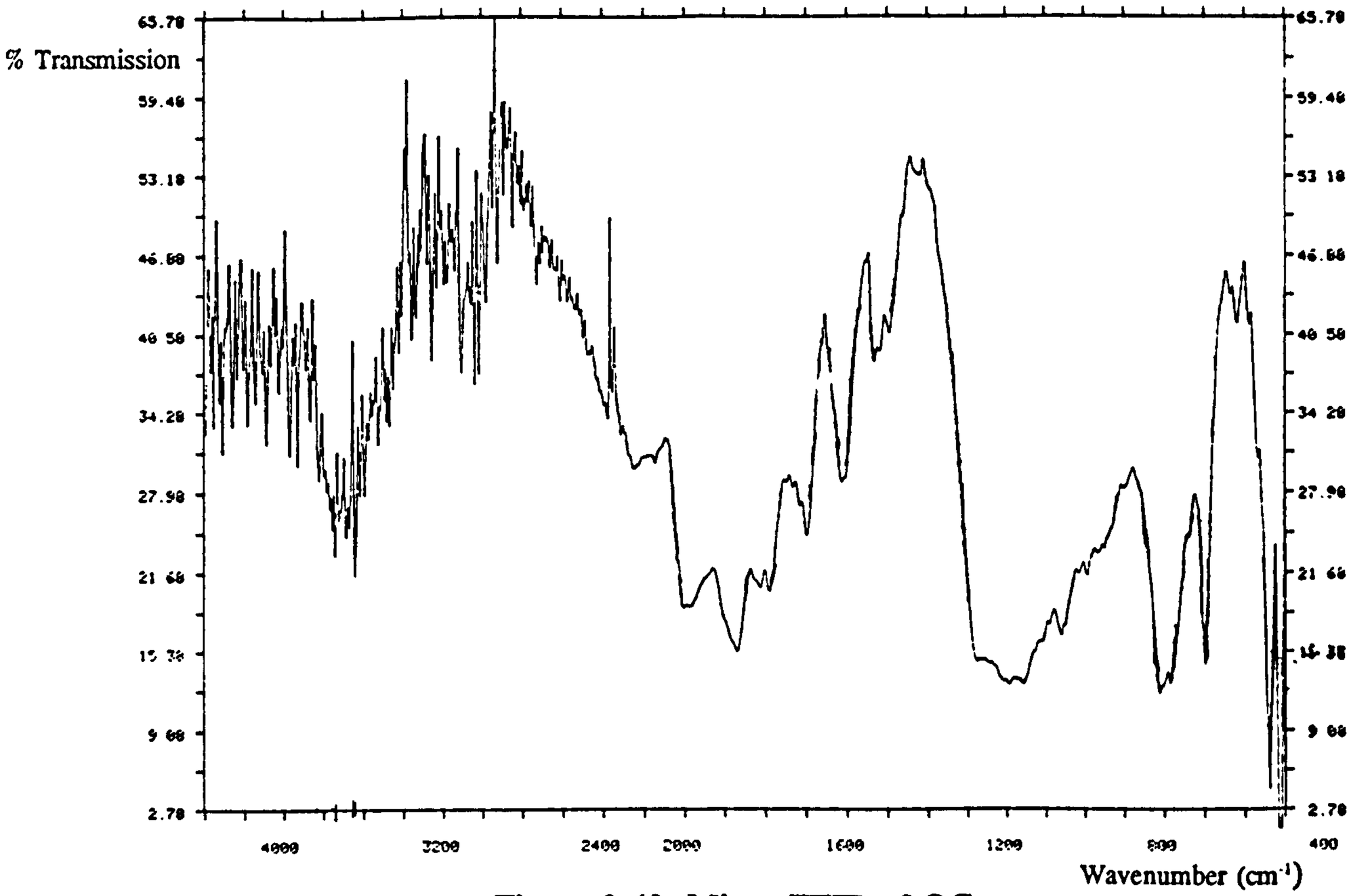

Figure 2.40: Micro-FTIR of QC.

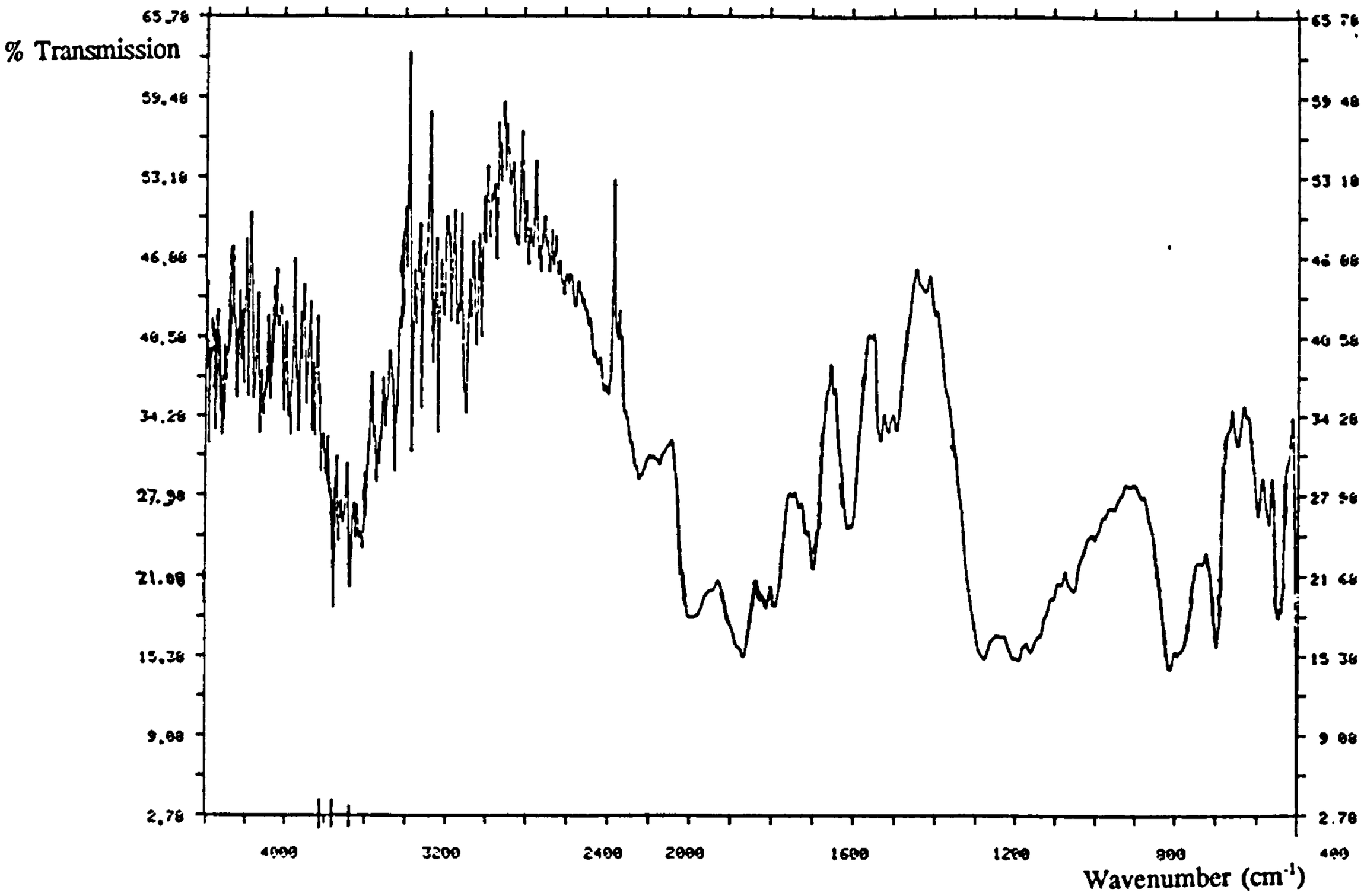

Figure 2.41: Micro-FTIR of QC, tumbled for 24h in distilled water.

2.20 BET Analysis of Total Surface Area. Theory and Experimental Analysis.

The surface area of the quartz was calculated using BET analysis. This uses the fact that an accurate measurement of the amount of a gas adsorbed by a solid can be used to obtain the surface area of that solid.

Brunauer, Emmett and Teller first developed their theory for multilayer gaseous adsorption onto solids in 1938 (37), based on initial work by Langmuir (38) who had considered adsorption of monolayers of gaseous molecules only.

The BET equation can be written as;

$$p / V_a(p_o-p) = mp/p_o + b$$

where p = adsorption equilibrium pressure,
p_o = saturation pressure of the adsorbate,
V_a = volume of gas adsorbed,
m and b = constants related to the adsorption enthalpy.
$m=(c-1)/V_m c$ [c is a constant related to the adsorption energy]
$b = 1/V_m c$

By plotting $p/V_a(p_o-p)$ vs. p/p_o, m and b can be calculated from the slope and intercept of the line respectively and V_m (the volume of an adsorbed monolayer of gas) can be calculated.

The total surface area can then be calculated from:

$$\text{Surface area} = V_m.a_{(N2)}.N_A / V_o.W$$

where N_A = Avogadros number,
$a_{(N2)}$ = cross-sectional area of adsorbent gas (nitrogen),
V_o = volume of 1 mole of ideal gas at STP (=22410cm^3mol^{-1}),
W = weight of the outgassed sample.

There are certain limitations of the BET theory due to assumptions made during the derivation. Firstly, the theory assumes an energetically homogeneous surface; this assumption becomes less important as the number of adsorbed layers increases. Secondly, the theory assumes no lateral interactions between adsorbed molecules on the adsorbent surface. This latter assumption is increasingly important as the adsorption progresses. Another questionable assumption of the BET theory is the equivalence of

the second layer of adsorbate to the subsequent layers since polarisation forces on the layers close to the substrate may still play a role in any interactions present.

The krypton BET surface area analyses were carried out at 77K using a Micromeritics Digisorb 2600 volumetric sorption analyser at the BP laboratories in Sunbury. The samples were outgassed for 16h at 393K. Table 2.4 shows the results obtained from this analysis, which are accurate to +/-0.01m^2/g.

2.21 Total Surface Area Results.

Table 2.4: Table of Total Surface Areas of the Quartz Samples Derived from BET Analysis.

Sample	Total Surface Area (m^2/g) Kr (BET)
QB	4.22+/- 0.01 4.21+/- 0.01
silica - calcined at 1273K for 1h	4.01+/- 0.01
silica - calcined at 1273K for 3h	3.19+/- 0.01
silica - calcined at 1273K for 10h.	3.77+/- 0.01

The desorption isotherm obtained during BET analysis can be used to calculate the radii of pores within a sample in order to get a measure of the pore size distribution. There are many methods used to calculate the variation of some pore parameter against the estimated pore radius. The most common approach is that devised by Barrett, Joyner and Halenda (BJH). These calculations only apply over the range of relative pressures where hysteresis occurs. On reducing the relative pressure of a gas upon a sample, desorption occurs. The largest pores empty at the highest relative pressure, due to their large diameters; as the relative pressure decreases the smaller pores empty. Also, as the pressure lowers, the larger pores that were emptied of their core liquid previously also lose some of the adsorbed film that does not desorb at the higher

pressures. This loss complicates the calculation of the weight loss of the adsorbate at each pressure and in order to account for this there are two radii associated with each relative pressure for every pore:

$$r_p = r_K + t$$

where: r_p = radius of the pore,
t = thickness of the adsorbed film,
r_K = Kelvin* radius

* from the Kelvin equation: $\ln(p/p_o) = (-2\gamma V_m/r_k RT).\cos\phi$ where:

p = equilibrium vapour pressure of the liquid in the pore,
p_o = equilibrium vapour pressure of the liquid on a plane surface,
γ = surface tension of the liquid,
ϕ = contact angle between the liquid and the wall of the pore.

BJH assumed that the film depth in a pore is the same as on a plane surface, so

$$t = (W_a/W_m)\Gamma$$

where: Γ = the thickness of a single monolayer,
W_a/W_m = number of statistical monolayers in the film.

As the film thickness can be estimated, then the radius of the empty pore and the pore area can be calculated. Unfortunately, the desorption isotherms measured were not made available for further analysis.

Kiselev et al (39) investigated the influence of temperature on pore structure and noted that the mean pore diameter of silica increased with thermal treatment. These observations suggest that a change of structure for the quartz into a more open and porous structure occurs. It is not entirely clear from SEM images measured for this thesis (see Figures 2.29-2.32) whether the quartz samples have any real porosity, or whether there are simply interparticle voids. However, for a model solid of non-porous spheres or cubes (which Silfraco quartz certainly is not) total surface area = $6000/(\rho_{quartz}\, d)$, where d is the average size of the quartz particles of density ρ_{quartz} (i.e. $2.65 g/cm^3$). Inserting the average value of the total surface area in Table 2.4 (i.e. $3.88 m^2/g$) into the above equation produces a value of d (i.e. $58.4 \mu m$) which is a factor of 10 higher in comparison with the SEM images. One would assume from this rather crude calculation that the Silfraco quartz was non-porous. Further study is required to investigate this stimulating topic.

References.

(1) N.M.A.Ibrahim; B.B.Wheals; Analyst, 121,239 (1996).

(2) S.J.Patterson; C.Scott; K.B.Tucker; J.Am.Oil Chem.Soc., 45,528 (1968).

(3) K.J.Bombaugh; J.Chrom., 53,27 (1970).

(4) F.P.B.Van der Maeden; J.Chrom., 149,539 (1978).

(5) F. Ysambertt; W.Cabrera; N. Marquez; J.L.Salager; J. Liquid Chrom., 18,1157 (1995).

(6) H.Suyani; J.Creed; T.Davidson; J.Caruso; J.Chrom.Sci., 27,139 (1987).

(7) P.J.Arpino; M.A.Baldwin; F.W.McCafferty; Biomedical Mass Spec., 1,80 (1974).

(8) S.C.Lamey; P.A.Hesbach; K.D.White; Energy and Fuels, 5,222 (1991).

(9) P.Sandra; P.Courselle; G.Steenbeke; M.Schelfaut; J.High Res.Chromat., 12,544 (1989).

(10) P.L.Desbene; B.Desmazieres; J.J.Basselien; L.Miussieux; Chromatographia, 24,558 (1987).

(11) P.L.Desbene; B.Desmazieres; V.Even; J.J.Basselier; L.Miussieux; Chromatographia, 24,857 (1987).

(12) G.R.Bear; J.Chromat., 459,91 (1988).

(13) P.L.Desbene; B.Desmazieres; J.J.Basselier; J.Chrom., 461,305 (1989).

(14) D.F.Anghel; M.Bakon; A.Voicin; M.Elien; J.Chrom., 668,375 (1994).

(15) N.Marquez; R.E.Anton; A.Usubilliya; J.Liquid Chrom., 17(5),1147 (1994).

(16) J.A.Pilc; P.A.Sermon; J.Chrom., 398,375 (1987).

(17) P.Jandera; J.Chrom., 449,361 (1988).

(18) A.Nakae; K.Tsuji; M.Yamanaka; Anal.Chem., 52,2275 (1980).

(19) G.P.Bera; J.Chromat., 371,387 (1986).

(20) D.J.Pietrzyk;P.G.Rigas; D.Yuan; J.Chrom.Sci., 27,485 (1989).

(21) I.Ogura, D.L.Duval, S.Kawakami, K.Miyajima; J. Am. Oil Chem. Soc., 73,137 (1996).

(22) L.Nitschke; R.Muller; G.Metzner; L.Huber; Fresnius,J.Anal.Chem., 342(9), 711 (1992).

(23) M.Ahel; W.Giger; Anal.Chem., 57,2584 (1985).

(24) M.S.Hott; E.H.McKerrell; J.Perry; R.J.Watkinson; J.Chrom., 362,419 (1986).

(25) E.Kubeck; C.G.Naylor; J.Am.Oil Chem.Soc., 67(6),400 (1990).

(26) Z. Lukaszewski, A.Szymanski; Mikrochimica Acta, 123,185 (1996).

(27) C.G.Naylor; J.P.Mieuvre; W.J.Adams; J.A.Weeks; F.J.Castaldi; L.D.Ogle; R.R.Romano; J.Am.Oli Chem.Soc., 67(6),400 (1990).

(28) Y.Mengerink; H.C.J.Deman; S.Vanderwal; J.Chrom., 552,593 (1991).

(29) Liquid Chromatography Technical Report, Du Pont, Delaware, USA (1982),

(30) N.Ibrahim; PhD Thesis, Brunel University (1995).

(31) H.Bennet;G.Oliver; XRF Analysis of Ceramics, Minerals and Allied Materials; J.Wiley&Sons, West Sussex, England (1992).

(32) C.D.Wagner; L.E.Davis; M.V.Zeller; J.A.Taylor; R.M.Raymond; L.H.Gale; Surf.Int.Anal.,3,211 (1981).

(33) J.I.Goldstein; D.E.Newbury; P.Echlin; D.L.Joy; A.D.Romij; C.E.Lyman; C.Fiori;E.Lifshin; SEM and X-ray Microanalysis, Plenum Press, New York (1994).

(34) K.K.Unger; Porous Silica. Elsevier Scientific Publishing Company, New York (1979).

(35) L.T.Zhuravlev; Langmuir, 3,316 (1987).

(36) D.M.Nevskaia; M.L.R.Cervantes; A.G.Ruiz; J.D.L.Gonzalez; J.Chem.Tech.Biotechnol., 63,249 (1995).

(37) S.Brunauer; P.H.Emmett; E.J.Teller; J.Am.Chem.Soc., 60,309 (1938).

(38) I.Langmuir; J.Am.Chem.Soc., 38,2221 (1916).

(39) A.V.Kiselev; V.M.Lukyanovich; Yu.S.Nikitin; E.B.Oganesyan; A.J.Sarakov; Kolloid. Zh., 31,388 (1969).

CHAPTER 3: Adsorption.

3.1 Theory of Adsorption.

In the bulk of a phase, irrespective of the state of the phase, the van der Waals forces between the molecules, atoms or ions are balanced. At the interface (or surface) of two phases, however, the forces become unbalanced due to the action on the molecules by both of the phases. These unbalanced forces cause changes in the number of molecules, atoms or ions to occur on the interface and this change in concentration is termed "adsorption". Adsorption results in the balance of forces at the interface being partly restored.

Adsorption may be a physical process (physisorption) which is dependent on intermolecular forces of attraction and repulsion (e.g. H-bonding or van der Waals forces) and thus is associated with relatively low binding energies of approximately 20kJ/mol. Alternatively it may be due to chemical processes, for example the sharing or transferring of electrons between the adsorbed species and surface species to form chemical bonds - associated with binding energies of approximately 200kJ/mol. Table 3.1 shows the distinctive properties of chemisorption and physisorption.

Table 3.1: Chemisorption and Physisorption.

Property	Physisorption	Chemisorption
Heat of Adsorption	small	large
Reversibility	easily reversed	extremely difficult
Thickness of Adsorbed Layer	multilayers capable of forming	monolayers only

The systems making up the interface can range from

(1) vapour/gas adsorption (VPA), to

(2) composite liquid adsorption (CLA), to

(3) solid solute adsorption (SSA).

Many treatments have been developed to describe the above adsorption processes and originally most of them dealt with VPA systems (1-3). Langmuir pioneered work on the kinetics of VPA systems (4) and also those of CLAs (5). Langmuir's work describing VPA in monolayers was later developed by Brunauer, Emmett and Teller (6) to include adsorbed multilayers. Theoretical treatments are numerous (7,8) although the work by Langmuir and Brunauer, Emmett and Teller is perhaps the best known; the latter named authors developed the BET equation that is widely used for the measurement of the specific surface area of finely divided solids by VPA. This work was again developed further for solids of low surface area using krypton as the adsorbate in place of nitrogen (9).

3.2 Adsorption at the Liquid/Solid Interface.

Adsorption at the liquid/solid interface forms the basis of many industrial processes, which include detergency, dyeing, pollution control, ion-exchange, surface area measurement and liquid/solid chromatographic techniques. The mechanism of adsorption at the liquid interface is dictated by the competition between solvent and solute molecules for surface sites and also by the chemistry of the surface. Adsorption at the solid/liquid interface is expressed in the form of an adsorption isotherm, which is a measurement of the amount of solute adsorbed as a function of its equilibrium concentration. Important factors such as mechanism of adsorption, rate of adsorption, adsorbed layer structure and the effects of pH and temperature can be predicted or explained using the adsorption isotherm.

The most common form of adsorption isotherm for adsorption of a liquid onto a solid is known as the Langmuir isotherm and is illustrated below:

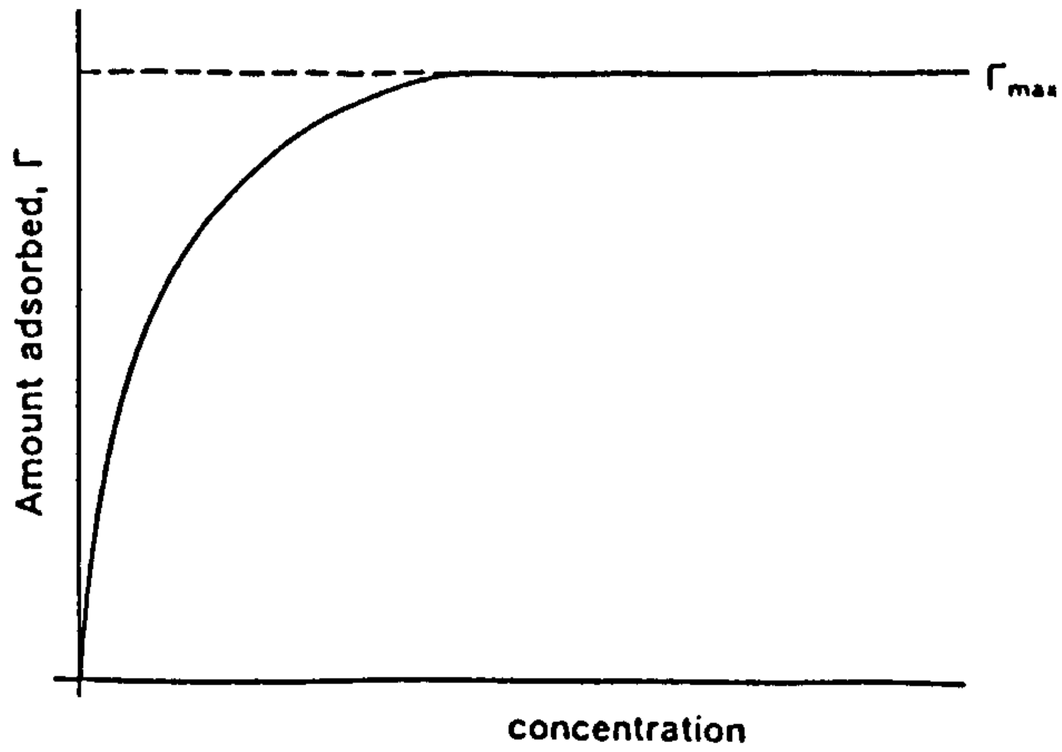

The slope of the curve of the initial section of the isotherm is a measure of the ease with which the liquid molecules are finding adsorption sites on the adsorbent surface. The slope falls steadily with rise in concentration since the availability of vacant sites decreases with an increase in surface coverage. Eventually, at the saturation point, the slope equals zero. Many isotherm types have been obtained for SSA systems and these have been extensively characterised theoretically and experimentally by Giles et al (10,11) (see diagrams below). Giles based his classification on the five principal forms of adsorption isotherms for gases proposed by Brunauer (12). Firstly, the isotherms are classified into four main sections based on their initial slope: class S, class L (Langmuirian), class H (having high adsorption affinity) and class C (constant partition of the substance between the surface layer and the bulk). Each of the four main classes have the subgroups 1,2,3,4 and max, which are distinguished by the shape of the isotherm at higher concentrations. Giles (11) has related the adsorption mechanism and the orientation of adsorbed molecules to the shape of the isotherm. For example, class S isotherms correspond to adsorbate molecules being perpendicular to the surface whereas class C isotherms are consistent with penetration into the structure of the solid by the liquid or solute.

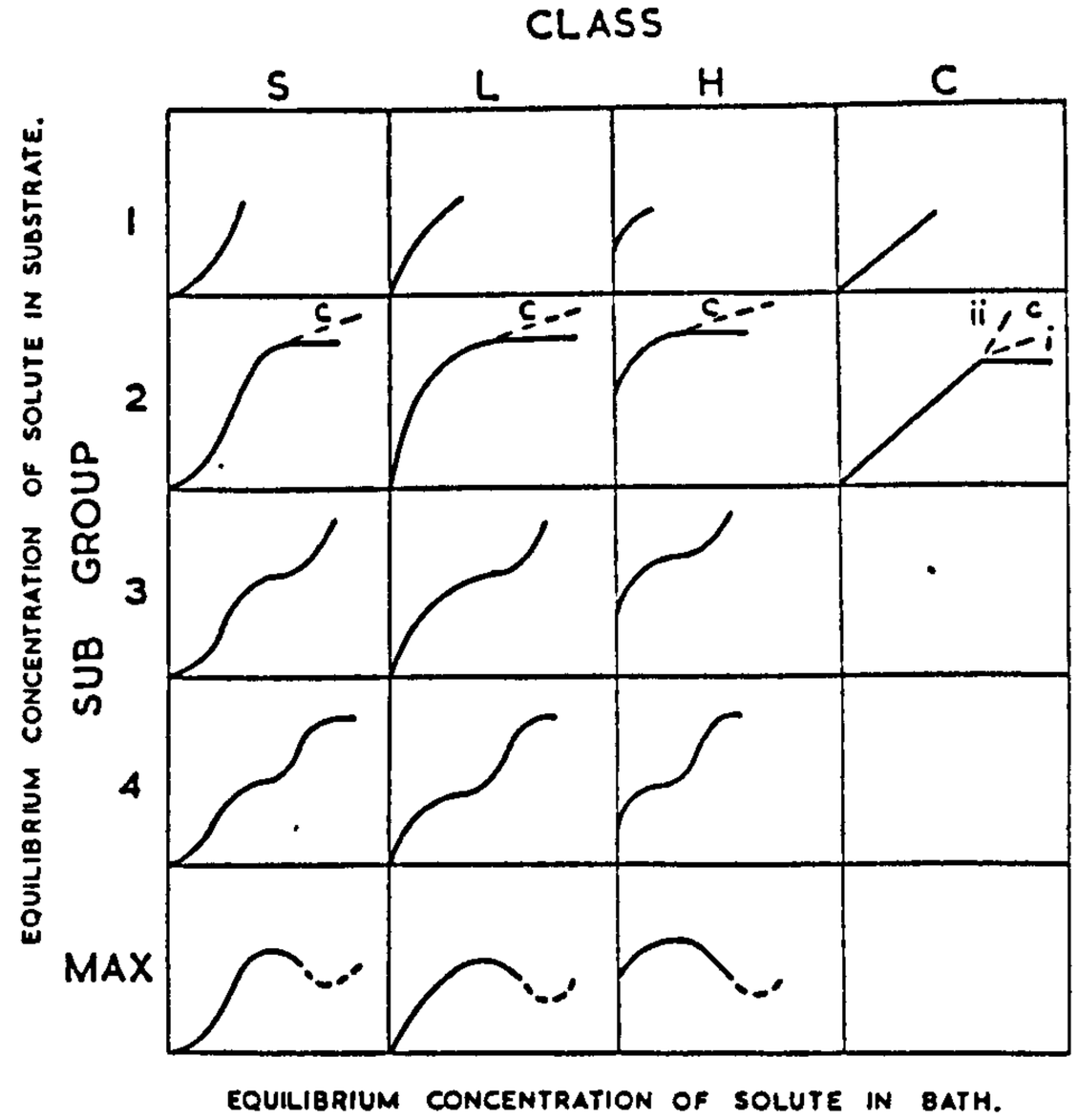

The Classification of Solid/Solute Adsorption by Giles (11).

3.3 The Derivation of the Langmuir Isotherm.

The rate at which adsorption occurs is proportional to the concentration of the solute and to the extent of free surface, and can be written as

$$\text{Rate of adsorption} = k_{ads}.(1-x).C \quad \ldots\ldots\ldots(1)$$

where x = fraction of the surface covered by adsorbed molecules,

C = concentration of the solute in solution,

k_{ads} = adsorption rate constant.

Similarly, the rate of desorption will be proportional to the fraction of covered surface and the rate constant of desorption k_{des}:

$$\text{Rate of desorption} = k_{des}.x \quad \ldots\ldots\ldots\ldots(2)$$

At equilibrium, the rate of desorption = rate of adsorption, so from equations (1) and (2) one has:

$$k_{des}.x = k_{ads}.(1-x).C$$

$$\therefore\ x/1-x = k_{ads}/k_{des}.C = KC$$

where K = equilibrium constant for the adsorption process.

Therefore, x = KC/1+KC, which is a form of the Langmuir isotherm.

3.4 Thermodynamics of Adsorption onto Solids.

An individual point on the adsorption isotherm can provide a value for the standard free energy of adsorption at that concentration as:

$$\Delta G^{\circ} = -RT\ln K$$

where G° is the standard free energy of adsorption, R is the gas constant, T is the absolute temperature and K is the relevant equilibrium constant.

If the isotherms are measured at several different temperatures, then the enthalpy of the

whole process at a certain value of x can be determined using:

$$\Delta H/T^2 = -\{d(\Delta G°/T) / dT\}_x$$

There are difficulties in choosing points on isotherms measured at differing temperatures which correspond to the same x values. The most reliable way in which to do this for liquids is to measure the heat of adsorption directly using microcalorimetry (13,14).

3.5 Surfactant Adsorption.

Surfactant adsorption onto mineral oxide surfaces has been of great interest for the past two decades due to their use, particularly in the 1970's, during EOR. The effects of temperature and salinity on their adsorption onto solid rock surfaces has been widely investigated (14-20). Scamehorn et al (18,19) did much to construct a general mechanism for surfactant adsorption. The adsorption isotherm of surfactants onto mineral surfaces can be split into three main sections as shown below:

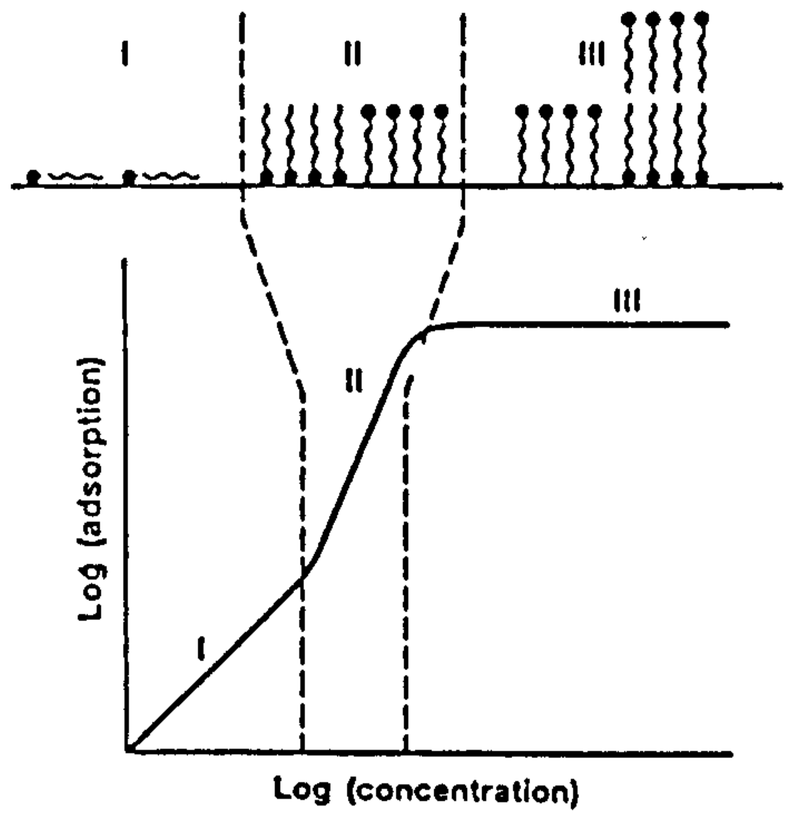

Section I occurs below the CMC at low surface coverage and corresponds to monomeric-driven adsorption onto the solid surface. These interactions can include H-bonding, geometric factors or electrostatic interactions depending on the nature of adsorbing surface and species, or surfactant.

Section II shows a rapid increase in adsorption and usually occurs at concentrations just below the CMC. This huge uptake of surfactant molecules is commonly thought to be due

to the onset of lateral interactions between adjacent adsorbed molecules (15).

Section III of the isotherm occurs at concentrations above the CMC of the surfactant at which point the slope of the isotherm decreases until a plateau is reached. The position of the plateau corresponds to a maximum adsorbed amount of surfactant, most commonly thought to be in the form of a bilayer of molecules (15).

This mechanism is a general one and the exact shape of the isotherm will depend on the species that make up the solid surface and the adsorbate.

3.6 Non-Ionic Surfactant Adsorption onto Mineral Oxides.

Many groups have studied the phenomenon of non-ionic surfactant adsorption onto mineral oxides (21-26); by combining isotherm determinations and adsorption calorimetry, a mechanism of adsorption of alkyl phenol polyethoxylates onto silica has been constructed and is generally agreed upon.

Adsorption Mechanism:

(i). At low surface coverages, isolated monomers are adsorbed via H-bonding of the polar chains of the surfactant to the acidic silanol groups on the surface. Groups differ in the opinion as to the region of the ethoxylate chain that initiates adsorption. Denoyel et al (24) assume contact between the surfactant and surface is made only via the end hydroxyl group of the surfactant, whereas Keith et al (27) have determined that all of the oxygen atoms within the ethoxylate chain of a monomer are used during this initial monomerically driven process. There is also the question of the position of water molecules in aqueous solution; Kong et al (28) carried out Monte Carlo simulations of a single poly(oxyethylene) chain attached to a hydrophobic wall and revealed that water molecules formed hydrogen-bonded bridges between adjacent oxygen atoms on the chain, and that these water-chain interactions increased with increase in temperature. Lindheimer et al (23) produced fundamental calorimetric studies on this type of adsorption and found the process to be exothermic.

(ii). At higher coverages, an aggregation process occurs which is endothermal and involves lateral interactions between the hydrocarbon chains of the preadsorbed molecules. The fluorescence studies of Levitz et al (22) showed that surface aggregation occurred at

surfactant concentrations well below the CMC. A monolayer of adsorbed surfactant is formed briefly which is known as a 'hemimicelle' layer. As the bulk concentration increases further, lateral interactions occur causing a bilayer of adsorbed surfactant most commonly known as an 'admicelle' (26). This is supported by contact angle measurements conducted by Gonzalez et al (29) which show a hydrophobization of the sample followed by hydrophilization below the CMC. Although groups do disagree on the exact coverage at which the bilayers are formed (23,29), it is thought to occur at coverages of $0.1 < x < 0.5$. This process becomes less endothermic as full coverage is approached, as the enthalpy effect of the transference of surfactant molecules from micelles in solution to admicelles is reduced. Eventually the process is non-thermal.

The time for the adsorption process to reach equilibrium is still a matter of contention. Equilibrium times vary from 3 hours (25) up to 24 hours (30), with some articles not mentioning a length of time at all (26)! The HPLC analysis carried out in this work showed that the equilibrium time for adsorption occurred at about 6 hours (see section 3.7.2 and figures therein).

3.7 Adsorption Isotherms on Quartz and Oligomeric Analysis of the Surfactants.

3.7.1 Experimental.

Initially, simple batch adsorption isotherms were measured for TX-100 onto silica in the form of quartz. The solid was a ground quartz (C-600 grade, Silfraco) that had an average surface area of $4.22 m^2/g$ (see section 2.21) and was pre-treated with conc.HCl as described in section 2.2. The surfactant used was Triton-X 100 and was purchased from Rohm and Haas of Germany.

0.7g of quartz samples were placed in contact with $7cm^3$ of aqueous TX-100 solutions of known concentration and the systems were tumbled for a kinetically pre-determined time of (7 h) in an oven. The suspensions were centrifuged at 3500 revs/min after tumbling and the supernatant analyzed by UV spectroscopy at 275nm in a Perkin Elmer Lamda 9 spectrophotometer. The pH measurements were made after tumbling.

For oligomeric analysis, the measurements are carried out in a similar fashion to the

method used for the adsorption isotherm, i.e. 0.7g of quartz were tumbled at varying times with 7cm^3 of a known concentration of surfactant in aqueous solution. The resultant mixtures were centrifuged and injected into the HPLC system. The gradient used for analysis was described in section 2.8 of this thesis. The heights of peaks in the chromatograms obtained were compared with a calibrant surfactant solution (the initial solution used for tumbling) and a percentage reduction of oligomer in solution was obtained. Oligomers having 3, 8, and 13 ethoxylate (EO) units were chosen as these represented both extremes of oligomeric size and an oligomeric size that was representative of the bulk of the surfactant. All values have an error of +/- 10% associated with them.

Results.

Figure 3.1 shows the adsorption isotherm for TX-100, the isotherm is S-shaped with a maximum adsorbed value of approximately 2 μmoles/m^2. Figure 3.2 shows the analysis of the three sizes of oligomer with position on the plateau and time. In all cases, the equilibrium time needed was in the region of 6 h. It can be seen from Figure 3.2 that the smallest oligomers are the most strongly adsorbed both at the plateau (x=1) and at x=0.5 (where x is the fraction of the surface covered).

Consider first the size effect on adsorption; the observed trend is what is expected as the smaller the oligomer, the less hydrophilic the oligomer. The components containing 13 EO units are extremely hydrophilic due to the long ethoxylate chain which forms complexes with water molecules. The smaller oligomers will attempt to separate themselves from the aqueous solution via adsorption onto the silica surface. The adsorption is slightly stronger for the smallest oligomers at x=0.5 because at this level of adsorption the molecules in solution are mostly in the monomeric form. Monomers are in a state of high free energy relative to micelles due to the hydrophobic parts of the molecules being subject to aqueous forces. In an attempt to lower their free energy the molecules will adsorb onto the surface. At x=1.0, the majority of surfactant in solution is in the form of micelles, which are in a relatively low state of free energy and which will incorporate the smallest oligomers. These small components will therefore be less likely to adsorb onto the quartz surface when compared to monomers.

3.7.2 Salinity Effects.

Figure 3.3 shows adsorption isotherms measured for TX-100 onto quartz at varying salinity. The values shown for salinity are those for the concentration of NaCl, although NaCl, $MgCl_2$ and Na_2SO_4 were added in the ratio of 10:1.25:1 respectively. This is a standard synthetic sea water. The results are in good agreement with the work of others (24,31), i.e. an increase in salinity displaces the plateau position towards lower equilibrium concentrations and increases adsorption of the surfactant at all positions along the isotherm. These are especially clear for salinities of 3% or higher. The onset of the plateau usually occurs at approximately the CMC of the surfactant and the trend of the plateau shift towards lower concentrations seems to follow the trend in reduction of the CMC of a surfactant with increasing salinity (24).

Schott et al (32) determined the effects of certain ions on the cloud point of a number of surfactants. Table 3.2 shows the effects of ions on the cloud point of TX-100. A negative effect represents a lowering of the cloud point and so a decrease in the temperature range over which the surfactant exists as an undersaturated solution and a positive value implies an increase in the temperature range over which an undersaturated surfactant solution predominates. Mg^{2+} ions increase the solubility of the surfactant by a complexation with ether linkages in the head group, whereas Na^{+} ions tend to decrease the solubility of the surfactant due to a dehydration process in which the sodium ions form complexes with water molecules and so dehydrate the ether chain of the head group. Schott calculated approximate values of reduction/increase in cloud point (Δx, where x is the cloud point of the surfactant) by appointing NO_3^- a Δ value of zero (32). The work suggested that the effects of ions on a surfactant in solution are cumulative. For the system used for this study, then, a simple addition of the values for all of the ions present suggests that a 'salting out' of the surfactant should occur, which seems consistent with observations. Another explanation for the rise in surfactant adsorption is that the ions in solution form a complex with the quartz surface. It has been well documented that coagulation of a mineral oxide is prevented in the presence of ionic solutions (33) due to the presence of a diffuse electrical double layer surrounding the surface.

At a pH value of approximately 5, the quartz surface carries a slight negative charge due

to the zero point of charge (zpc) of silica being in the region of pH 2 (24,30), and so a diffuse layer of positively charged ions may develop about the surface (34). This layer may not only stabilise the quartz suspension but also attract the electron-rich oxygen atoms of the polyethylene oxide chains of the surfactant molecules towards the surface and so induce the adsorption process to begin at lower equilibrium concentrations.

Table 3.2 Effects of Ions on TX-100 Solubility (32).

ION IN SOLUTION	EFFECT ON THE CLOUD POINT OF TX-100 (K).
Cl^-	-10.5
Na^+	-6.5
SO_4^{2-}	-25.0
H^+	+15.5
Mg^+	+4.5

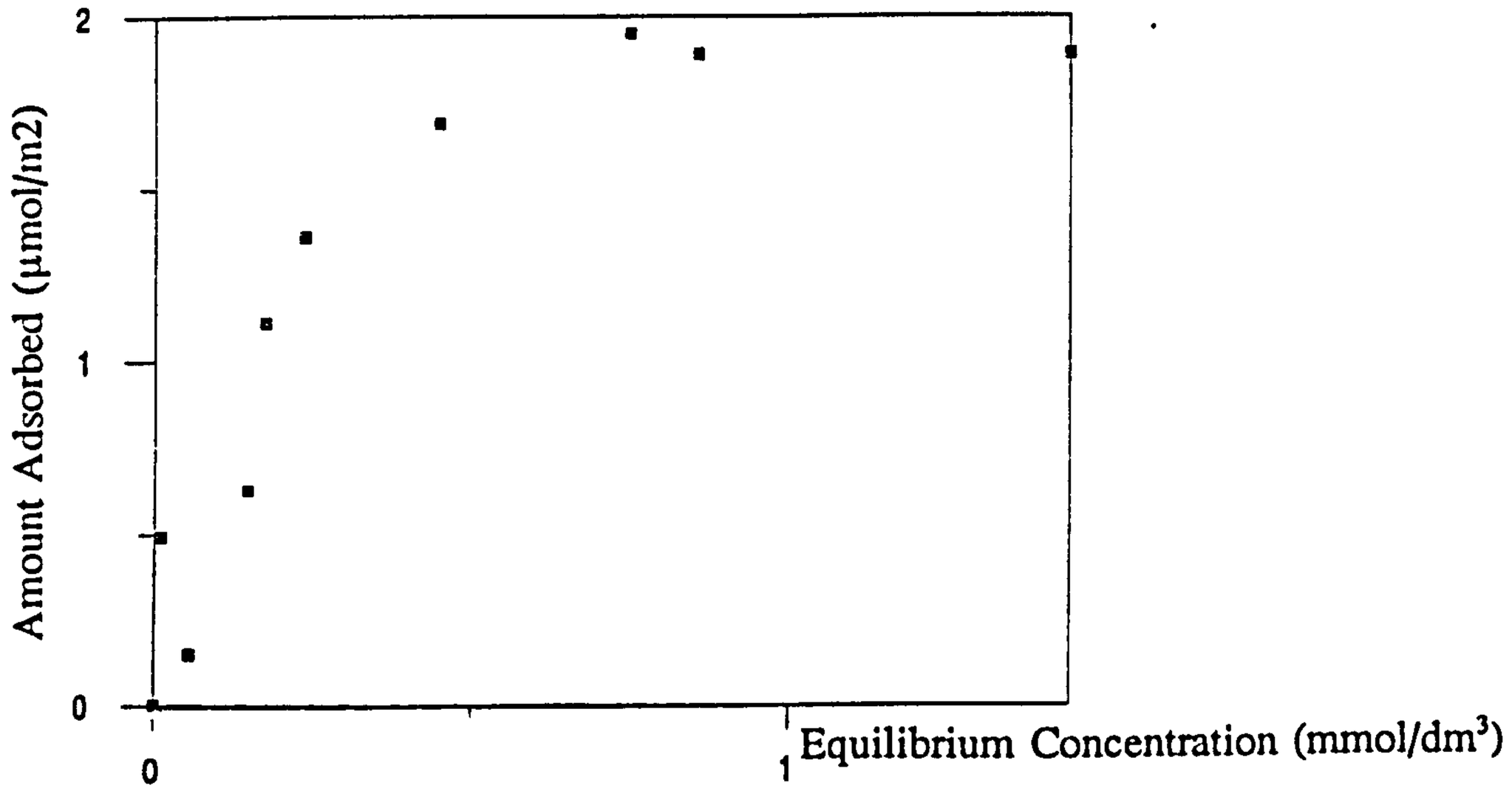

Figure 3.1: Adsorption Isotherm of TX-100 onto Quartz QB from Aqueous Solution at pH6 and 298K.

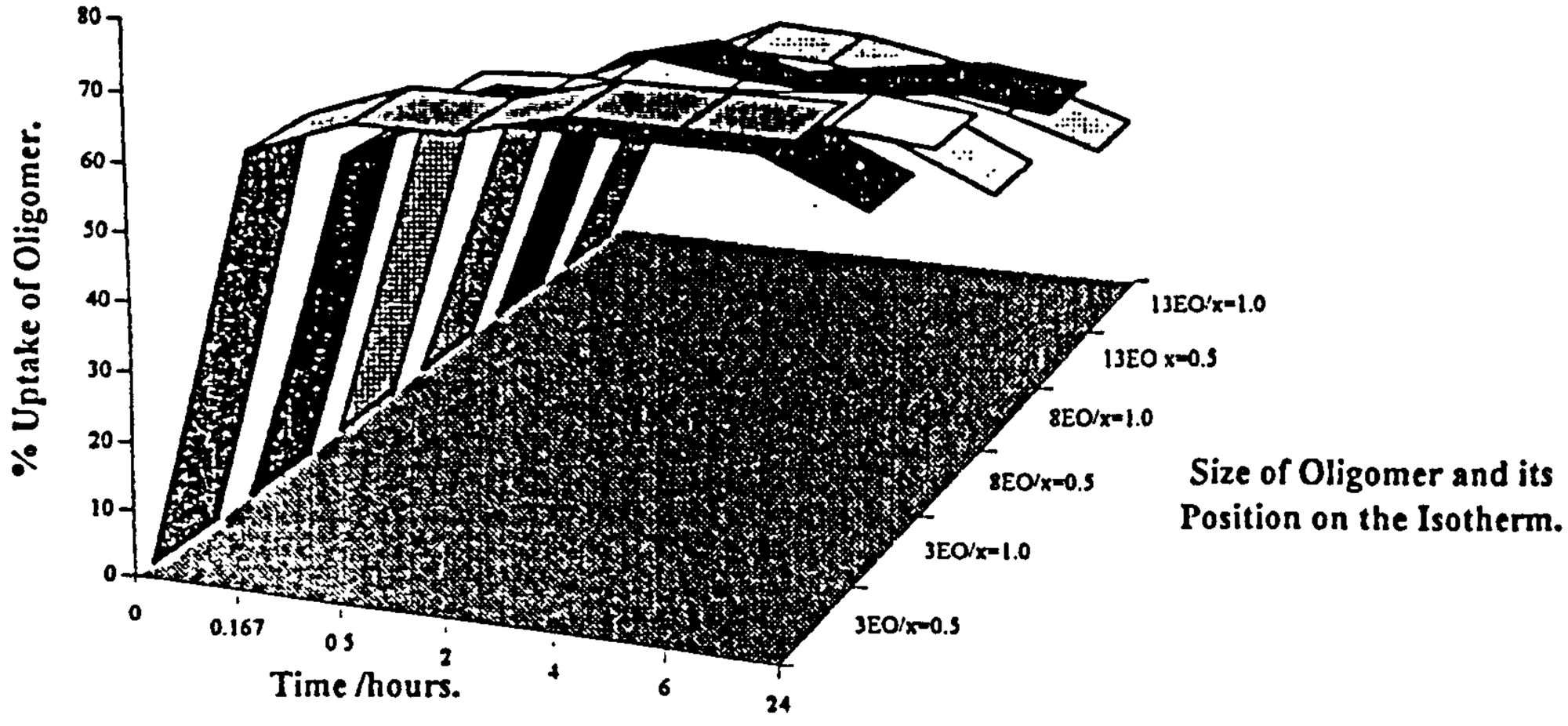

Figure 3.2: Variation of Oligomer Uptake on Quartz QB with Size of Oligomer, Time and Position on the Isotherm at pH6 and 298K.

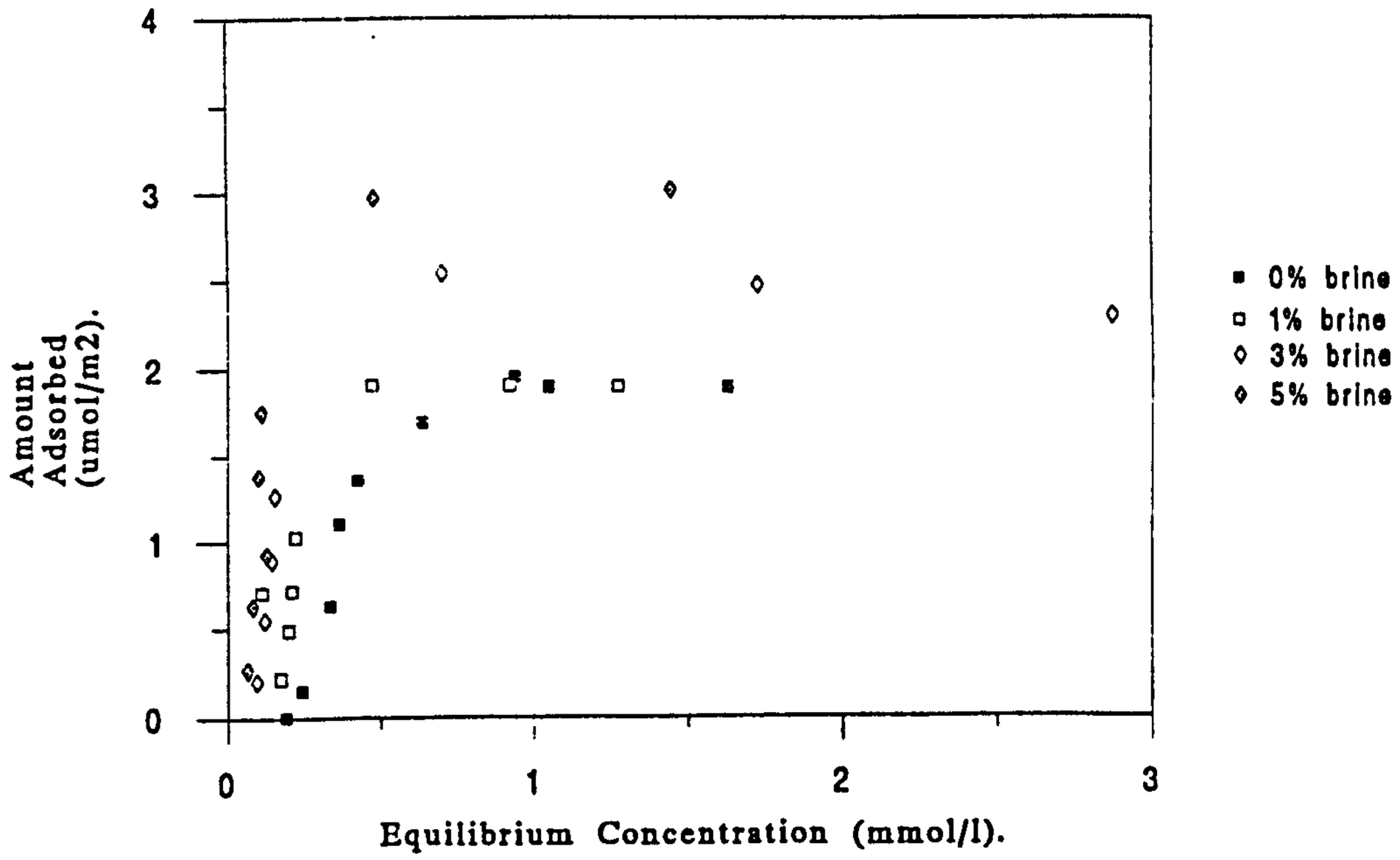

Figure 3.3: Adsorption Isotherm of TX-100 onto Quartz QB from Aqueous Solution and with Increasing Salinity.

Oligomeric Analysis.

Figures 3.4-3.6 show the uptake of all sizes of surfactant oligomer in the absence of additional ions and in the presence of NaCl and $MgCl_2$. At the plateau of the isotherm.

It can be seen that both types of ions cause an increase in adsorption for all sizes of oligomer, with the singly charged cation having the largest effect. This effect is expected if one refers back to Table 3.2. Figure 3.7 shows the effects of adsorption of oligomers on adding NaCl only and the synthetic brine solution. The brine solution increases adsorption slightly relative to the NaCl solution, most probably due to the added effects created by the extra ions capable of salting out the ether linkages in aqueous media. The effect seems strongest for the smaller oligomers. Figures 3.8-3.13 show the effects on oligomeric adsorption of increasing concentrations of synthetic brine solution. It can be seen in all cases that brine addition increases adsorption at all levels on the isotherm and for all oligomeric size. At x=0.5, in all cases, the adsorption rises steadily and the effect is strongest for the smallest oligomers due to this oligomer having the least number of ether linkages within its structure which thus renders it the easiest to salt out of solution. At the plateau, the effect can again be clearly seen for the components containing 3EO units; for the larger oligomers the effect is not so strong at 1% brine which may be due to the high stability of these larger components when in the micellar state. Above 1% brine, however, the micelles of the larger oligomers are overcome by the extremely high levels of ion in solution.

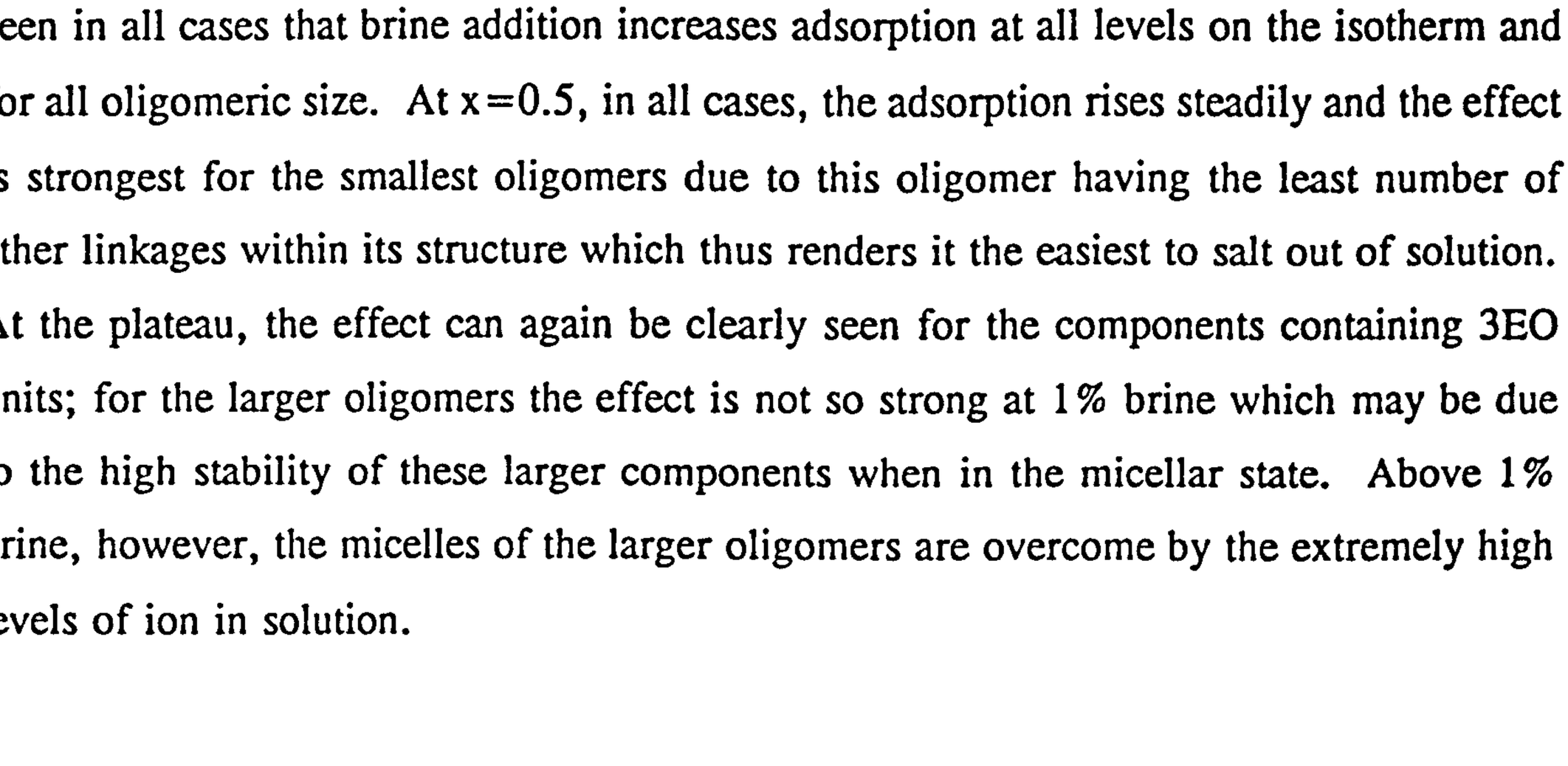

Figure 3.4: Variation of 3EO Oligomer Uptake on Quartz QB with Time and Salinity at x=1.0 and pH6 and 298K.

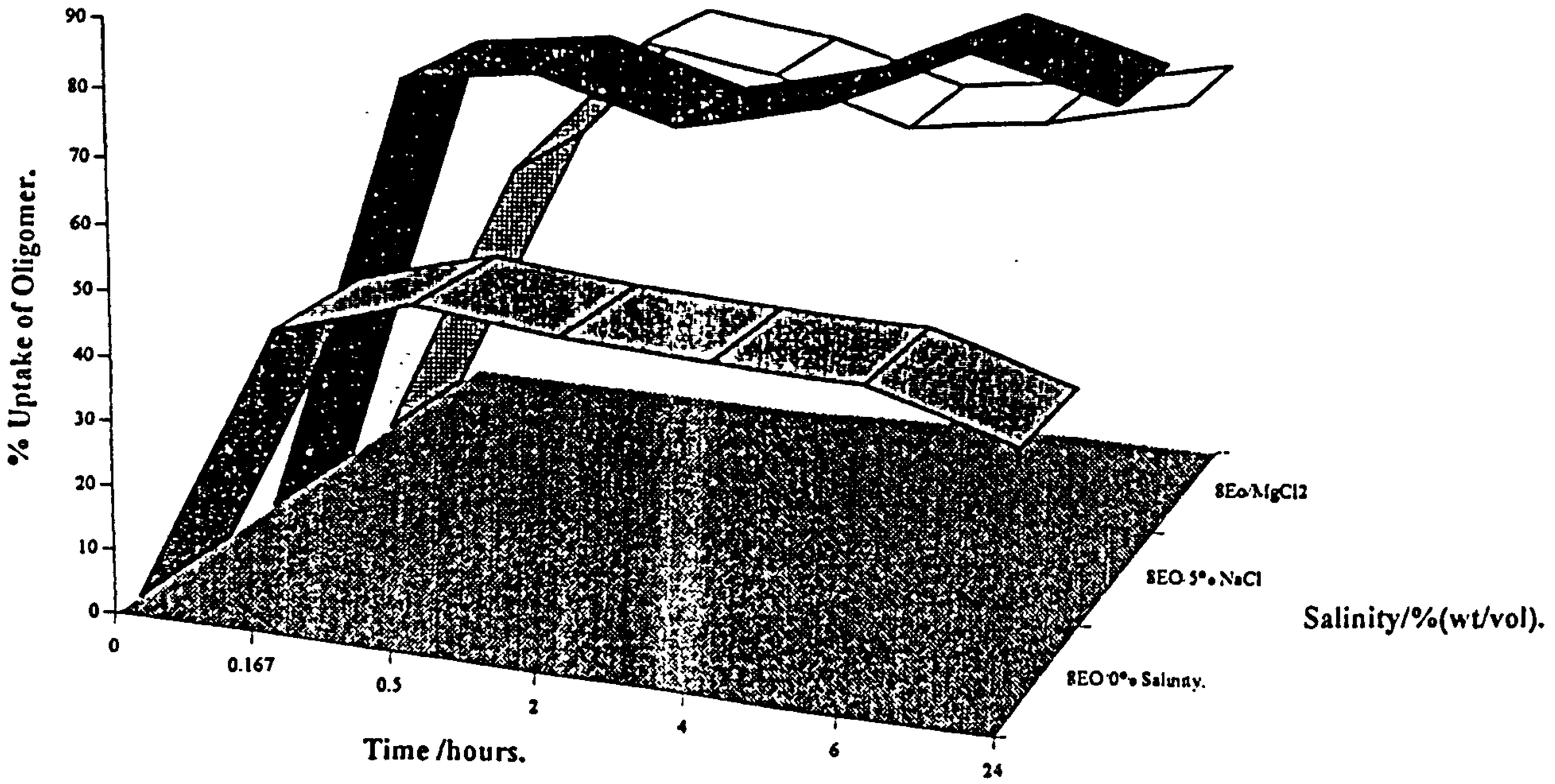

Figure 3.5: Variation of 8EO Oligomer Uptake on Quartz QB with Time and Salinity at x=1.0 and pH6 and 298K.

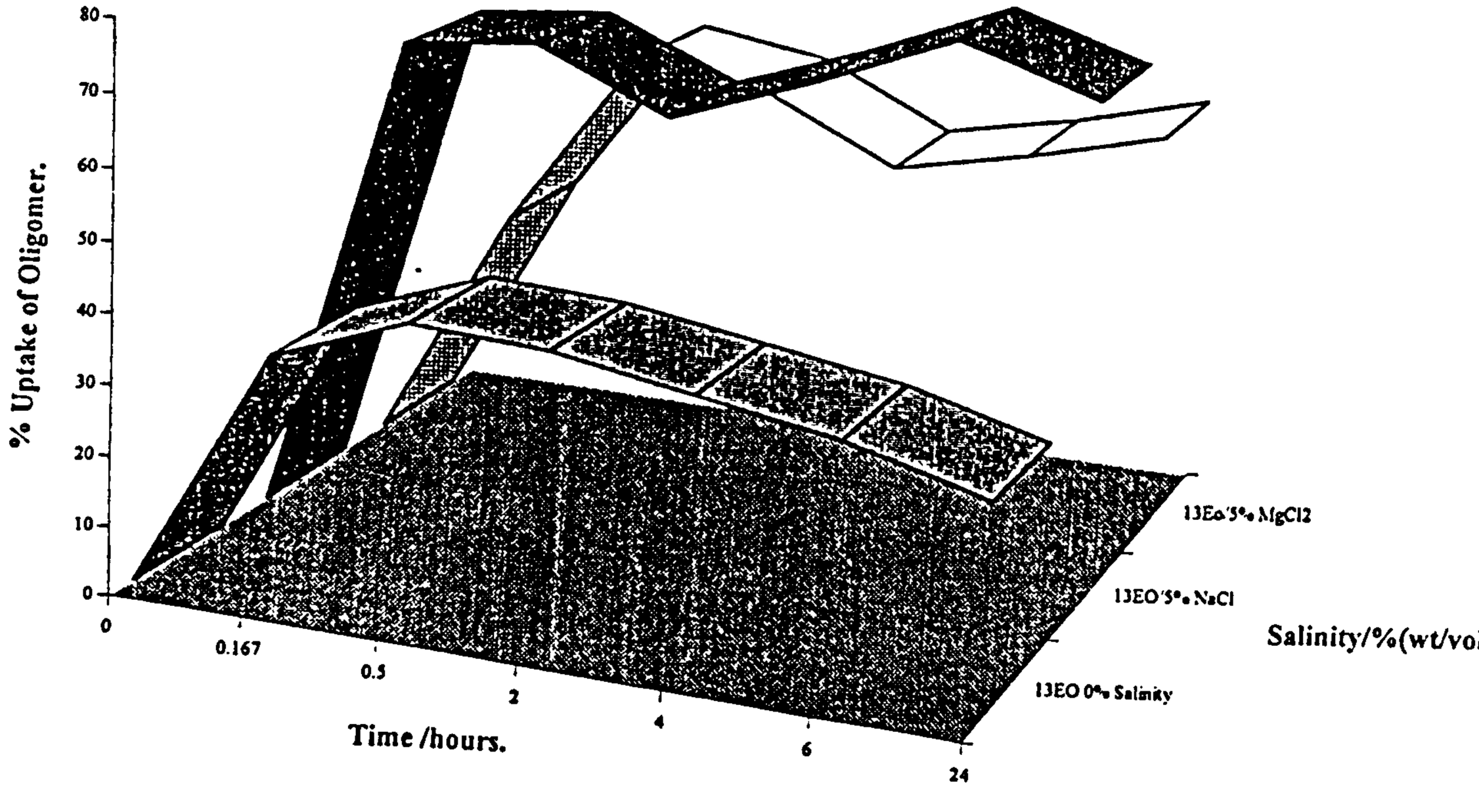

Figure 3.6: Variation of 13EO Oligomer Uptake on Quartz QB with Time and Salinity at x=1 and pH6 and 298K.

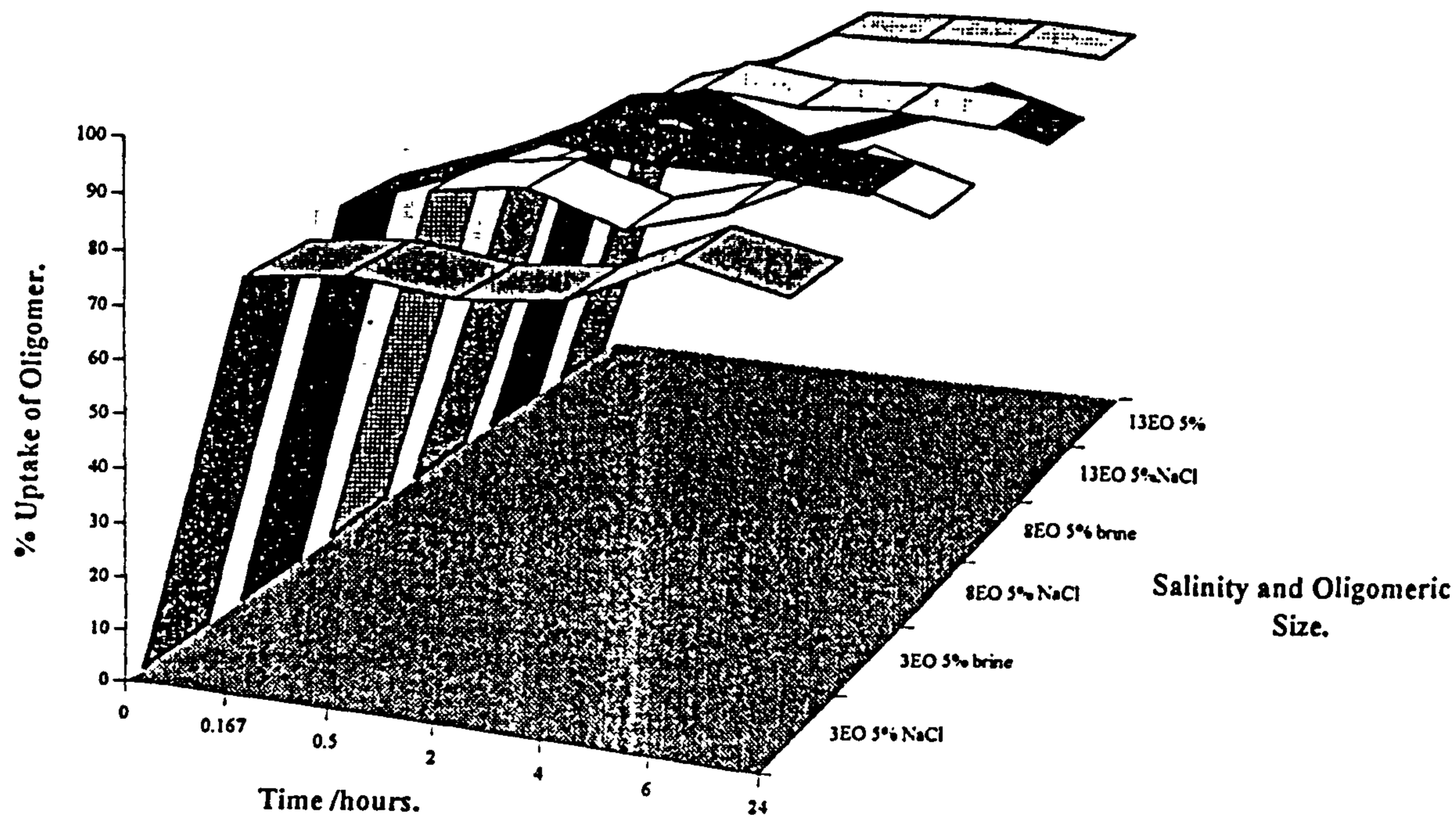

Figure 3.7: Variation of Oligomer Uptake on Quartz QB with Time and Salinity at x=1 and pH6 and 298K.

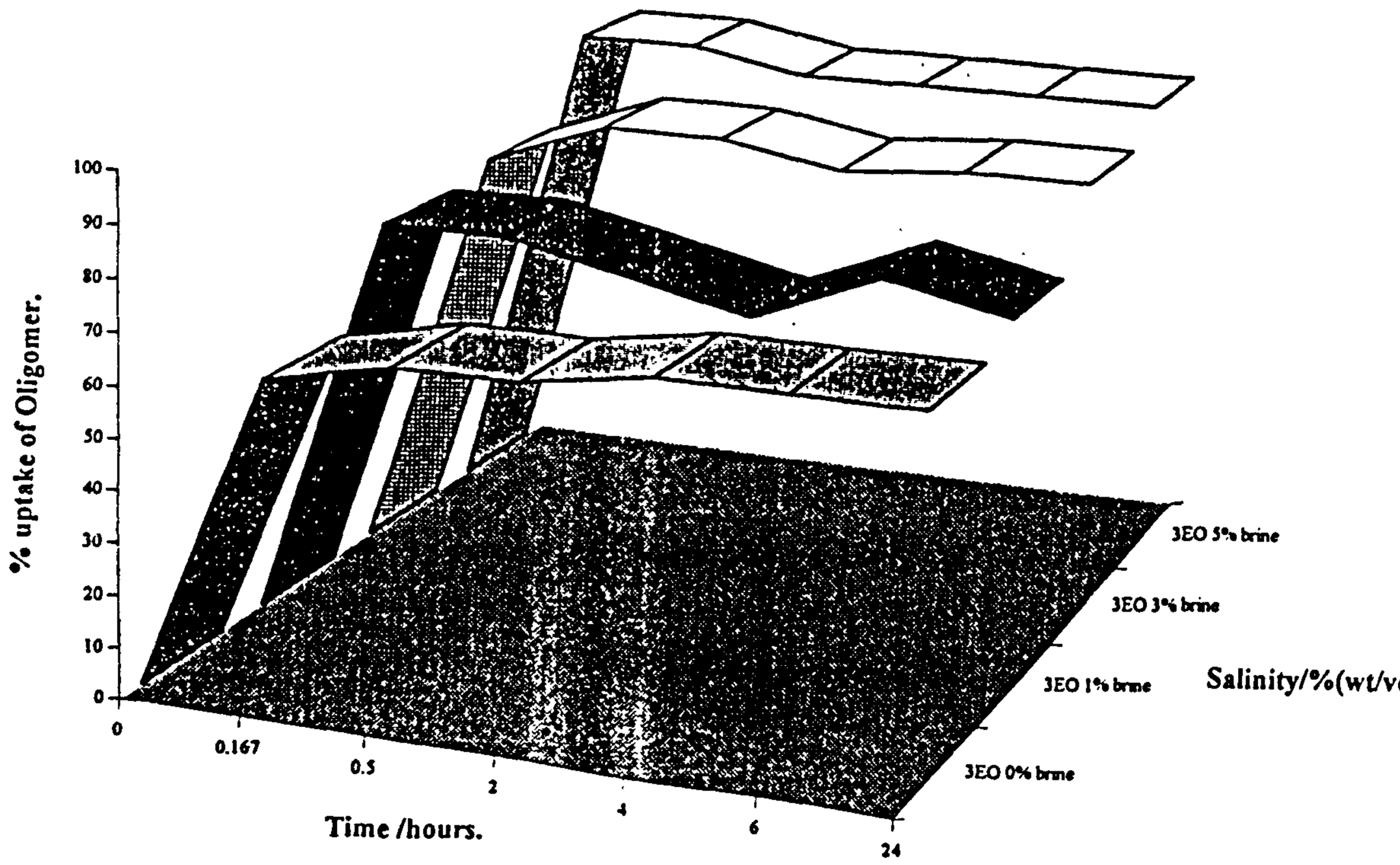

Figure 3.8: Variation of Oligomer Uptake on Quartz (QB) with Time and Salinity at x=0.5 and pH6 and 298K.

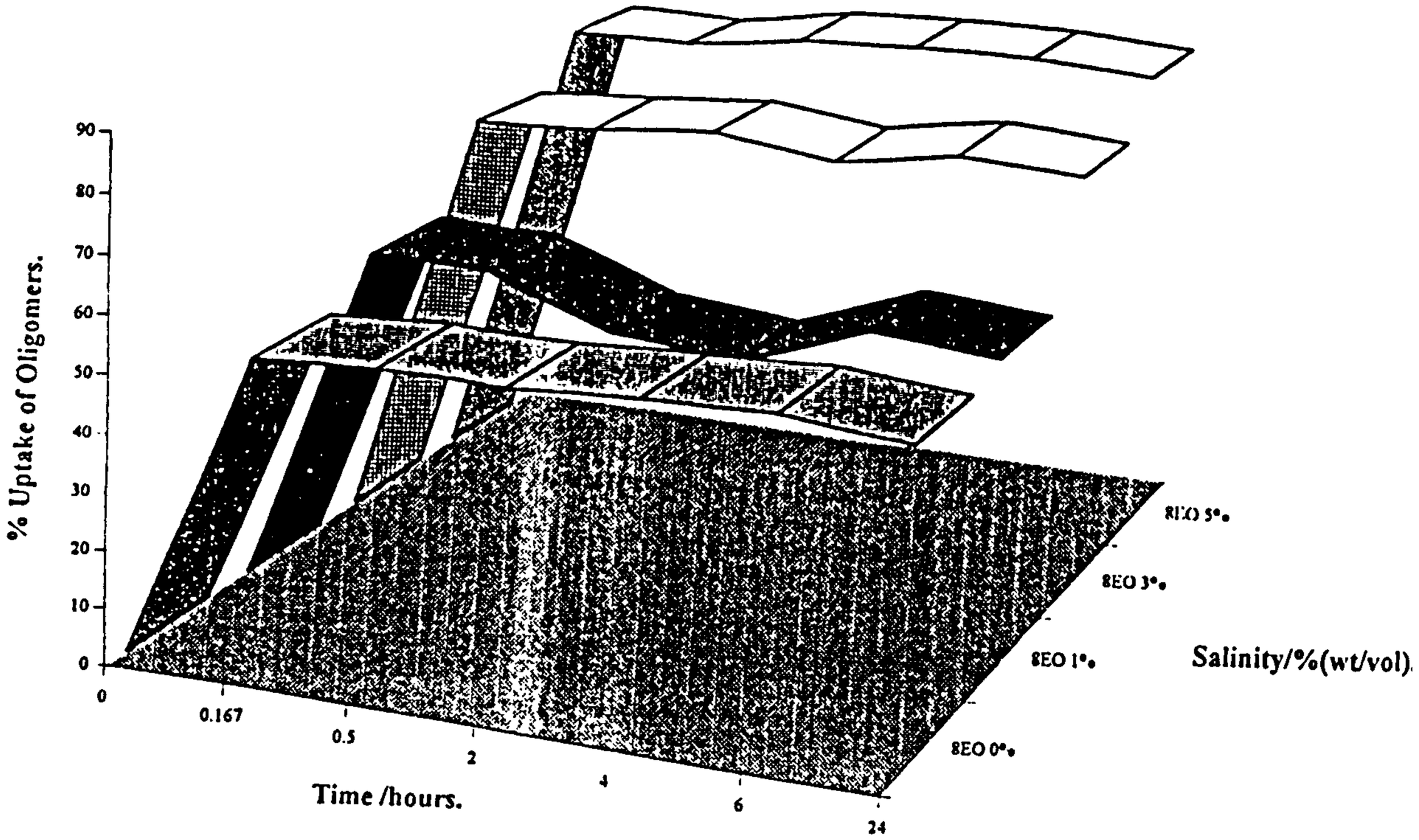

Figure 3.9: Variation of Oligomer Uptake on Quartz QB with Time and Salinity at x=0.5 and pH6 and 298K.

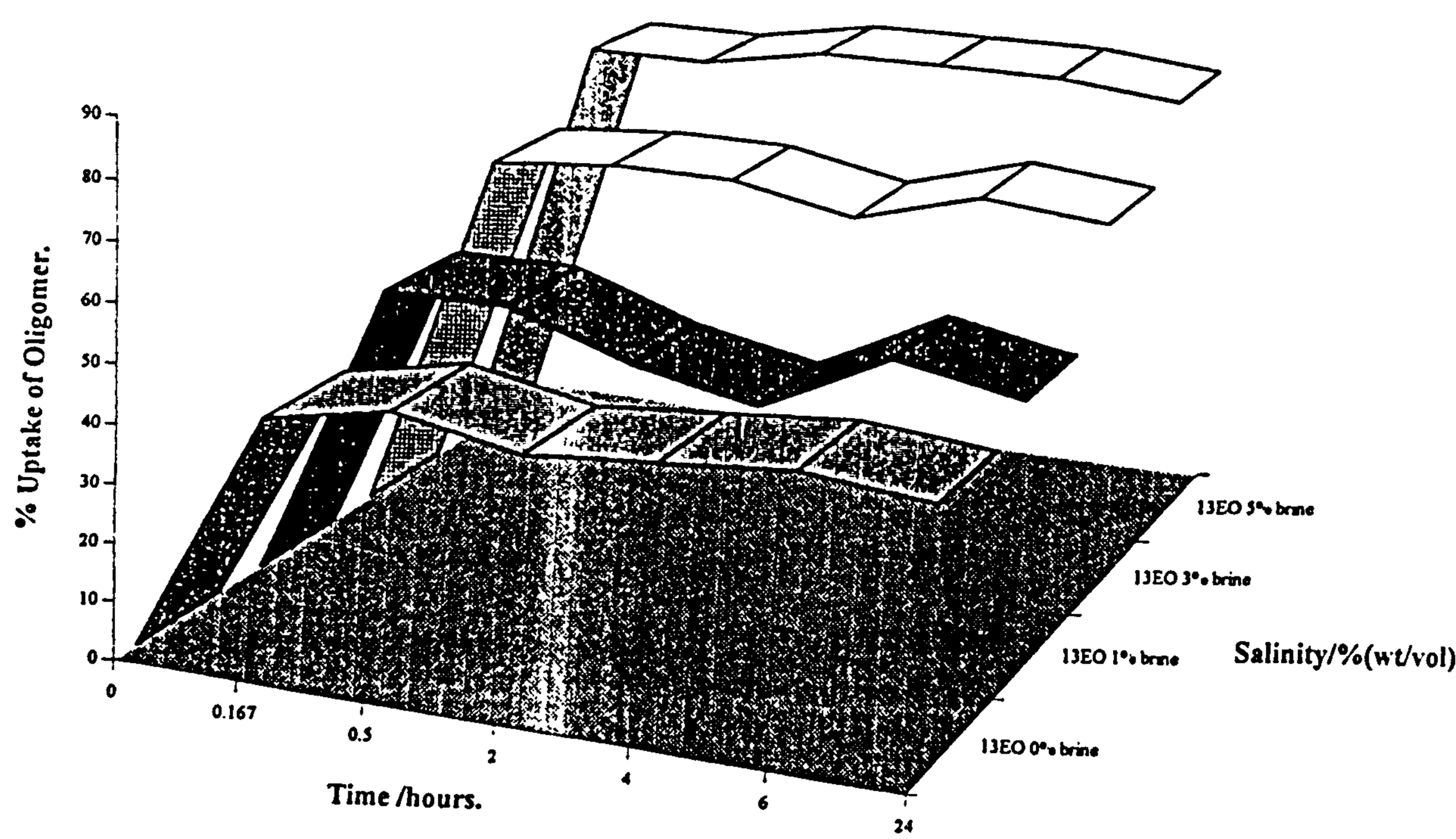

Figure 3.10: Variation of Oligomer Uptake and Quartz QB with Time and Salinity at x=0.5 and pH6 and 298K.

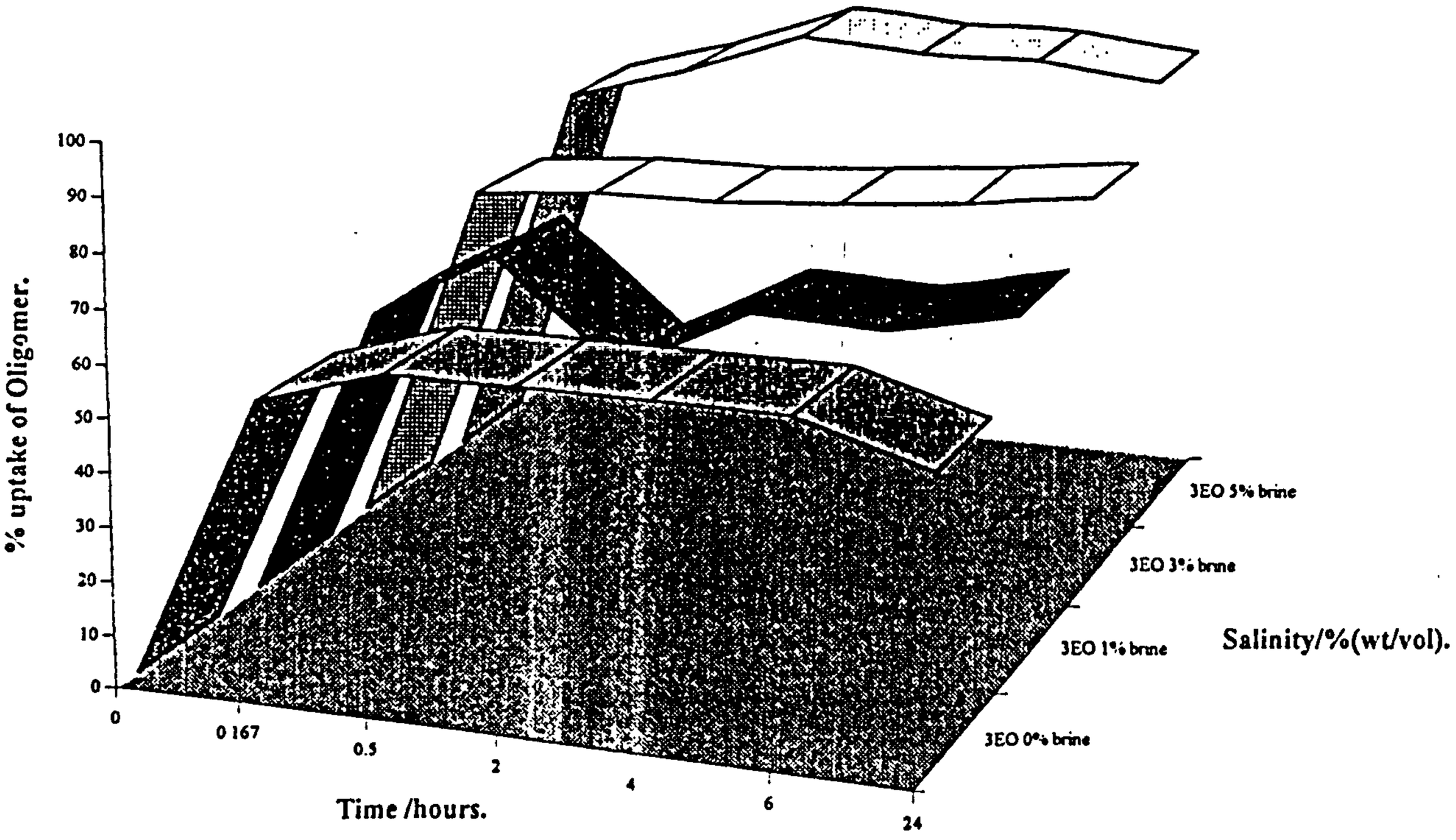

Figure 3.11: Variation of Oligomer Uptake on Quartz QB with Time and Salinity at x=1 and pH6 and 298K.

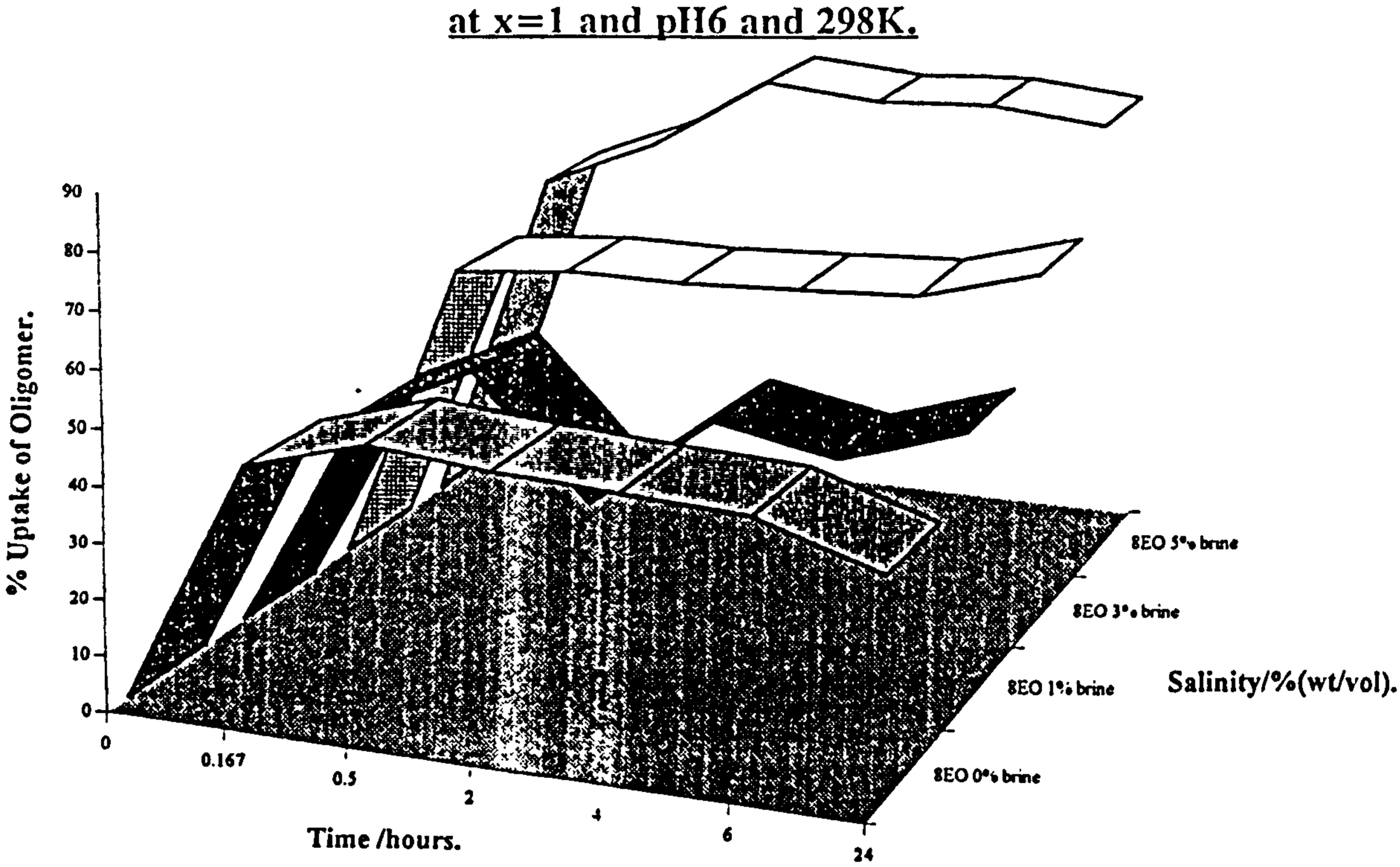

Figure 3.12: Variation of Oligomer Uptake on Quartz QB with Time and Salinity at x=1 and pH6 and 298K.

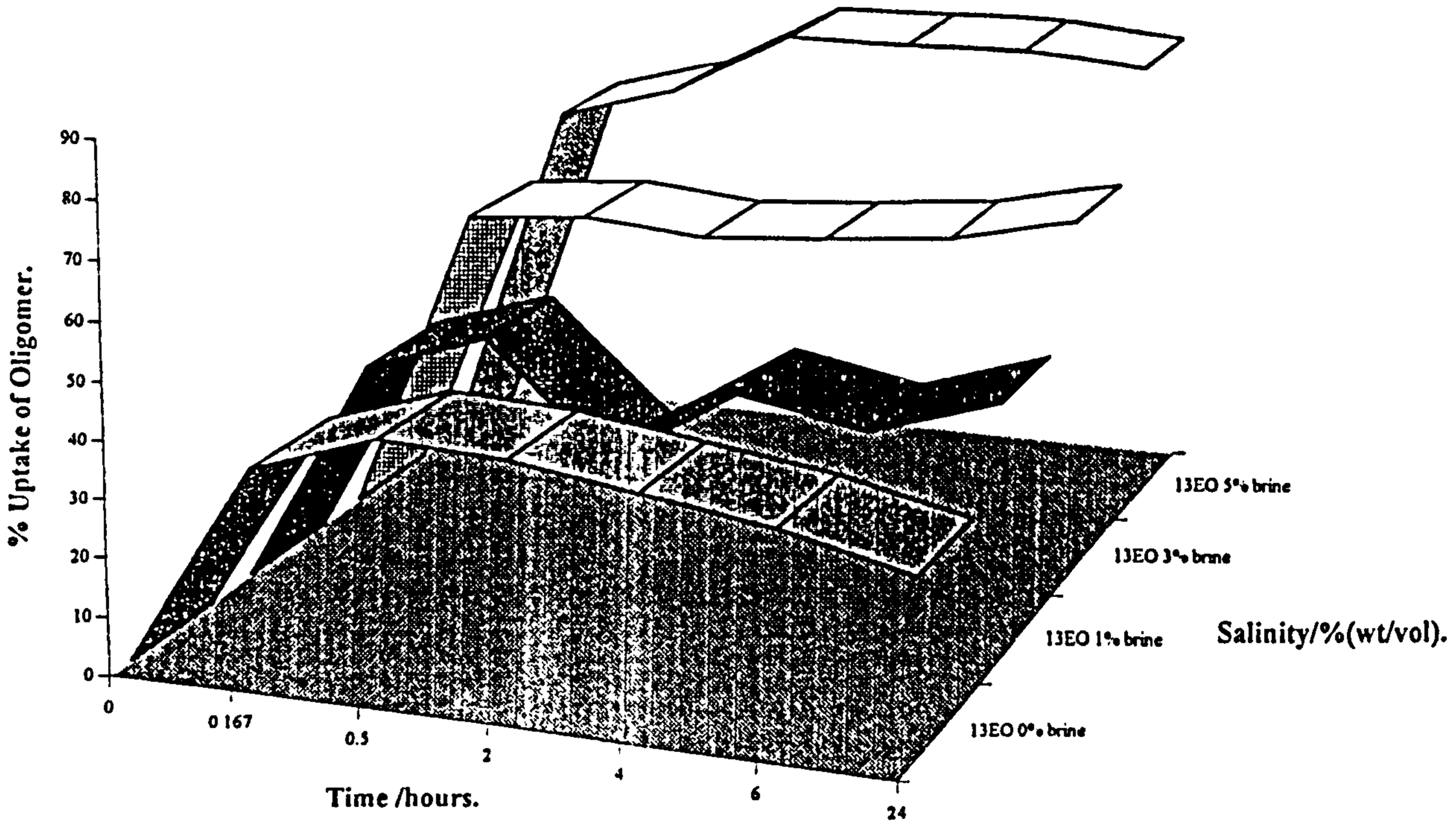

Figure 3.13: Variation of Oligomer Uptake on Quartz QB with Time and Salinity at x=1 and pH6 and 298K.

3.7.3 Temperature Effects.

Figure 3.14 shows the adsorption isotherms for TX-100 at increasing temperatures. At lower equilibrium concentrations the amount adsorbed decreases slightly with an increase in temperature, whereas the plateau value of the extent of adsorption increases with temperature. This is also in general agreement with other work (21,23). It is thought that the reduction in surfactant adsorption at lower coverages with temperature is due to an increased interaction of the surfactant chains with the solvent (21,24). Also, at this stage in the adsorption process the system is exothermic and therefore it follows that the amount of adsorbed surfactant will be lower when energy is added to the system. At the position on the isotherm where the process is endothermic (and driven by micellisation rather than individual monomer interaction with the surface), the opposite is true and adsorption is enhanced by the extra energy available. Also, at this stage the adsorption process is driven by the lateral interactions between the hydrocarbon tails of the surfactant molecules, and the process is thought to be equivalent to micellisation in solution (23). Micellisation is known to be induced by an increase in temperature and so it is valid to assume that

admicellisation would also be induced by elevated temperatures.

Figure 3.15 shows the adsorption isotherm measured at a temperature of 353K, approximately 15K above the cloud point. As can be seen it was difficult to obtain a plateau region for this temperature. Initially the adsorbed amount increases but reaches an amount at the plateau that is below that measured at 323K. The cloud point of TX-100 occurs at 338K (32) and the supersaturation of the surfactant at this and higher temperatures may induce the surfactant to remain in solution rather than adsorb onto a surface. Also, despite the fact that the solutions were centrifuged immediately on their removal from the oven the temperature drop will cause errors in the final result.

Oligomeric Analysis.

Figures 3.16-3.18 show the % uptake of the oligomers with temperature, time and position on the isotherm. Considering the extents of adsorption at 323K, it can be seen that the adsorption is increased at both the plateau region and x=0.5 of the isotherm for all sizes of oligomer, when compared to the extent of adsorption at 298K. Again the smallest oligomer is taken up the strongest by the quartz QB. Increasing the temperature of a surfactant solution is known to decrease the value of the CMC. Increasing the temperature of a micellar solution results in the dehydration of micelles and eventually causes a supersaturation of the aqueous surfactant solution (ie. the cloud point of the surfactant is reached). In the case of adsorption, the temperature increase may induce adsorption of the surfactant onto the quartz as micelles in an attempt to separate from the aqueous phase. At x=0.5 and 353K, the adsorption of the larger oligomers decreases when compared to their adsorption at 298K. In the monomeric form at increased temperatures the larger surfactant components will most likely have increased interaction with the solution (c.f. the Flory-Huggins parameter for polymers), these components would therefore resist adsorption at elevated temperatures. As previously mentioned, the isotherm at 353K was difficult to measure due to the wide scatter of experimental data most probably due to the phase separation of the surfactant at this temperature. At the plateau of the isotherm the adsorption is increased to a great extent, particularly for the larger oligomers, again probably due to the fact that the temperature increase induces the micellisation process and would therefore enhance admicellisation also.

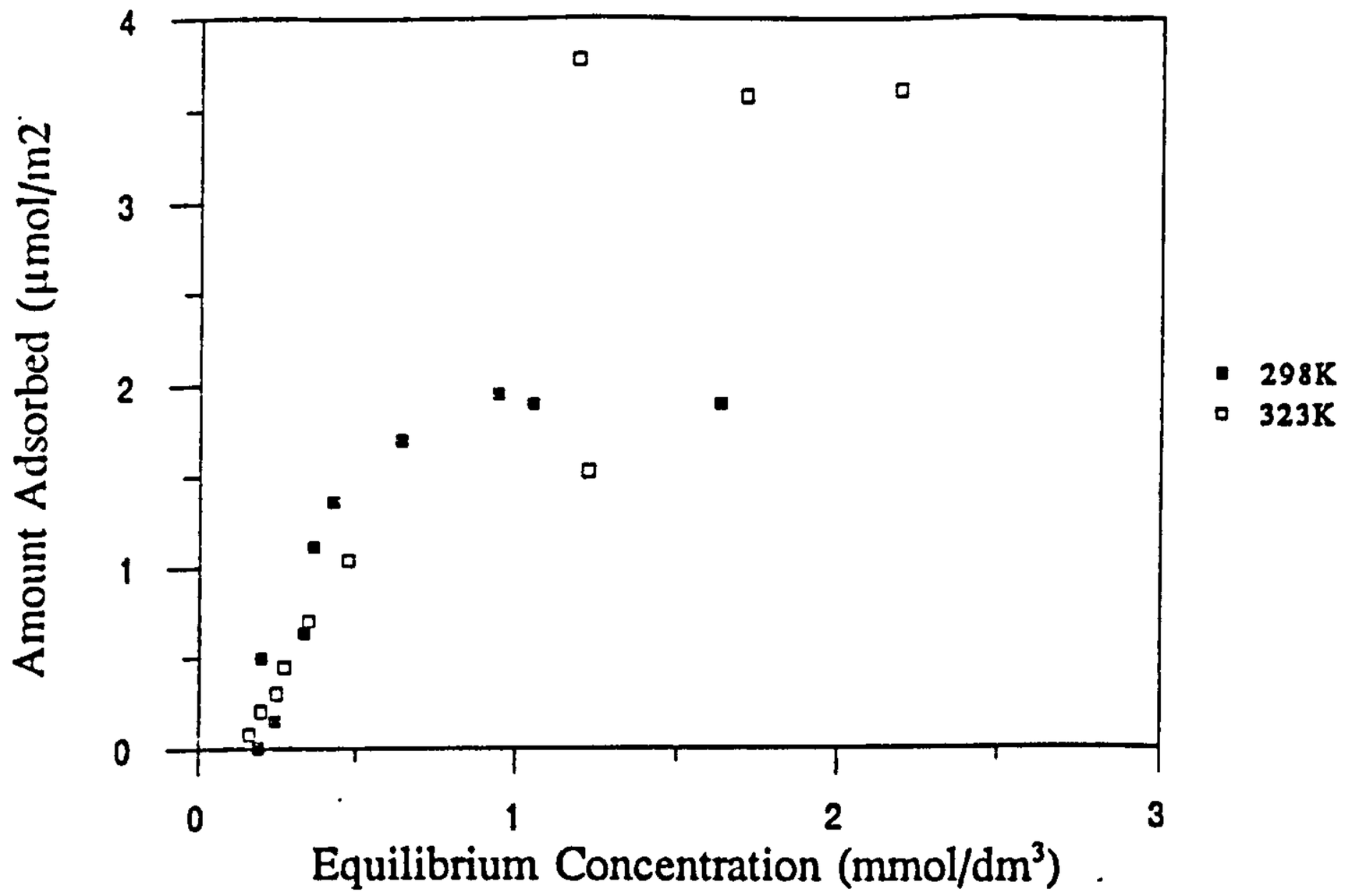

Figure 3.14: Adsorption Isotherm of TX-100 from Aqueous Solution (pH6) onto Quartz QB at Increasing Temperature.

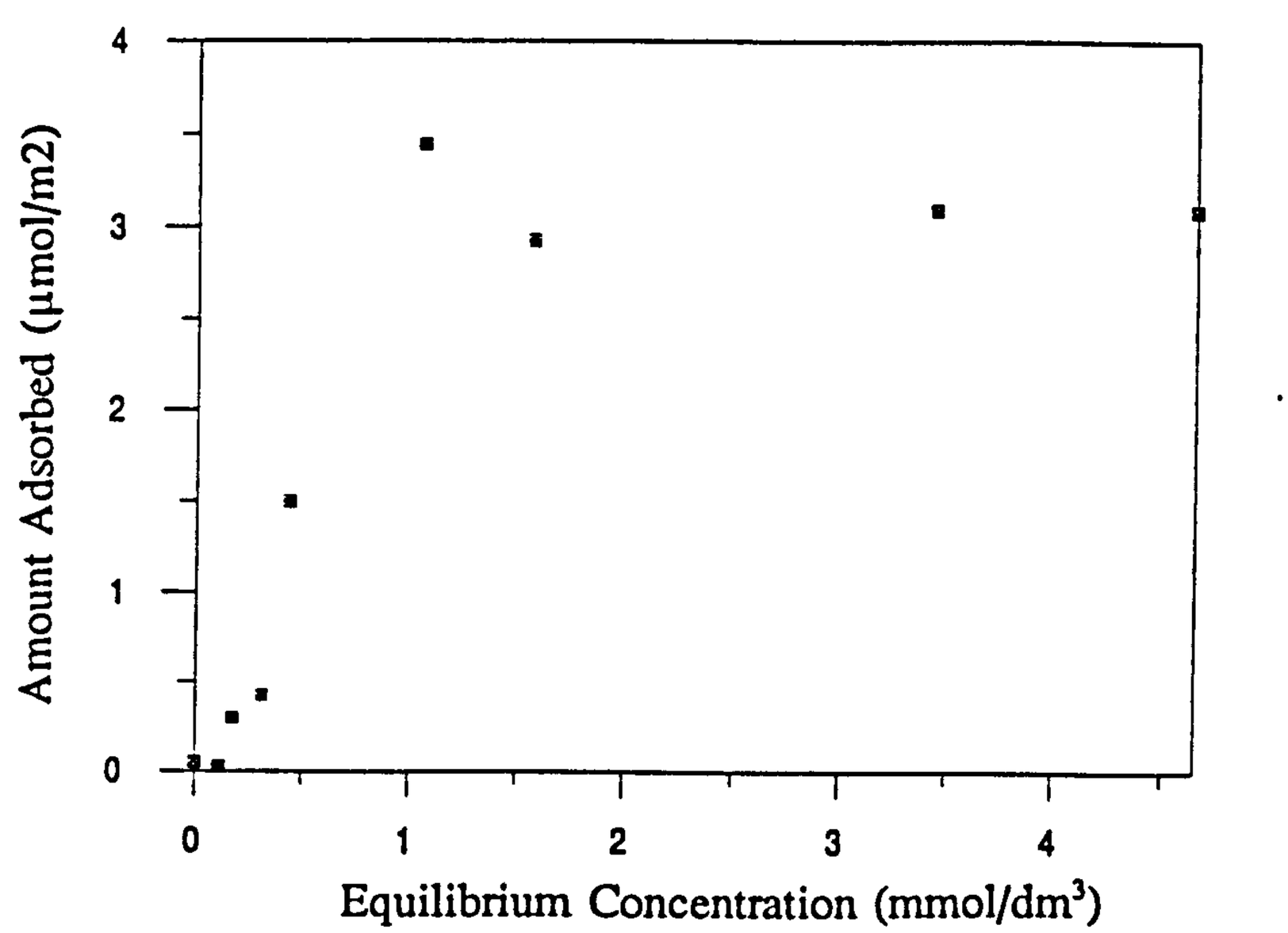

Figure 3.15: Adsorption Isotherm of TX-100 from Aqueous Solution onto Quartz QB at 353K.

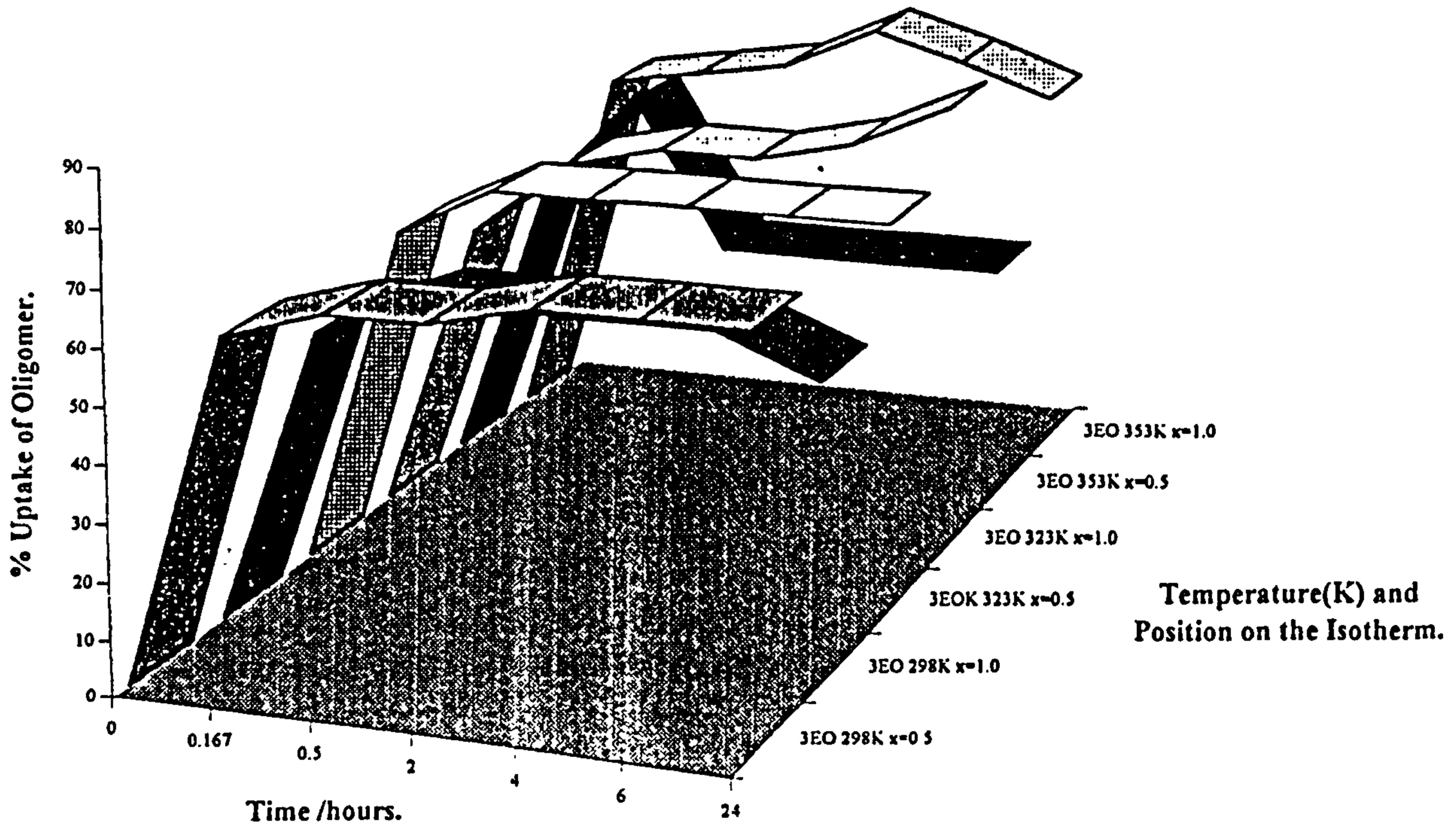

Figure 3.16: Variation of Oligomer Uptake on Quartz QB with Time and Temperature.

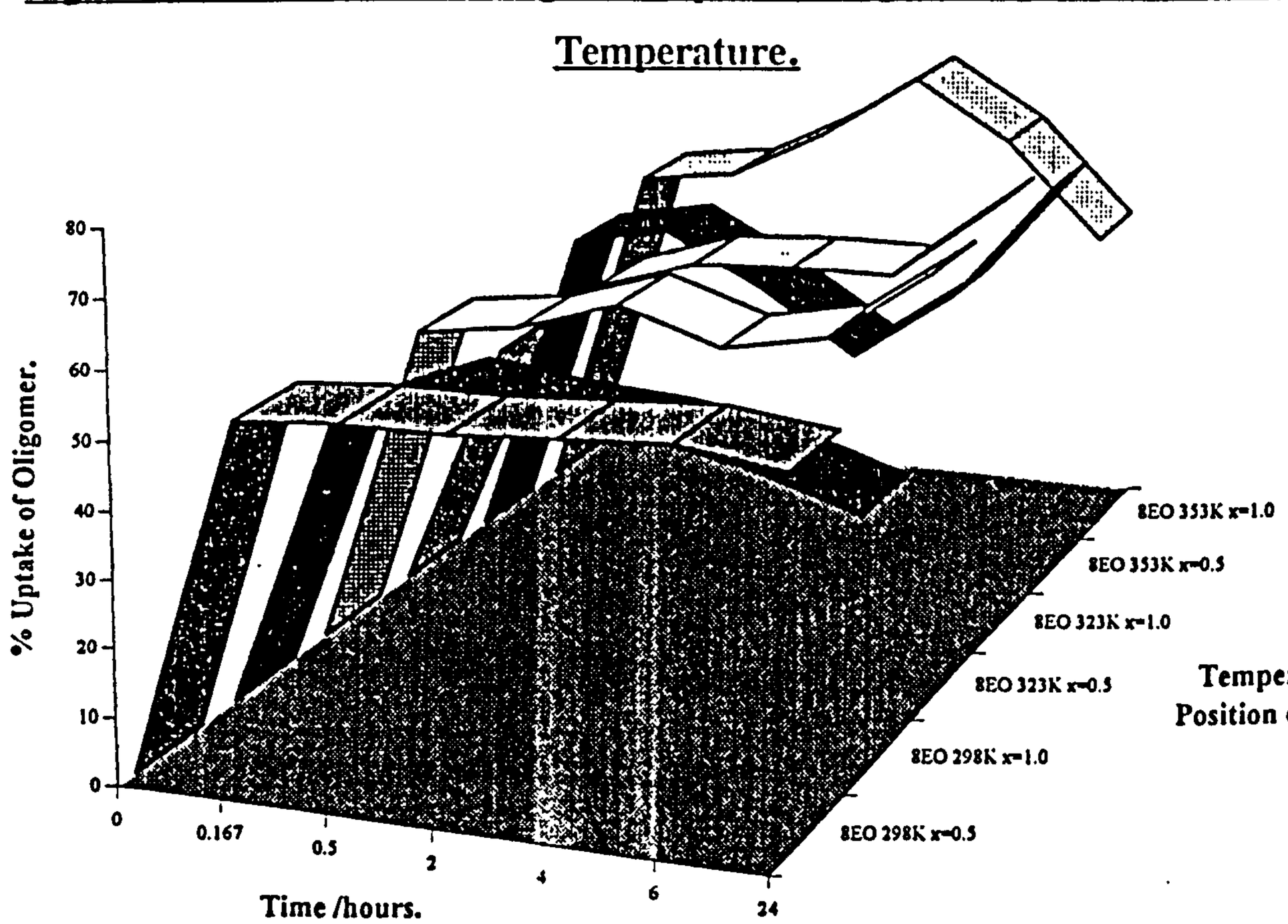

Figure 3.17: Variation of Oligomer Uptake on Quartz QB with Time and Temperature.

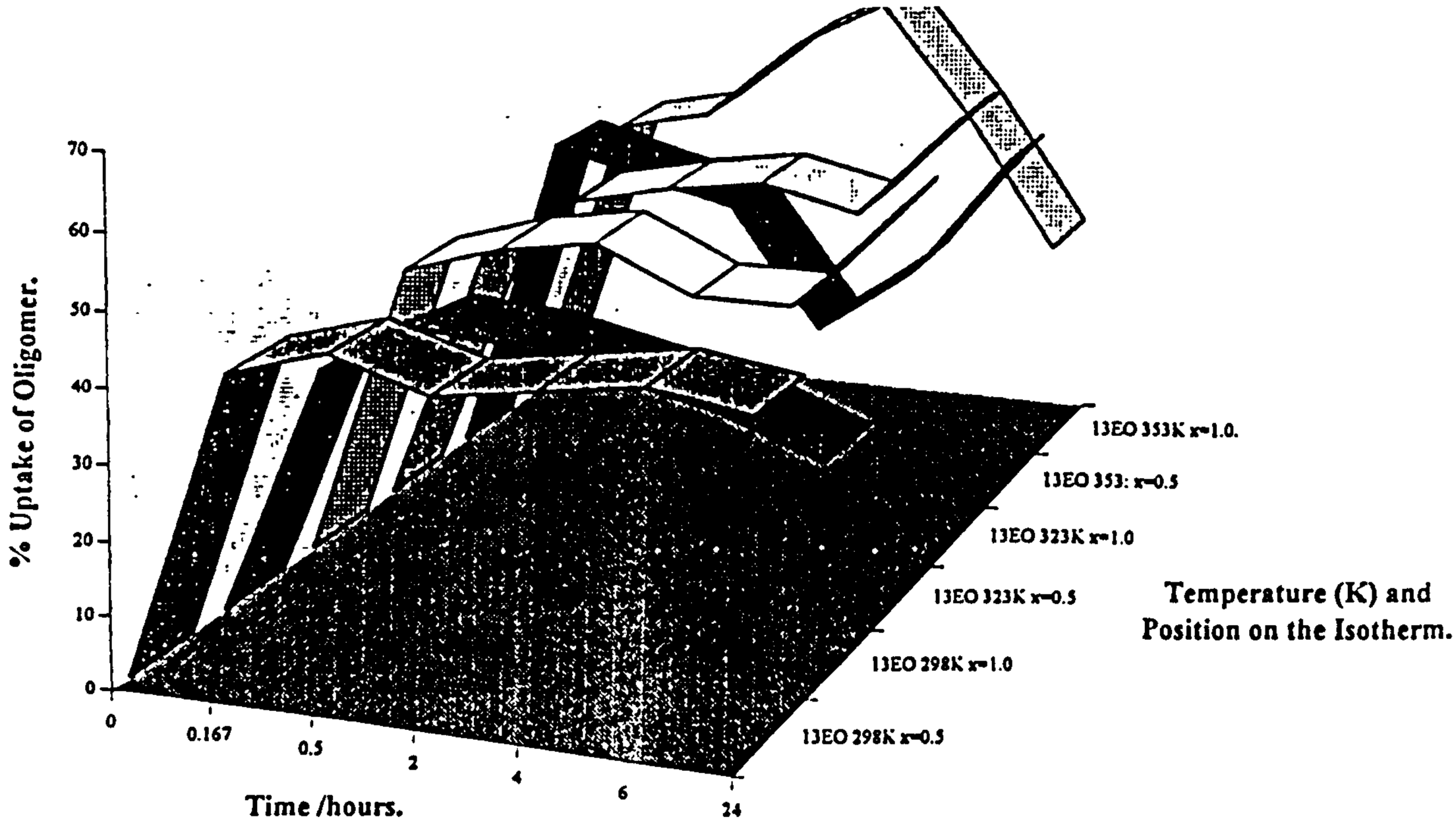

Figure 3.18: Variation of Oligomer Uptake on Quartz QB with Time and Temperature.

3.8 Effects of Heat Treatment of the Silica Surface on Surfactant Adsorption.

Figure 3.19 shows the adsorption isotherm for calcined quartz QC. It was observed that the amount adsorbed at the plateau increased considerably with heat treatment of the quartz sample, despite the findings described in Chapter 2 stating that the hydroxyl number decreases with heat treatment of the quartz together with the specific surface area of the sample (see sections 2.18 and 2.21, respectively).

The reactivity of silica is known to depend on the number and nature of the surface hydroxyl groups, via which the surfactant molecules form H-bonds. There are several different types of hydroxyl groups: free (isolated), bridged (hydrogen-bonded) hydroxyls and hydroxyl groups that are bound to water at the surface of the sample. Varying the numbers of silanol groups therefore can modulate the adsorptive properties of the silica. Zhuravlev (35) completed a thorough study of surface silanol groups on amorphous silicas, and concluded that silanol group concentration is independent of the structural characteristics of the sample (e.g. specific surface area and pore size distribution). On heating the quartz the number of hydroxyl groups on the surface of the silica decreases; heating at 1673K is known to result in the complete removal of the hydroxyl groups from the surface. Initially, the bridged groups condense, and at temperatures of 1073K and above, the hydroxyl group population is reduced to almost zero.

All of the factors described above point to the adsorption of materials onto heat-treated silica being reduced. When an adsorption isotherm is measured using a calcined silica sample, rehydroxylation of the sample cannot be ruled out. Indeed, Chapter 2 of this thesis shows that free and bound hydroxyl groups may reappear on submersion of the calcined sample in water. Kiselev et al (36) investigated the influence of temperature and the duration of hydrothermal treatment on the pore structure of silicas. It was found that although the specific surface area of the silicas is reduced upon heat treatment, the mean pore diameters vastly increased. It is possible in the light of these data that the micropores present in the silica samples are changing to mesopores on heat treatment. Certainly, the sample has a brittle feel to it when compared to the powder texture before treatment. It is possible then, that the increased surfactant adsorption is due to an increased porosity of the quartz upon heat treatment. Also, as was indicated by the XRF and XPS data described in sections 2.13 and 2.15, any carbonaceous material and ions present on the silica are removed by heat treatment. This would leave the hydroxy groups present on the silica surface free from perturbation and therefore at liberty to form bonds with the surfactants.

The increased adsorption of surfactant onto calcined quartz is most likely due to the removal of impurities from the surface of the quartz and/or an alteration of pore structure on heat treatment. Further experimentation is needed to investigate this problem which would involve careful measurements of the changes in adsorbed amounts of surfactant with changes in treatment of the quartz surface.

3.9 Effect of Changing the End of the Ethoxylate Chain.

To study the effect of changing the end hydroxyl group of the ethoxylate on the extent of adsorption, TX-100 was sulphonated in the organic chemistry department at Brunel University. The sulphonation was carried out via the scheme set out below.

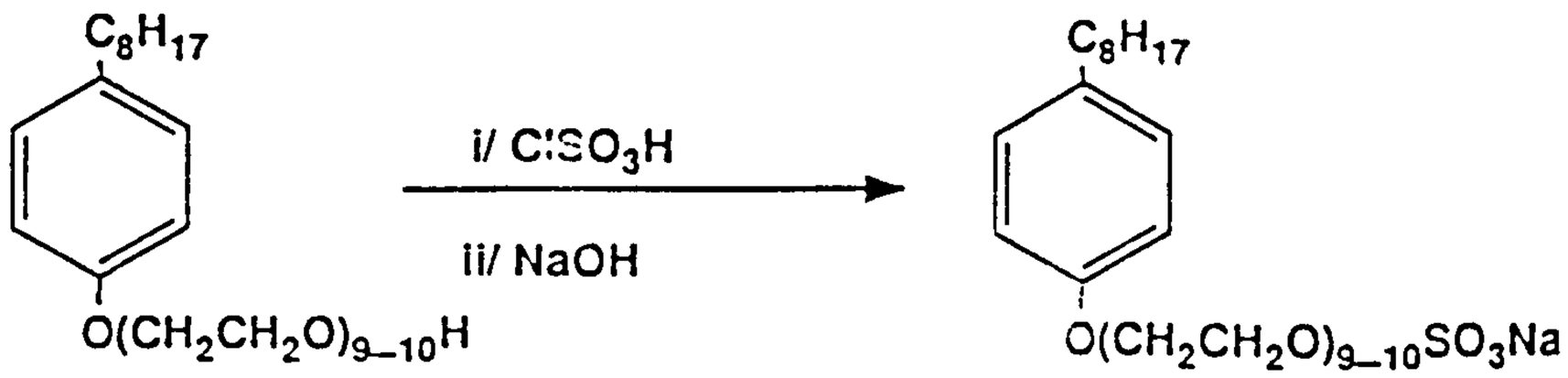

The adsorption isotherm obtained for this surfactant on QB is shown in Figure 3.20. As one can see the surfactant was only slightly adsorbed onto the silica; from these results we could assume that the negative charge on the sulphonated surfactant was repelled by the negative charge on the silica surface.

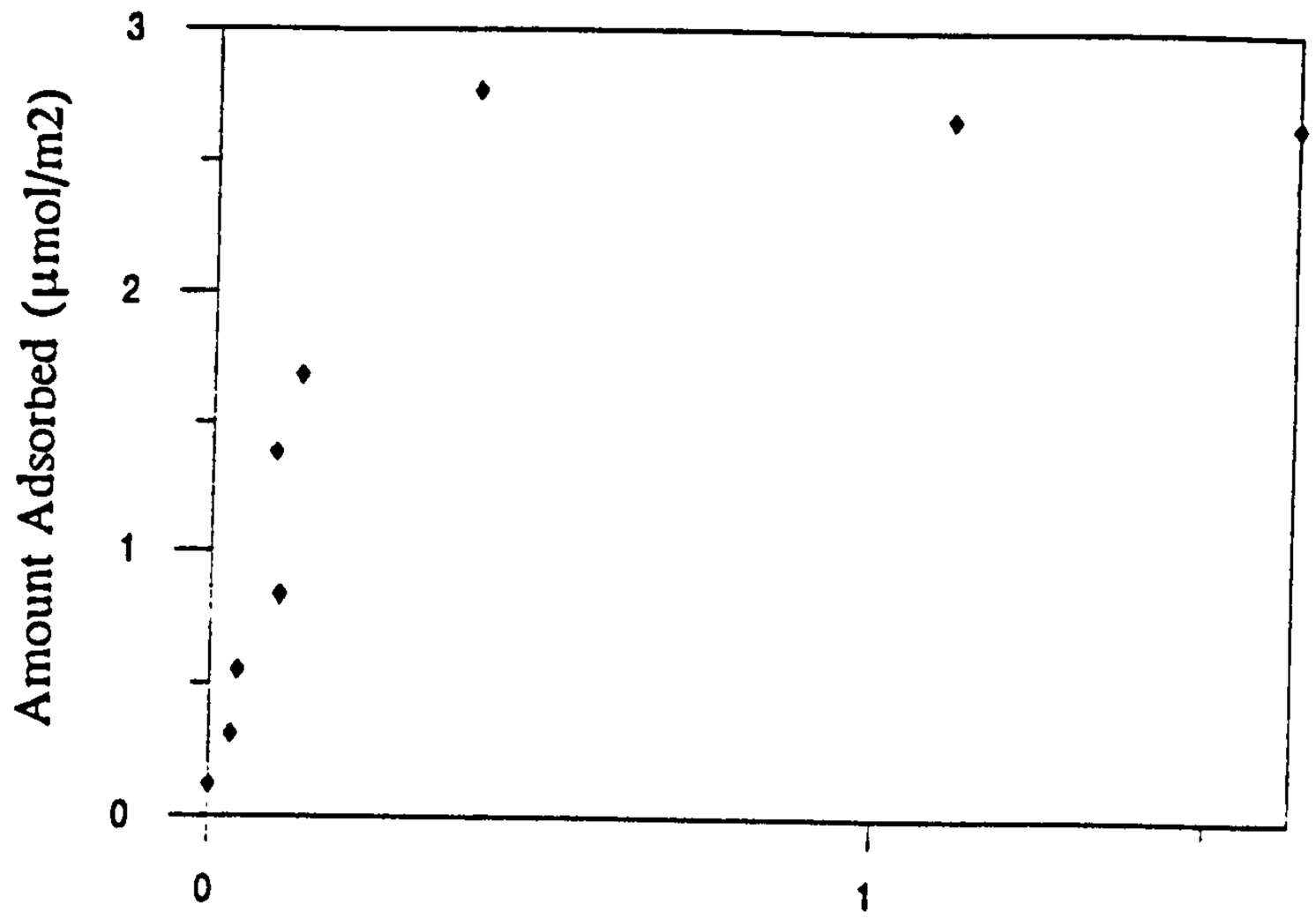

Figure 3.19: Adsorption Isotherm of TX-100 from Aqueous Solution (pH7) onto Calcined Quartz QC.

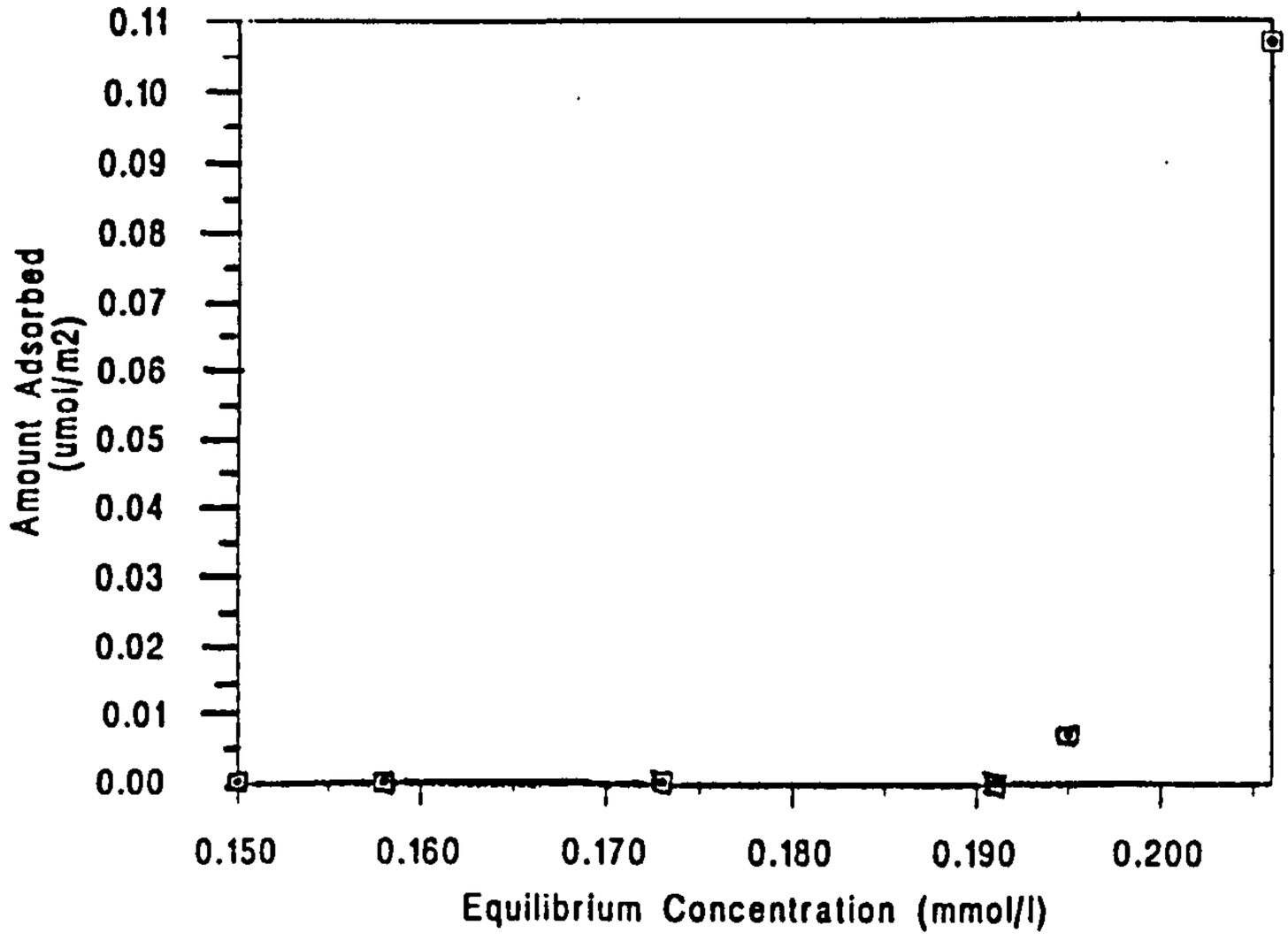

Figure 3.20: Adsorption Isotherm of Sulphonated TX-100 from Aqueous Solution (pH6.0) onto Quartz (QB).

3.10 Flow Rig Analysis.

A rig was constructed (see Figure 3.21), based on HPLC, in order to observe surfactant depletion from solution as a result of adsorption onto quartz in a dynamic environment. Aqueous solutions of known concentrations of the surfactant were placed at the inlet of the system and pumped through a column (that was prepared at Brunel and contained a known weight of quartz, QB)) at a known flow rate for a measured length of time. The profiles of surfactant concentration at the outlet of the column were measured as a function of time using a UV detector. Measurements were made at different temperatures and salinities of the TX-100 solution. Relevant data are shown in Figures 3.22 and 3.23. It was assumed that the plateau of the profile was equivalent to the surfactant concentration at the inlet. Initially all surfactant entering the column was adsorbed and after approximately 45 min on stream the TX-100 surfactant was detected at the outlet. It can be seen that increasing the temperature and brine concentration caused a reduction in the time taken for the TX-100 to be eluted at a value that was comparable to the inlet concentration. Hence there was a reduction in the amount of surfactant adsorbed onto the quartz surface.

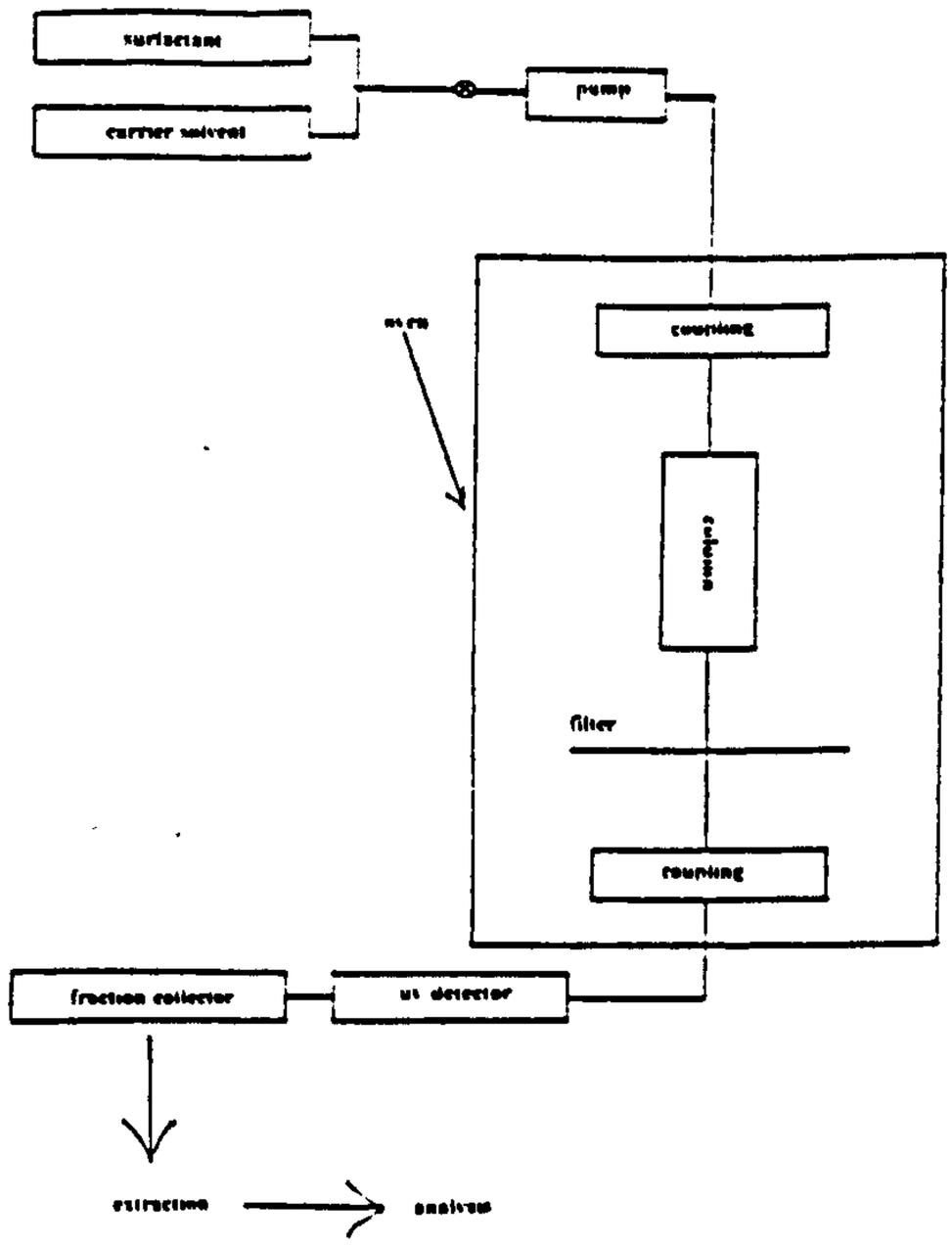

Figure 3.21: System used to Measure Adsorption Kinetics.

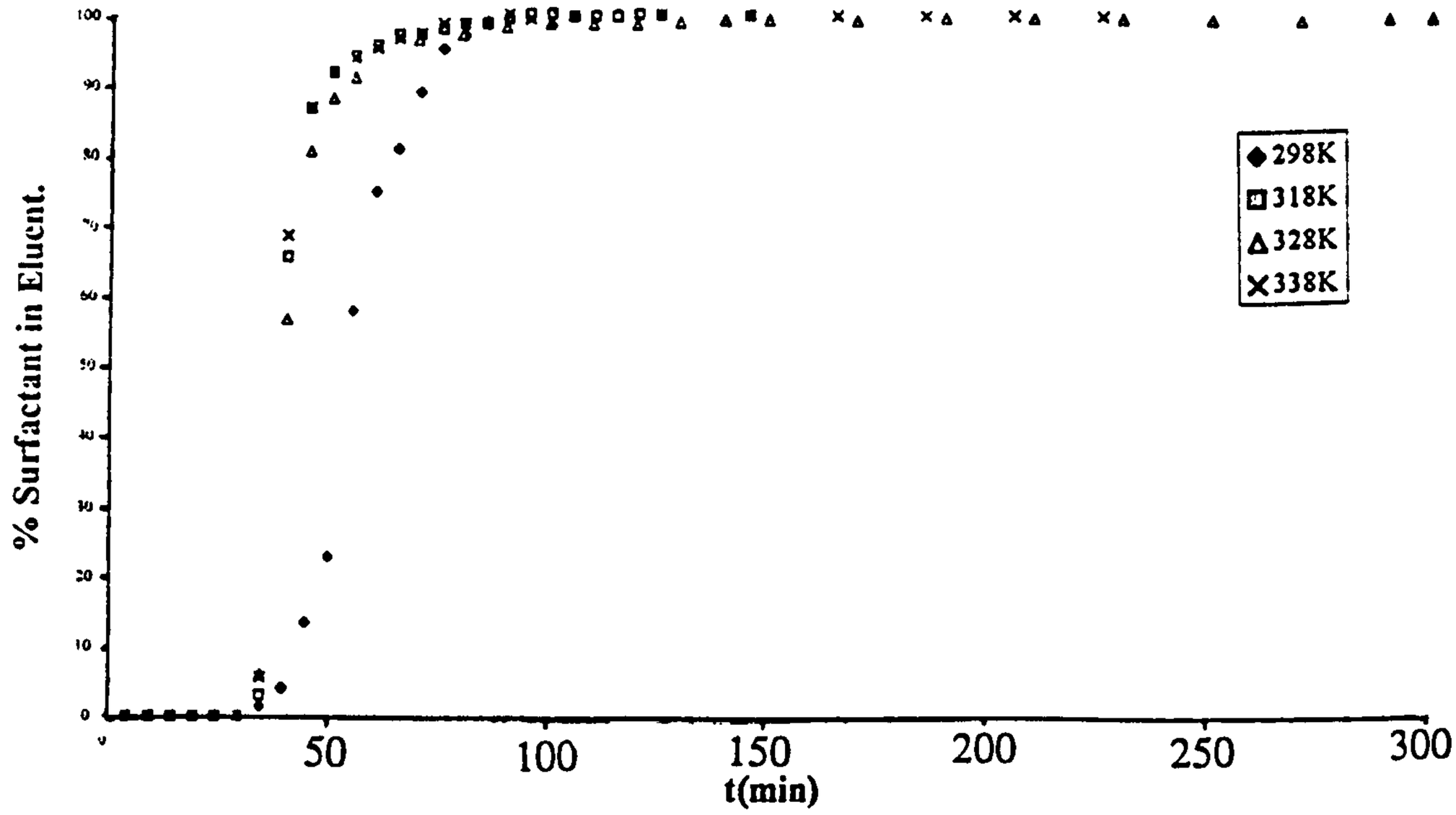

Figure 3.22: Measurements of (2.5 mol dm^{-3}) TX-100 Adsorption on to Quartz QB from Aqueous Solution with Time and Temperature.

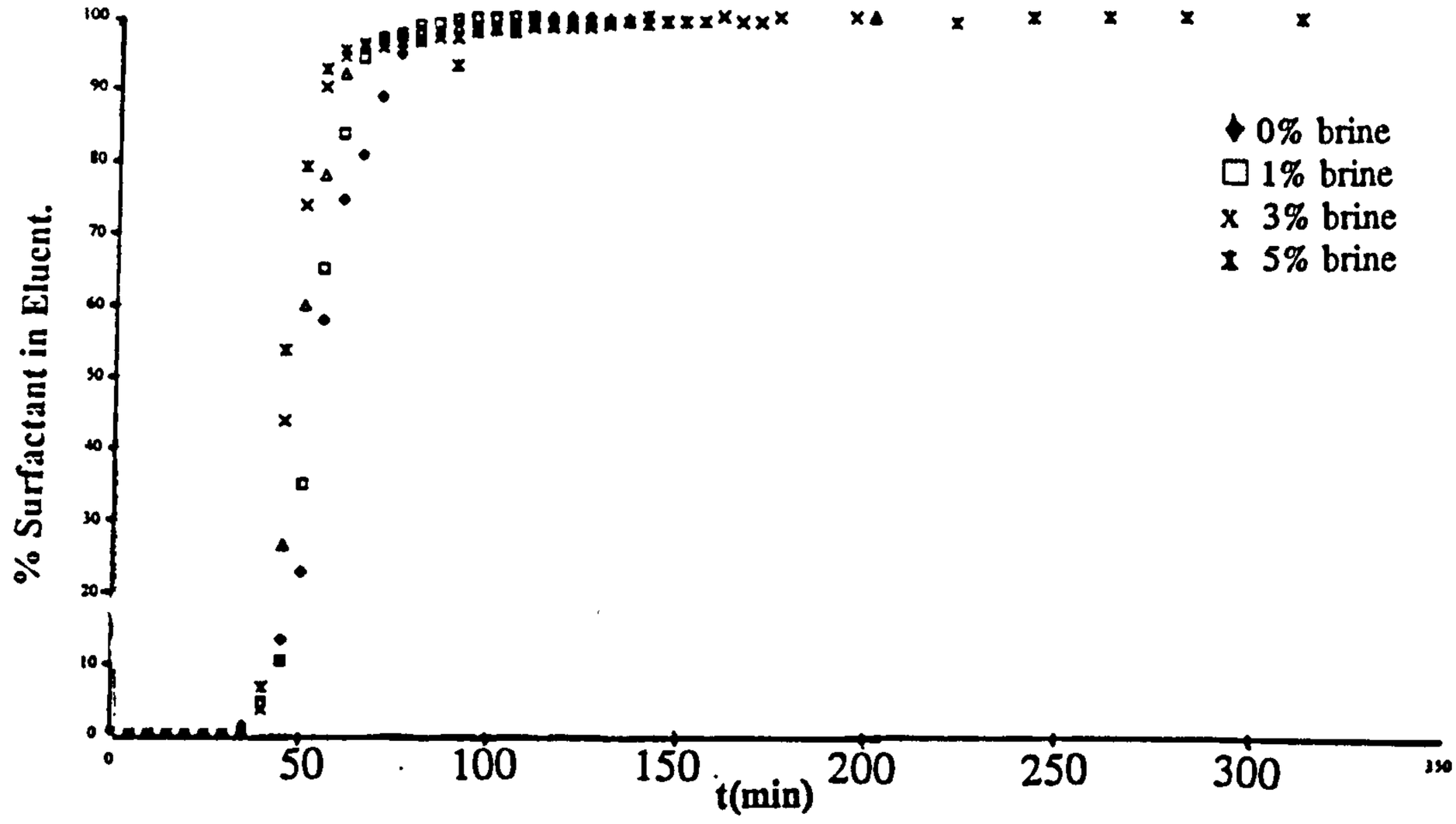

Figure 3.23: Measurements of (2.5 mol dm3) TX-100 Adsorption onto Quartz (QB) from Aqueous Solution with Time and Salinity.

3.11 Calculation of the Extent of Surfactant Adsorption.

The number of moles of surfactant which passed through the column per min., while the concentration of surfactant detected at the outlet was zero, were calculated (solution flow rates and inlet concentration values were known). As the weight of quartz in the column was known together with its surface area, one could calculate the amount of surfactant adsorbed onto the quartz column in moles per square metre. This calculation was repeated until the surfactant began to appear at the outlet.

At points where a percentage of the inlet surfactant concentration was being eluted, the concentration of the surfactant being held in the system at a given time was calculated by subtraction of the concentration of surfactant eluted from the column (calculated from the assumption that the level of the plateau on the profile was equivalent to the inlet concentration and that the concentration of surfactant at the outlet was directly proportional to the UV absorption shown on the profile) from the initial concentration of surfactant at the inlet. This concentration was then used as previously to calculate the number of moles taken up by the column, and so the amount adsorbed for that particular time interval was

calculated. All the increments of adsorbed surfactant were then added together and the total cumulative amount adsorbed for each time interval was calculated. These calculations are open to errors as the outlet concentration drifted somewhat and never quite reached the inlet concentration; errors of up to 10% occurred.

As can be seen from Table 3.3, the amount of surfactant that adsorbed onto the column seemed to decrease with increase in temperature and on the addition of brine. Batch isotherm measurements show an increase in adsorption with brine at all points on the isotherm, whereas increase in temperature shows a decrease in adsorption at low values of x and an increase in adsorption at the plateau of the isotherm. The observations made during batch experimentation are very different from the observations made for the dynamic measurements and are also difficult to explain. The dynamic system is much more complicated to describe as the adsorption process is not at equilibrium.

Table 3.3: Amounts of TX-100 Adsorbed onto Quartz QB in a Dynamic Environment Compared to those seen in Batch Experiments.

System T(K); % brine	Γ (μmol/m^2) (dynamic)	Γ (μmol/m^2) (batch)
298K, 0% brine	1.93	1.90
328K, 0% brine	1.70	3.70 (323K)
298K, 3% brine	1.74	2.5
298K, 5% brine	1.65	3

The anomalous results of the dynamic apparatus are due to the many limitations of this apparatus. Firstly, the inlet surfactant concentration was never quite achieved at the outlet for the time lengths used (and up to 24h); this was also found on a system that was used at CNRS, Marseille (37). This problem may have been due to detector drift caused either by particulate disturbance, as the system did not include a filter (because the operating

pressure of the system rose to an impractical level when a filter was used), or by bubble disturbance, when the oven was used during experiments involving higher temperatures. Also, density variations of the solvent and surfactants on heating during analysis may have caused errors in the UV absorption readings. The considerable amount of errors present in these results cause us to regard them as highly dubious. They are, however, considered to be a good starting point for future study.

Comparison of Various Methods of the Measurement of Surfactant Adsorption.

Both batch and dynamic methods for measuring the adsorption of aqueous solutions of surfactant onto quartz have their sources of error and uncertainty. The main source for both methods seems to be the detection of the equilibrium concentrations of the surfactant. It is my belief that small particles of quartz are never completely removed from the surfactant solution, and thus the UV absorption measurements taken after adsorption are effected.

Another source of error for both methods occurs when the temperature of the quartz/surfactant/aqueous systems are raised. If the temperature is raised above, or close to, the cloud point of the surfactant then the adsorption process becomes complicated by surfactant molecules interacting more strongly with the solvent and with each other. Particularly, batch measurements taken at higher temperatures showed much deviation.

As a consequence of the above points, it is feasible to state that adsorption measurements of aqueous solutions of surfactant onto quartz, while not useless, give only approximate values of the extent of adsorption and an approximate picture of the mechanism of adsorption.

Recent literature (38,39) has shown that the differential molar enthalpy of adsorption is very sensitive to the different stages of the mechanism of surfactant adsorption. In future work, the author would use a mix of adsorption and enthalpy studies to determine extents and mechanisms of surfactant adsorption onto solid surfaces.

References.

(1) K.Fishbeck; H.Maas; H.Meisenheimer; Z.Physik.Chem., A171,385 (1934).

(2) E.Cunningham; J.Phys.Chem., 39,69 (1935).

(3) A.S.Coolidge; J.Am.Chem.Soc., 48,1795 (1926).

(4) I.Langmuir; J.Am.Chem.Soc., 38,2221 (1916).

(5) I.Langmuir; J.Am.Chem.Soc., 39,1848 (1917).

(6) S.Brunauer; P.H.Emmett; E.Teller; J.Am.Chem.Soc., 60,309 (1938).

(7) H.K.Livingston; J.Chem.Phys., 15,617 (1947).

(8) O.Redlich; D.L.Peterson; J.Phys.Chem., 63,1024 (1959).

(9) P.J.Malden; J.D.F.Marsh; J.Phys.Chem., 63,1309 (1959).

(10) C.H.Giles; D.Smith; J.Coll.Int.Sci., 47,755 (1974).

(11) C.H.Giles; A.P.D'Silva; J.A.Baston; J.Coll.Int.Sci., 47,766 (1974).

(12) J.O.Oscik; Adsorption, Ellis Horwood Ltd., UK. (1982).

(13) S.Partyka; M.Lindheimer; S.Zaini; E.Keh; B.Bruni; Langmuir, 2,101 (1986).

(14) J.Seidel; Thermochim.Acta, 229,257 (1993).

(15) F.J.Trogus; T.Sophany; R.S.Schechter; Soc.Pet.Eng.J., 17(5),337 (1977).

(16) L.A.Noll; T.E.Burchfield; W.D.Wood; 5th Am.Symp.EOR & Improved Drilling Technology, B9/1-B9/5 (1979).

(17) W.P.Ramirez; P.J.Shuler; F.Friecman; Soc.Pet.Eng.J., 20,430 (1980).

(18) J.F.Scamehorn; R.S.Schechter; W.H.Wade; J.Coll.Int.Sci., 85(2),463 (1982).

(19) J.F.Scamehorn; R.S.Schechter; W.D.Wade; J.Coll.Int.Sci., 85(2),479 (1982).

(20) L.T.Lee; J.Lecourtier; G.Chauretean; Acs.Symp.Series, 396,224 (1989).

(21) Th.Van den Boomgard; Th.F.Tadros; J.Lyklema; J.Coll.Int.Sci., 116(1),8 (1987).

(22) P.Levitz; H.Van Damme; J.Phys.Chem., 90,1302 (1986).

(23) M.Lindheimer; E.Keh; S.Zaini; S.Pertyka; J.Coll.Int.Sci., 138(1),83 (1989).

(24) R.Denoyel; J.Rouquerol; J.Coll.Int.Sci., 143,555 (1990).

(25) J.Anstad; T.Loevereide; K.Olsik; J.Pet.Sci.Eng., 6,107 (1991).

(26) F.Giordano-Palmino; R.Denoyel; J.Rouquerol; J.Coll.Int.Sci., 165,82 (1994).

(27) S.Keith; C.H.Rochester; J.Chem.Soc.Far.Trans.I, 84,3641 (1988).

(28) Y.C.Kong; D.Nicholson; N.G.Parsonage; L.Thompson; J.Chem Soc. Faraday Trans.,91,4261 (1995).

(29) G.Gonzalez; A.M.Travailloni-Louvisse; Langmuir, 5,26 (1989).

(30) D.M.Nevskaia; unpublished data; UNED, Madrid (1994).

(31) J.G.Quian; J.P.Wu; T.R.Gu; Chem. J. China Univ., 17,933 (1996)

(32) H.Schott; A.E.Royce; S.K.Han; J.Coll.Int.Sci., 98(1),196 (1984).

(33) G.A.Parkes; Equilibrium Concepts in Natural Water Systems, W.Stumm (Ed).; Adv.Chem.Ser. 67,121 (1966).

(34) R.L.Rea; G.A.Parkes; ACS.Symp.Ser., 416,260 (1990).

(35) L.T.Zhuravlev; Langmuir, 3,592 (1980).

(36) A.V.Kiselev; V.M.Lukyanovich; Yu.S.Nikitin; E.B.Oganesyan; A.J.Sarakhov; Kolloidn.Zh., 3,388 (1969).

(37) R.Denoyel; personal communication (1994).

(38) J.Seidel; C.Wittrock; H.-H.Kohler; Langmuir, 12,5550 (1996).

(39) J.Seidel; C.Wittrock; H.-H.Kohler; Langmuir, 12,5557 (1996).

CHAPTER 4: Light and Neutron Scattering.

4.1 Light Scattering.

Light scattering can be observed nearly everyday of our lives: gas molecules present in the atmosphere scatter light causing us to see the sky as a vivid blue colour on a clear day, whereas the poor visibility in fog arises from light scattering by airborne water droplets (1). John Tyndall and Lord Rayleigh first studied the scientific phenomenon of light scattering theoretically by relating the properties of the scatterer (i.e. size, shape and refractive index) to the angular distribution of the scattered light (2). Indeed, isolated particles which are small when compared to the wavelength of light (the rule for Rayleigh's theoretical treatment) are known as point Rayleigh scatterers.

When light impinges upon matter, the electric field of the light falling incident on that matter causes a fluctuating polarisation of the electrons in the molecules constituting that matter. This means that the electrons are forced to move in one direction and the nuclei are forced to move in the opposite direction. The molecules diffuse randomly and subsequently radiate light (i.e. scattered light) in all directions. Most of the scattered light has the same wavelength as the incident beam (i.e. elastic scattering) and a small amount has a higher or lower wavelength (i.e. inelastic scattering). In static light scattering, the former is used.

Light scattering is widely used to obtain information such as molecular weight, size, shape and intermolecular structure of particles in solution. The contrast required to study particles in solution is provided by the difference in refractive indices of the particle and medium. The particles may be surfactant micelles, polymer aggregates or some other colloidal system.

There are many types of light scattering theories that consist of models that correspond to differing systems (i.e. small molecules, liquids and solutions of small molecules and large molecules). In this work, dynamic light scattering was used to measure the motion of dilute solutions of small particles.

4.2 Dynamic Light Scattering.

Dynamic light scattering analysis of particles in solution allows the time scale over which the translational motion of particles takes place to be monitored. This information can be used to calculate the translational diffusion coefficient (D_z) of the particles. There are two methods of measuring this motion: quasi-elastic light scattering (QELS) and photon correlation spectroscopy (PCS). The random motion of particles in solution movements fluctuates with time (i.e. they undergo Brownian motion). This fluctuation in motion with time, which gives information about the movement or dynamics of the particles, causes light scattered by the particles to possess a range of frequencies that differ very slightly from that of the incident beam. The scattering is then said to be *quasi-elastic* (i.e. the light scattering is not quite elastically scattered). These frequency shifts can be measured using spectrum analysers and incident light sources that have extremely narrow frequency bands (i.e. lasers). This was the first dynamic approach. The advent of high speed correlators made it easier to work at fixed light wavelength and study fluctuations in the scattered signal with time.

PCS measures the fluctuations in intensity of the scattered light with time. To explain the phenomenon of fluctuations in scattered light intensity, consider the volume element from which light is scattered into the photomultiplier to contain, on average, 1000 particles. As a result of the random motion of these particles in and out of the sample volume this number may temporarily increase to 1001, 1002,...etc, or decrease to 999, 998...etc. It is clear, then, that the number of particles being sampled by the incident beam will not be constant and that the rate of change of the intensity of scattered light, I, given by the photomultiplier detector will depend on the rate of motion (D_z) of the particles in and out of the sample element (see Figure 4.1). In order to detect the fluctuations in intensity of scattered light when they are at a maximum, photodiode detectors with small apertures are used so that the scattered light entering the detector can be assumed to have originated from a very small volume element in the solution. The detector measures the number of photons of scattered light entering the detector during a specified, pre-set time interval (see Figure 4.1) that is varied during the analysis. Typically, 64 regularly increasing time values are chosen for the basis of the computer calculations (i.e. 1μs to 64μs). The incremental increase in time is known here as τ.

Over short time delays, measured photon counts will be comparable and are said to be correlated, that is I(t) and I(t+τ) are comparable values (where I(t) is the measured intensity at some time, t, and I(t+τ) is the measured intensity at some time, t+τ, later). If τ is large, the corresponding counts will not be correlated, that is, I(t) does not equal I(t+τ).

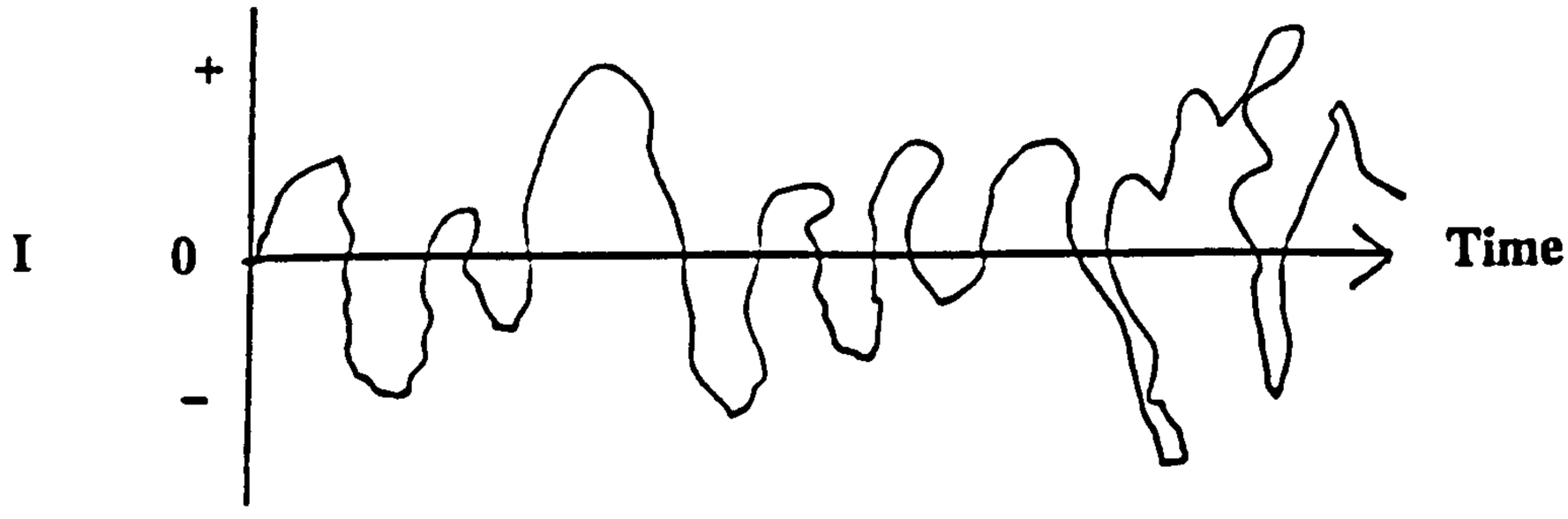

Figure 4.1: The Fluctuation of Intensity of Scattered Light Detected by the Photomultiplier.

A photomultiplier detects the fluctuations in intensity of the scattered light and its output is fed to a correlator, which calculates the 'autocorrelation function' of the process measured by the detector. The autocorrelation function is calculated by multiplying the incoming intensity with the stored intensity and adding this number to the accumulated correlation coefficient. The autocorrelation function has the form:

$$G_2(t) = \int_0^\infty I(t).I(t+\tau)\delta\tau = \langle I(0)I(t)\rangle$$

where: I(0) = scattering intensity at t=0,

I(t) = scattering intensity at time, t.

As I(t+τ) increases, an exponential decay function of scattered intensity is observed for translational (random) motion of equal sized particles. $G_2(t)$ (also known as the smooth decay function) is the time correlation function of the scattered light for polydisperse particles undergoing Brownian motion and is expressed as:-

$$G_2(t) = A + Bg_1(t)$$

where A and B are constants and,

$g_1(t) = \exp(-\Gamma_0 t)$ (for monodisperse spherical particles in solution).

Γ is the characteristic decay rate which is related to the z-average translational diffusion coefficient, D_z, of the particles.

$$\Gamma = D_z q^2,$$

where q is the scattering vector $= 4\pi n_0 \sin(\theta/2) / \lambda$
n_0 = refractive index of the solvent,
θ = angle through which the incident beam is scattered,
λ = wavelength of the monochromatic incident beam.

The Hydrodynamic Radius.

The diffusion coefficient, D_z, is defined by the Stokes-Einstein equation:

$$D_z = KT/6\pi\acute{\eta}R_H$$

where K = Boltzmann constant,
T = absolute temperature,
$\acute{\eta}$ = solvent viscosity,
R_H = the z-average hydrodynamic radius.

The speed with which the correlogram is resolved will depend on the number of scattering particles in the beam, the volume of the particles and the difference in refractive indices of the particles and medium.

4.3 Experimental.

Dynamic light scattering measurements were made in order to attempt to measure the thickness of an adsorbed layer of surfactant on spherical silica particles. The silica used for the experiments was in colloidal form and was purchased from Aldrich (commercial name: Ludox Cl-X). The physical attributes of this silica as defined by Aldrich are given in Table 4.1. Also, Figure 4.2 shows a TEM of the Ludox as received.

Dynamic light scattering experiments were carried out using a Malvern Zetasizer 3. Figures 4.3a and b show diagrams of the equipment used. The machine uses a 5mW

Helium Neon laser with a wavelength of 633nm. The measurements were taken at an angle of 90°. The mixtures were filtered into 1cm polystyrene cuvettes through a 0.2μm filter. If a value for refractive index was not known precisely then a default value corresponding to that for the solvent being used was inserted.

Table 4.1: The Physical Attributes of Ludox CL-X.

Property	CL-X
Average particle diameter/nm.	22
Specific surface area /m^2/g	130
Specific gravity (298K) (g/cm^3)	1.37

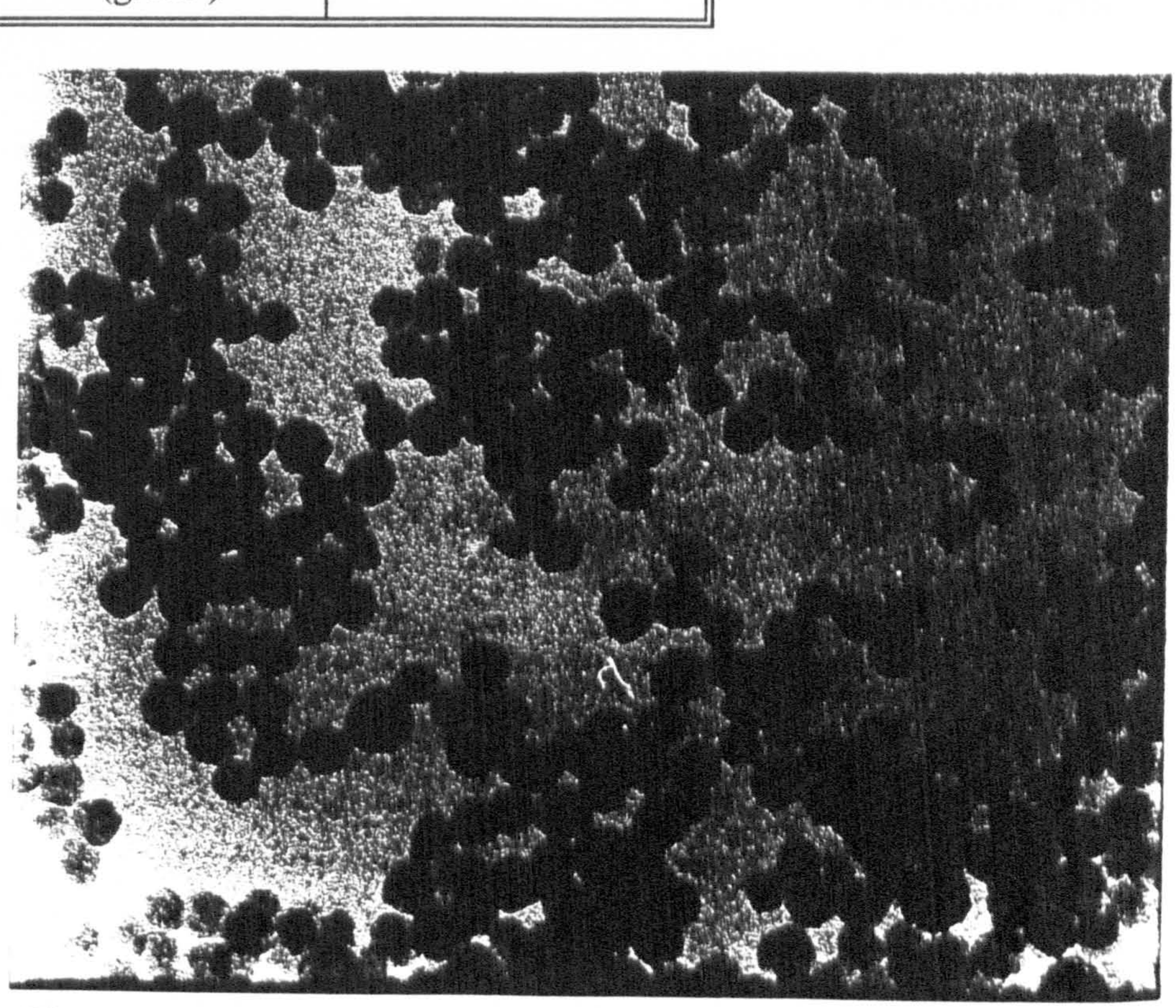

Figure 4.2: TEM of Ludox CL-X at 1/10 dilution magnified to 100K (1cm=0.1μm).

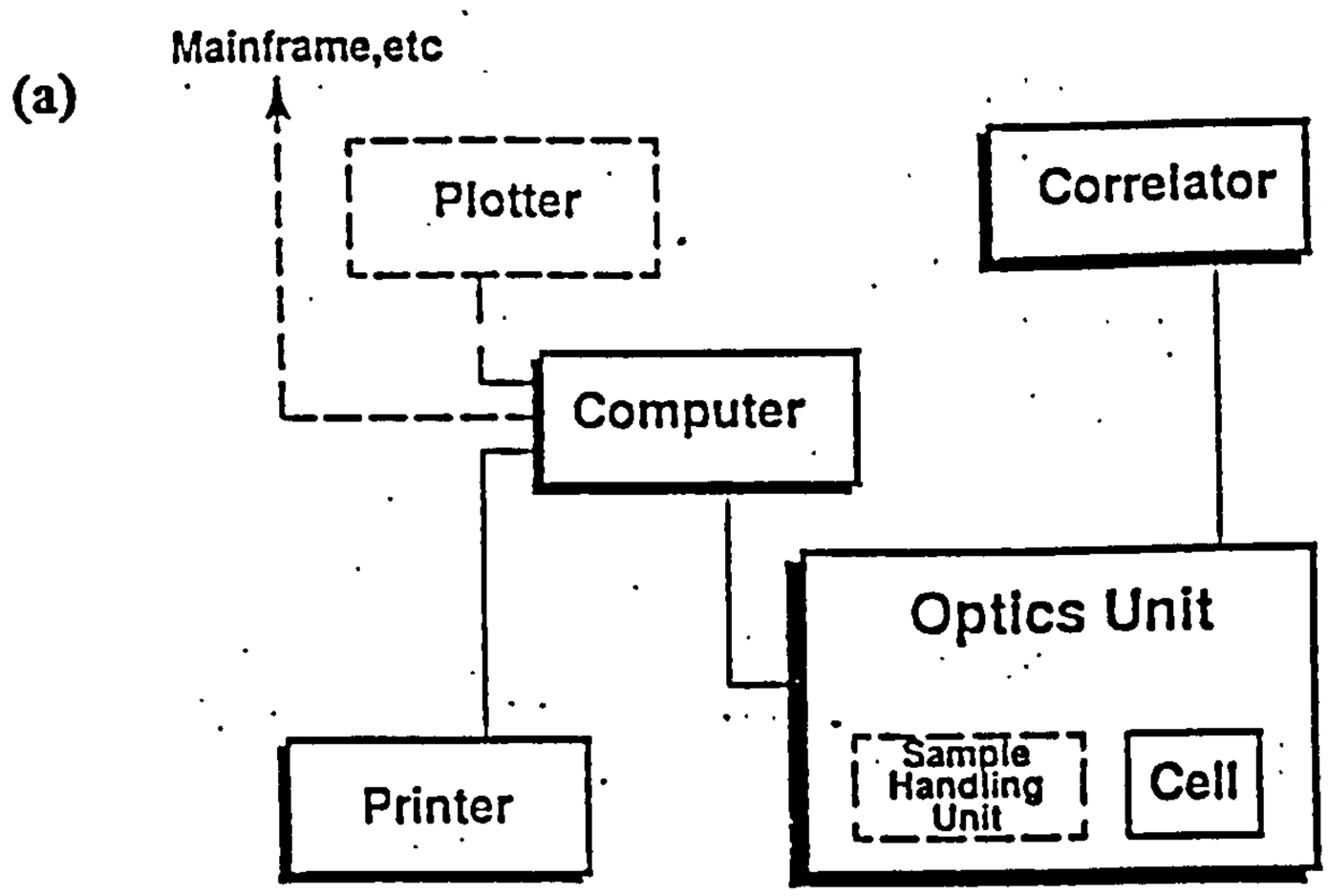

Figure 4.3: (a) Schematic Diagram of Equipment used for Dynamic Light Scattering.

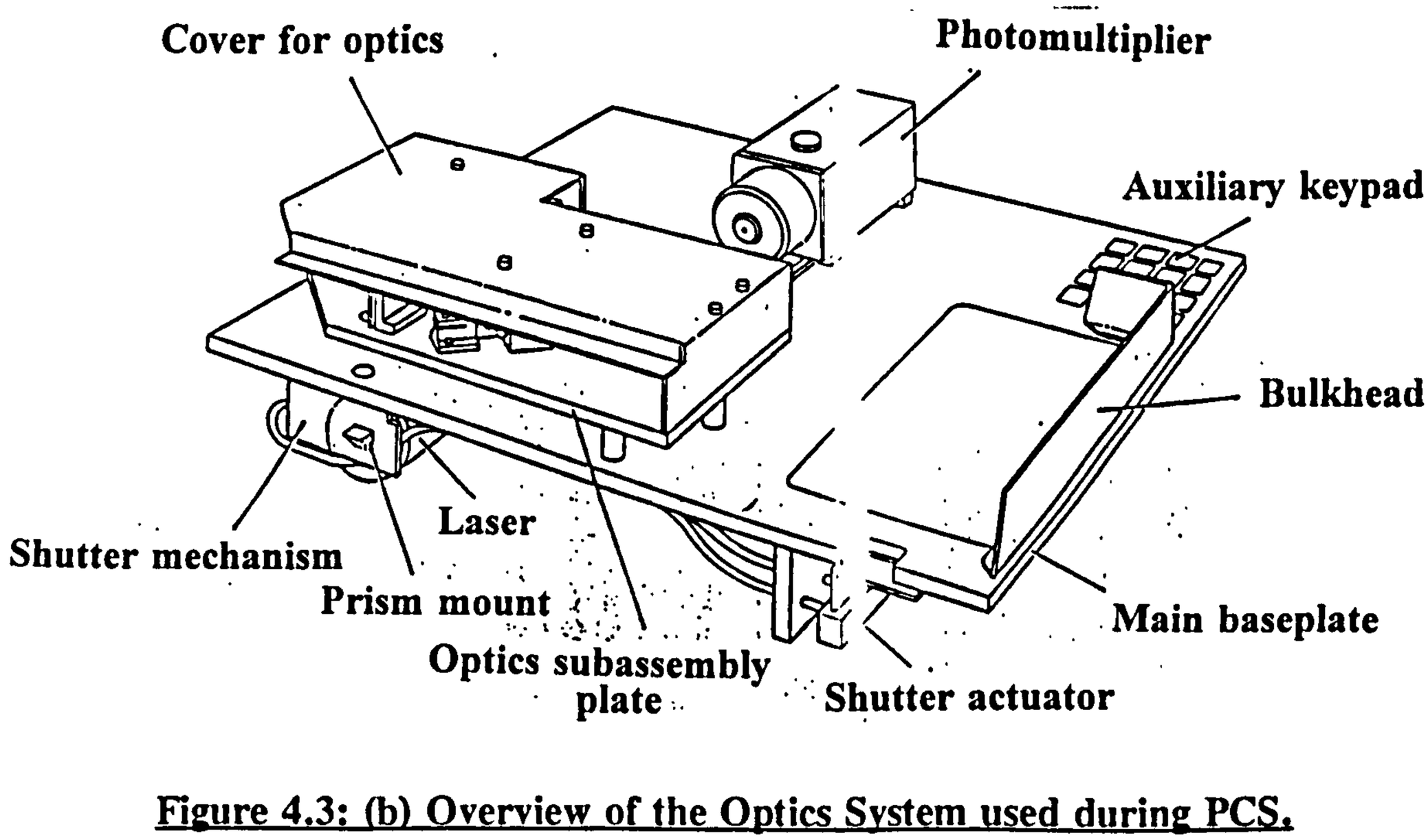

Figure 4.3: (b) Overview of the Optics System used during PCS.

Before light scattering measurements were made, a measurement of the adsorption isotherm of TX-100 onto the silica sol was needed so that it would be possible, when the dynamic light scattering measurements were carried out, to estimate the extent of

coverage of the silica at certain thicknesses or the thickness at an average coverage. Cummins et al (3) have previously used surface tension as a method of measuring the adsorption isotherm of surfactant onto the sol; they made the assumption that the surface tension of the bare sol was that of water. The surface tension of a mixture of surfactant and silica sol would give the amount of surfactant still left in solution (i.e. not adsorbed onto the silica surface); after measuring a standard surface tension curve for the surfactant alone, the adsorption isotherm of a series of mixtures of known concentrations of surfactant on a given volume of silica could be calculated. 2wt% solutions of the Ludox sol were made up using distilled water and known masses of surfactant were added. These mixtures were then left to equilibrate overnight. 2% solutions of the silica sol were chosen since Ramsay et al (4) concluded in an earlier paper that above this concentration the particles would not be arranged at random and would have some short range ordering present, thus complicating the values of scattered intensity obtained. The adsorption isotherm of TX-100 on the silica was measured in this way and is shown in Figure 4.4; the shape of the isotherm is comparable to those measured in the afore-mentioned paper (4) and indicated that, at the equilibrium concentrations of surfactant used, a maximum extent of adsorption was not being reached. Unfortunately, if higher concentrations of surfactant had been used, the increased viscosity of the surfactant/silica mixture would not have allowed accurate surface tension measurements to have been taken as the solution surface would be saturated with surfactant molecules (i.e. $d\gamma/dc$ is then 0). The results gained from this method of measuring the adsorption isotherm of surfactant onto silica sol were not taken as 'real' because the silica had a tendency to precipitate out of solution, thus making the calculations inaccurate.

A second attempt was made to measure an adsorption isotherm using visking tubing. The pore size of the visking tubing (2.8nm) is similar to the length of a single TX-100 molecule (approximately 2.5nm). A known volume of the suspension of silica and surfactant was inserted into a length of visking tubing and tumbled for a pre-determined time of 48h in a beaker of distilled water, again of known volume. The system reached equilibrium when the concentrations of molecules inside the tubing equals the concentration of molecules in the beaker. As the total volume of distilled

water in the beaker and visking tubing was known and the concentration of surfactant in the distilled water could be calculated from UV analysis, then the concentration of surfactant left in solution after adsorption could be calculated and hence the amount of surfactant adsorbed could be calculated. The adsorption isotherm measured by this method is shown in Figure 4.5. This time larger equilibrium concentrations were reached and, although there is some scatter of experimental results, the amount adsorbed seems to reach a plateau value of approximately 10μmol/m^2 at an equilibrium concentration of approximately 5mmol/dm^3. A model of the Freundlich isotherm (5) was superimposed onto the experimental data and gave a reasonable fit at low coverages of the silica. The difference at high concentrations may be due to the presence of higher initial concentrations of surfactant in the visking tubing which, because of the limiting size of the pores in the tubing, may have hindered the diffusion of the surfactant molecules into the beaker of distilled water, and therefore caused the calculated amount of surfactant adsorbed onto the silica to be more be higher than it actually was.

Despite a number of experimental uncertainties, the results obtained for the adsorption of TX-100 onto the silica sol using the visking tubing method were used as an initial guide when setting up the light scattering measurements. The larger molecule TX-305 was also studied as a comparison to TX-100.

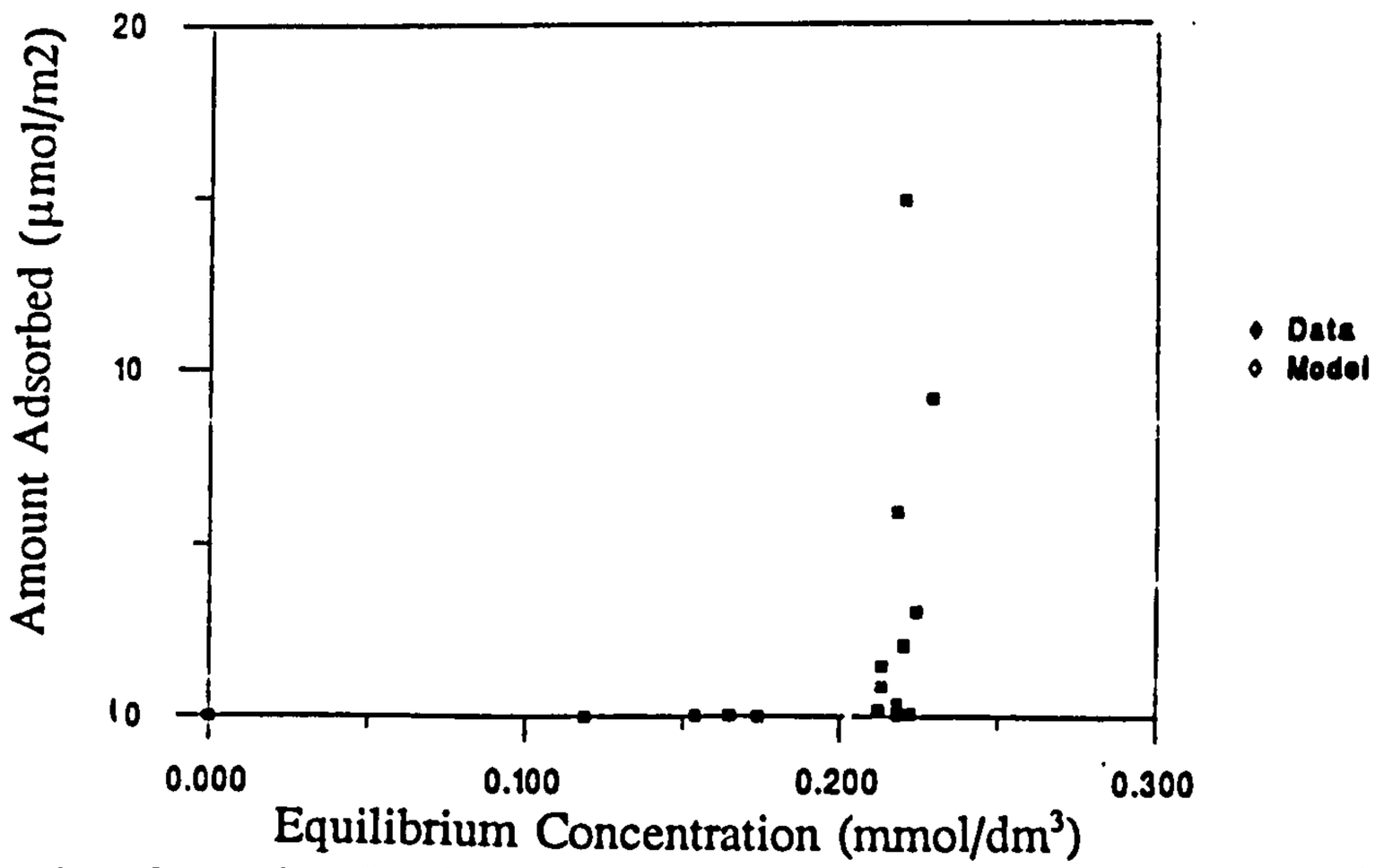

Figure 4.4: Adsorption Isotherm of TX-100 onto Ludox Silica (2wt%) at 298K and pH7.

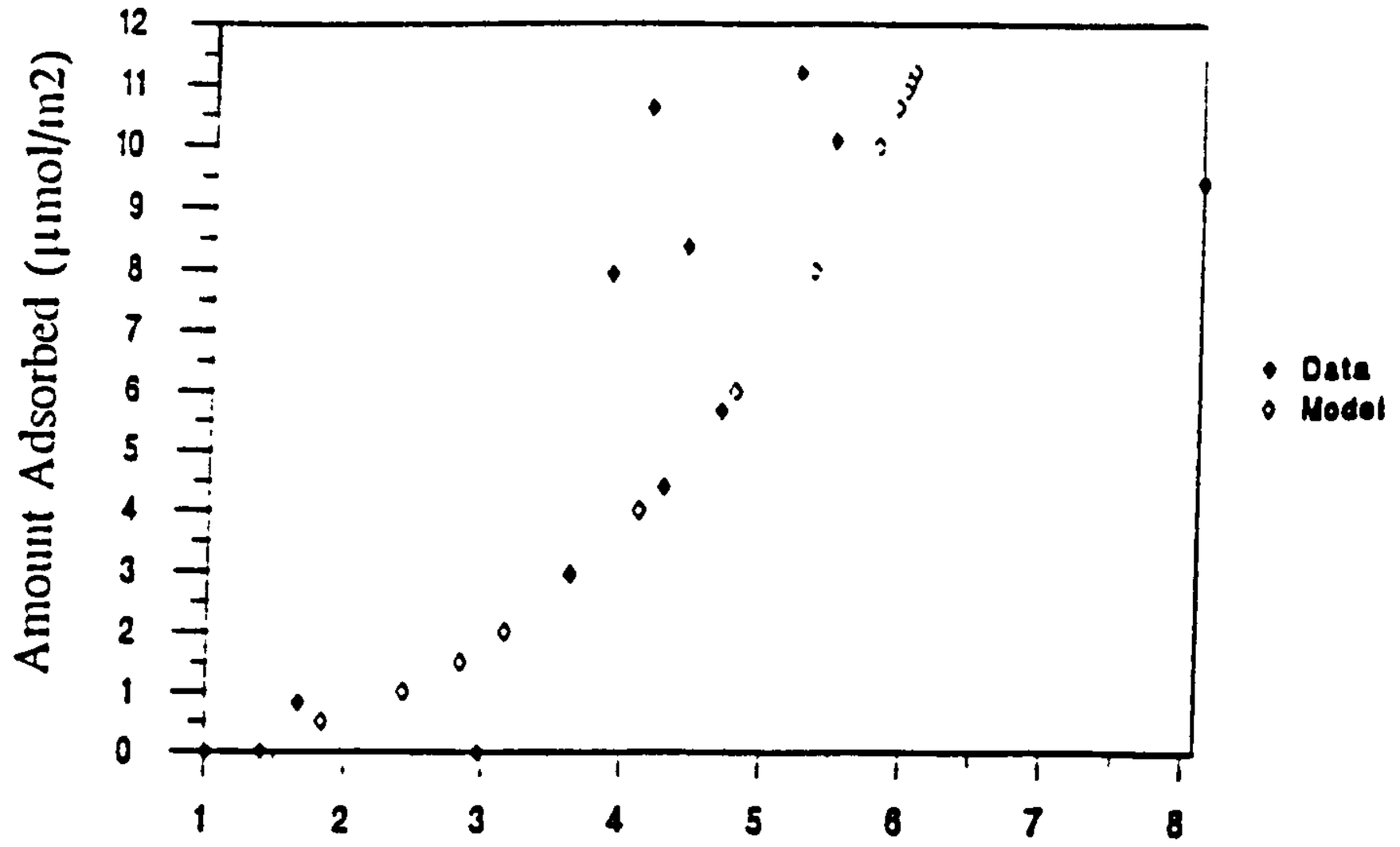

Figure 4.5: Adsorption Isotherm of TX-100 onto Ludox Silica (2wt%) using Visking Tubing at 298K and pH7.

igures 4.6 and 4.7 show the thickness of adsorbed surfactant layer obtained by light attering for mixtures of surfactant and silica. The thickness of adsorbed layer of rfactant was calculated by subtraction of the value obtained for the diameter of the re silica particles from the diameter measured for the silica particle when covered th surfactant (and multiplying by 0.5). As can be seen, the thickness of the TX-100 orbed layer appeared to reach a plateau at 2nm at approximately 2mmol/dm^3 of ed surfactant; this seemed to predict a monolayer of surfactant being formed on the a surface which was not expected from the usual adsorption theory for non-ionic factants. The TX-305 did not reach a plateau extent of adsorption at these low centrations, so it was decided to increase the amount of both TX-305 and TX-100 d to the silica suspension.

res 4.8 and 4.9 show the increase in the thickness of the adsorbed layer of TX-100 TX-305 respectively on the silica sol. There is a steep rise in adsorbed layer ness initially for both surfactants. At an adsorbed layer thickness of oximately 6nm, a plateau appears to have been reached, but on further addition of tant to the solution, the layer thicknesses appeared to increase still further. There veral possible causes of these curious results: (i) multilayers of surfactant may be ng on the silica surface (although this did not agree with the general theory of tant adsorption onto silica surfaces discussed in Chapter 3), (ii) interparticle

frictional effects may well have slowed the particles down (giving larger sizes as estimated by dynamic light scattering than in reality) and (iii) micelle aggregation could have caused the apparent increase in hydrodynamic radius.

As there was no way of deciding (by light scattering) which of the above was the real cause of the continued increase in apparent size of the surfactant-coated silica particles, neutron scattering was used to examine the adsorption of the surfactant on the silica. This approach and the results obtained are now described.

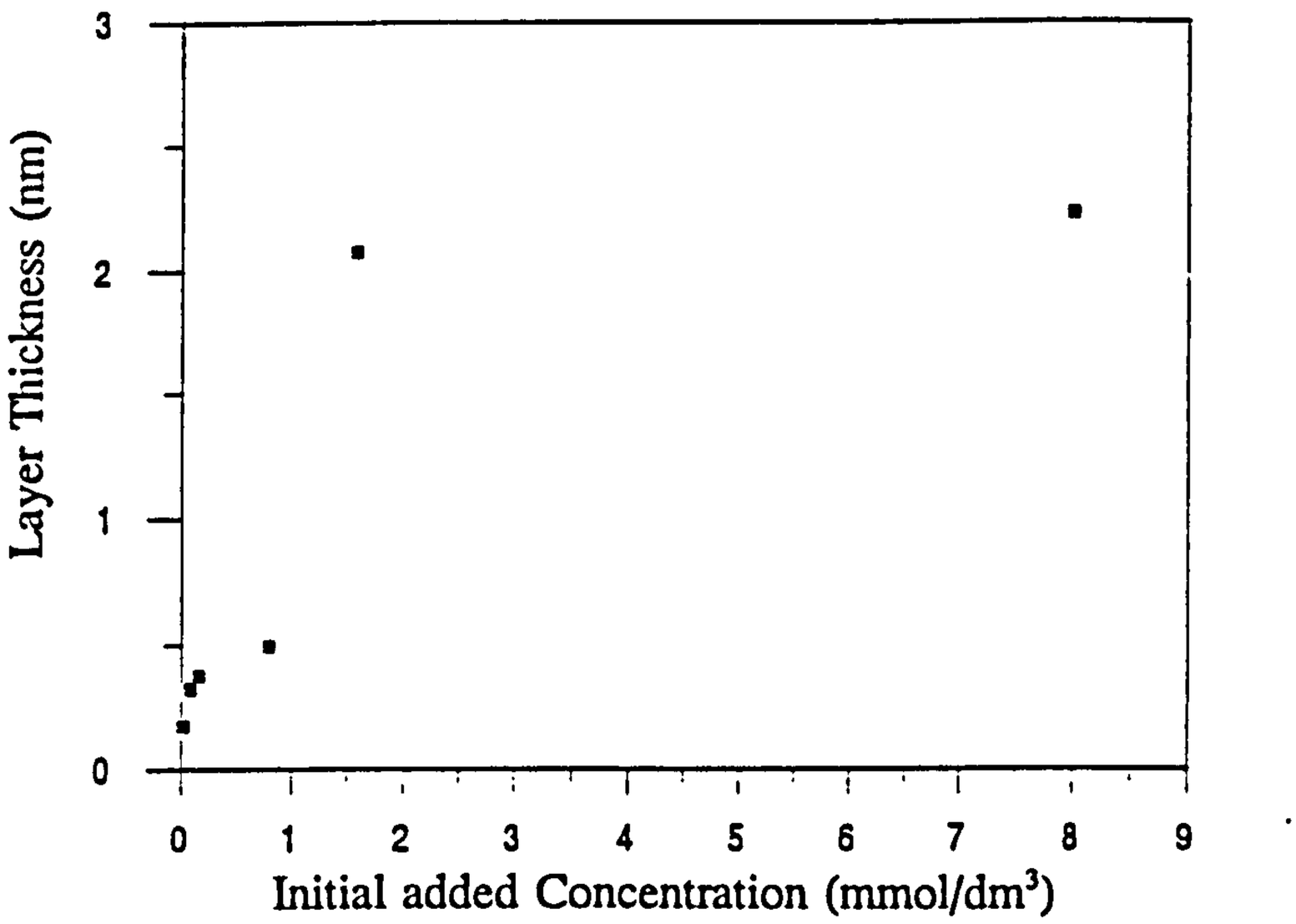

Figure 4.6: Increase in the Thickness of the Adsorbed Layer of TX-100 onto Ludox CL-X (2wt%) with Increasing Concentration of Surfactant at 298K.

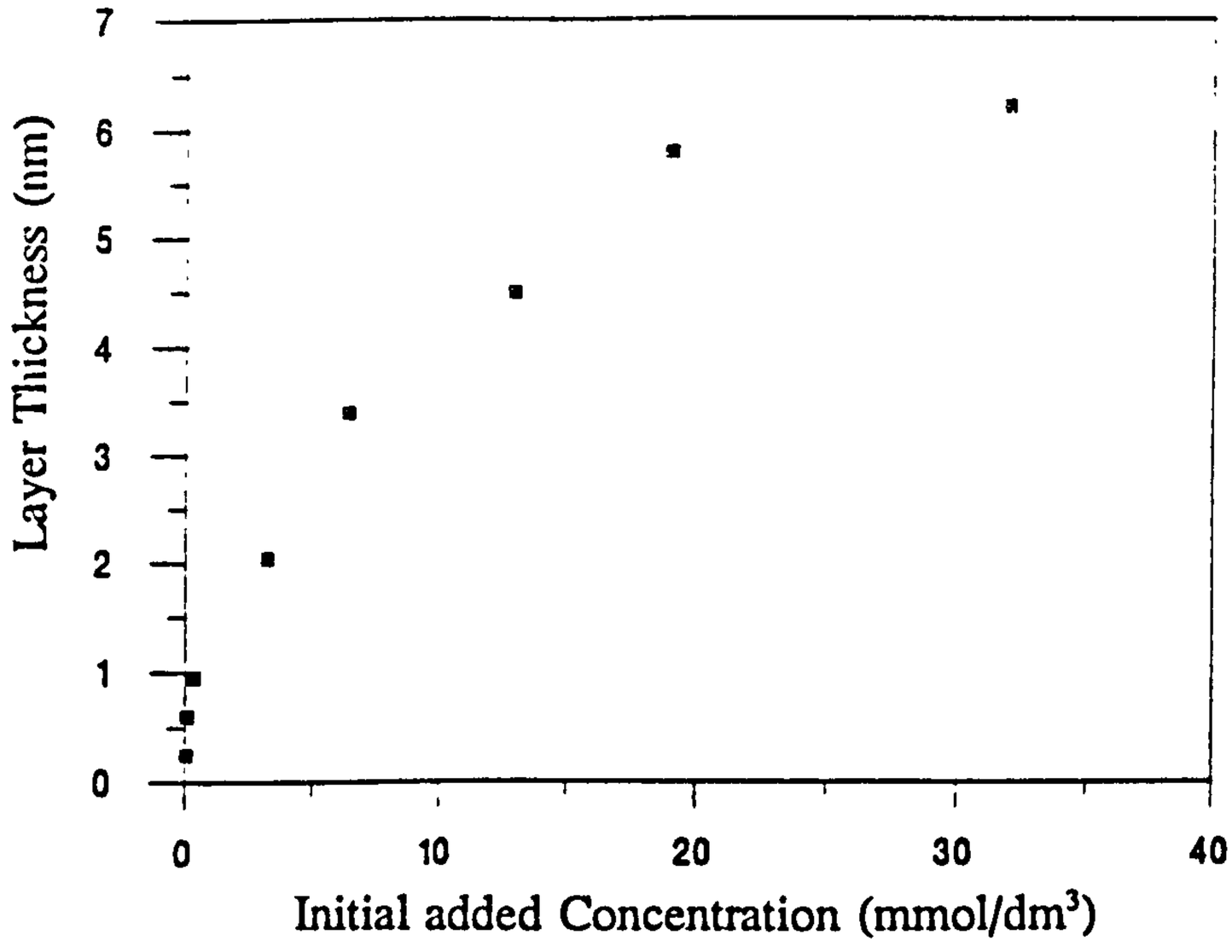

Figure 4.7: Increase in the Thickness of the Adsorbed Layer of TX-305 onto Ludox Silica (2wt%) with Increasing Concentration of Surfactant at 298K.

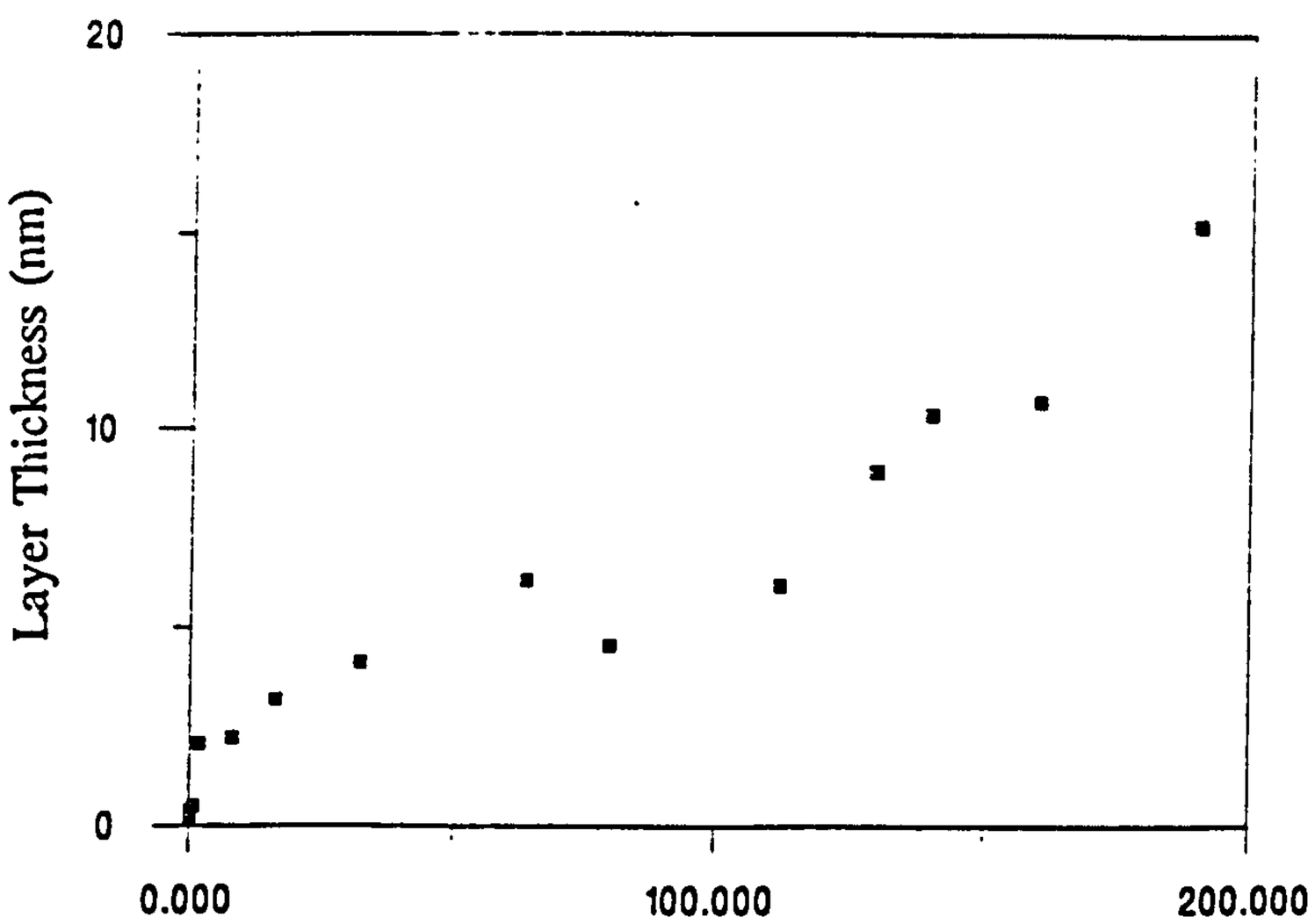

Figure 4.8: Increase in the Thickness of the Adsorbed Layer of TX-100 onto Ludox Silica (2wt%) with Increasing Concentration of Surfactant at 298K.

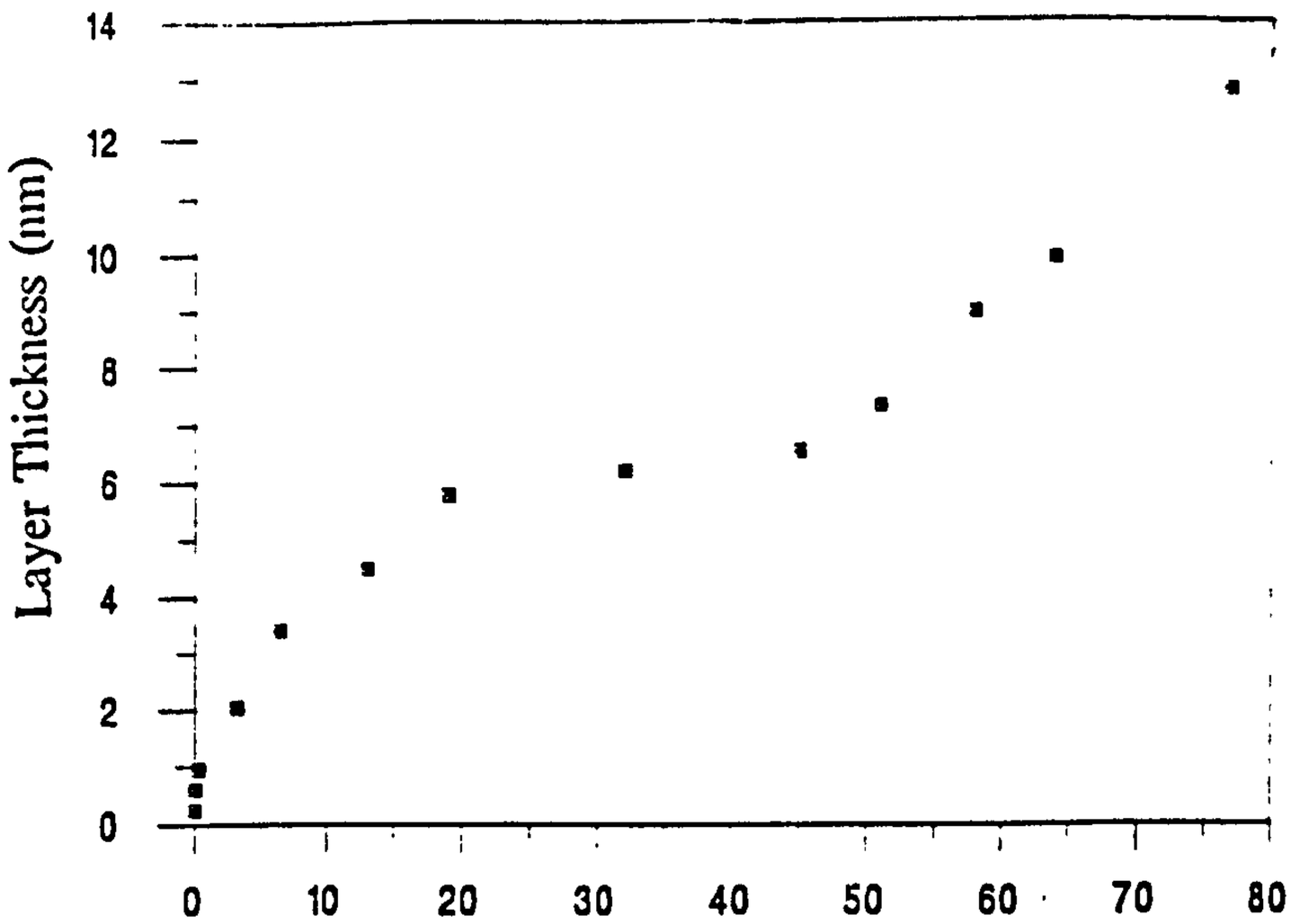

Figure 4.9: Increase in the Thickness of the Adsorbed Layer of TX-305 onto Ludox Silica (2wt%) with Increasing Concentration of Surfactant at 298K.

4.4 Neutron Scattering Theory.

The theory of neutron scattering has some similarities with light scattering. Indeed, the basic equations for both sets of theory are the same, provided that an optical constant, k, is used to take into account the differing origins of the scattering involved. Visible light scattering arises from differences in *polarisability of particles* (see section 4.1) whereas neutron scattering originates from differences of *neutron scattering length densities* between particles.

Thermal neutrons are uncharged particles of mass, m, 1.68×10^{-27}kg, spin 1/2 and wavelength, λ (=0.1-1nm); λ and m are related by the De Broglie equation:

$$\lambda = h/m\upsilon$$

where h is Planck's constant and υ is the velocity of the particle. As the wavelength of neutrons is very much smaller than that of visible light (e.g. 1nm versus 500nm), they are capable of giving information about much smaller particles. This information is obtained from neutrons that are scattered from different parts of the same particle. Measurements are made at very small scattering angles by placing the detector at long

distances (1-40m) from the sample to keep the path length differences of the scattered beams small.

Neutron scattering experiments involve measuring the properties of neutrons scattered from an object located in the beam onto a multi-detector placed at a distance, d from the object and perpendicular to the beam (see Figure 4.10(a)). In Figure 4.10(b), the direction of propagation of the incident neutron beam of wavelength λ_o travelling with velocity, v_0, is represented by the vector k_0, and that of the scattered neutron beam travelling with velocity, v, by k. k is equal to $2\pi mv/h$. Q is the scattering vector and is equal to $k - k_0$, and has units of reciprocal length. Q can also be written as $(2\pi mv/h) - (2\pi mv_0/h)$. Q can also be calculated by using the cosine rule:

$$Q = k^2 + k_o^2 - 2kk_0\cos 2\theta.$$

where $k_o = 2\pi/\lambda_o$.

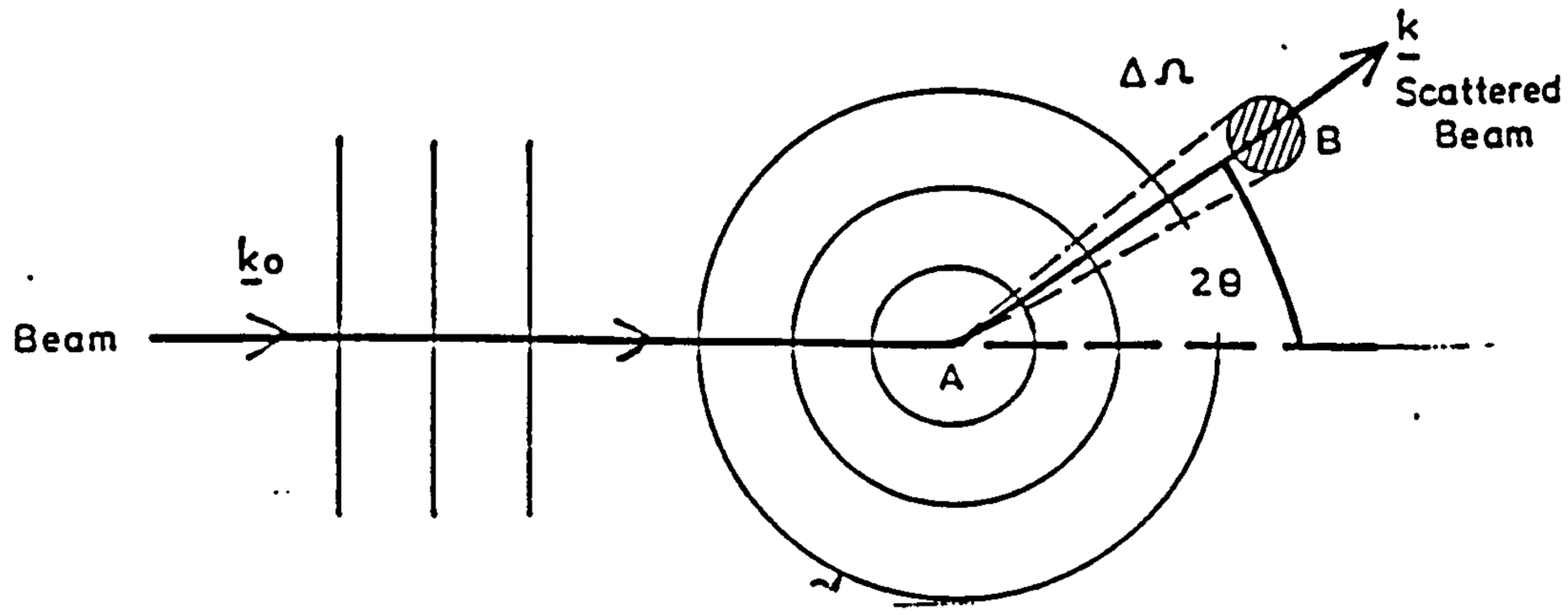

Figure 4.10: (a) Illustration of the Neutron Scattering Process.

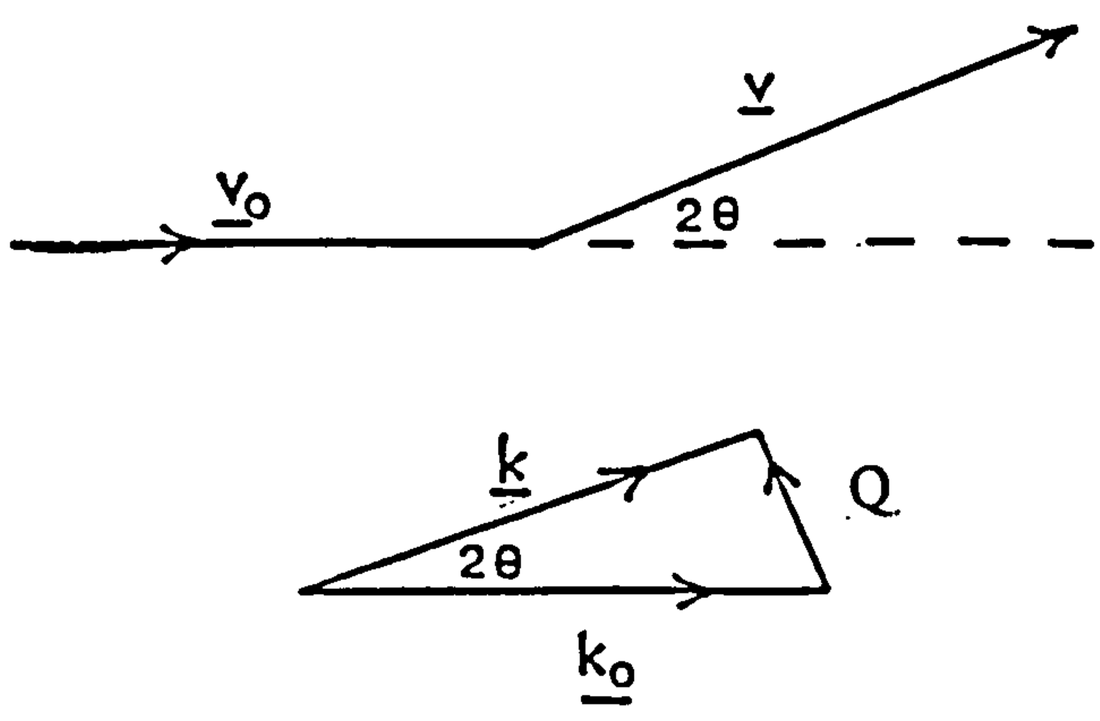

(b) Illustration of the Neutron Scattering Vector.

The energy change upon scattering can be calculated as energy = $1/2(mv^2)$ and $k = 2\pi mv/h$

$$\Delta E = E - E_0 = (h^2/2m)(k^2 - k_0^2)$$

where E_0 and E are the initial and final energies of the neutron beam.

In elastic scattering (which is the method of analysis used in our experiments), there is no change in energy since k changes in direction but not in magnitude. Thus $k = k_0$ and

$$Q = k_0 \sin 2\theta = 2k_0 \sin\theta = (4\pi/\lambda)\sin\theta$$

and since $\sin\theta \sim h/d$
where: h = half the detector height,
d = the object to detector distance,
$Q = (4\pi/\lambda)h/d$

Inelastic scattering involves a finite energy change (ΔE) which can be positive or negative depending upon whether the neutrons have gained or lost energy to molecular motion. The total scattering measurement at the detector shows no distinction between elastic and inelastic scattering and integrates over neutrons of all energies.

<u>Nuclear Scattering Cross-Section.</u>

The scattered neutron wave is spherically symmetrical and of an amplitude (b) known as the scattering length of the nucleus from which the wave emanates. The scattering length is dependent on the nature of the scattering nucleus. When assemblies of atoms or molecules are considered, two types of scattering can arise:

1) coherent scattering: which is brought about by interference of waves that have been scattered from atoms in differing spatial positions.

2) incoherent scattering: this is not an interference effect and is due to elemental isotopes or nuclei of the same element having different nuclear spin states. The intensity is not a function of Q and so it appears as background scattering.

No structural information can be gained from incoherent scattering but coherent scattering is directly related to structure.

Incoherent scattering produces a background effect which must be subtracted from the total measured scattering. The scattering cross-section is therefore:-

$$\sigma = \sigma_{inc} + \sigma_{coh}$$

where $\sigma_{coh} = 4\pi b^2_{coh} = 4\pi <b>^2$

$\sigma_{inc} = 4\pi[<b^2> - <b>^2]$

The values of some relevant coherent scattering lengths b_i are given in Table 4.2.

Hydrogen gives a particularly large incoherent scattering due to its' many spin states, which have scattering lengths of different signs. There is an appreciable difference between the scattering length for hydrogen and deuterium nuclei (see Table 4.2). Thus, the contrast of a particle or solvent in neutron terms can often be changed by replacing the hydrogen therein by deuterium. This allows the selective examination of various parts of molecules or assemblies of molecules while leaving the structural properties essentially unchanged.

Table 4.2: Scattering Lengths for some Atoms.

Element	Scattering length (b_i) /10^{-12}cm
H	-0.374
D	0.6674
C	0.665
O	0.58
Si	0.41491

When scattering measurements are made on molecules, a coherent neutron scattering length density, ρ, for that molecule is obtained by integrating over all atomic elements in the molecular volume to give:

$$\rho = \Sigma b_i / V_m$$

where b = coherent neutron scattering length of isotope, i,
V_m = molecular volume of sample.

Table 4.3 shows calculated values of the coherent neutron scattering length densities for molecules relevant to this work.

Table 4.3: Calculated Coherent Scattering Length Densities.

Molecule	Total b_i (10^{-12}cm)	V_m ($10^{-23}cm^3$)	ρ ($10^{10}cm^{-2}$)
H_2O	-0.168	2.99	-0.56
D_2O	1.914	2.99	6.36
SiO_2	1.575	4.056	3.89
TX-100	5.595	147	0.3806
TX-305	1.410	1760	0.0384

Analysis of Scattering.

For a monodisperse system of dilute, spherical, non-interacting particles, the scattered intensity I(Q) (which has units of cm^{-1}) can be written (5,6) as a function of the scattering vector Q in the form:-

$$I(Q) = I(0)P(Q)$$
$$= A(\rho_p-\rho_s)^2V_p^2N_pP(Q)$$

where: I(0) = scattered intensity at Q=0
A = a constant taking into account instrumental factors,
ρ_p = coherent neutron scattering length density of the particle,
ρ_s = coherent neutron scattering length density of the solvent,
V_p = particle volume,
N_p = average number of particles per unit volume in solution,
P(Q) = a factor dependent upon particle shape,
($Q = (4\pi/\lambda)\sin\theta$, for a scattering angle of 2θ and wavelength λ,).

For a system of monodisperse, non-interacting, spherical particles each surrounded by a 'shell' consisting of, for example, a layer of adsorbed surfactant, I(Q) is written as:

$$I(Q) = A[\ (\rho_p-\rho_s)^2V_p^2N_p^2P(Q) + (\rho_{sh}-\rho_s)^2\{V_T^2N_p^2P_T(Q)-V_p^2N_p^2P(Q)\}\ ]$$

where: ρ_{sh}=coherent neutron scattering length density of the shell,
V_T= particle volume (with shell),
$P_T(Q)$=form factor of particle and shell.

This equation takes into account the scattering intensity of the core particle and the shell separately.

For monodisperse spheres of radius R, the single particle shape factor is given by the equation:

$$P(Q) = \{3(\sin QR - QR\cos QR) / (QR)^3\}^2 \qquad [A]$$

In dilute dispersions there are only a small number of interparticle interactions, but as the concentration of scattering units increases the particles will interact and some degree of ordering occurs as a consequence of this. The scattering intensity is then:

$$I(Q) = A(\rho_p - \rho_s)^2V_p^2\ N_p.P(Q).S(Q)$$

where S(Q)= the structure factor, this is equal to unity for dilute solutions or large values of Q and is given by:

$$S(Q) = 1 + (4\pi N_p/Q)\int_0^\infty[(g(r) - 1]\sin QRdr.$$

where g(r) = the particle pair distribution function,
r = centre-to-centre interparticle separation.

Figure 4.11 shows an example of the scattering pattern observed for monodisperse spherical particles (S(Q) taken to be unity).

The maxima and minima observed in this scattering curve are due to interference

effects between the neutron scattering from differing parts of the same particle, according to equation [A].

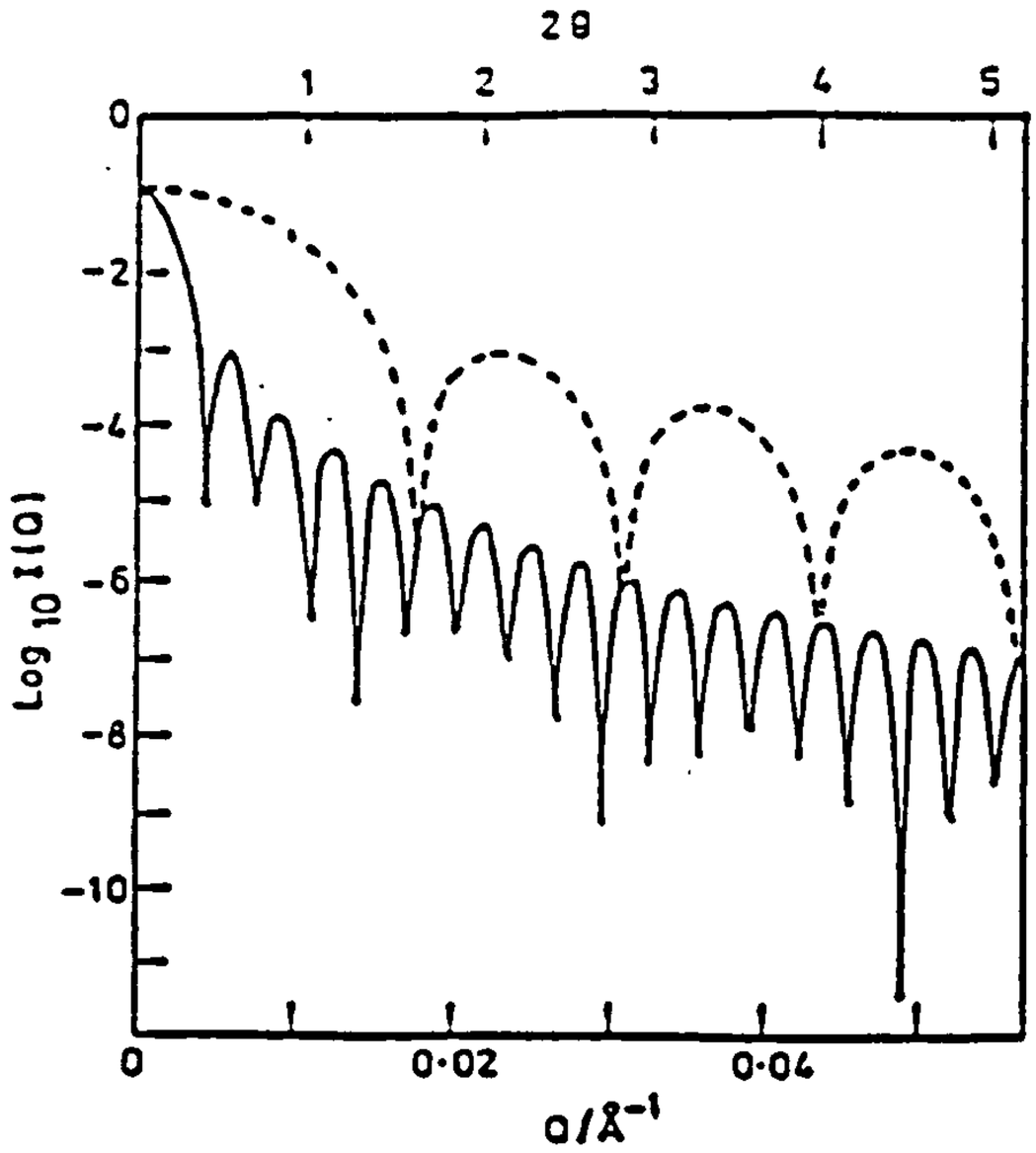

Figure 4.11: Scattering Pattern obtained for Spherical Particles in Solution

(- - - denotes particles of radius 25nm; —— denotes particles of radius 100nm).

At zero Q the particle form factor, P(Q), becomes unity and so

$$I(Q) = A(\rho_p-\rho_s)^2V_p^2N_p$$

P(Q) can be used to calculate such parameters as the radii of micelles in solution or the core radius in core/shell models. There is a different P(Q) equation for rods and discs.

Contrast Matching.

As already noted it is possible to vary the scattering length density of the particle or solvent by totally or partially substituting the H atoms by D in the molecules; a linear dependence of $\sqrt{I(Q)}$ versus ρ_s would be obtained from the equation given for I(0) above. It is clear that for $\rho_p = \rho_s$, so-called zero contrast, the scattering is zero at all Q values and is known as a contrast match point. The contrast match variation method allows the observation of separate discrete parts or domains of complex particles. Figure 4.12 shows an example of a spherical particle with an adsorbed layer. In (a),

the scattering length densities of all three domains are different and so the whole unit scatters. In (b) there would be scattering from the core only since $\rho_s = \rho_{sh}$ (where ρ_s is the scattering length density of the solvent and ρ_{sh} is the scattering length density of the shell). In (c) there would be scattering from the shell as $\rho_s = \rho_p$ (where ρ_p is the scattering length density of the core). Table 4.3 shows the scattering length densities for various molecules; the silica and solvent were contrast matched using these values and the equation: [(-0.56)x + (1-x)6.36 = 3.89], where x is the fraction of H_2O needed in the solvent mix of D_2O and H_2O. When x is found then the ratio of H to D that will equal the scattering length density of silica sol can be found. From this equation it was calculated that all measurements of surfactant/silica mixtures were to be made in a part deuterated solvent of 61%:39% (D_2O:H_2O), if the adsorbed surfactant layer only was to be highlighted during neutron scattering analysis (condition (c) in 4.12).

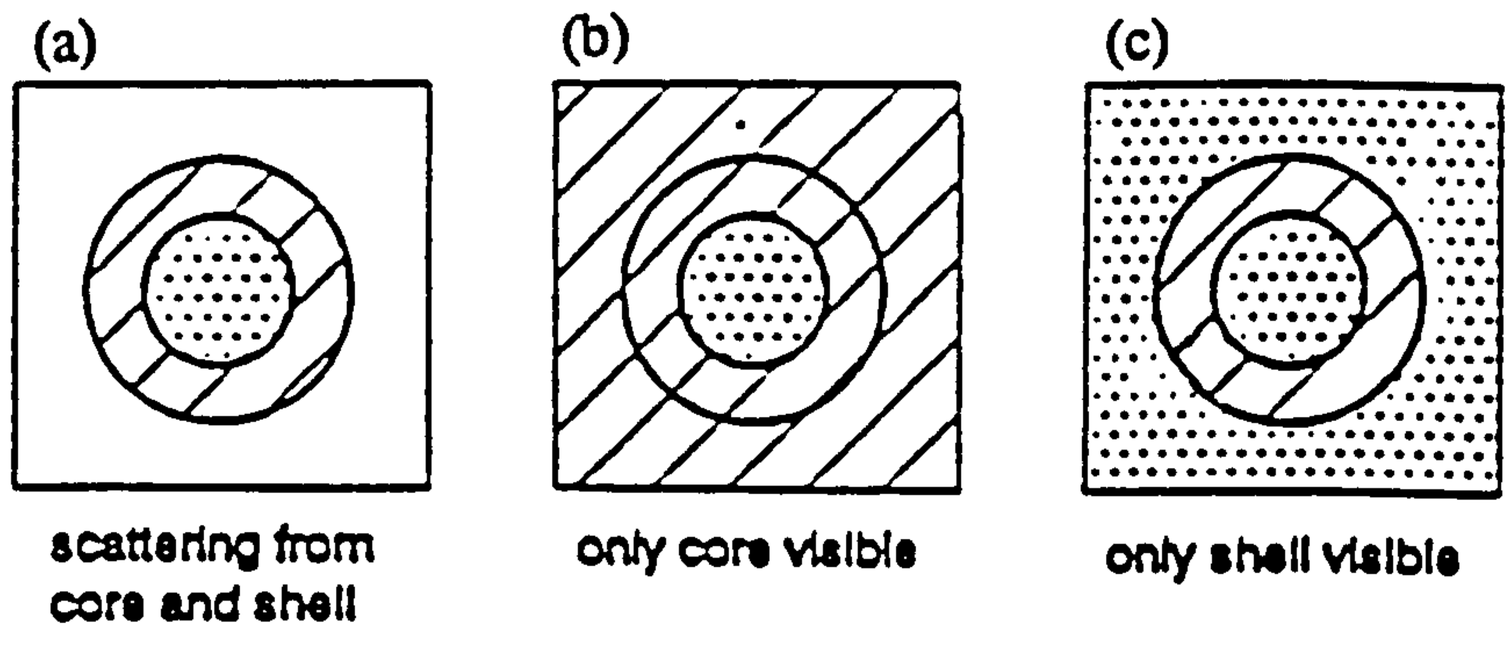

Figure 4.12: Samples which may be Analysed by the Contrast Variation Method.
(where the blank, striped and dotted sections denote areas of the systems having different scattering length density)

Radius of Gyration (R_g).

For the condition that $QR_g < 1$, the terms in P(Q) can be expanded to the 'Guinier Approximation':-

$$I(Q) = I(0)\exp(-Q^2R_g^2/3)$$

Therefore plotting ln I(Q) against Q^2 should give a straight line of gradient ($R_g^2/3$) and intercept of I(0).

4.5 Experimental.

It was the purpose of these experiments to study the nature of the adsorbed surfactant layer having obtained some preliminary thickness data by dynamic light scattering. Other groups have studied similar surfactant and silica systems using neutron scattering (3,7), although none have included TX-100. The work most commonly involved alkyl polyoxyethylene non-ionic surfactants on silica sols and concluded that the adsorbed layer of surfactant was in the form of a bilayer and was present in 'patches' around the surface of the silica.

SANS measurements were obtained using the D17 diffractometer at Institut Laue-Langevin in Grenoble. This instrument is shown schematically in Figure 4.13. Neutrons with a wavelength of 1.5nm were collected on a 64x64cm^2 multidetector. A Q range of 0.006 to 0.22Å^{-1} was obtained with the detector positioned at a distance (D_{s-d}) of 4.43m from the sample. Quartz cells (1mm path length) were used as sample holders as quartz materials display very little small angle neutron scattering. The raw data measured consisted of the average number of counts in the detector as a function of r, the distance from the centre to the edges of the detector. 'r' was converted to Q to give I(Q) versus Q using, $Q = (4\pi/\lambda)(h/d)$.

The measured intensity $I_s(Q)$ was corrected for background and solvent/sample container scattering [(B(Q)], and then normalised using the scattering from water [$I_w(Q)$] (from which a background had also been removed [WB(Q)] - that of the empty cell) to give the scattering from the dispersion using the equation:

$$I(Q) = [I_s(Q) - T_sB(Q) / I_w(Q) - T_wWB(Q)].[(d\sigma/d\Omega)_w.T_wd_wA_w / T_sd_sA_s]$$

This gave the intensity, I(Q), (in cm^{-1}). In this equation T_s and T_w are the transmission of the sample and water respectively, d_s and d_w are the sample and water thickness respectively, A_s and A_w are the area of beam incident on the sample and water respectively and $d\sigma/d\Omega$ is the differential cross-section of water. The transmission values were obtained from the relative intensities of the direct (straight-through) beam from the sample and an 'empty beam'.

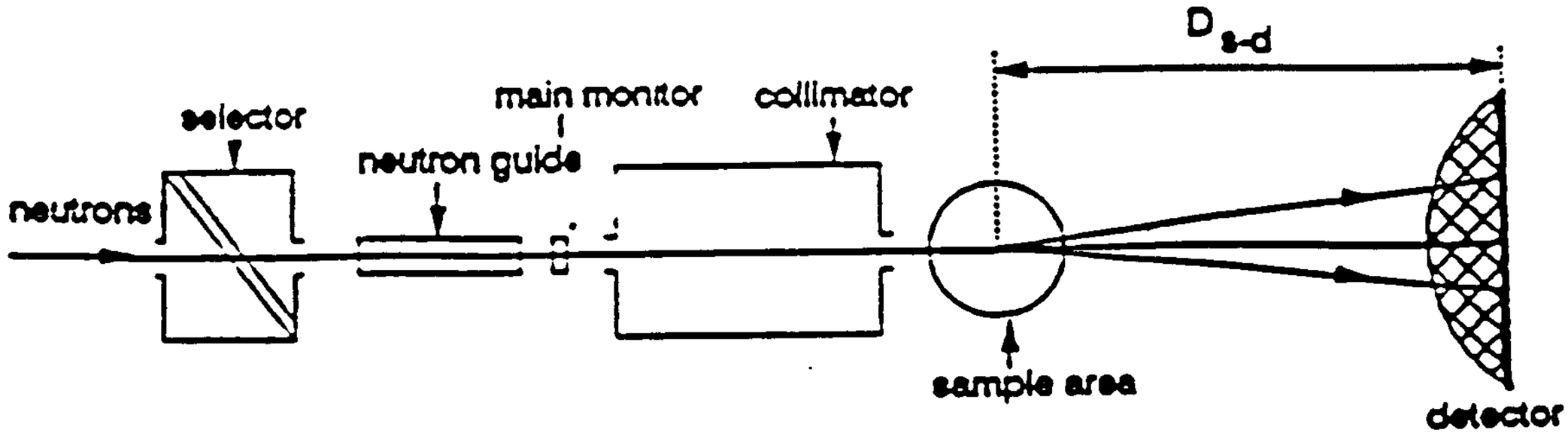

Figure 4.13: Schematic Diagram of the D17 Diffractometer at Institut Laue-Langevin.

4.5.1 Surfactant Micelle Sizes.

Figures 4.14-4.19 show the results of the Guinier analyses of the surfactant solutions, assuming the micelles to be hard spheres. The radii of gyration R_g for the surfactant micelles were obtained from these plots and the apparent radii R_{app} were then obtained by using:

$$R_g^2 = (3/5)R_{app}^2$$

Table 4.4 gives values of R_g and R_{app} for micelles of TX-100 and TX-305 in aqueous solution. Averaging the final results gives values of 4.1nm for the apparent radius of TX-100 (this matches well with literature (8)) and 3.5nm for the apparent radius of TX-305. The smaller radius of the TX-305 molecule (which has the larger molecular weight) is due to the cmc of the surfactant not yet being reached. TX-305 molecules have long ethene oxide chains that repel one another in aqueous solution; this surfactant therefore undergoes full micellisation at large concentrations of monomer.

Surfactant	Surfactant Concentration (mmol/l)	R_g (nm)	R_{app} (nm)	Average R_{app} (nm)
TX-100	8.0	3.097	3.998	
TX-100	16.0	3.234	4.175	
TX-100	24.0	3.244	4.188	4.145
TX-100	32.0	3.267	4.218	
TX-305	3.3	2.82	3.641	3.493
TX-305	6.6	2.59	3.344	

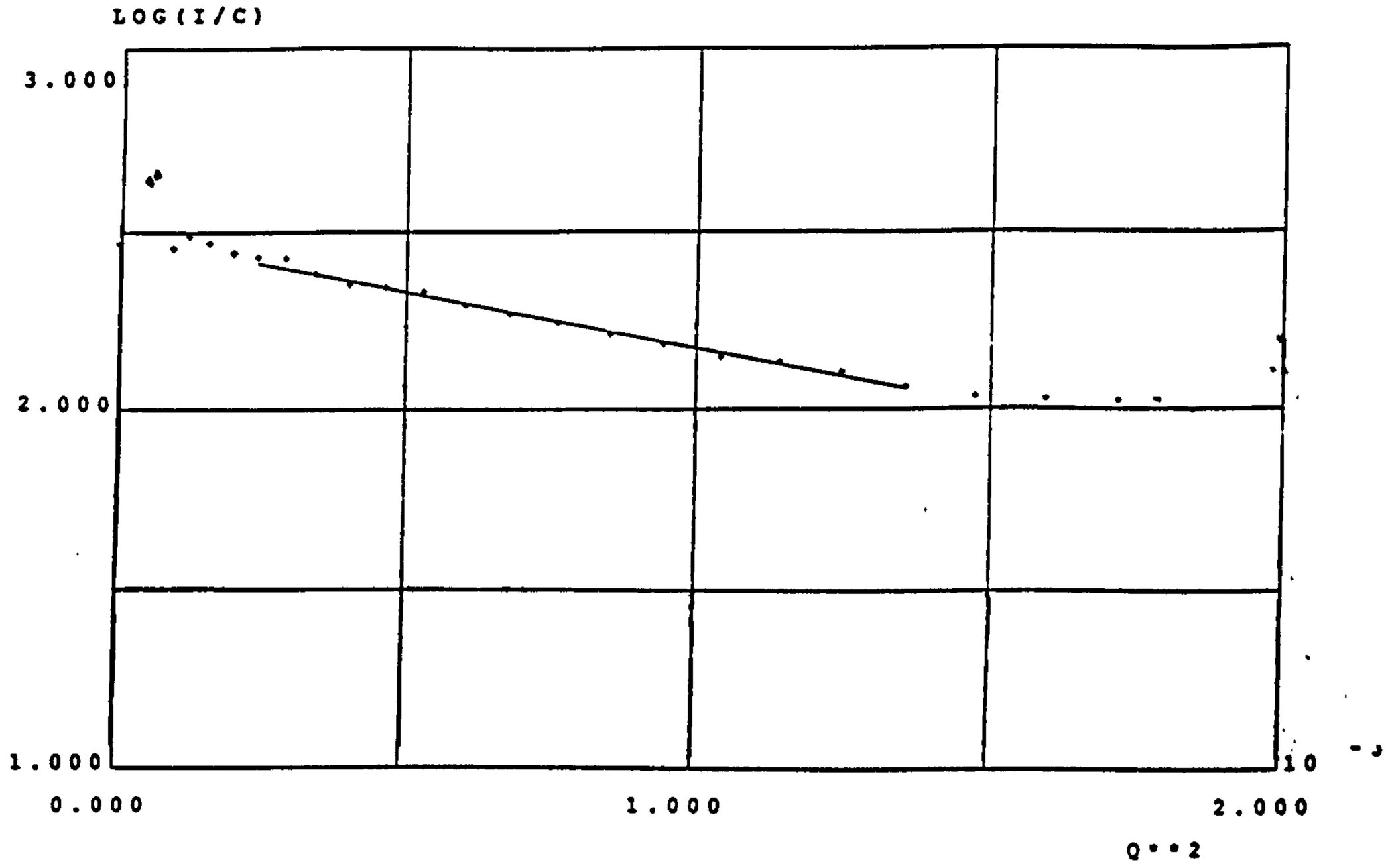

Figure 4.14: Guinier Analysis of 8mmol/l (0.5%) TX-100, R_g = 30.97Å.

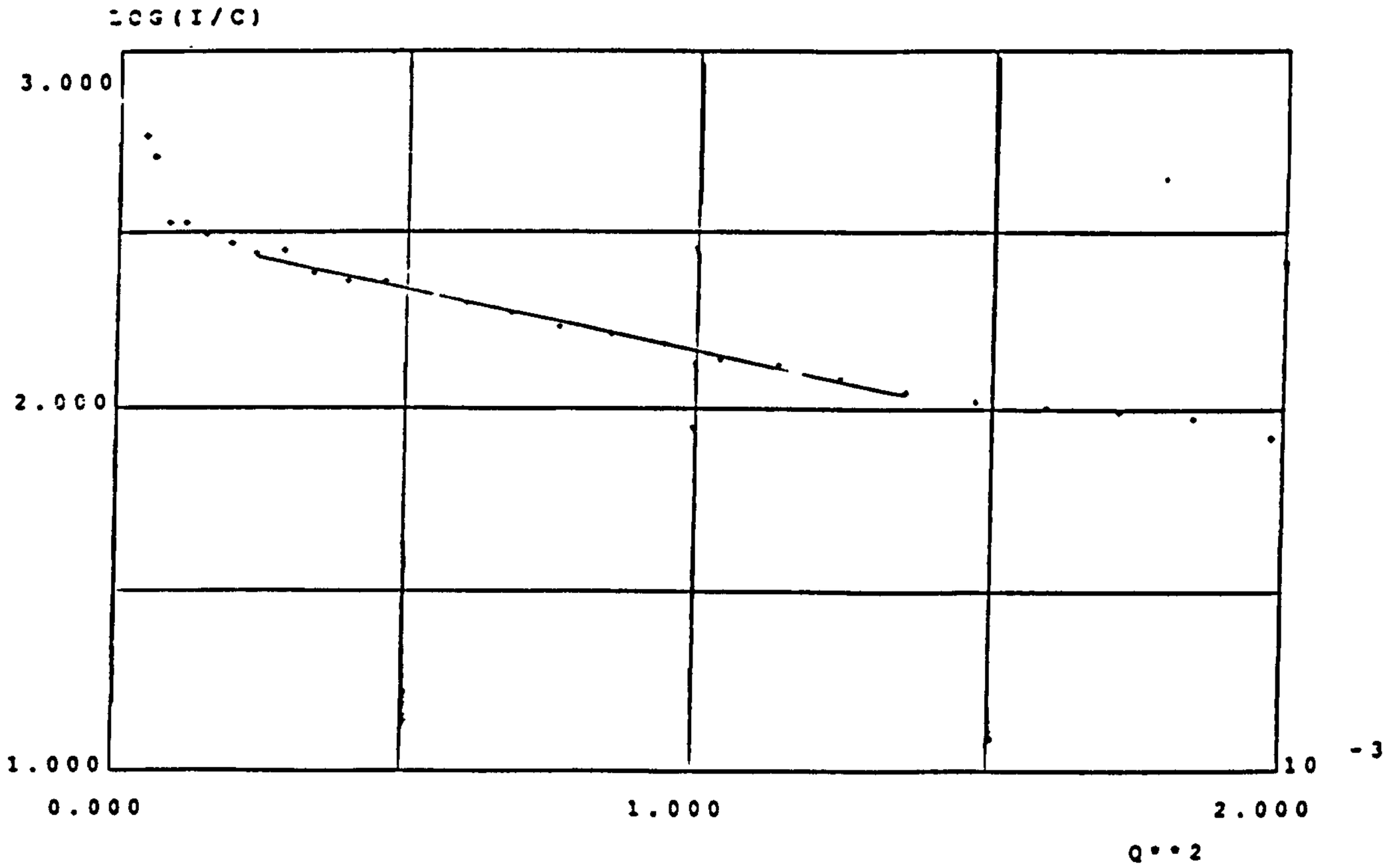

Figure 4.15: Guinier Analysis of 16mmol/l (1%) TX-100, R_g = 32.34Å.

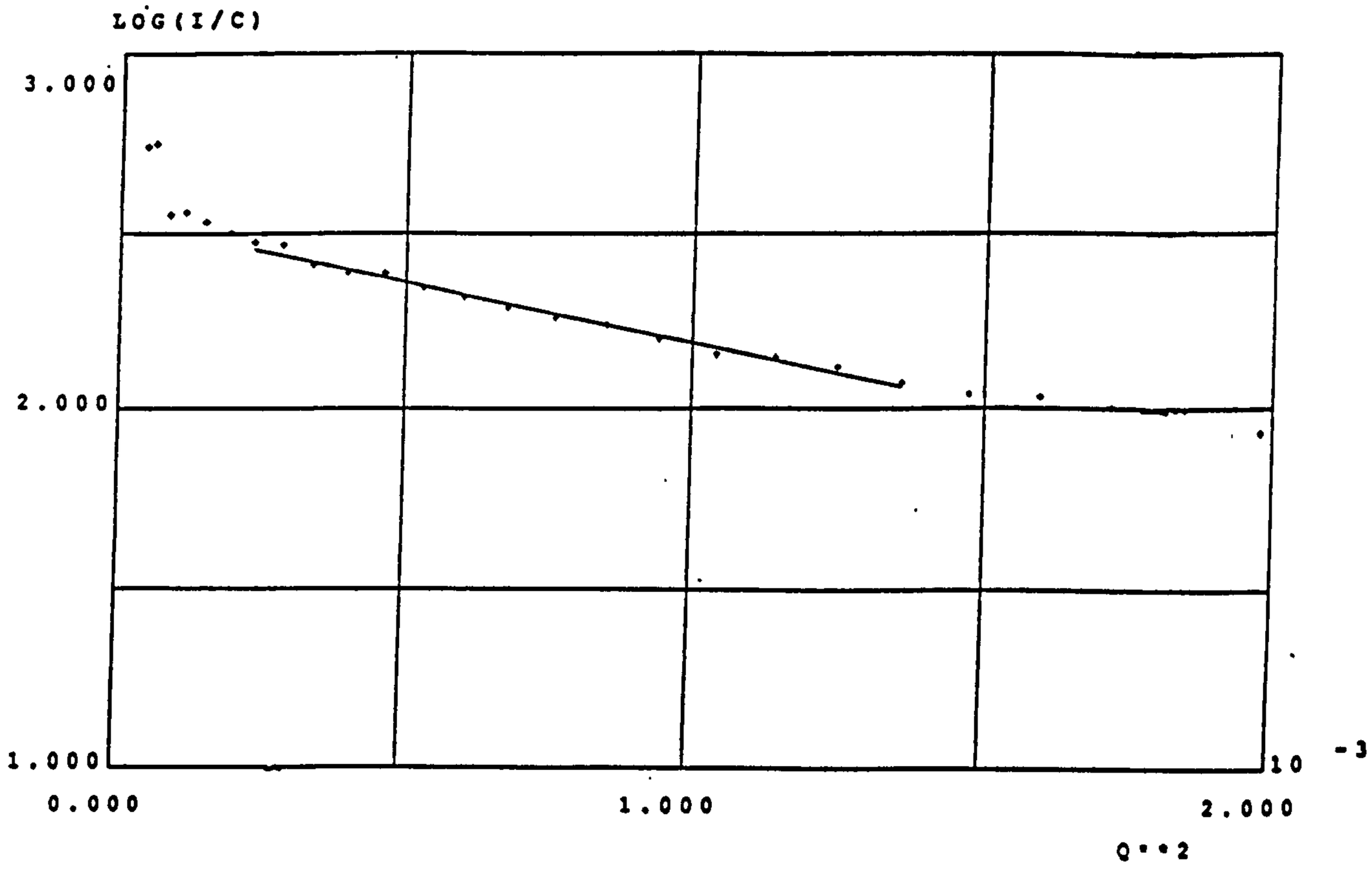

Figure 4.16: Guinier Analysis of 24mmol/l (1.5%) TX-100, R_g = 32.44Å.

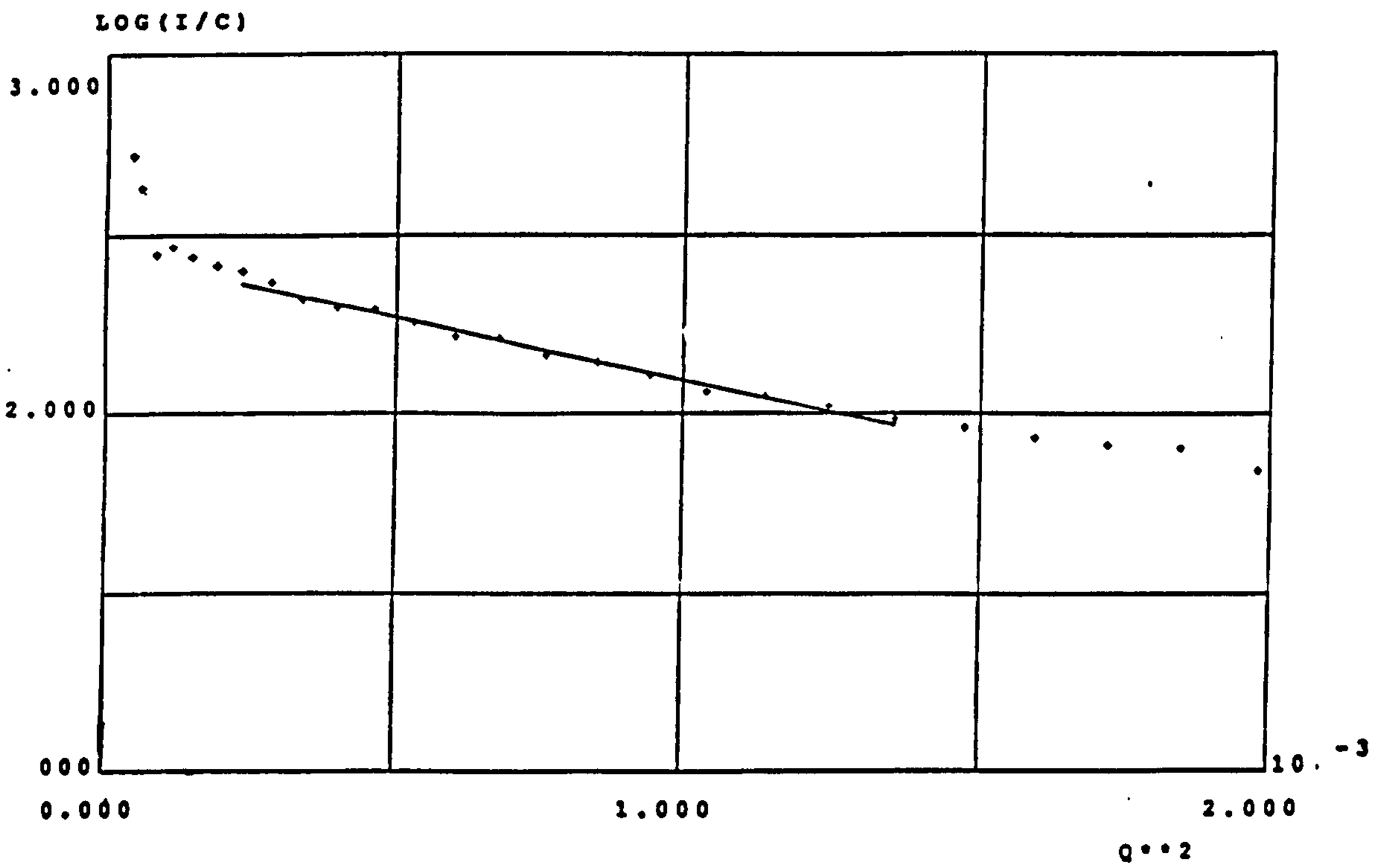

Figure 4.17: Guinier Analysis of 32mmol/l (2.0%) TX-100, R_g = 32.67Å.

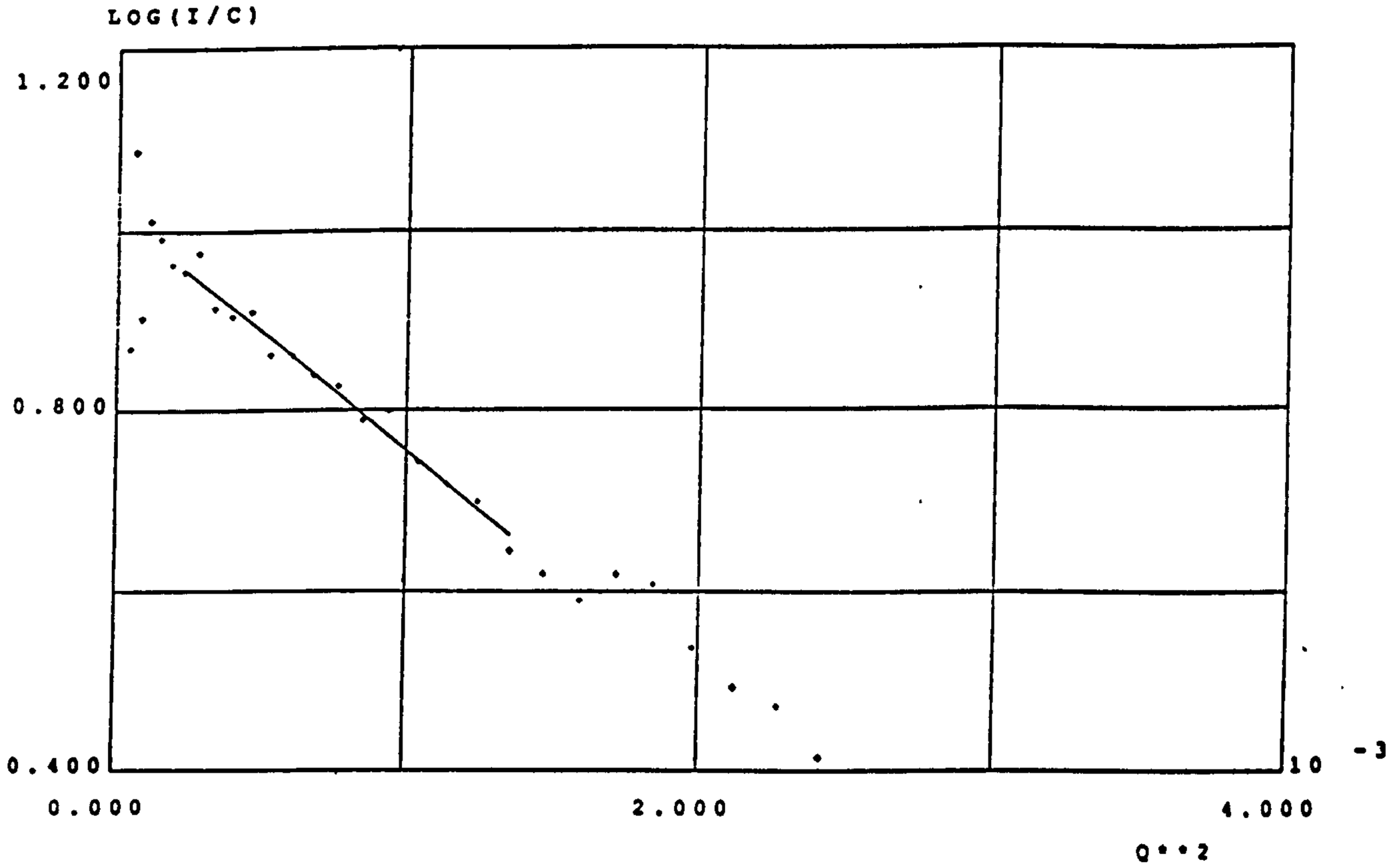

Figure 4.18: Guinier Analysis of (3.3mmol/l) 0.5% TX-305, R_g = 28.2Å.

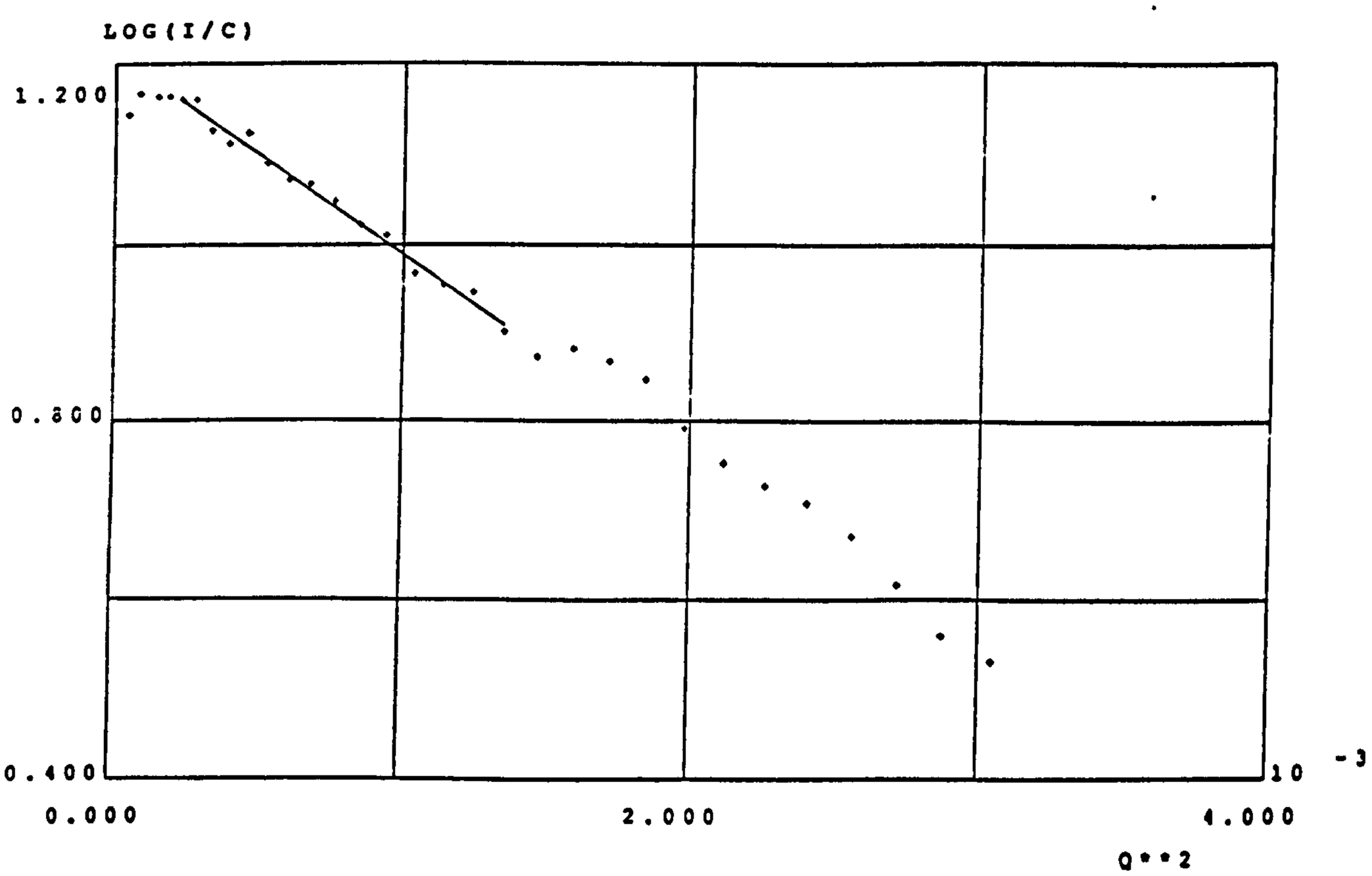

Figure 4.19: Guinier Analysis of (6.6mmol/l) 1.0% TX-305, R_g = 25.9Å.

4.5.2. Bare Silica Particles.

Figure 4.20 shows the scattering obtained for aqueous dispersions of the Ludox silica sol at differing concentrations of silica. This pattern is a model example of the scattering pattern obtained for spherical, monodisperse particles (Fig. 4.11). Figure 4.21 shows the scattering obtained for 2% silica sol with the scattering from a 1% silica dispersion subtracted. It is seen that the scattering patterns of the two superimpose and this proves that there is no interparticle scattering caused by interactions between the silica particles at these concentrations.

4.5.3. Silica and Surfactant Mixtures.

Figures 4.22-4.26 show the scattered intensities (after subtraction of solvent scattering) measured for mixtures of silica sol and TX-100 (at varying concentrations). As the surfactant concentration decreases (see Figure 4.26) the errors in measured scattering increase at higher Q (to approximately 5%), due to the scattering from sample and solvent being very close; Figures 4.27 and 4.28 show these curves superimposed. On examination of Figure 4.27 (i.e. the low surfactant concentrations) it is observed that the scattered intensity increases with surfactant concentration at all values of Q, whereas Figure 4.28 shows that at high surfactant concentrations, the scattering at low Q values becomes a constant. These patterns suggest that at lower values of surfactant concentration (ie. 0.1%, 0.25% and 0.5%) the adsorbed layer of the surfactant on the silica surface is increasing in thickness. For higher surfactant concentrations (ie. 1.0% and 2.0%) the thickness of the adsorbed layer then increases no further indicating that a maximum extent of adsorption has been reached. At high Q values, the scattered intensity increased at all levels of surfactant, and is thought to be due to scattering from the micelles formed in the solution. These scattering curves suggest that multilayers of surfactant are not formed on colloidal silica. Indeed an adsorption maxima is reached between 4mmol/l (0.25%) and 8mmol/l (0.5%) of TX-100 is added to a 2% solution of silica sol. This is in general agreement with the adsorption isotherm measured for silica sol and TX-100 using the visking tubing in section 4.3 of this thesis.

Figures 4.29-4.32 show similar scattering patterns obtained for TX-305 and the silica;

these curves are superimposed in Figure 4.33. These scattering patterns are rather more difficult to interpret as the scattered intensities from micelles in solution dominate the results. Using a similar argument to above, these data suggest that maximum extents of adsorption of TX-305 on the silica had already occurred at 0.5% of added surfactant. Further experimentation is necessary in order to fully interpret these results.

A check was needed to ensure that the extra scattering observed at high Q values for both surfactants was due to micelles in solution and not to interactions between the surfactant-coated silica particles. Assuming that the scattered intensities measured for mixtures of the surfactant and the silica <u>above</u> the maximum extent of adsorption are due to the scattering from the silica core and the adsorbed layer of surfactant and the scattering from the surfactant micelles (provided that the samples are made up in the same solvents) one obtains the equation

$$I_{si+1\%TX100} = I_{si+0.5\%TX100} + I_{0.5\%mic}$$

assuming 0.5% TX-100 is equivalent to 100% coverage of the silica

The surfactant solutions were measured in D_2O and so a constant (z) was first calculated to account for the extra scattering that would be attributable to the hydrogenous solution; i.e.

$$I_{0.5\%mic(d/h)} = zI_{0.5\%mic(d)}$$

At some value of Q (say, Q=0.03), the intensities for all of the solutions were taken and used to calculate z. The whole of the data for the micelle scattering were then multiplied by this value and subtracted from the scattering measured for the surfactant/silica mixture in question. Figures 4.34-4.37 show the curves at maximum extents of adsorption of surfactant and the corrected curves for surfactant/silica mixtures above the maximum extent of adsorption. It can be seen in each case that the curves superimpose upon one another well, thereby showing that any additional scattering is due to micelles in solution.

Calculation of the Thickness of the Adsorbed Layer of Surfactant on the Colloidal Silica.

A) Core Modelling.

The scattering patterns obtained for the bare silica sol were fitted to the model of P(Q), the particle form factor (see Figure 4.38), by a process that involved estimating the value of I(0) and the radius of the surfactant-covered particle (assuming monodispersity). For this model, the peaks at higher Q are much clearer than in the patterns obtained for the 'real' systems, this is due to the fact that the peaks at higher Q for polydisperse systems are usually smeared out.

$$P(Q) = \{3(\sin QR - QR\cos QR) / (QR)^3\}^2$$

Figures 4.39 and 4.40 show how the model was modified for different values of R and I(0), respectively. The y-axis, P(Q), is equivalent to the scattered intensity divided by I(0). The x-axis is equivalent to the angle at which the scattering was measured (Q) multiplied by R, the radius of the scattering particles in Å. Figures 4.41-4.43 show the basic data that was obtained for a 2% solution of colloidal silica and fitted to the model of P(Q). The data were modified for values of I(0) (to enable the fitting of this data to the model) by dividing the measured intensity by values estimated to be I(0) (as I(0) was not known exactly). The model was varied for differing values of R. The best fit of the data to the model was then found by superimposing these plots; the values of I(0) and R at the best fit were taken to be the values of I(0) and the radius of the core particle, R_c for the particular system being analyzed. Results are shown in Table 4.5.

B) Core and Shell Modelling.

Core and shell modelling was carried out in a similar fashion to the core fitting. Initially, the fitting was completed using the equation given in section 4.4 that takes into account the scattering from the core and the shell, however, the scattering patterns were dominated by scattering involving the core, and the scattering from the shell (which was small in comparison) was masked. As a consequence of this, the equation usually used for the core alone was incorporated.

Table 4.5: Surfactant Layer Thicknesses.

System	I(0) Value	Total R (nm)	Shell Thickness (nm)
2% silica	187 +/12.5	13.0+/- 0.25	0.00
2% silica + 0.1% TX100	6.24	17.0	4.0+/- 0.5
2% silica + 0.25% TX100	19.9	18.0	5.0+/- 0.5
2% silica + 0.5% TX-100	59.3	19.5	6.5+/- 0.5
2% silica + 0.5% TX-305	32.36	18.0	5.0+/- 0.5

The scattering of the free surfactant in the silica sol and surfactant mixtures was not subtracted as the analysis was carried out only for the systems that had not reached full adsorption; it was assumed that there was either minimal or no free surfactant in solution for these cases.

Figures 4.44-4.46 show the calculation of I(0) and the subsequent fitting of the data for 2% silica and 8mmol/l (0.5%) TX-100 to the model. The value for I(0) was calculated (using the Guinier approximation) from a plot of lnI(Q) vs. Q^2 (see Figure 4.44). This process was repeated for all systems of TX-100 and TX-305 mixtures. Table 4.5 shows the values obtained for the thicknesses of the adsorbed surfactant layers. Fitting was not carried out for the mixtures above the adsorption maxima. Comparison of the adsorbed layer thickness with the radius of gyration for the TX-100 and TX-305 micelles shows that maximum extent of adsorption of TX-100 onto colloidal silica corresponds to approximately a bilayer of surfactant (or admicelle) being formed on the silica surface. This is in general agreement with the work of other groups of workers

(7). The systems that contained the silica and surfactant at less than full coverage appeared to have thicknesses of surfactant that corresponded to approximately a monolayer.

Some groups have found that the surfactant aggregated on the silica surface in patches, although the scattering patterns obtained for the systems under study here did not seem to show this; the spheres appeared to be monodisperse in size. This could be due to the effects on scattering of the presence of polyethylene glycol (PEG) (covering the silica in the sol and acting as a stabilizer).

As the coverage of the silica surface increased for both surfactants, it was increasingly difficult to fit the data to the model, due to the data profile flattening out. It must be pointed out that this modelling was only used to find an approximate value for the surfactant shell thickness. Also, despite the fact that it was proved that all scattering came from either the silica particles or from the Triton surfactants, the presence of even small amounts of PEG may well have influenced the amounts of TX-100 and TX-305 that were adsorbed onto the silica surface. Recent adsorption isotherms of PEG onto silica measured at Brunel showed that PEG is adsorbed onto silica at higher levels than alkyl phenols (approximately 25 times [in μmol/g] more PEG adsorbed than Triton) (9).

Luciani (10) conducted ellipsometry analysis on systems containing TX-100 and TX-305 and a silicon wafer with an oxidised surface, and found that the average layer of surfactant above the CMC was 6.3nm in thickness (for TX-100) and 7.8nm in thickness (for TX-305). If the results from neutron scattering are compared with those from ellipsometry, we can say that the neutron scattering carried out on the systems containing TX-305 was inaccurate, most probably due to misleading neutron scattering intensities caused by micelle aggregation.

Figure 4.47 shows the scattering intensities obtained for a mixture of 8mmol/l (0.5%) TX-100 and 2% silica at increasing temperature. It can be seen that the scattered intensity increased slightly, at high Q values, with temperature. Many groups have

studied the effects of temperature on micellar solutions of non-ionic surfactants using light and neutron scattering (11-14) and found that micelles in solution increase in size with increasing temperature due to dehydration of the surfactant molecules causing changes in micellar geometry (i.e. from long, flexible, rod-like surfactants to shorter rigid lamellar-type structures). The increase in intensity observed in Figure 4.47 may be due to desorption of micelles from the silica surface into solution.

Cummins and Staples (13) carried out a similar experiment on the effects of temperature on the nature of adsorbed layers and suggested that the extra scattering observed at high Q values was due to a re-organisation of the adsorbed layers on the silica surface as opposed to desorption effects; although it is unlikely that one would see this at high Q. Interparticle attractions may also occur at increasing temperature as the admicelles may become entangled at higher temperatures causing aggregation of the silica particles. Again, however, one would not usually expect to see this at high Q. The experiments carried out here seem to suggest that there is more surfactant in the micellar form in solution, and therefore I propose that there is a desorption of surfactant from the silica surface and an increase in free micelles present in solution.

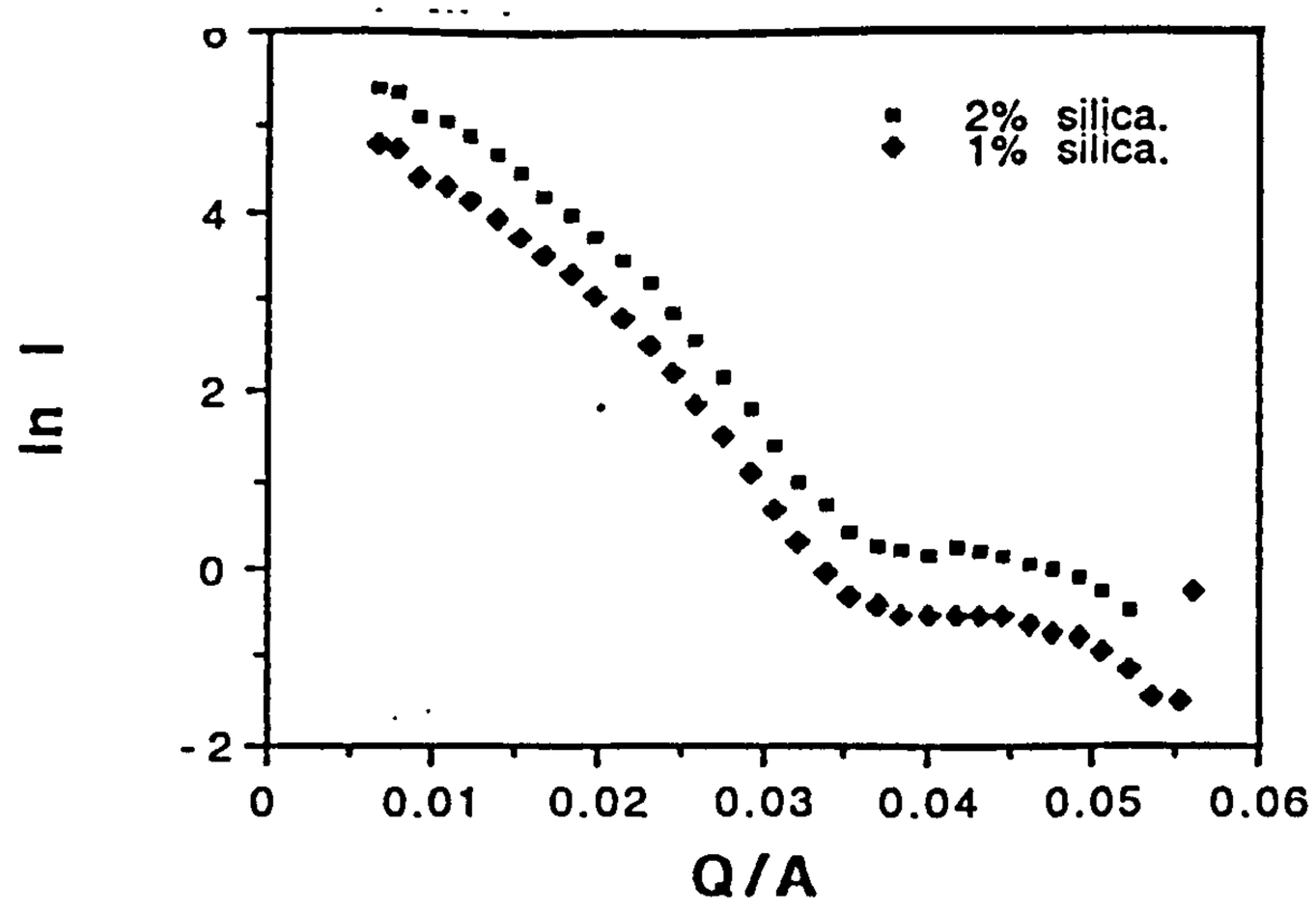

Figure 4.20: Scattered Intensity from 1% and 2% Ludox Silica Sols.

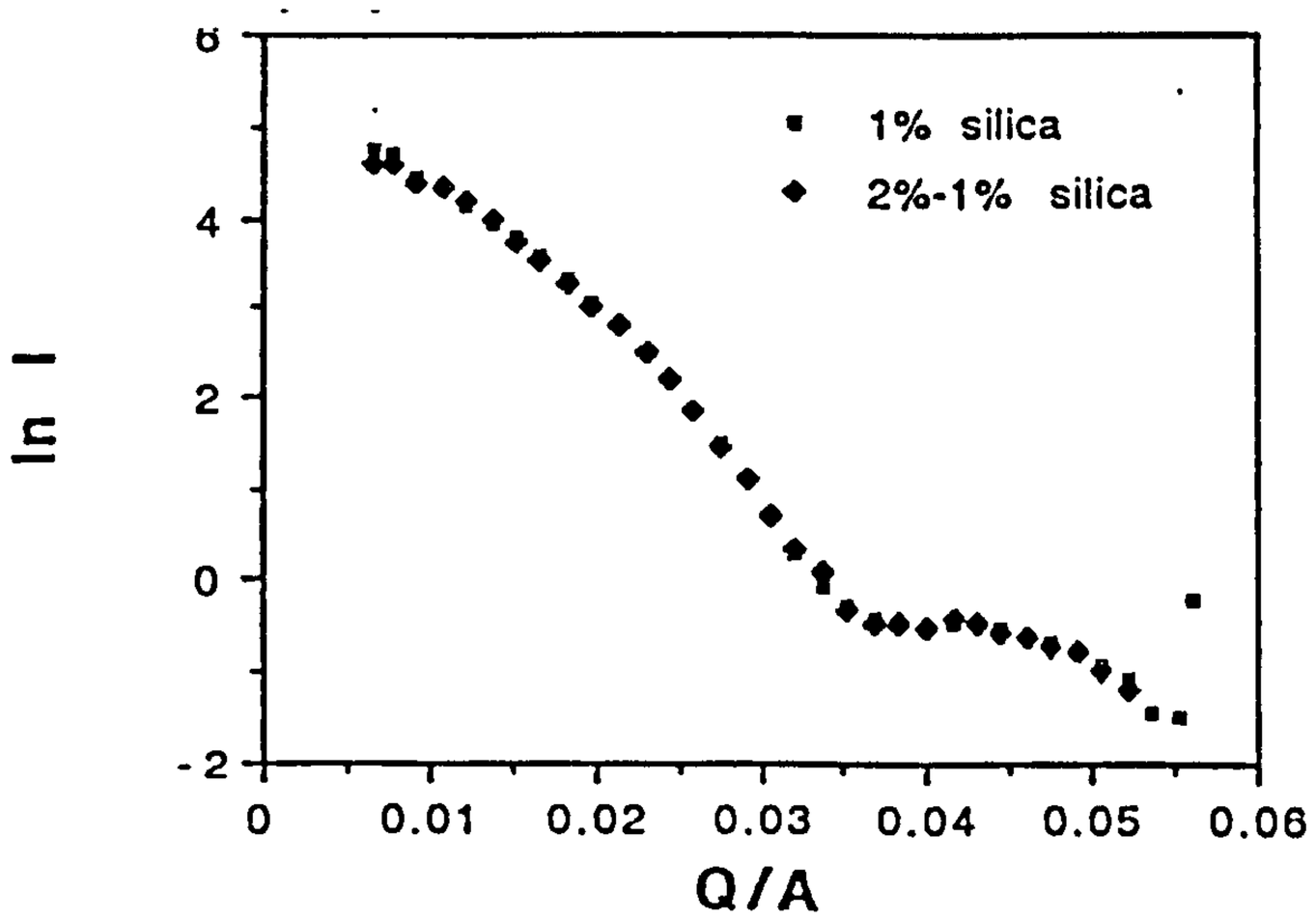

Figure 4.21: Superimposition of the Scattering Intensities from 1% and 2%-1% Ludox CL-X.

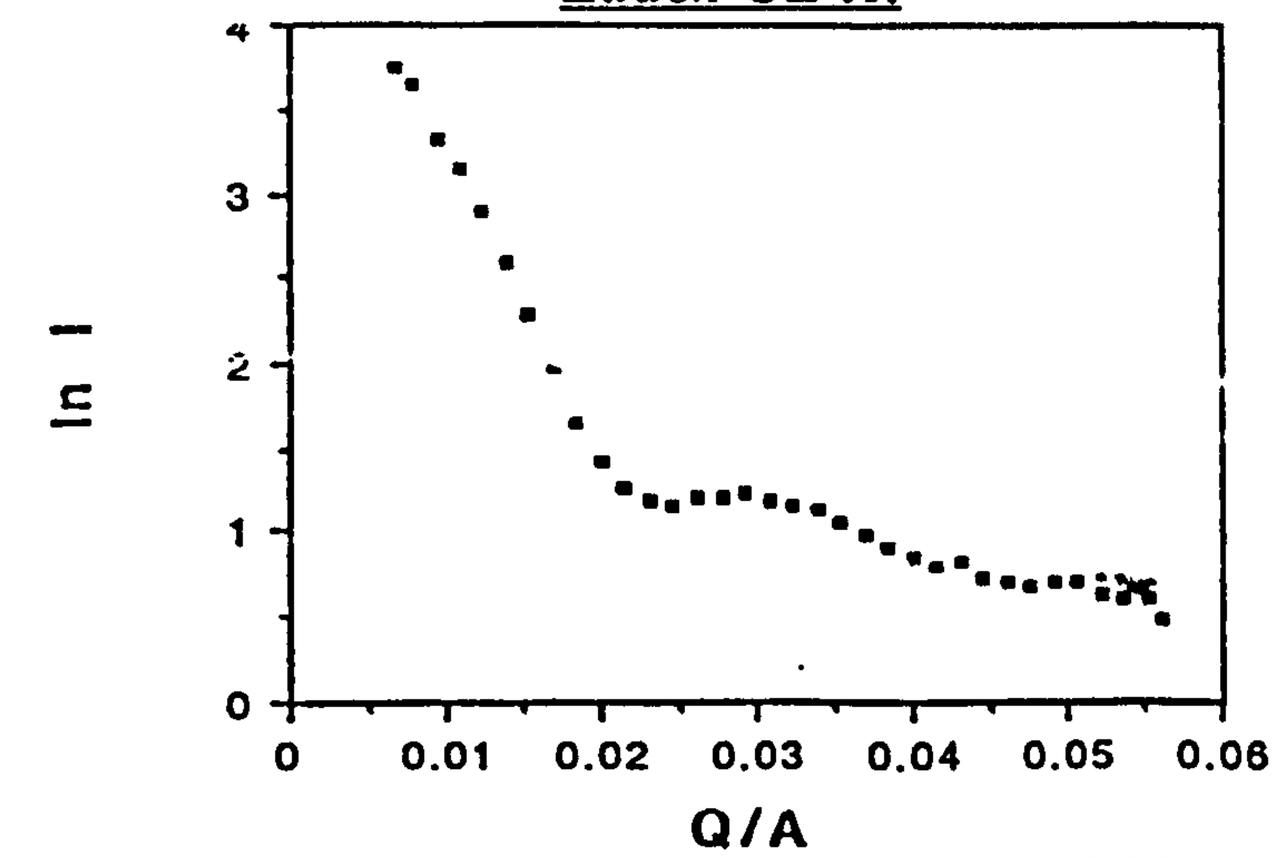

Figure 4.22: Scattering Intensity of 2% Silica Sol and 32mmol/l (2%) TX-100.

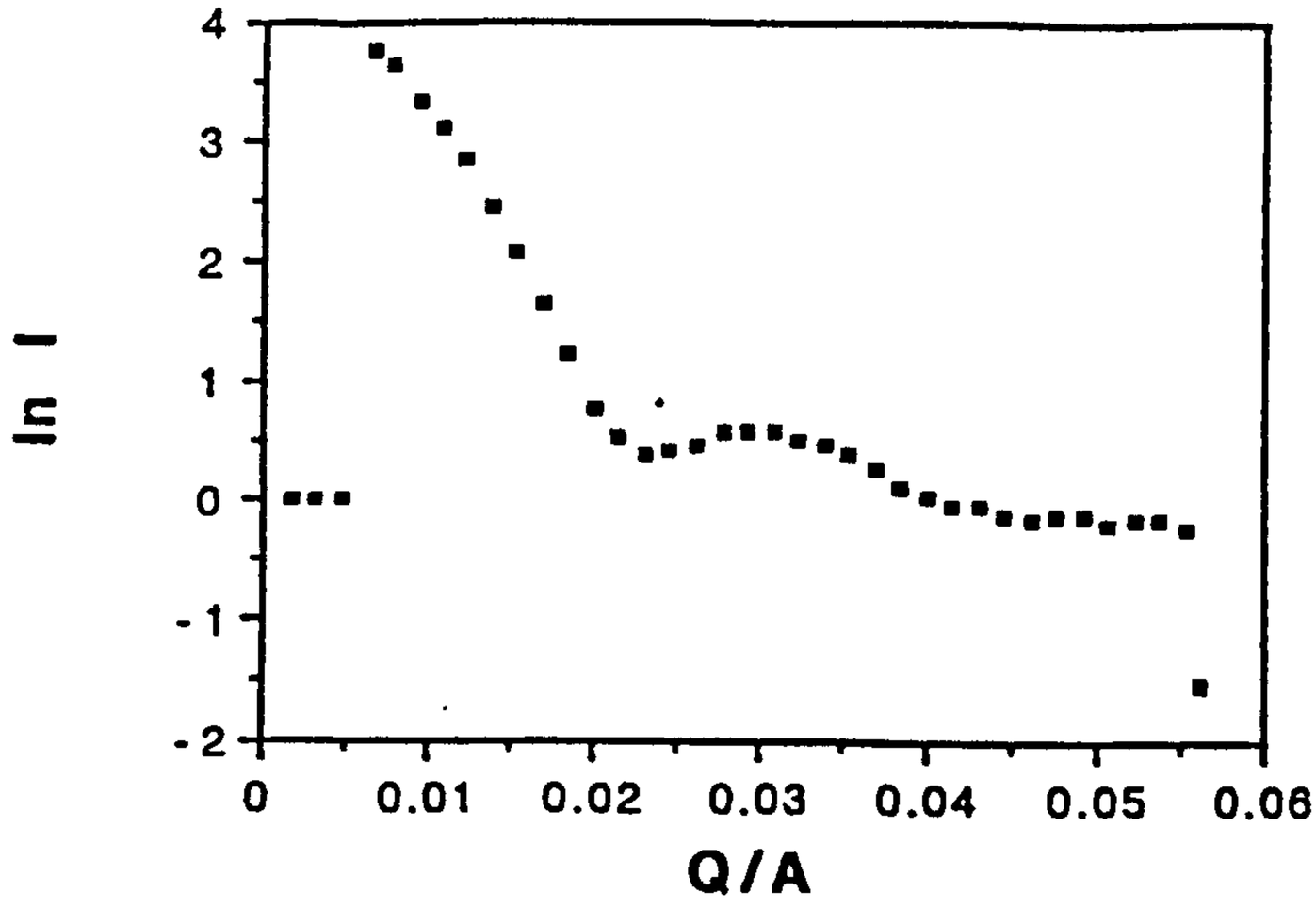

Figure 4.23: Scattering Intensity of 2% Silica Sol and 16mmol/l (1%) TX-100.

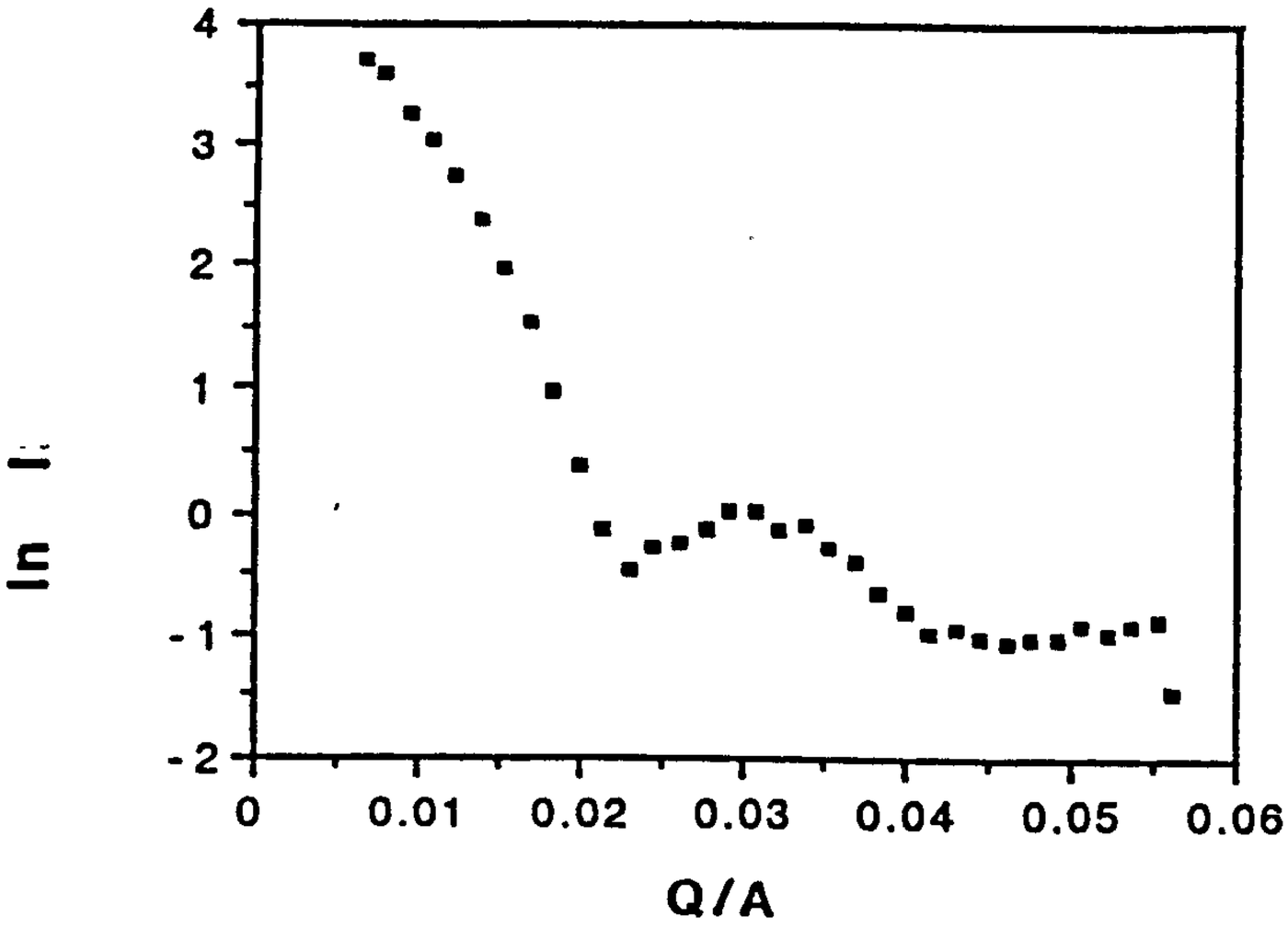

Figure 4.24: Scattering Intensity for 2% Silica Sol and 8mmol/l (0,5%) TX-100.

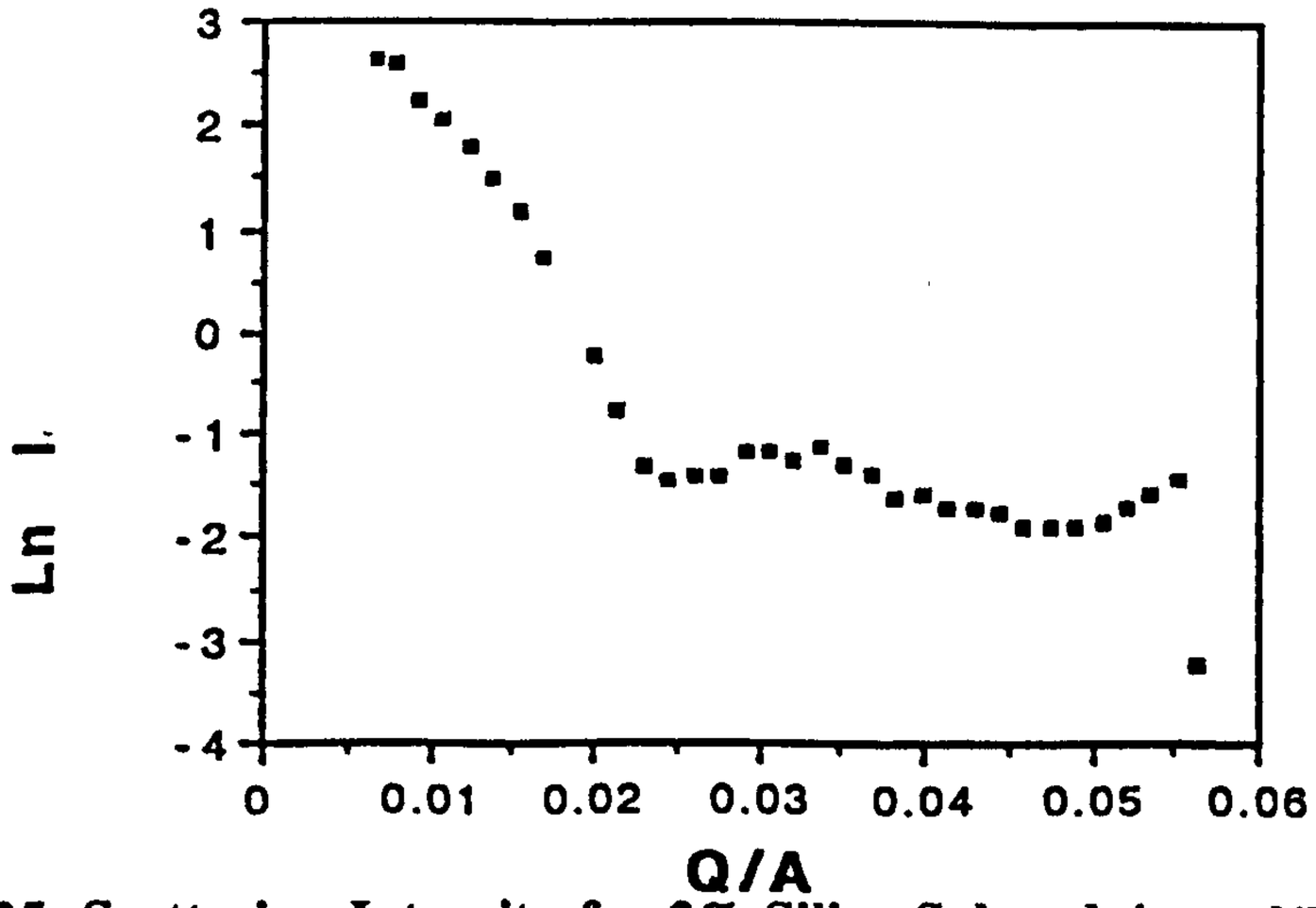

Figure 4.25: Scattering Intensity for 2% Silica Sol and 4mmol/l (0,25%) TX-100.

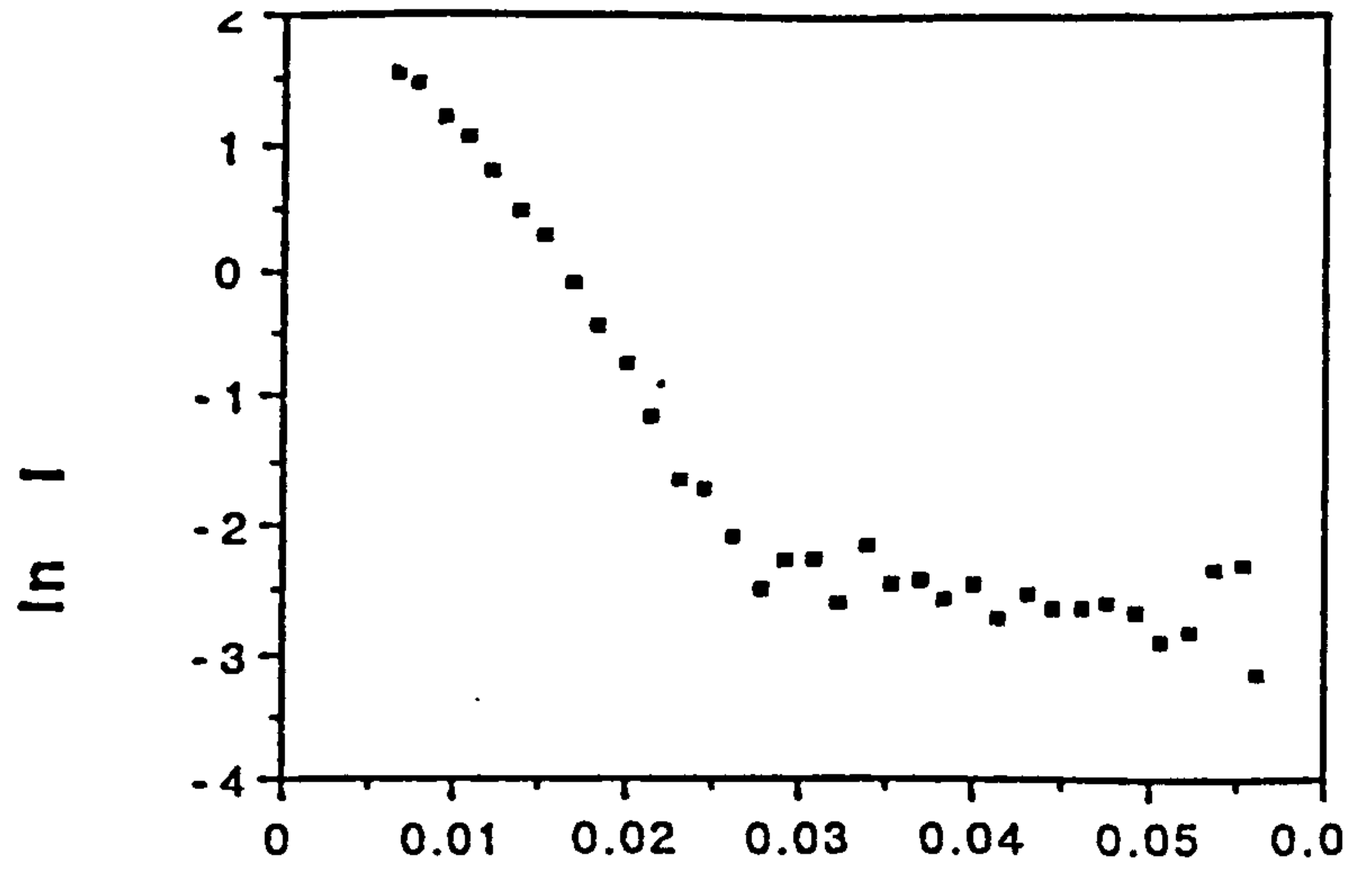

Figure 4.26: Scattering Intensity for 2% Silica Sol and 1,6mmol/l (0,1%) TX-100.

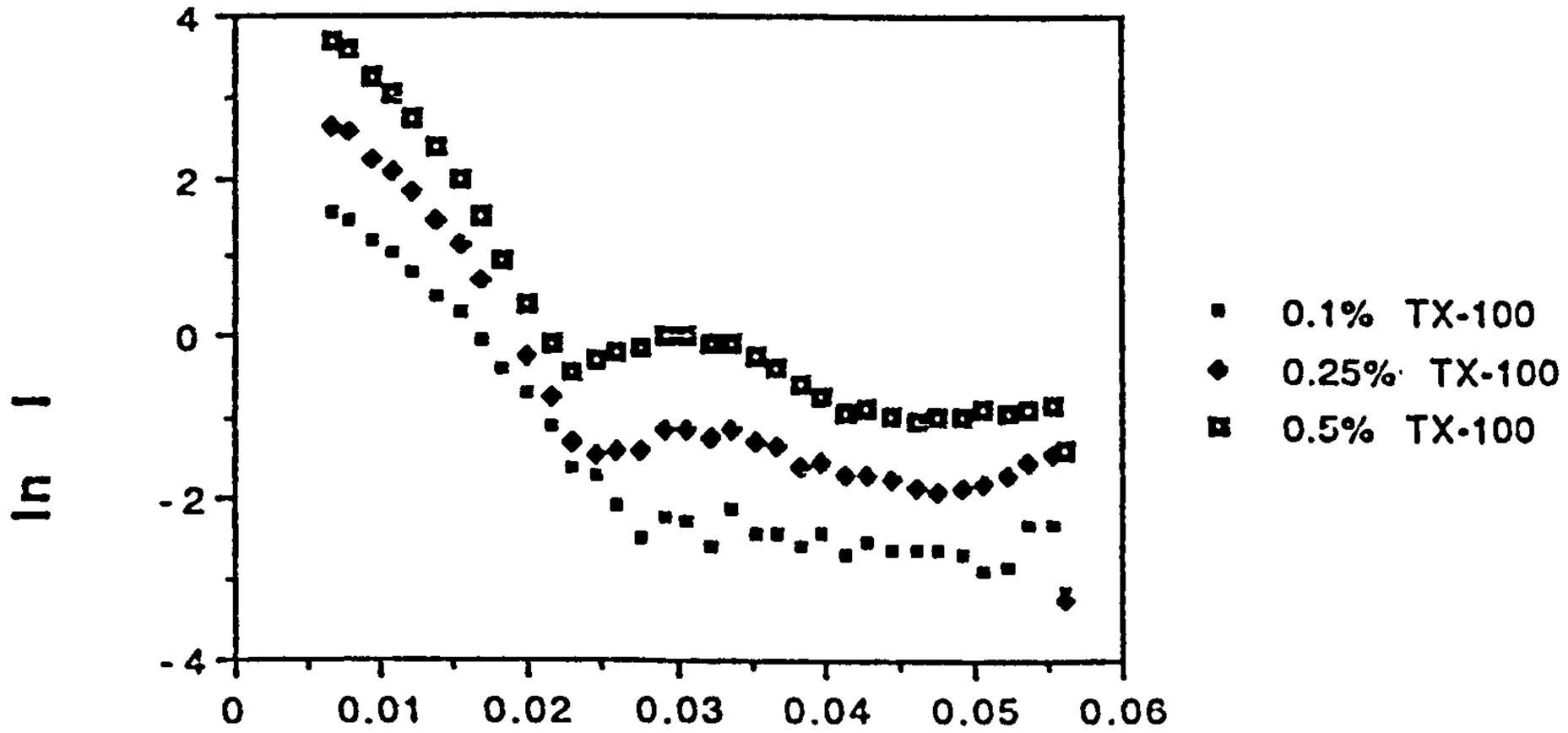

Figure 4.27: Superimposition of the Scattering Intensities of 0,5%, 0,25% and 0.1% TX-100.

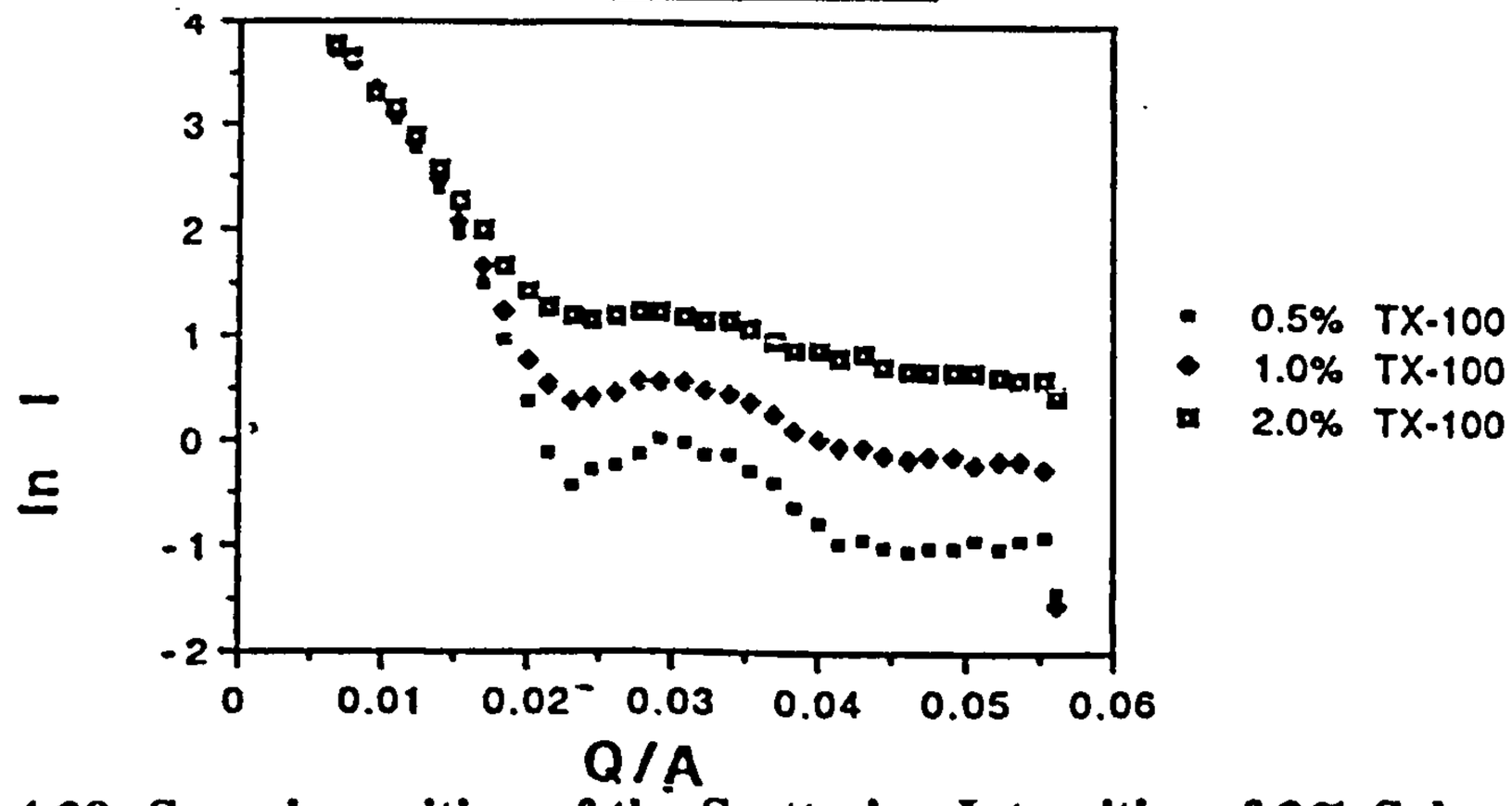

Figure 4.28: Superimposition of the Scattering Intensities of 2% Sol and 0,5%, 1% and 2% TX-100.

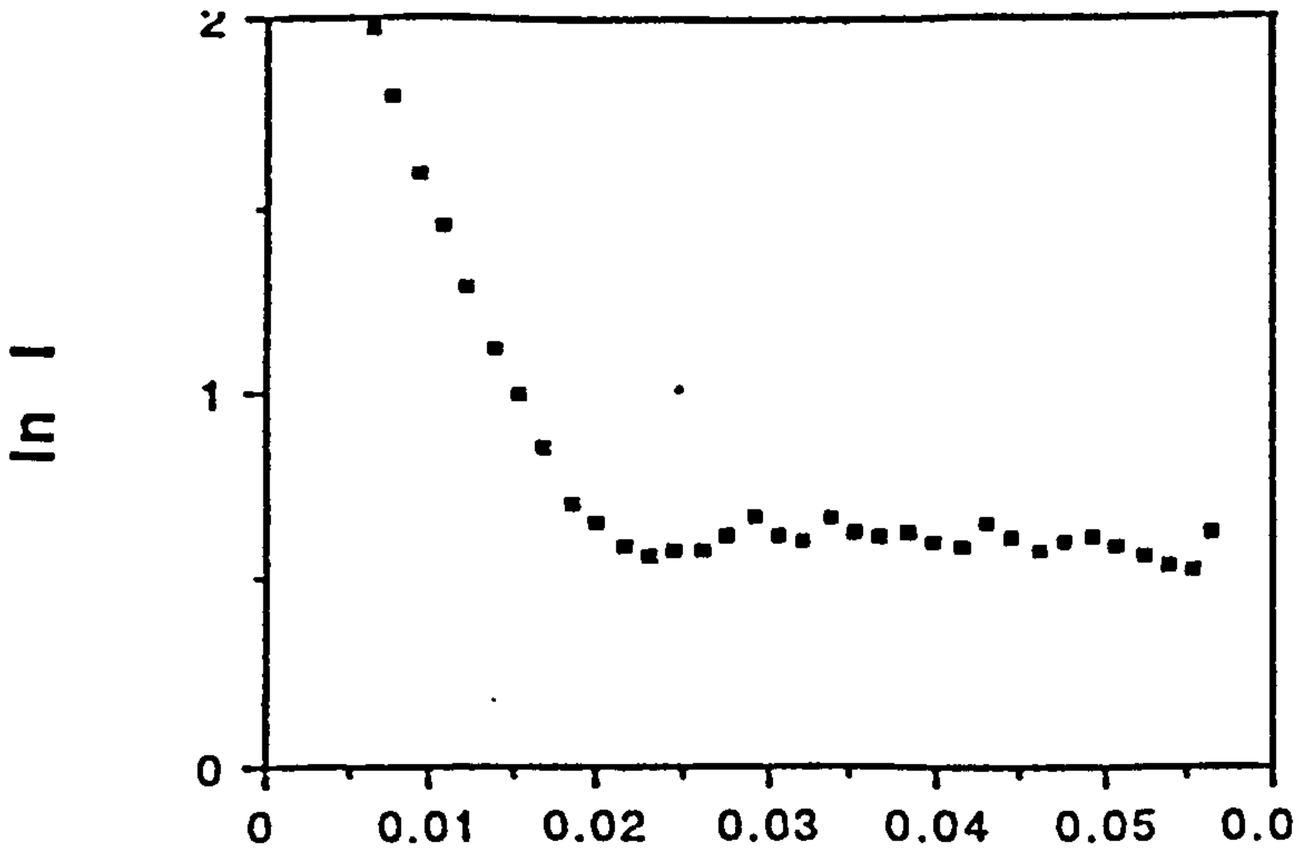

Figure 4.29: Scattering Intensity from 2% Silica Sol and 33mmol/l (5%) TX-305.

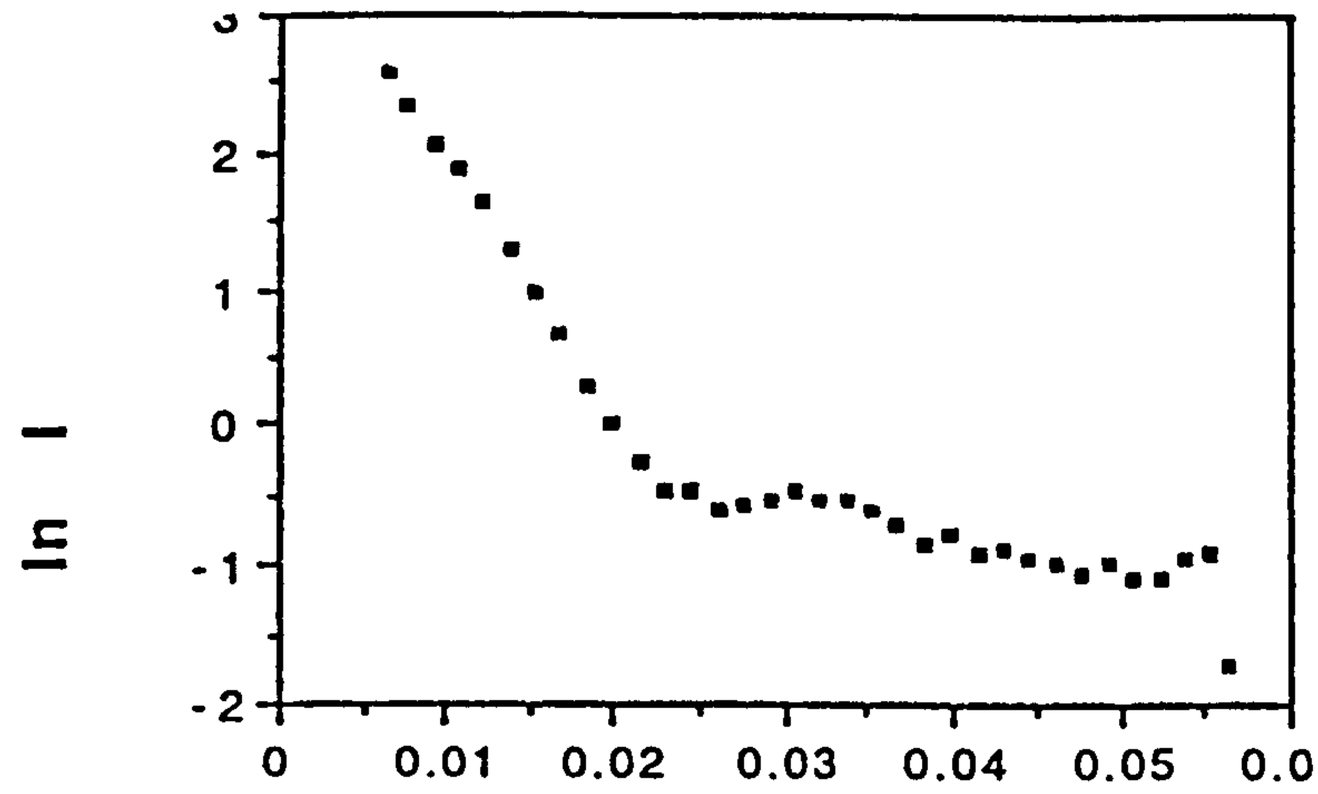

Figure 4.30: Scattering Intensity from 2% Silica Sol and 6.6mmol/l (1.25%) TX-305.

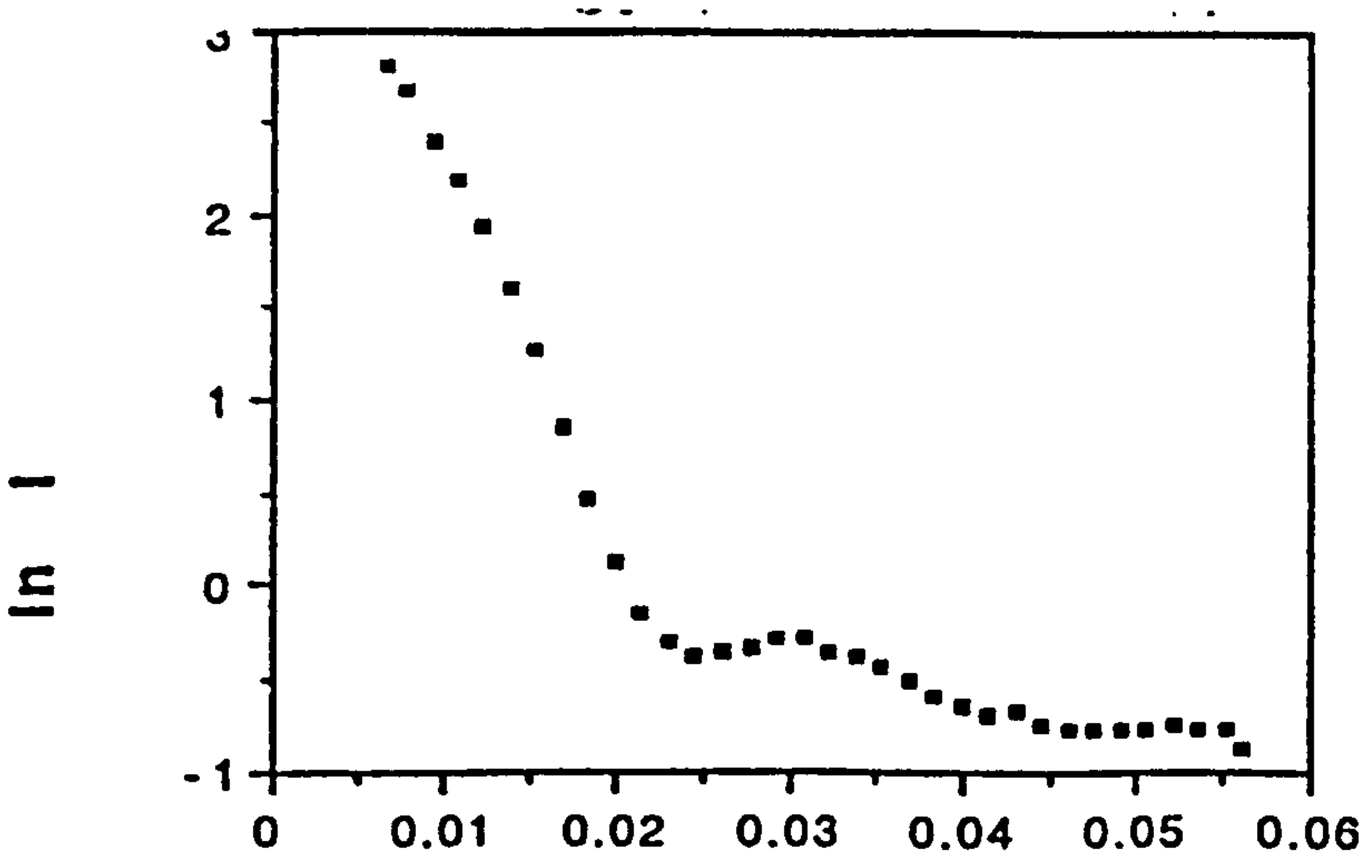

Figure 4.31: Scattering Intensity for 2% Silica Sol and 4.1mmol/l (0.625%) TX-305.

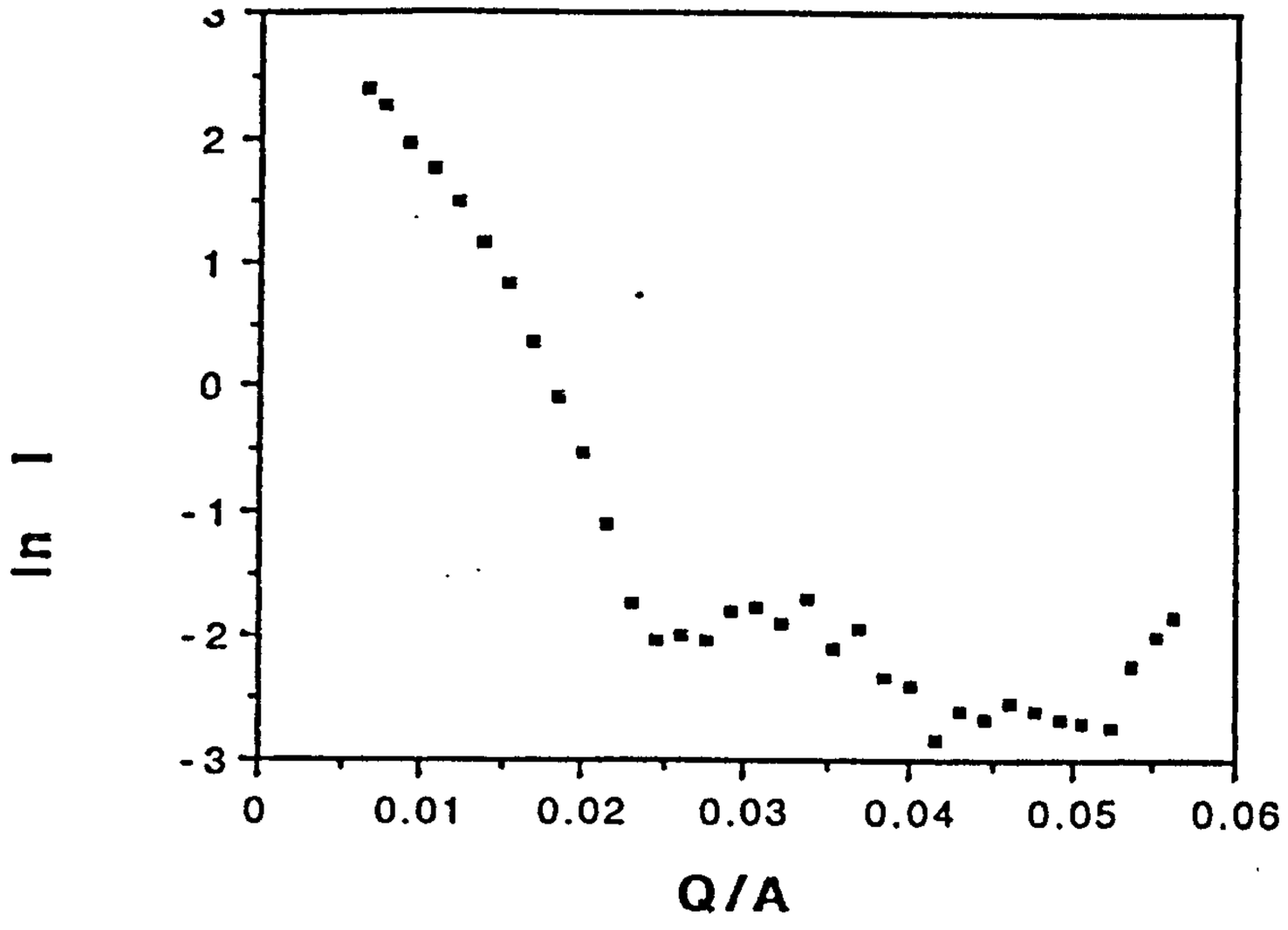

Figure 4.32: Scattering Intensity for 2% Silica Sol and 3.3mmol/l (0,5%) TX-305.

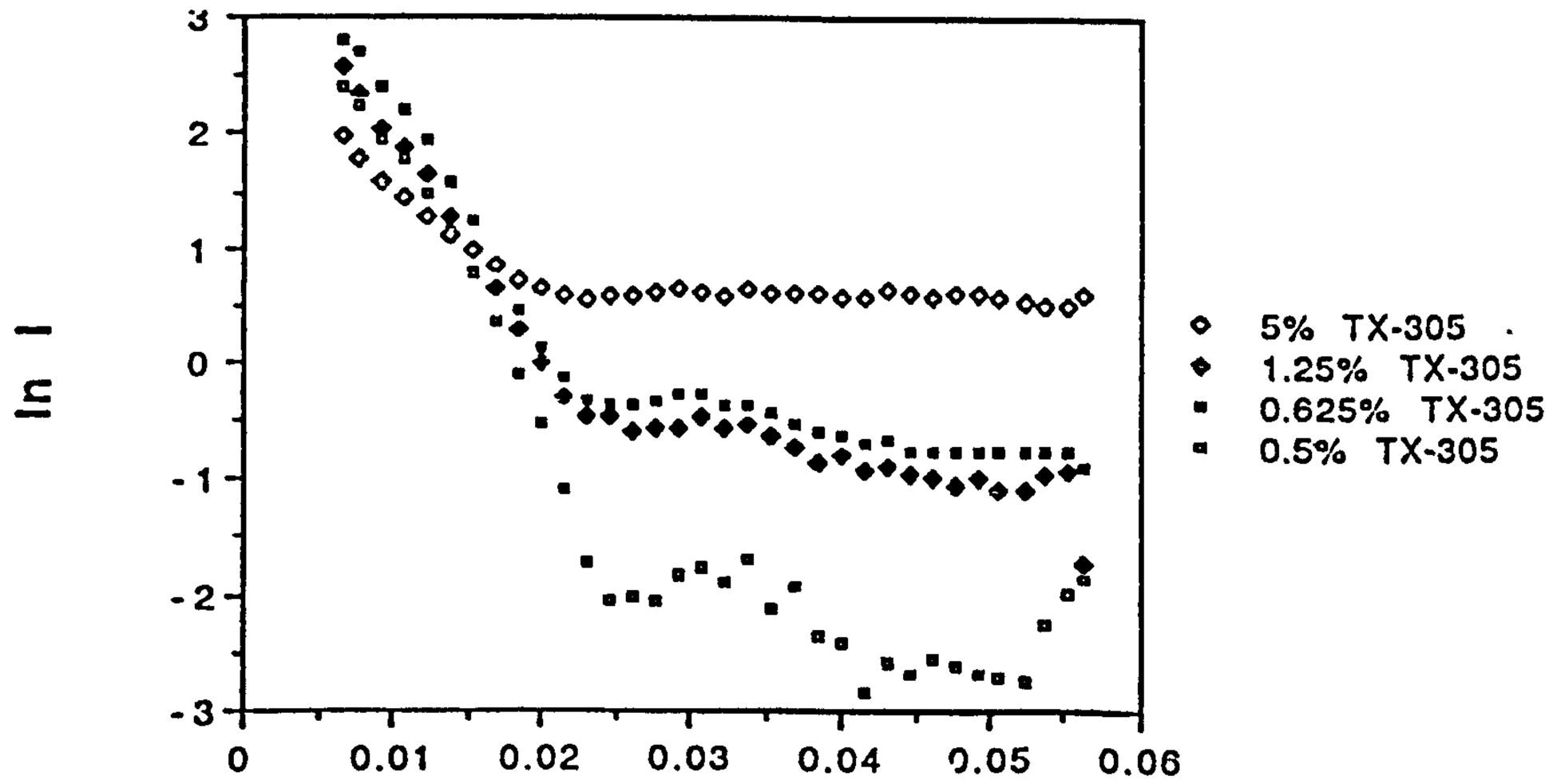

Figure 4.33: Superimposition of the Scattering Intensities for 5%, 1.25%, 0.625% and 0.5% TX-305 onto 2% Silica Sol.

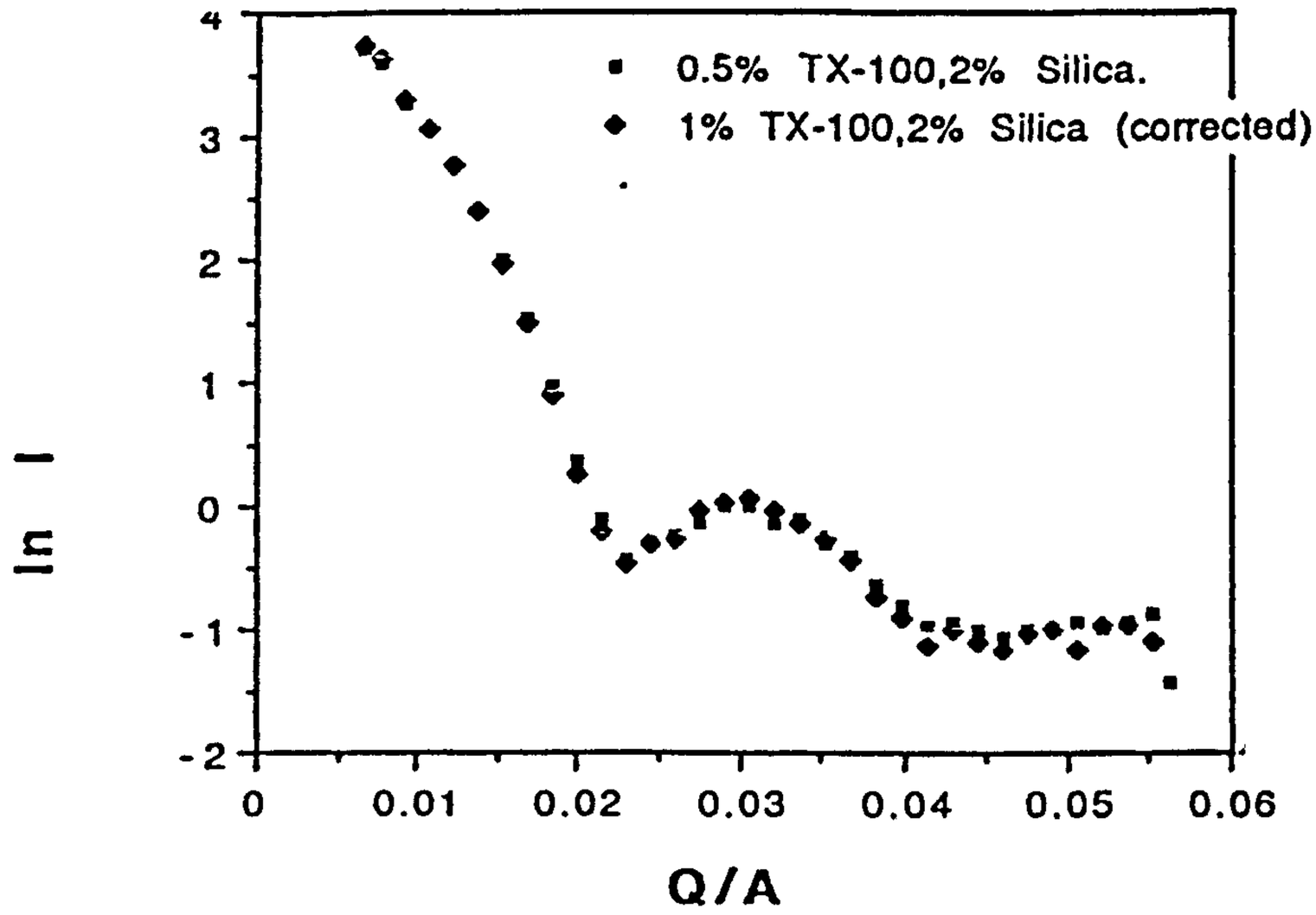

Figure 4.34: Scattering Intensity of 2% Silica Sol corrected for extra Micellar Scattering

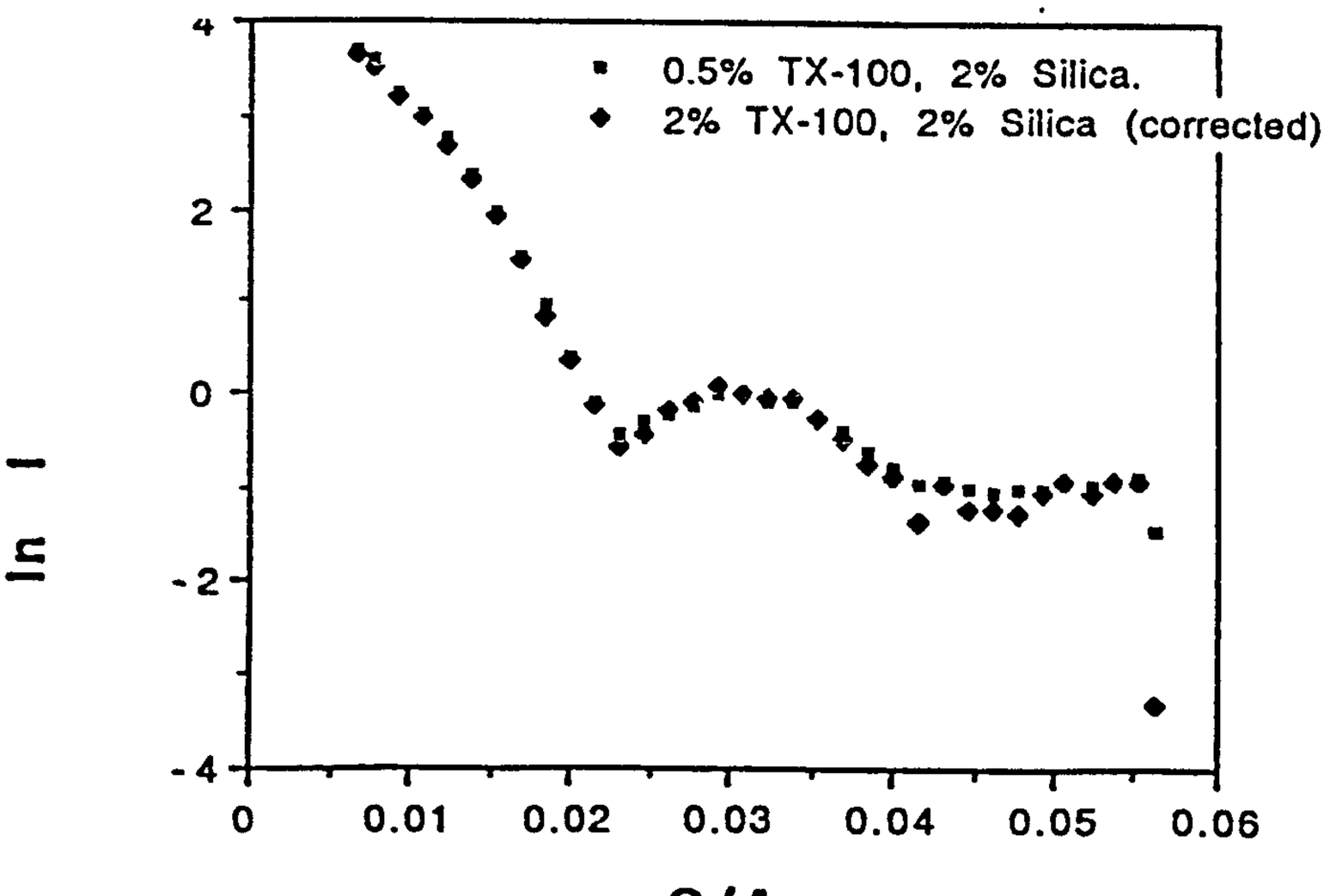

Figure 4.35: Scattering Intensity from 32mmol/l (2%) TX-100 and 2% Silica Sol Corrected for Micellar Scattering.

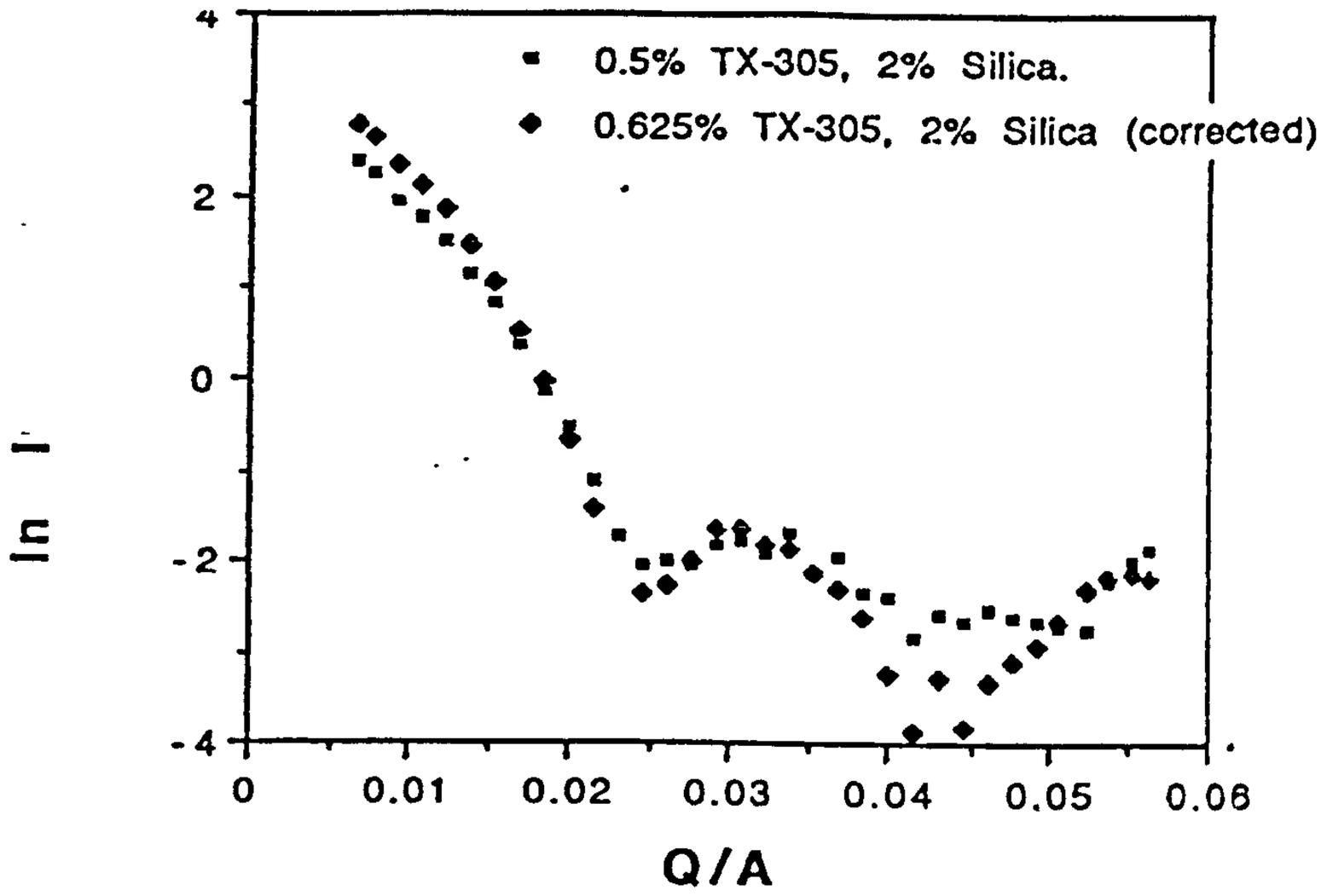

Figure 4.36: Scattering Intensity from 4.1mmol/l (0.625%) TX-305 and 2% Silica Sol Corrected for Micellar Scattering.

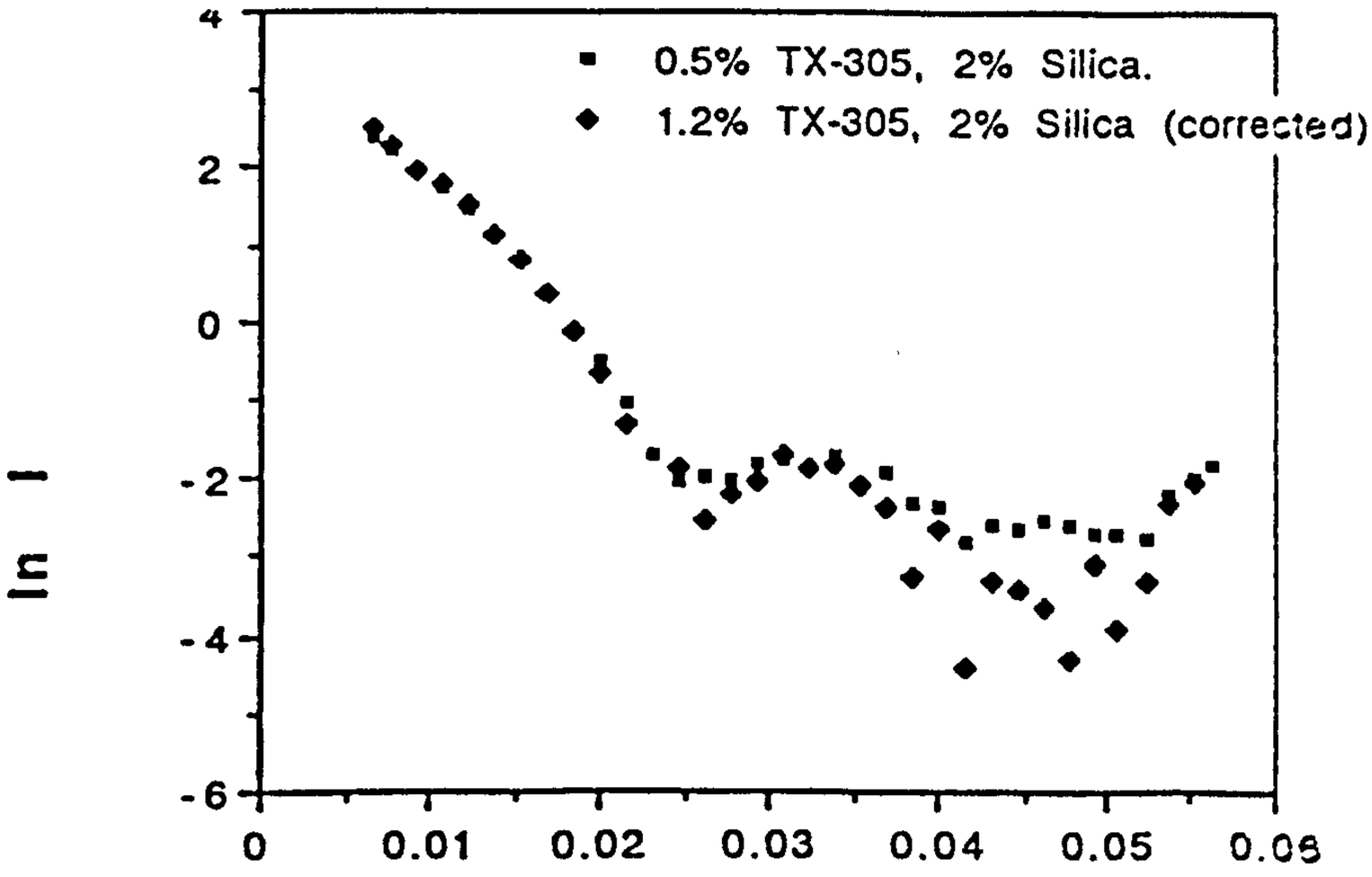

Figure 4.37: Scattering Intensity from 6.6mmol/l (1.25%) TX-305 and 2% Silica Sol Corrected for Micellar Scattering.

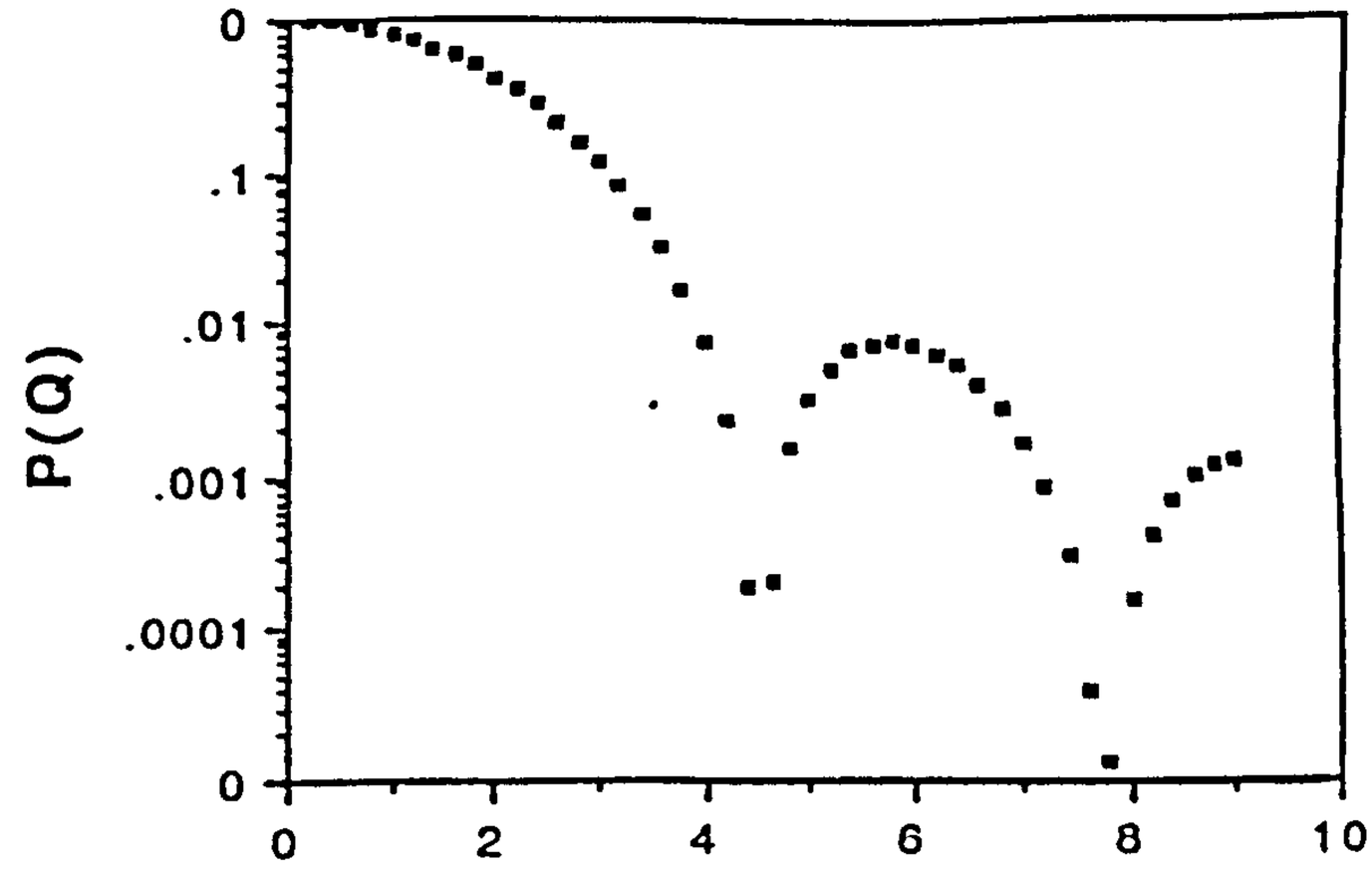

Figure 4.38: Model of P(Q)

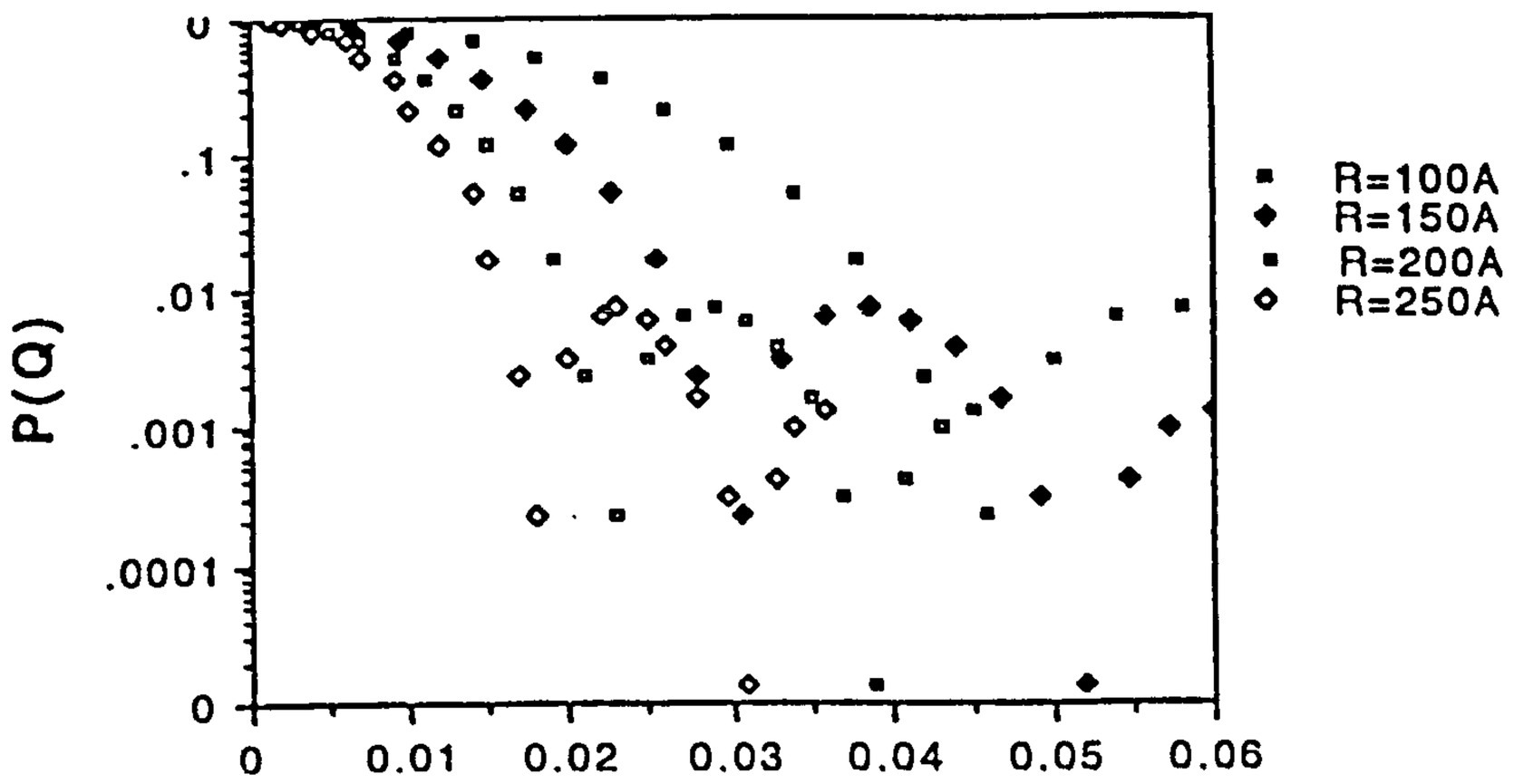

Figure 4.39: Varying the Value of 'R' in the Model.

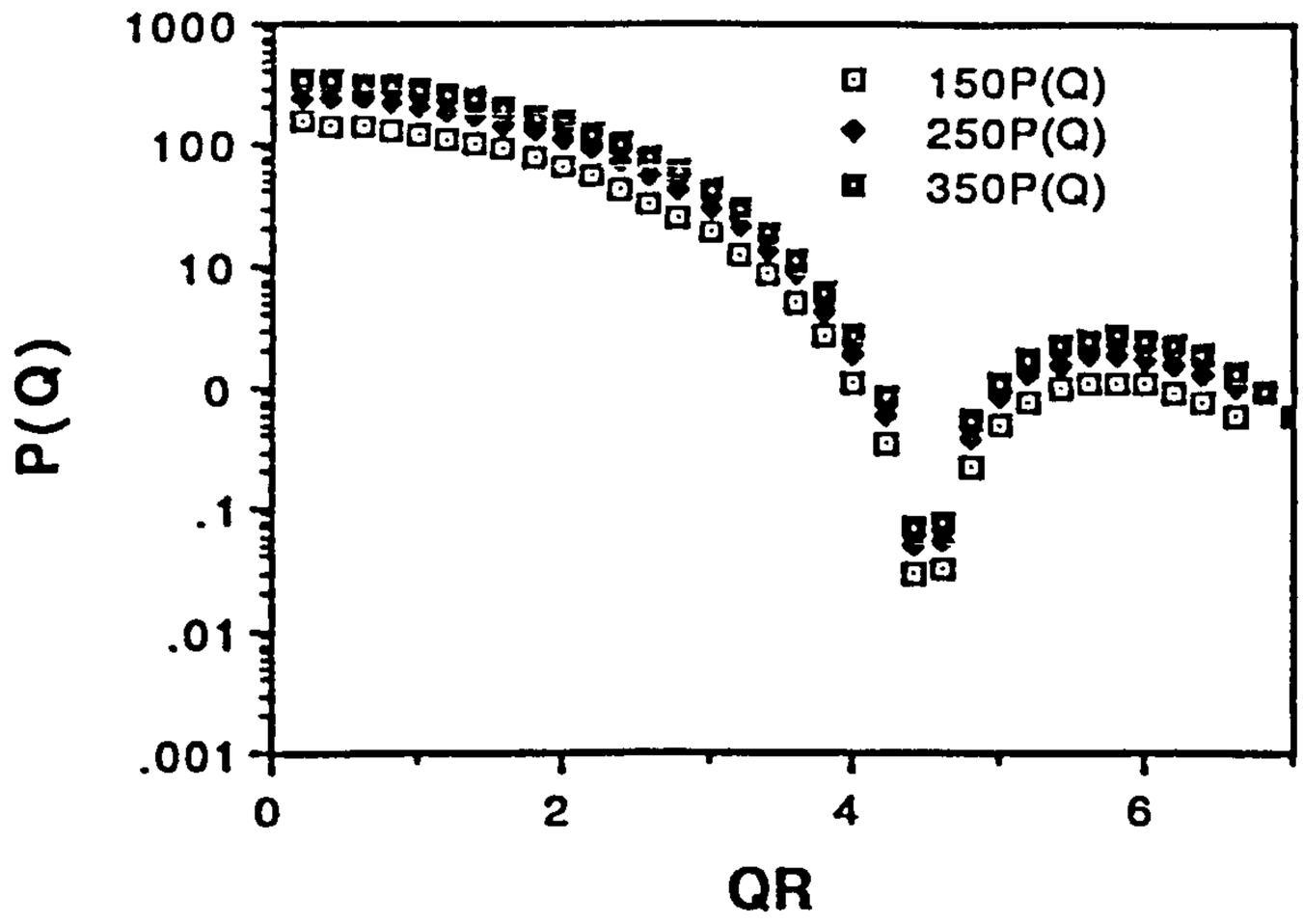

Figure 4.40: Varying I(0) of the Model.

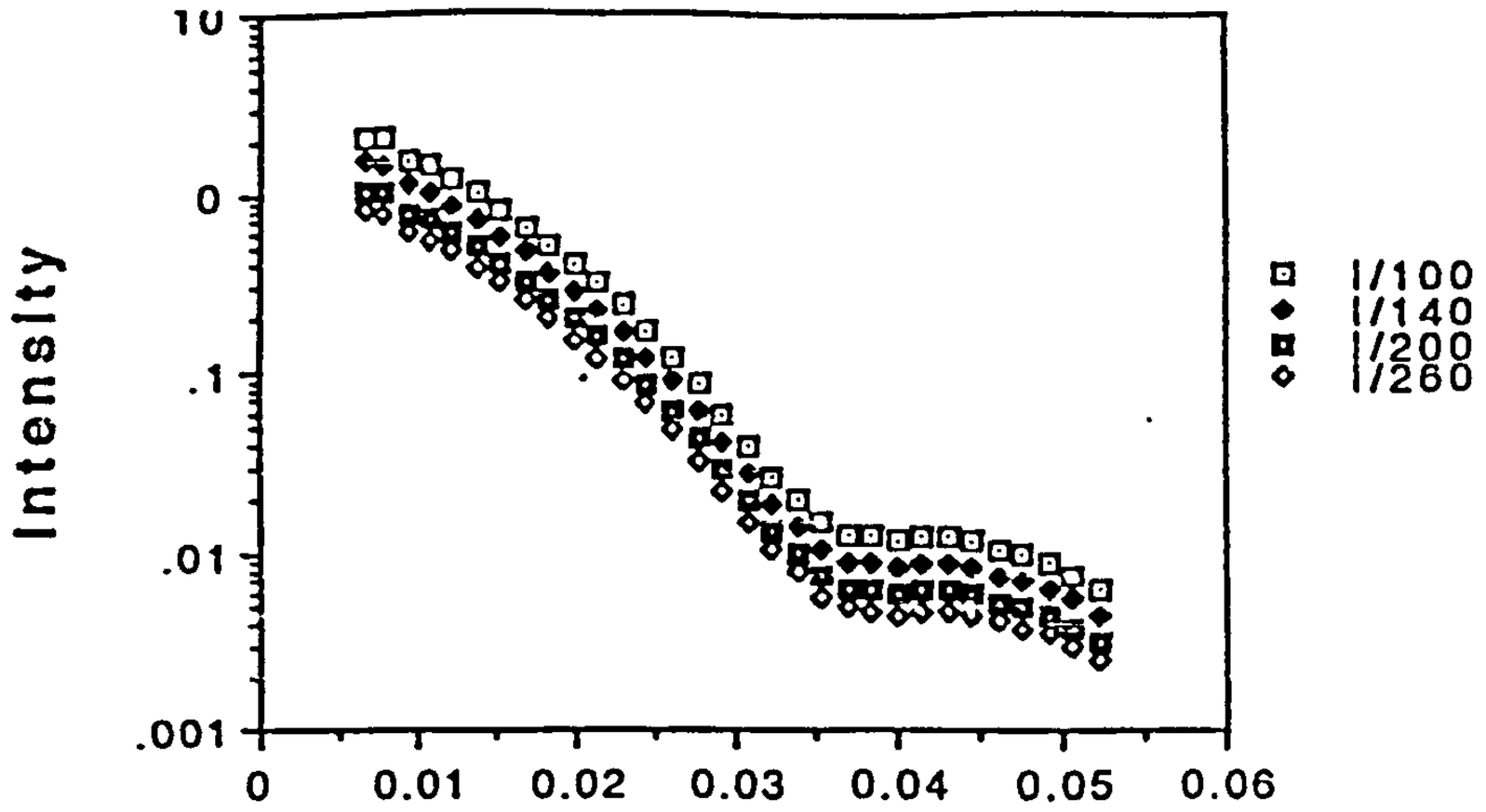

Figure 4.41: Data for the Bare Silica modified for Differing Values for I(0).

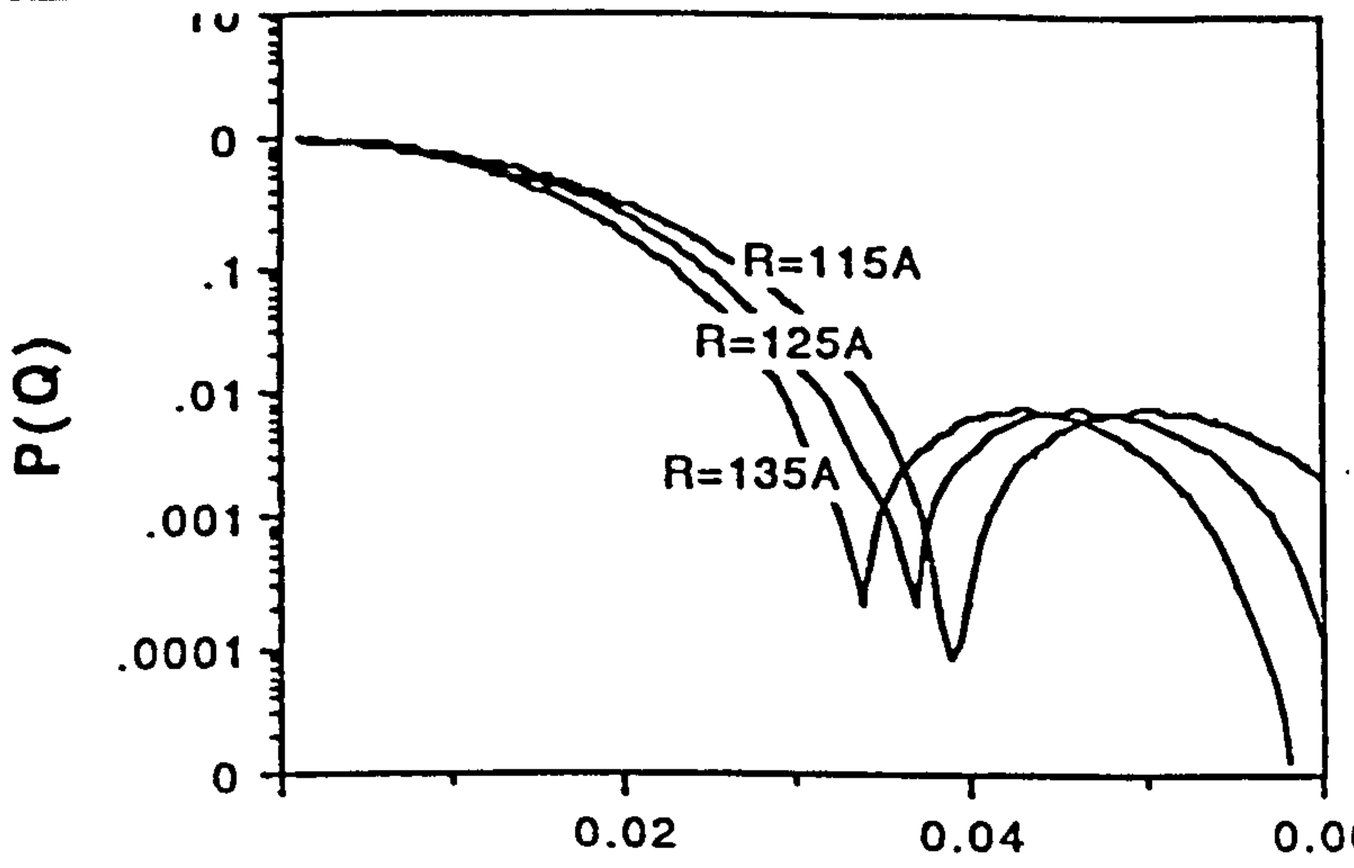

Figure 4.42: Varying 'R' of Model P(Q) to fit to Data for Bare Silica.

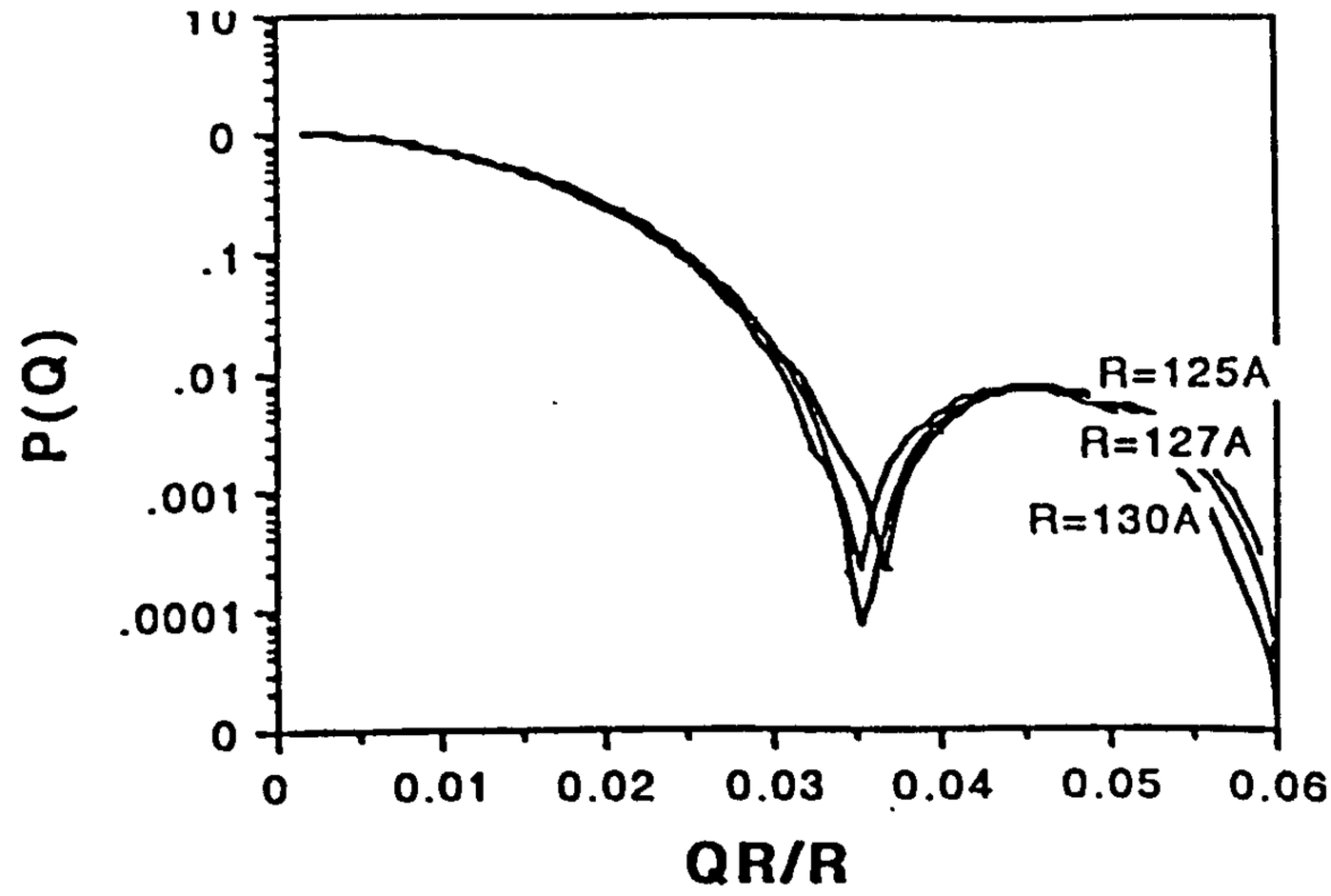

Figure 4.43: Varying 'R' of Model P(Q) to fit to Data for Bare Silica.

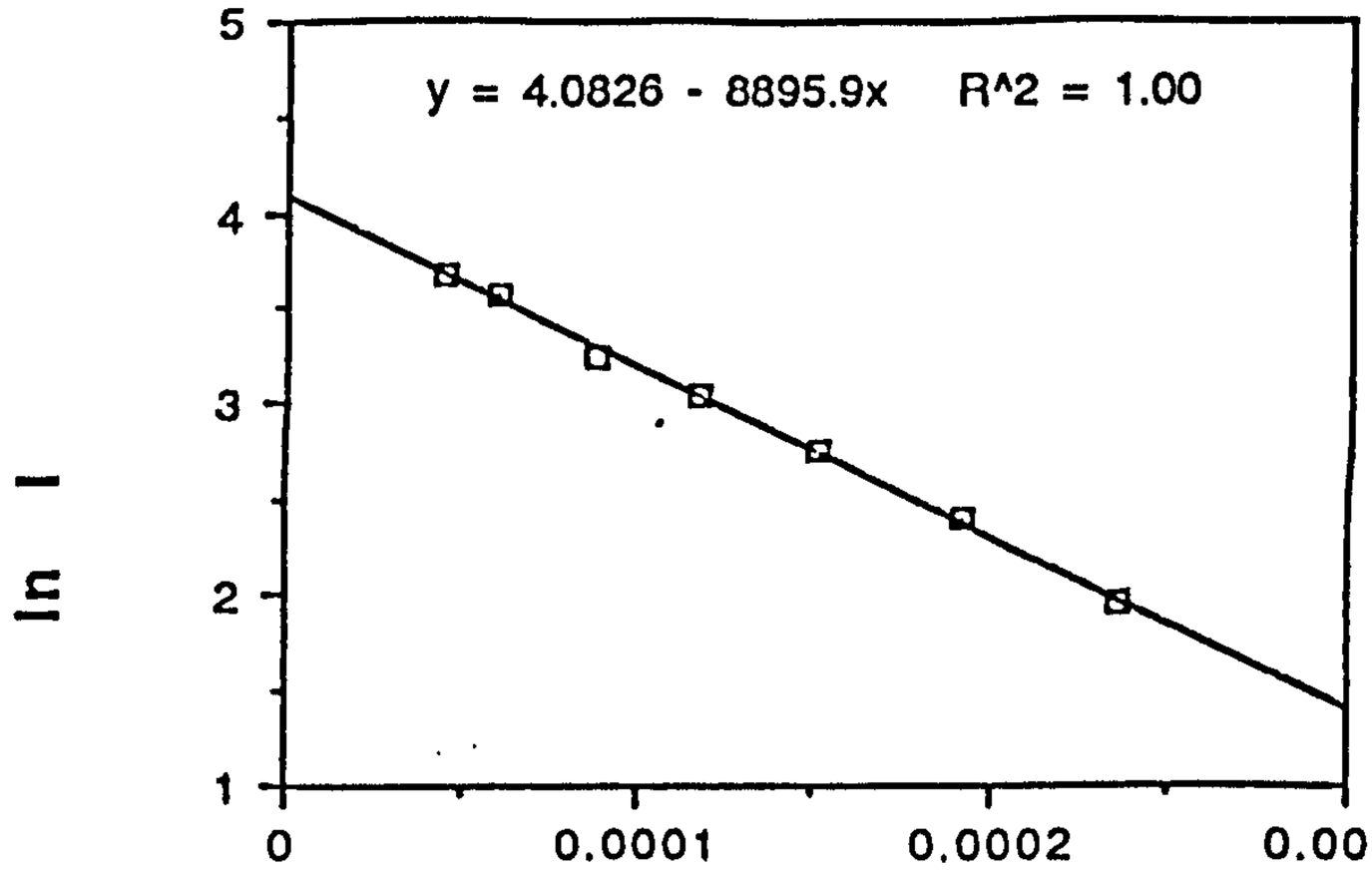

Figure 4.44: Calculation of I(0) for 8mmol/l (0.5%) TX-100 and 2% Silica by Guinier Analysis.

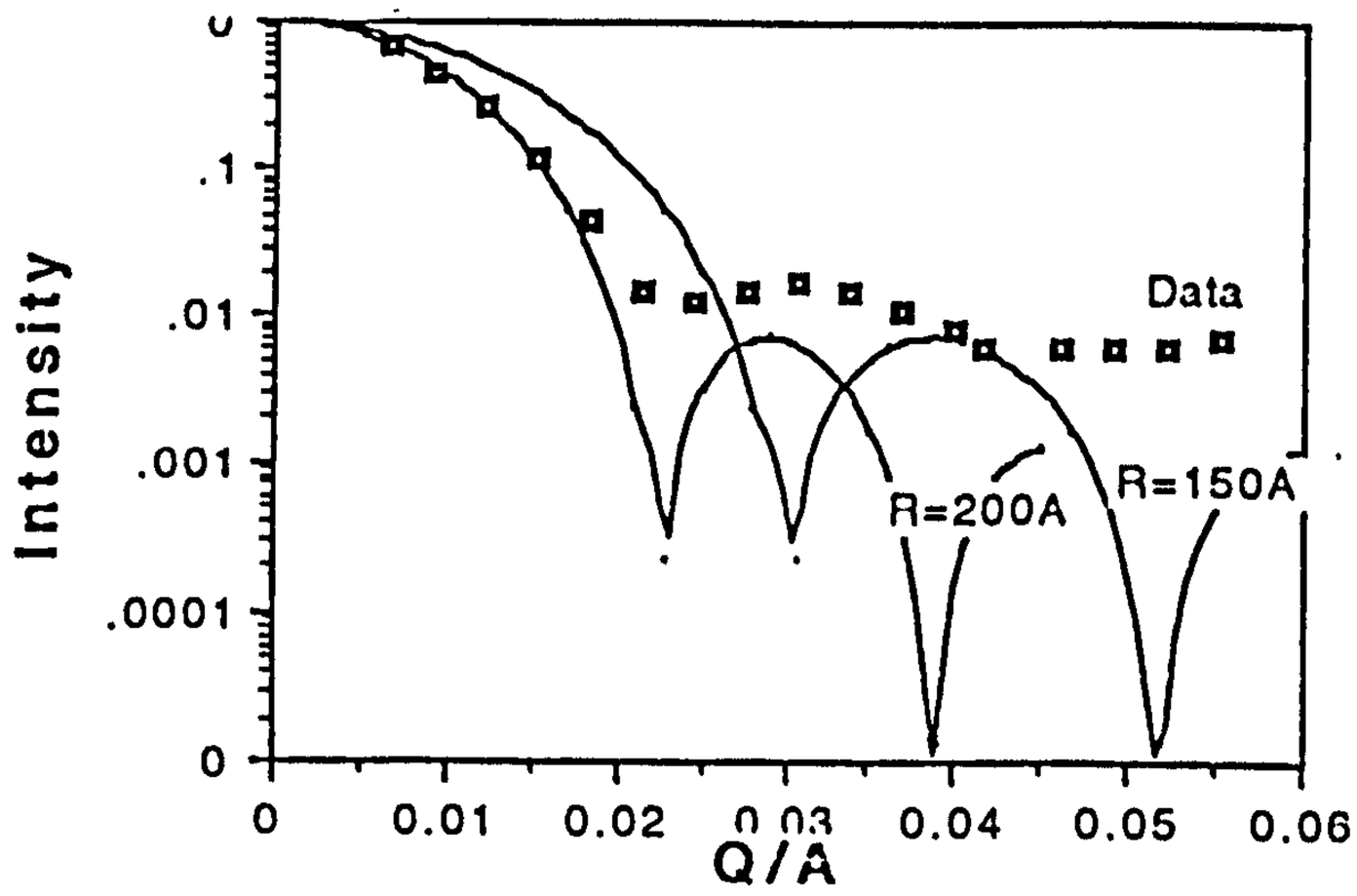

Figure 4.45: Fitting the Data to the Model of P(Q) for 0.5% TX-100 and 2% Silica.

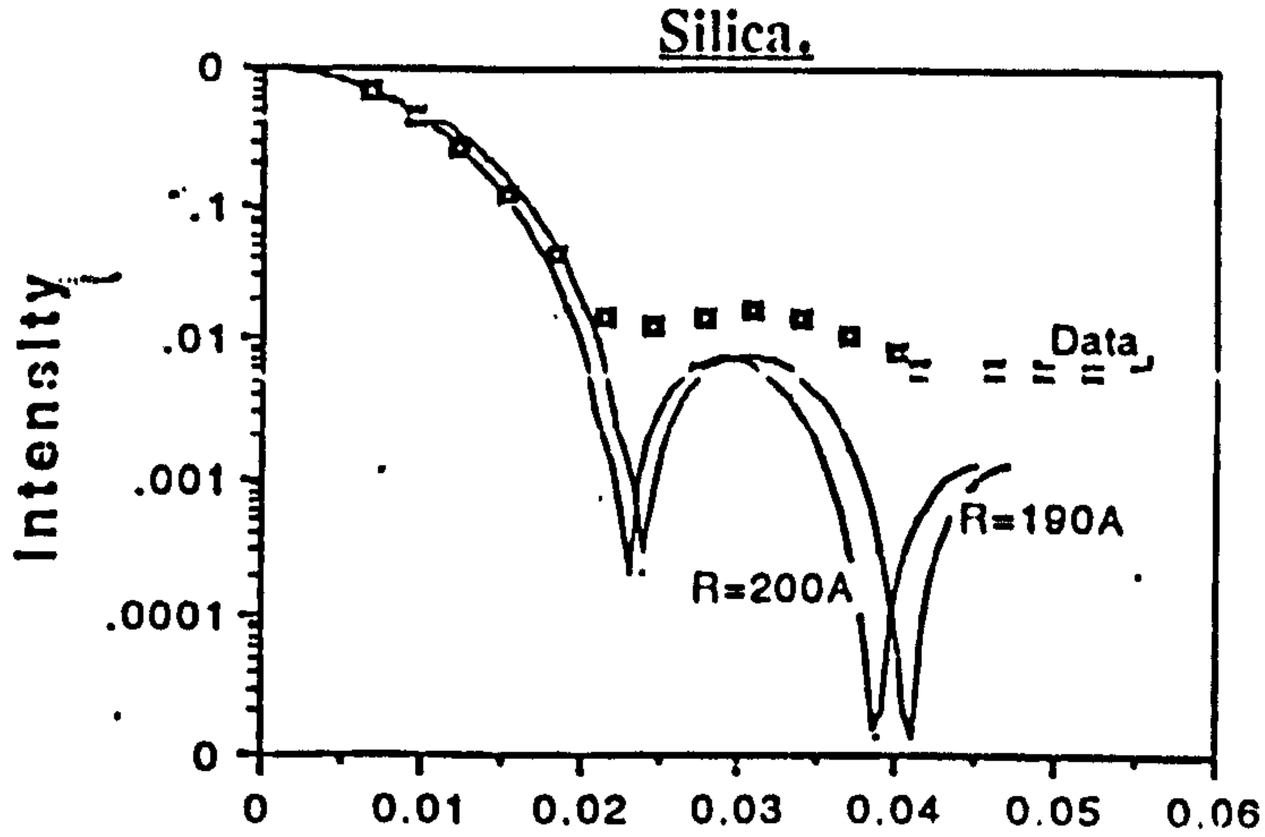

Figure 4.46: Fitting the Data to the Model of P(Q) for 0.5% TX-100 and 2% Silica.

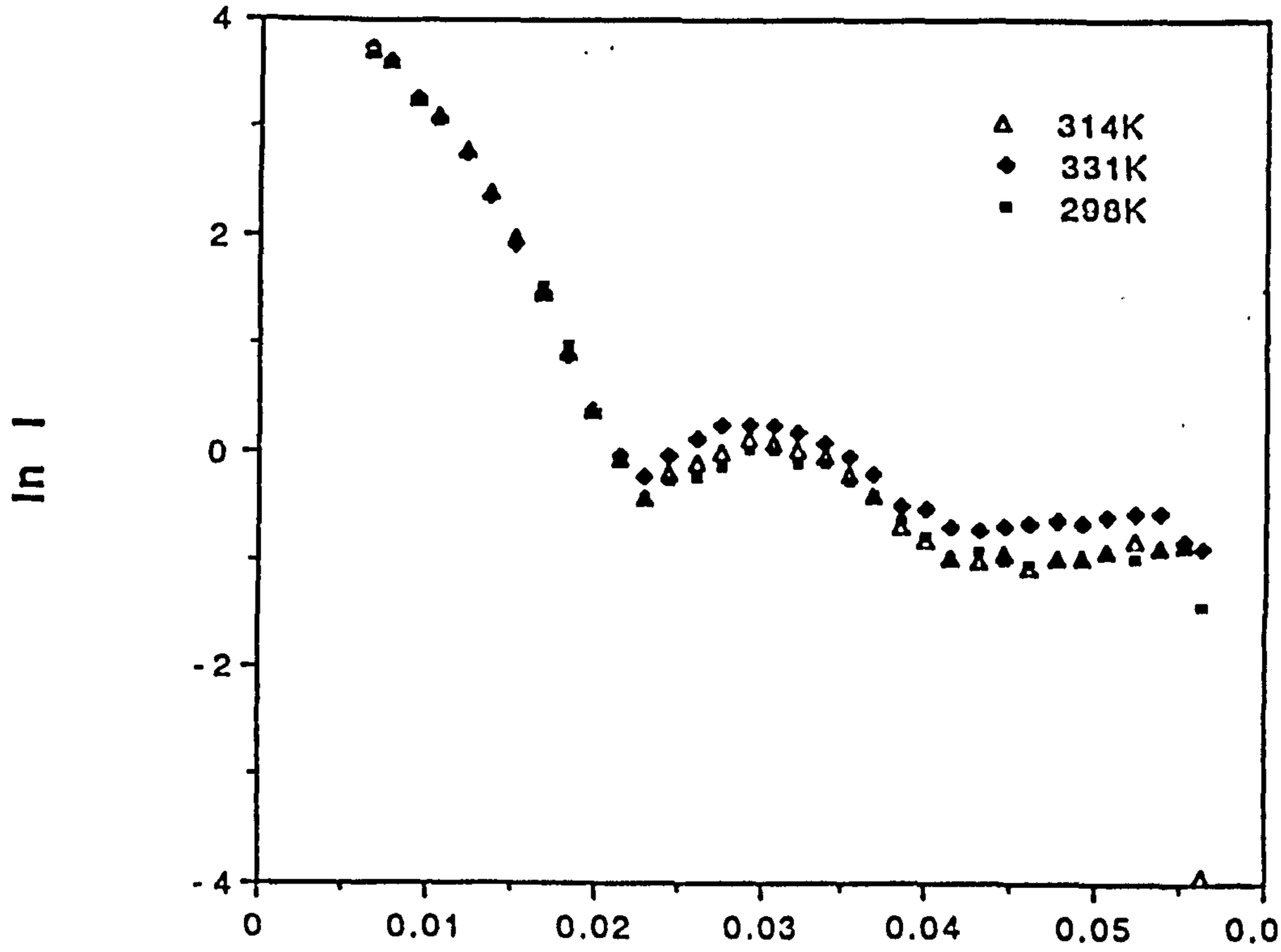

Figure 4.47: Scattered Intensities at Increasing Temperature for 0.5% TX-100 and 2% Silica.

4.6 Atomic Force Microscopy (AFM) Analysis.

AFM, invented in 1986 by Binnig, Quate and Gerber (15), allows one to directly visualise thin films in the nanometre scale. The conventional atomic force microscope traces out lines of constant force on a surface. During the measuring process the interactions between a probe and the features on a substrate surface are measured. A silicon nitride tip, supported by a cantilever, is placed in contact with the substrate. A piezoelectric scanner rasters the sample beneath the tip and topographical variations in the surface deflect the cantilever. The top of the cantilever reflects a laser beam onto a photodetector, which then records the topographical variations. A constant force is maintained between the tip and the sample. An image is built up of many scans, each scan being slightly offset from the previous one. This form of AFM is known as 'contact mode AFM'. Several new modes of AFM imaging have been developed, these are known as non-contact mode AFM. Manne and Gaub (16) used long range forces to deflect the cantilever rather than contact forces, and were able to view hemicylindrical micelles that were loosely bound onto graphite. Other methods of AFM include electric force microscopy (which measures electric field gradients near a sample surface) and friction force microscopy (which measures the lateral or friction force between the tip and sample in addition to changes in topography). Zasadzinski has reviewed scanning force microscopy in its many forms (17). Figure 4.48 shows a schematic diagram of the detection system for the scanning probe microscope.

4.6.1 Experimental.

The AFM was used here to see if the technique could be used to view surfactant that had been adsorbed onto quartz. The AFM measurements were carried out using a Park Scientific Instruments Autoprobe in the contact mode. This is not an ideal mode for the systems being studied as surfactant coatings are soft and tend to be disturbed by the tip of the cantilever, however, non-contact mode fittings were not available at Brunel during the time of experimentation. Quartz disks (cut from sheets of quartz in the Glass Workshop at Brunel University, polished by the supplier, and kept in covered petri dishes when not involved in experimentation) were dip coated, at a speed of 5mm sec^{-1}, in aqueous solutions of TX-100. Figure 4.49 shows the AFM image obtained for the bare quartz disk; the surface appears flat. Figure 4.50 shows the image obtained

for quartz disks that had been dipped in TX-100 of concentration $8x10^{-5}$mol dm^{-3} (i.e. under the CMC, see Chapter 2, Table 2.1). The surface is uneven when compared to the bare quartz, and the image appears to show 'patches' of surfactant. Figure 4.51 shows the image obtained for the disks that had been dipped in surfactant solution having a concentration of surfactant that was well above the CMC (i.e. $3.0x10^{-3}$mol dm^{-3}). The surface appears to be almost smooth. The patches that appeared for the previous images disappeared at this higher concentration of TX-100. There are also slight 'pin pricks' in the surface that are most likely due to the evaporation of water from the surfactant solution adsorbed at the surface. McDermott et al (7) observed, using neutron reflection, that non-ionic surfactant solutions were adsorbed onto silica surfaces in these non-continuous 'islands', although they saw this phenomenon at concentrations of surfactant well above the CMC. In order to obtain a greater accuracy for the surfactant/silica sol systems, a non-contact AFM system should ideally be utilized to avoid the disturbance of the soft surfactant layer by the AFM tip.

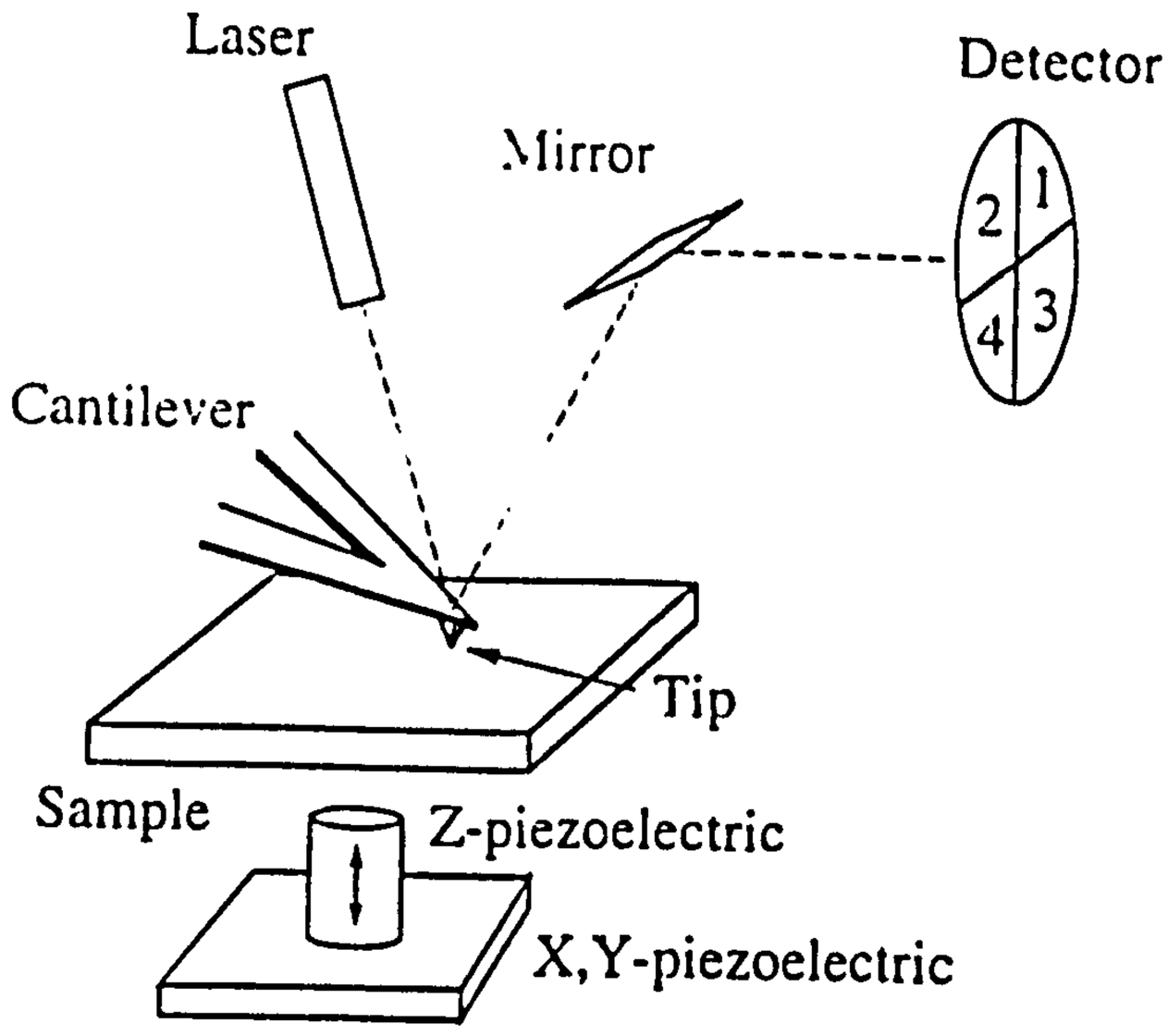

Figure 4.48: Schematic Diagram of the Atomic Force Microscope.

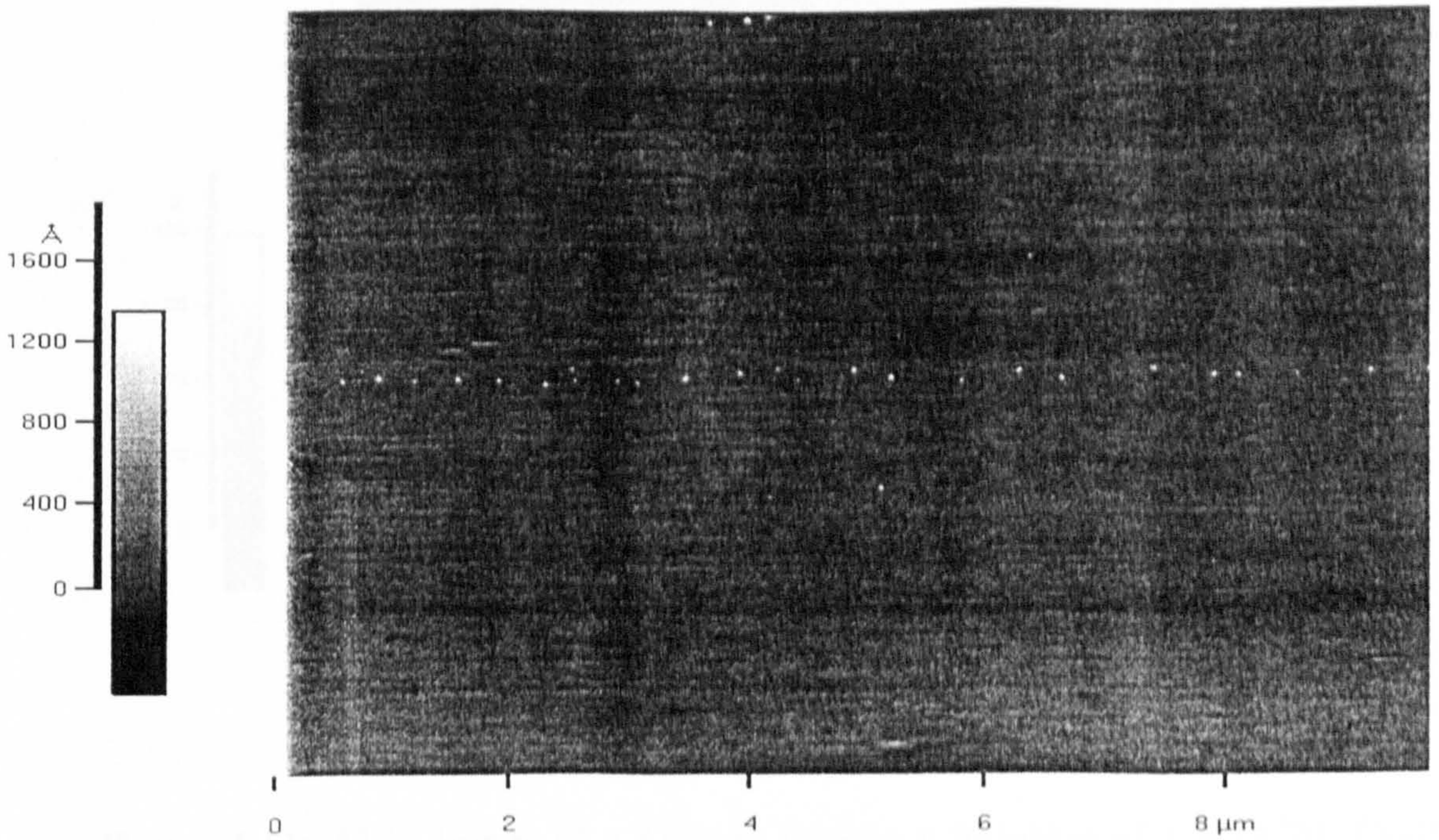

Figure 4.49: AFM Image of a Bare Quartz Disk.

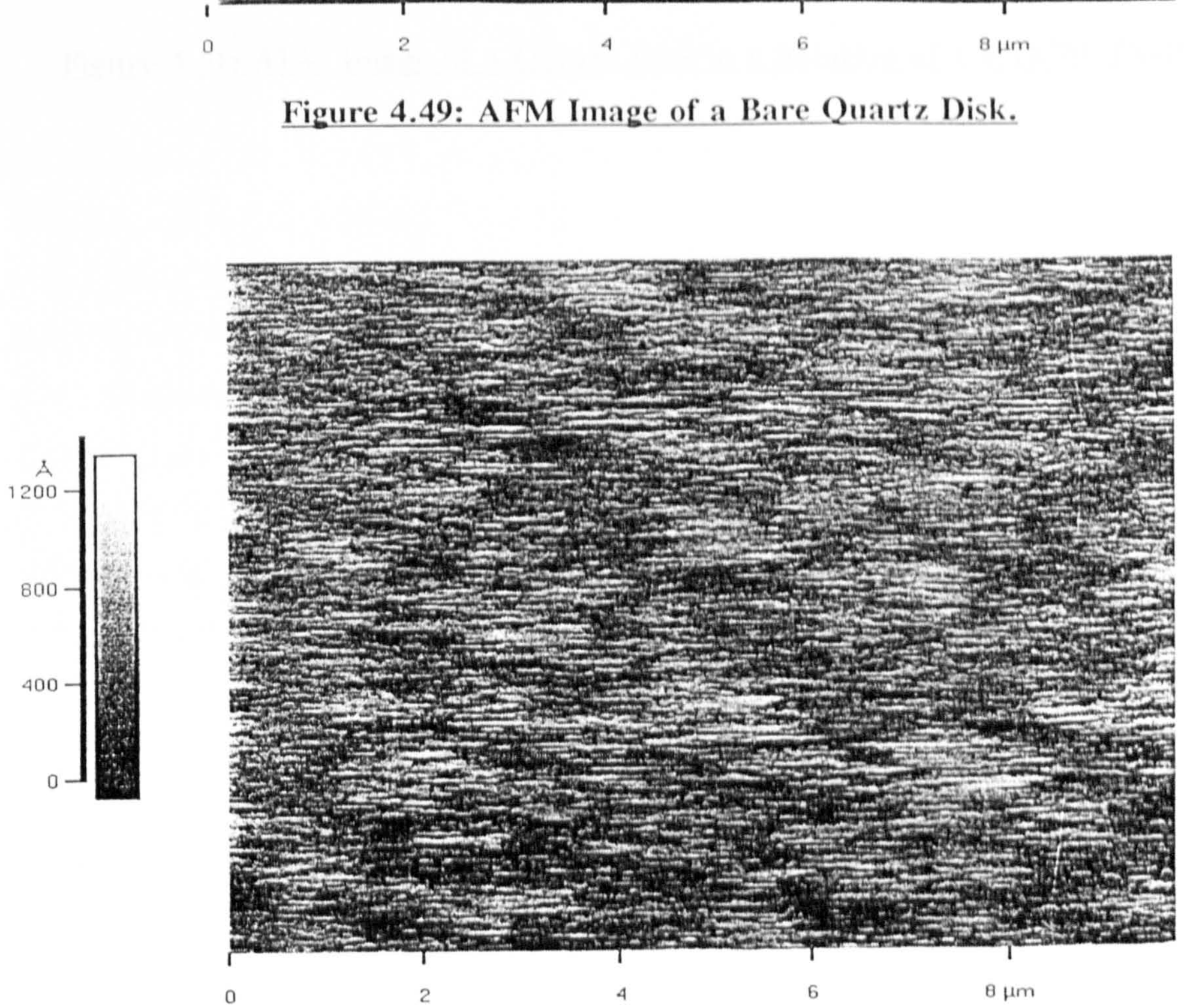

Figure 4.50: AFM Image of a Quartz Disk dipped in a Solution of 8.5 x 10^{-5}M TX-100.

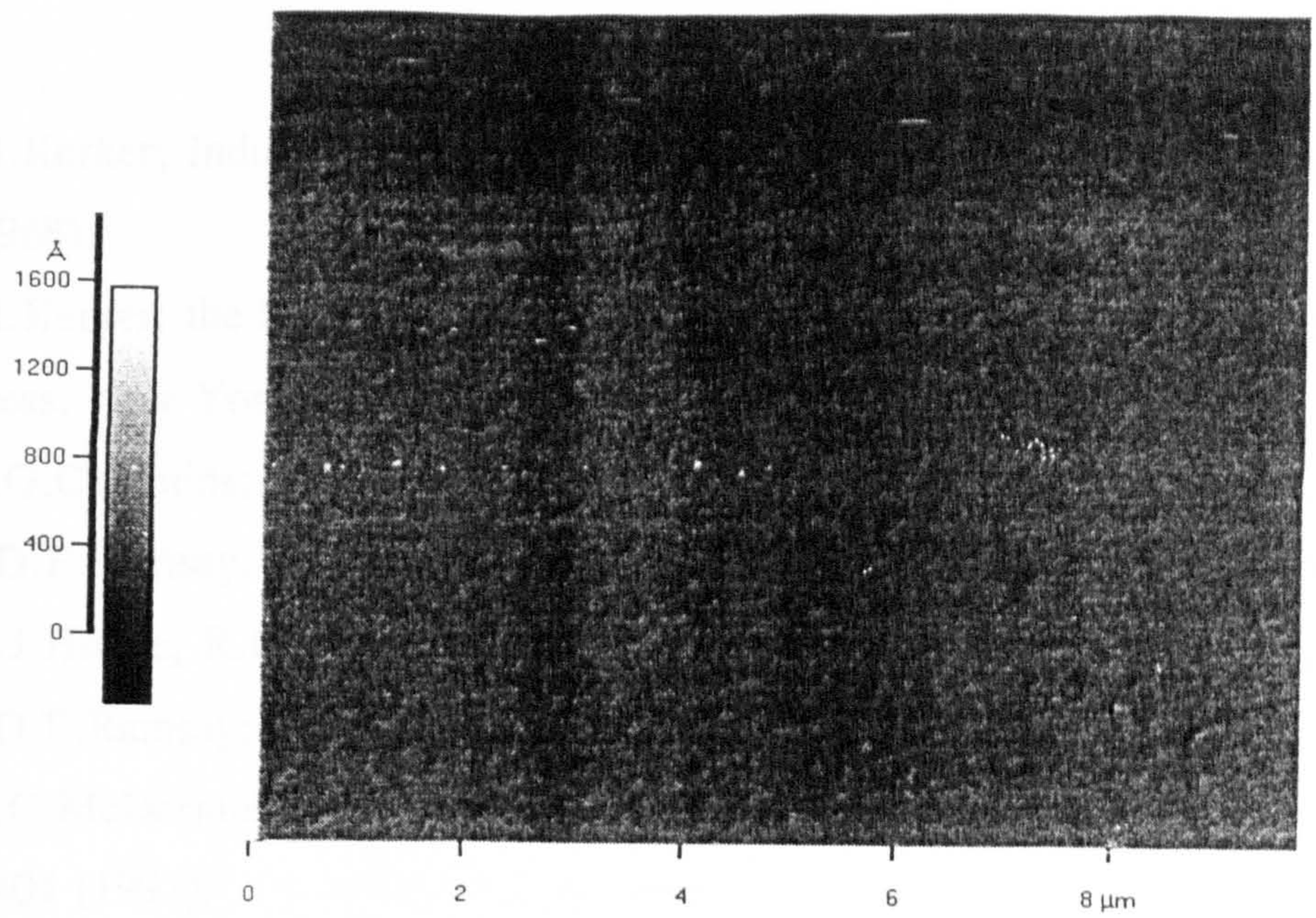

Figure 4.51: AFM Image of a Quartz Disk in a Solution of 1 x 10^{-3}M TX-100.

References.

(1) M.Kerker; Industrial and Engineering Chemistry (The Interface Symposium), 60,31 (1968).

(2) M.Kerker; the Scattering of Light and other electromagnetic Radiation. Academic Press; New York and London (1969).

(3) P.G.Cummins; E.Staples; J.Penfold; J.Phys.Chem., 94,3740 (1990).

(4) J.D.F.Ramsay; B.O.Booth; J.Chem.Soc.Faraday Trans.1, 79,173 (1983).

(5) D.J.Hodge; R.G.Laughlin; R.H.Ottewill; A.R.Rennie; Langmuir, 7,878 (1991).

(6) J.D.F.Ramsay; R.G.Avery; L.Benest; Far.Discuss.Chem.Soc., 76,1 (1983).

(7) D.C.McDermott; J.R.Lu;E.M.Lee; R.K. Thomas; A.R.Rennie; Langmuir, 9(9), 2404 (1993).

(8) W.Brown; R.Rymden; J. van Stam; M.Almgren; G.Svensk; J.Phys.Chem., 93, 2512 (1989).

(9) F.Mahmood; P.A.Sermon; unpublished data, Brunel University (1996).

(10) L Luciani; PhD Thesis, L'Universite Aix-Marseille, Marseille, France (1995).

(11) T.Kato; S.Anzai; T.Seimiya; J.Phys.Chem., 91,4655 (1987).

(12) T.Kato; S.Anzai; T.Seimiya; J.Phys.Chem., 94,7255 (1990).

(13) J.Penfold; E.Staples; P.G.Cummins; Adv.Coll.Int.Sci., 34,451 (1991).

(14) P.G.Cummins; E.Staples; J.Phys.Chem., 95(15),5902 (1991).

(15) G.Binnig; C.F.Quate; C.Gerber; Phys. Rev. Lett., 56,930 (1986).

(16) S.Manne; H.E.Gaub; Science, 270,1480 (1995).

(17) J.A.Zasadzinski; Curr. Opin. Colloid Interface Sci.,1, 264 (1996).

CHAPTER 5: Discussion.

5.1. Aim of Work Carried out for this Thesis.

A surfactant's behaviour in aqueous solution determines its environmental feasibility. Surfactants are used in detergents, paints, stabilisers in biological systems, flocculant in the water industry, EOR and in agricultural chemicals. Many of these applications are controlled by surfactant adsorption at an interface.

The work carried out for this thesis aimed to deal with the problem of analysing oligomeric non-ionic surfactants, of the polyethoxylate type, directly from aqueous solution, and understanding the mechanism of a successful analysis; and following on from that to elucidate the mechanism of adsorption of these surfactants onto oxide surfaces and the nature of the adsorbed layer.

5.2. Mechanism of Adsorption.

The behaviour of oligomeric surfactants during their adsorption onto silica from aqueous solution is an extremely complex process that depends on the nature of the adsorbate and the ionic impurities present in the aqueous solution. A basic mechanism of adsorption of such surfactants is set out below, and is based on the mechanism gleaned from literature and the results given in section 3.6 of this thesis.

5.2.1. Initial Stage of Adsorption.

This exothermic process occurs at concentrations of surfactant well below the CMC, it consists of isolated monomers adsorbing, via H-bonding between hydroxyl groups on the silica surface and the hydroxyl groups of the surfactant head group, onto the mineral oxide surface. Experiments carried out with sulphated TX-100 (TX-100S) showed that the surfactant adsorbed only onto silica at very high equilibrium concentrations. This surfactant carried a negative charge and so suggests that the molecule must have been repelled by the negative charges on the silica surface. These results suggest that monomeric adsorption taking place at low equilibrium concentrations is governed by the end hydroxyl group of the surfactant. Although Keith et al (1) showed that other ethene oxide linkages in the surfactant head group are also involved in hydrogen bonding between

the monomer and the surface. I would propose, then, that initially, the onset of monomeric adsorption is governed by the end hydroxyl group; once this initial attachment has been established, then other ethene oxide linkages become attached to the surface.

Adsorption is enhanced by heat treatment of the silica. This result appears to be contrary as calcination is known to reduce the surface area of silica and the number of silanol groups on the silica surface. Calcination, however, is also known to cause the removal of calcium from the silica surface and increase the number of unperturbed hydroxyl groups on the silica surface. This suggests that the oxide will be 'cleaner' after calcination; there will be more silanol groups that are free for bonding with surfactant molecules.

An increase in salt concentration causes a reduction in the CMC of certain surfactants, and this is mirrored by an increase in the adsorbed amount of the bulk surfactant at low equilibrium concentrations. The ions present in solution cause a reduction in the inter-head group repulsion between monomers already attached to the surface, and also a 'salting out' of the surfactant from aqueous solution takes place. These factors are key in the enhancement of surfactant adsorption onto a surface.

An increase in the temperature of the system at low equilibrium concentrations causes a decrease in the adsorbed amount of the bulk surfactant. The ethylene oxide chains of the surfactant molecules will have an enhanced solubility in the aqueous solution at the elevated temperatures, thus reducing the likelihood of their being adsorbed onto the silica surface.

5.2.2. Final Stage of Adsorption.

At the plateau stage on the adsorption isotherm, the process is endothermal and is driven by lateral interactions between the hydrocarbon chains of the surfactant molecules. Again, the adsorption is enhanced by heat treatment of the silica.

The addition of ions to the system at the isotherm plateau causes an increase in the adsorbed amount of the bulk surfactant. Sodium chloride causes the largest increase in adsorption when compared to magnesium chloride. The presence of the magnesium ions

causes an increase in the solubility of non-ionic surfactants (see Table 3.2, Chapter 3) and hence has a smaller effect on the increase in surfactant adsorption than the sodium chloride. Lateral attractions between surfactant molecules already on the surface are enhanced, thus causing an increase in adsorption of the surfactant.

The results for increased brine concentration were of a similar nature: the adsorbed amount of surfactant increases with increase in brine concentration. The adsorbed amounts do not change significantly at the plateau region for 1% brine, as seen in the isotherms when sodium chloride and magnesium chloride are present in the system. It would appear that there needs to be a certain initial concentration of brine before the enhanced adsorption effects can take place, due to the larger concentrations of surfactant and therefore the larger amounts of head group repulsion to overcome.

An increase in temperature of the system at this point on the isotherm is accompanied by an increase in adsorption of the bulk surfactant. The increase in temperature causes a dehydration of the head groups and this drives the micelles out of solution and onto the silica surface.

5.3. HPLC Analysis of Surfactants.

A good HPLC gradient, which would provide a quick, accurate system for separating the oligomers of the surfactants (see Section 2.1), was required. The gradient eventually used was peculiar in that it was neither reversed nor normal phase HPLC, although a tentative explanation of how it worked is possible. The curious point regarding this system is that it was only successful on a certain type of silica. It is the author's belief that the pre-treatment of a silica surface strongly affects its adsorptive properties, and that the effects need to be studied more by experimentalists working in this field.

Calcination of the silica surface, in particular, seems to alter the surface structure of the material. There have been very few recent papers published that have examined this phenomenon and the work carried out for this thesis seemed to produce more unanswered questions. For example, is it true that the surface area of the silica is reduced upon heat treatment, or is it that the pore structure is changed, thereby rendering BET analysis to

be not a true indication of surface structure? Are any micropores present changed to mesopores (although changes were not seen directly with SEM)? When standard adsorption isotherms were measured for TX-100 on calcined silica, the adsorbed amount at the plateau of the isotherm was shown to increase, it may be that silicas bought from different commercial sources have been pre-treated by different methods and thus are more or less susceptible to the adsorption of surfactants. Unfortunately, very few commercial suppliers are willing to give out information such as this.

5.4. Oligomeric Analysis of Surfactants.

Following the discovery of a gradient that was capable of separating the oligomers, the relative amounts of oligomer adsorbed onto the silica surface could be examined in a similar fashion to the way in which adsorption isotherms of the bulk surfactant had been measured.

It was found that the smallest oligomers were preferentially adsorbed onto the silica surface at all sections on the isotherms, most probably due to the hydrophobic nature of the smaller components relative to the larger ones.

The addition of sodium chloride and magnesium chloride to the systems caused an increase of adsorption of all sizes of oligomer at the plateau of the isotherm. The largest effect was seen for sodium chloride (see Figure 3.4), due to the large salting out effects of this salt. The increase in adsorption was largest for the largest oligomer due to their having the longest head groups and thus being more susceptible to the salting out of the ions.

The addition of brine also caused an increase in adsorption of all oligomers at all positions along the isotherm. At 1% brine, however, there appears to be little or no increase in adsorption, particularly for the two larger sizes of oligomers studied. A group at UNED, Madrid, have also found similar results for the bulk surfactants but have not published or attempted to explain these results. It may be that initially the ions are adsorbed onto the silica surface, thus preventing the surfactant molecules from adsorbing due to the formation of an electrical double layer around the silica particles. At concentrations of brine above 1%, there are enough ions to salt out the surfactant's head groups and this

overrides the effects of ion complexation with the surface.

An increase in temperature shows a steady increase in adsorption of oligomeric sizes. At 253K, however, there is a drop in adsorption at x=0.5. An increase in temperature may cause an increase in interaction of the head group with water for individual monomers thus causing a decrease in adsorption. At concentrations above the CMC, interactions between the head groups may increase and so the adsorption is enhanced by lateral interactions between the head groups within micelles.

Table 5.1 shows the amounts of differently sized oligomer that are taken up by the silica surface at differing system conditions.

5.5. Neutron Scattering.

Neutron scattering results showed the adsorbed surfactant at the plateau of the isotherm as approximately a bilayer, they also showed the point at which saturation of the colloidal silica surface with surfactant took place and were extremely valuable in this respect. AFM measurements showed a relatively flat surface. The AFM image showed 'pin pricks' to be present in the adsorbed layer of surfactant. These are most probably due to water, once part of the adsorbed layer, that has evaporated off the surface.

5.6. Conclusions and Future Work.

This study has attempted to thoroughly analyse the adsorption of oligomers of non-ionic, oligomeric surfactants onto silica surfaces from aqueous solution. These types of surfactants form the basis of many industrial processes and industrial/domestic cleaners and thus their environmental impact is at present in the media 'spotlight'. Hopefully, this work has provided, in a small way, an increase in the understanding of these complex systems. If similar work continues, the industrial chemist will be able to predict the behaviour of such chemicals in aqueous solution and thus ensure a decrease in the pollution of our rivers and coastlines by these soaps.

There are many ways in which the work in this thesis can be extended. A more in-depth look at the structure of the adsorbed layer on surfaces needs to be undertaken, particularly

now that AFM analysis is being developed which will allow this sort of examination to be made with ease. It would be exciting to analyse the results gained from neutron scattering using more sophisticated mathematics in order that the actual structure of the adsorbed layer of surfactant be studied. Also, it would be profitable to look at mixed solutions of surfactants; the system used in this work was ideal, usual systems consist of a blend of anionic/cationic and non-ionic surfactants. Of course, this would require the HPLC (or other) apparatus to be developed to incorporate the extra components. Another look at the true effects of various pre-treatments of silica would also be beneficial to experimentalists working in this area.

At a more applied level, the study of adsorption of these surfactants from oil-based systems would also be invaluable, particularly for those chemicals used during the emulsification of oil slicks. It would be interesting to study the degradation of non-ionic surfactants in waste-water systems and the natural environment as this is a popular field of research recently (2-6). Also, it would be very interesting to look at the solubilisation of certain molecules by admicelles; TX-100 admicelles have recently been used to solubilise (or 'ad-solubilise') steroids. This work is extremely important in the development and complete understanding of new pharmaceutical and biological processes (7,8).

As can be seen, this work can be extended in a huge number of ways. The possible practical applications will ensure that research in this area of colloid chemistry will always be active.

Table 5.1. The Behaviour of Oligomers of TX-100 in Aqueous Solution.

Uptake of Oligomers from Solution (>90% = HH; 70%-90% = H; 50%-70% = M; 0%-50% = L).												
	298K		**323K**		**353K**		**1% brine**		**3% brine**		**5% brine**	
	x=0.5	x=1.0	x=0.5	x=1.0	x=0.5	x=1.0	x=0.5	x=1.0	x=0.5	x=1.0	x=0.5	x=1.0
3EO	H	M	H	H	M	H	H	H	HH	HH	HH	HH
8EO	M	L	M	M	M	H	M	M	H	H	H	H
13EO	M	L	M	M	M	M	M	M	H	H	H	H

References.

(1) S.Keith; C.H.Rochester; J.Chem.Soc.Far.Trans.I, 84,3641 (1988).

(2) J.A.Field; T.M.Field; T.Poigner; H.Siegrist; W.Giger; Water Research, 29,1301 (1995).

(3) M.Ahel; C.Schaffner; W.Giger; Water Research, 30,37 (1996).

(4) M.Ahel; W.Giger; M.Koch; Water Research, 28,1131 (1994).

(5) M.A.Blackburn; M.J.Waldock; Water Research, 29,1623 (1995).

(6) P.Van der Meeren; W.Verstraete; Curr. Opin. Colloid Interface Sci., 1,624 (1996).

(7) J. Jansen; C. Treiner; C.Vaution; J. Colloid Interface Sci., 179, 578 (1996).

(8) S.Keith; C.H.Rochester; J.Chem.Soc.Far.Trans.I, 84,3641 (1988).

(9) R.Nagarajan; Curr. Opin. Colloid Interface Sci., 2,282 (1997).